THE UNIVERSITY
of ADELAIDE

Role of Voltage-gated Sodium Channel Isoforms in Electrophysiological Properties of Neurons Innervating the Viscera in Mice

Andelain Kristiseter Erickson

School of Medicine
Discipline of Medicine
The University of Adelaide

Thesis submitted for the degree of Doctor of Philosophy
17th May 2019

Table of Contents

Citation listing

Grundy, L*, Erickson, A* & Brierley, SM 2018, 'Visceral Pain', *Annu Rev Physiol*, Oct 31 (**Chapter 1**). *Contributed equally to this work.

Erickson, A, Deiteren, A, Harrington, AM, Garcia-Caraballo, S, Castro, J, Caldwell, A, Grundy, L & Brierley, SM 2018, 'Voltage-gated sodium channels: (Na$_v$)igating the field to determine their contribution to visceral nociception', *J Physiol*, vol. 596, no. 5, pp. 785-807 (**Chapter 2**).

Salvatierra, J*, Castro, J*, Erickson, A*, Li, Q, Braz, J, Gilchrist, J, Grundy, L, Rychkov, GY, Deiteren, A, Rais, R, King, GF, Slusher, BS, Basbaum, A, Pasricha, PJ, Brierley, SM & Bosmans, F 2018, 'Na$_v$1.1 inhibition can reduce visceral hypersensitivity', *JCI Insight*, vol. 3, no. 11, Jun 7 (**Chapter 10**). *Contributed equally to this work.

Grundy, L, Erickson, A, Caldwell, A, Garcia-Caraballo, S, Rychkov, G, Harrington, A & Brierley, SM 2018, 'Tetrodotoxin-sensitive voltage-gated sodium channels regulate bladder afferent responses to distension', *Pain*, vol. 159, no. 12, Dec, pp. 2573-2584 (**Chapter 11**).

Abstract

Chronic visceral pain is a poorly managed symptom of functional and inflammatory gastrointestinal disorders and there is a lack of suitable analgesics that are efficacious without gastrointestinal side effects. Voltage-gated sodium (Na_v) channels regulate action potential generation and cell membrane excitability in sensory neurons and are implicated in several enhanced pain and loss-of-pain phenotypes in humans. Pharmacological modulation of Na_v channels has been investigated as a therapeutic strategy for the past two decades in a range of pain modalities, including somatic, neuropathic, and more recently - visceral pain. In this thesis, gene transcripts for the nine Na_v channel isoforms ($Na_v1.1$-$Na_v1.9$) were detected in dorsal root ganglia (DRG) neurons retrogradely labeled from the colon and bladder in mice, and the contribution of different isoforms to active electrophysiological properties in these neurons was evaluated using Na_v-selective modulators. An evaluation of electrophysiological properties of colon-innervating DRG neurons from healthy and chronic visceral hypersensitivity (CVH) mice was also conducted and did not provide sufficient support for a model-related phenotype *in vitro*. In the pharmacological part of this thesis, it was found that inhibition of tetrodotoxin-sensitive Na_v channels ($Na_v1.1$-$Na_v1.4$, $Na_v1.6$ and $Na_v1.7$) effectively altered electrophysiological responses in colon-innervating and bladder-innervating neurons, and furthermore reduced bladder afferent responses to distension and nociceptive signaling to the spinal cord. Electrophysiological responses in colon-innervating DRG neurons were also modulated by less selective Na_v modulators, such as veratridine, which targets all Na_v channel isoforms, and more selective Na_v modulators, such as Hs1a, which targets $Na_v1.1$, $Na_v1.2$, $Na_v1.3$, $Na_v1.6$, and $Na_v1.7$; OD1, which targets $Na_v1.4$, $Na_v1.6$, and $Na_v1.7$; ICA-121341, which targets $Na_v1.1$-$Na_v1.3$; A-803467, which targets $Na_v1.8$; and Compound B, which targets $Na_v1.1$. inhibition of $Na_v1.1$ using Compound B was furthermore shown to be effective in reducing pain responses to colorectal distension in CVH mice.

Declaration of originality

I certify that this work contains no material which has been accepted for the award of any other degree or diploma in my name in any university or other tertiary institution and, to the best of my knowledge and belief, contains no material previously published or written by another person, except where due reference has been made in the text. In addition, I certify that no part of this work will, in the future, be used in a submission in my name for any other degree or diploma in any university or other tertiary institution without the prior approval of the University of Adelaide and where applicable, any partner institution responsible for the joint award of this degree.

The author acknowledges that copyright of published works contained within this thesis resides with the copyright holder(s) of those works.

I give permission for the digital version of my thesis to be made available on the web, via the University's digital research repository, the Library Search and also through web search engines, unless permission has been granted by the University to restrict access for a period of time.

<table>
<tr><td></td><td>17/5/19</td></tr>
<tr><td>Andelain Kristiseter Erickson</td><td>date</td></tr>
</table>

Acknowledgments

Abbreviations

A/M-IBS	Alternating/Mixed irritable bowel syndrome
ACc	Anterior cingulate cortex
Adrα2A	α2A-adrenoceptors
ATP	Adenosine 5'-triphosphate
BOTOX	Botulinum toxin type A
Ca_v	Voltage-gated calcium
CGRP	Calcitonin-gene related peptide
CHRNA3	Nicotinic acetylcholine receptor subunit alpha 3
CIP	Congenital insensitivity to pain
CNS	Central nervous system
CRD	Colorectal distension
CRF	Corticotrophin-releasing factor
CRF_1Rs	Corticotrophin-releasing factor 1 receptors
CSF	Cerebrospinal fluid
CTB	Cholera toxin subunit B
CTB-488	Cholera toxin subunit B conjugated to Alexa Fluor 488
CVH	Chronic visceral hypersensitivity
DCN	Dorsal root ganglia commissure
DGC	Dorsal gray commissure
DH	Dorsal horn
DRG	Dorsal root ganglia
DSS	Dextran sodium sulfate
EC	Enterochromaffin
EMG	Electromyogram
ENS	Enteric nervous system
FBD	Functional bowel disorder
G-CSF	Granulocyte colony-stimulating factor
GAG	Glycosaminoglycan
GPCR	G-protein coupled receptor
HC	Healthy control
Hm1a	δ-theraphotoxin-Hm1a
HPA	Hypothalamic-pituitary-adrenal
IBD	Inflammatory bowel disease
IBS	Irritable bowel syndrome
IBS-C	Constipation-predominant irritable bowel syndrome
IBS-D	Diarrhea-predominant irritable bowel syndrome

IC/BPS	Interstitial cystitis/bladder pain syndrome
IR	Immunoreactive
K2P	Two-pore domain K
KOR	κ-opioid receptor
K_v	Voltage-gated potassium
LI	Laminae I
LS	Lumbosacral
LV	Laminae V
Na_v	Voltage-gated sodium
$Na_v1.7^{Nav1.8}$	$Na_v1.7$-knock out in $Na_v1.8$-expressing cells
NGF	Nerve growth factor
NSAIDs	Non-steroidal anti-inflammatory drugs
OTR	Oxytocin receptor
P-CTX-1	Pacific ciguatoxin 1
PAG	Periaqueductal gray
PBMCs	Peripheral blood mononuclear cells
PBS	Phosphate buffered saline
PDE4	Phosphodiesterase 4D
pERK	Phosphorylated MAP kinase ERK 1/2
PGE2	Prostaglandin E2
PI-IBS	Post-infectious irritable bowel syndrome
PK	Pharmacokinetic
PNS	Peripheral nervous system
RT-qPCR	Reverse-transcription quantitative polymerase chain reaction
SDH	Superficial dorsal horn
SNI	Spared nerve injury
TK	Toxicokinetic
TL	Thoracolumbar
TNBS	Trinitrobenzenesulfonic acid
TNF-α	Tumor necrosis factor-α
TrkA	Tropomysin-related kinase A
TrkC	Tropomysin-related kinase C
TRP	Transient receptor potential
TTX	Tetrodotoxin
TTX-R	Tetrodotoxin-resistant
TTX-S	Tetrodotoxin-sensitive
VFH	Von Frey hair
VMR	Visceromotor reflex

X
`

Statement of Authorship

Title of Paper	Visceral Pain

Publication Status	☑ Published	☐ Accepted for Publication
	☐ Submitted for Publication	☐ Unpublished and Unsubmitted work written in manuscript style

Publication Details	Grundy, L., Erickson, A., & Brierley, S. M. (2018). Visceral Pain. Annu Rev Physiol. doi:10.1146/annurev-physiol-020518-114525

Principal Author

Name of Principal Author (Candidate)	Andelain Erickson		
Contribution to the Paper	Planning, writing, and editing of manuscript		
Overall percentage (%)	30		
Certification:	This paper reports on original research I conducted during the period of my Higher Degree by Research candidature and is not subject to any obligations or contractual agreements with a third party that would constrain its inclusion in this thesis. I am the primary author of this paper.		
Signature		Date	15/1/2019

Co-Author Contributions

By signing the Statement of Authorship, each author certifies that:

    i.   the candidate's stated contribution to the publication is accurate (as detailed above);

    ii.   permission is granted for the candidate in include the publication in the thesis; and

    iii.   the sum of all co-author contributions is equal to 100% less the candidate's stated contribution.

Name of Co-Author	Luke Grundy (equal first author)		
Contribution to the Paper	Planning, writing, and editing of manuscript.		
Signature		Date	19.3-19

Name of Co-Author	Stuart Brierely (corresponding author)		
Contribution to the Paper	*[handwritten]* project lead / co-ordination writing / editing manuscript / corresponding author.		
Signature		Date	14/3/19

Please cut and paste additional co-author par

1

Chapter 1 Visceral Pain

Grundy L*[1,2], Erickson A*[1,2], Brierley SM[1,2]

[1]Visceral Pain Research Group, College of Medicine and Public Health, Centre for Neuroscience, Flinders University, Bedford Park, South Australia 5042, Australia [2]Centre for Nutrition and Gastrointestinal Diseases, University of Adelaide, South Australian Health and Medical Research Institute (SAHMRI), Adelaide, South Australia 5000, Australia. *These authors contributed equally to this article.
Corresponding author: stuart.brierley@flinders.edu.au.

1.1 Abstract

Most of us live blissfully unaware of the orchestrated function that our internal organs conduct. When this peace is interrupted, it is often by routine sensations of hunger and urge. However, for >20% of the global population, chronic visceral pain is an unpleasant and often excruciating reminder of the existence of our internal organs. In many cases, there is no obvious underlying pathological cause of the pain. Accordingly, chronic visceral pain is debilitating, reduces the quality of life of sufferers, and has large concomitant socioeconomic costs. In this review, we highlight key mechanisms underlying chronic abdominal and pelvic pain associated with functional and inflammatory disorders of the gastrointestinal and urinary tracts. This includes how the colon and bladder are innervated by specialized subclasses of spinal afferents, how these afferents become sensitized in highly dynamic signaling environments, and the subsequent development of neuroplasticity within visceral pain pathways. We also highlight key contributing factors, including alterations in commensal bacteria, altered mucosal permeability, epithelial interactions with afferent nerves, alterations in immune or stress responses, and cross talk between these two adjacent organs.

1.2 Introduction

Our internal or visceral organs undertake a variety of physiological functions that are essential for sustaining life. We are generally unaware of these complicated processes, but when awareness is triggered, it is usually by sensations of hunger, fullness, or urge. Akin to pain arising from other regions of the body, visceral pain alerts us of potential or actual tissue damage. Visceral pain encompasses a plethora of common acute and chronic clinical conditions that are experienced by millions of people around the globe. This includes sudden onset pain associated with serious clinical conditions, such as peptic/intestinal ulcers, cholecystitis, and appendicitis. However, visceral pain also encompasses wide-ranging chronic syndromes, including noncardiac chest pain, functional abdominal pain, endometriosis, pancreatitis, as well as chronic pain from the bladder and bowel. While some of these clinical entities have a clear underlying pathology, in many cases there is no obvious reason for the pain, and they are therefore often referred to as idiopathic or functional disorders. This is particularly troubling for the afflicted individual and makes accurate diagnosis difficult, particularly when the diagnosis is based on exclusion of other serious diseases. To further complicate diagnosis, visceral pain is poorly localized and diffuse, often affecting multiple organs at once, with visceral differentiation often relying on the determination of associated pathology and changes in organ function.

In this review, for brevity, we discuss key mechanisms contributing to chronic abdominal and pelvic pain. In particular, it covers pain originating from the colon and bladder and the highly prevalent clinical conditions they are associated with. These include interstitial cystitis/bladder pain syndrome (IC/BPS), irritable bowel syndrome (IBS), and inflammatory bowel disease (IBD), which are major and debilitating forms of chronic visceral pain. A lack of suitable treatments for these disorders is a major contributing factor to their debilitating nature and the large socioeconomic cost accrued by patients, their families, and society (1, 2). Conventional analgesics, such as nonsteroidal anti-inflammatory drugs and opioids, are unsuitable for therapy, as they are associated with severe side effects. This includes tolerance, a lack of efficacy and, importantly for some inflammatory disorders, the potential to exacerbate the disease (3, 4). Chronic use of opioids for pain management causes dependence and reduced analgesic efficacy, resulting in the current opioid epidemic (5). Importantly, chronic opioid use also causes severe

constipation, which is already a common symptom of many patients with IBS, making opioid use even more problematic in this patient cohort. Consequently, understanding the underlying etiology of these disorders is the first step in identifying new effective analgesic treatments for visceral pain syndromes.

1.3 Clinical relevance

IBD, which includes ulcerative colitis and Crohn's disease, is a chronic, relapsing inflammatory disorder of the gastrointestinal tract that affects 0.5% of the Western population, including 2.5 million in Europe and 1 million people in the United States (6). Although the exact etiology of IBD is unclear, development likely occurs in genetically susceptible individuals through an inadequately suppressed or exaggerated immune response to luminal antigens, probably derived from gut microbiota (7). Abdominal pain, diarrhea, and gastrointestinal bleeding are the major clinical symptoms of IBD, with medical and surgical therapies aimed at resolving mucosal inflammation and correspondingly reducing symptoms (7). Accordingly, IBD has considerable economic costs totaling >$6 billion per annum in the United States alone (1, 6).

In contrast, IBS is a chronic functional gastrointestinal disorder characterized by abdominal pain or discomfort associated with altered bowel habits. IBS is subclassified as constipation-predominant IBS (IBS-C), diarrhea-predominant IBS (IBS-D), alternating or mixed IBS (A/M-IBS), and postinfectious IBS (PI-IBS). IBS is distinct from IBD in that it presents without overt inflammation-induced pathology to the intestine and is diagnosed based on the Rome IV criteria (1). IBS affects more than 11% of the global population, with ~65% of patients being female (1, 8). The etiology of IBS is multifactorial, and additional risk factors may be required for development, including altered stress and immune responses in afflicted individuals, with a strong correlation between a prior exposure of the patient to gastrointestinal infection and symptom occurrence (8, 9). This includes a preceding bout of gastroenteritis induced by pathogens such as *Escherichia coli, Campylobacter, Giardia lamblia*, and *Salmonella*, with symptoms potentially lasting for more than eight years after the initial infection (9, 10). IBS patients report a reduced quality of life and have additional clinical symptoms, including stool irregularities, as well as somatic and visceral comorbidities, with higher levels of anxiety and depression than healthy people (1, 8, 11). In the United States, the total direct and indirect cost of IBS is ~$30 billion per annum (12).

IC/BPS is a prevalent, chronic bladder disorder affecting >5% (11% of women and 5% of men) of the Western population (13–15). Patients with IC/BPS exhibit sensations of bladder fullness, urge to void, and allodynia and hyperalgesia to cystometric bladder filling compared to healthy controls; they also report sensations of urgency and pain at lower bladder distension volumes (16). Although the pathophysiology of IC/BPS is not completely understood, prior bladder E. coli infection, stress, and changes to neural pathways likely play key roles in the associated urgency, frequency, and pain (17). In the United States alone, IC/BPS costs ~$20–40 billion per annum to treat (15).

1.4 Visceral comorbidities

Although these conditions exist as distinct clinical entities, it is becoming clear that they do not occur in isolation, with considerable overlap in symptom profiles across patient cohorts. For example, ~40% of IBD patients in remission from inflammation meet the diagnostic symptom criteria for a functional gastrointestinal disorder (18), with incidence of IBS 2–3 times higher in IBD patients in remission from inflammation than in the general population (19). IC/BPS patients are 100 times more likely to have concurrent IBD than healthy controls (20), whereas bladder dysfunction is significantly more common among IBS patients than in healthy subjects (21). Correspondingly, patients with IBS are more likely to report bladder symptoms, including nocturia, urgency, and in some cases, urge incontinence (22). Conversely, 20–30% of men and women with IC/BPS have IBS among their most common comorbidity (20, 23). Recent evidence suggests that these clinical comorbidities are likely underscored by the overlap of colonic and bladder sensory networks, which ensure homeostatic coordination of these organs (11). Sensory signals emanating from these visceral organs project to the dorsal horn of the spinal cord where they activate postsynaptic pathways responsible for spinal and supraspinal autonomic reflexes. If the signal is of sufficient intensity, brain stem, limbic, and cortical regions provide emotional affective and conscious modulation of visceral sensation. As such, visceral sensations are susceptible to modulation

3

at each stage along this pathway, and the induction and maintenance of visceral pain have been investigated as a consequence of peripheral and central sensitization of the afferent pathways. Supraspinal modifications such as emotional state and stress can have significant effects on the perception of visceral pain.

1.5 Extrinsic sensory afferent innervation of the colon and bladder

The colon/rectum and bladder are innervated by specialized spinal sensory afferents traveling via two distinct anatomical spinal pathways: the lumbar splanchnic and sacral pelvic nerves (7, 24, 25) (**Figure 1.1**). Colon-innervating splanchnic and pelvic afferents have their cell bodies located within the thoracolumbar (TL; T10–L2) and lumbosacral (LS; L5–S1) dorsal root ganglia (DRG), respectively. These afferents synapse in the dorsal horn of the spinal cord with excitatory and inhibitory interneurons and second-order neurons of the dorsal column, spinothalamic tract, and spinoparabrachial pathway. The spinoparabrachial pathway is made predominantly of superficial dorsal horn projections associated with autonomic and affective responses to painful stimuli, whereas the spinoparabrachial projections feed into limbic and cognitive centers, including the amygdala, hypothalamus, and periaqueductal gray (PAG). The spinothalamic tract signal is relayed via the thalamus to cortical areas for sensory discrimination and localization via somatosensory inputs, while also feeding into limbic areas for the emotional component of the pain response (3, 26). The thalamus influences prefrontal cortex signaling associated with visceral pain responses, including those in the anterior cingulate cortex (ACc). Output from the cortical and limbic regions in response to pain activates descending inhibitory circuitry within the brainstem that causes release of inhibitory neurotransmitters within the dorsal horn of the spinal cord to regulate autonomic output responses (3, 26).

Neuronal cell bodies of bladder-innervating afferents are distributed within DRG at TL (T10–L2) and LS (L5–S1) spinal levels, with a predominance within LS DRG and the LS spinal cord (27, 28) (**Figure 1.1**). The spinal cord terminals of bladder afferents are found predominantly in the lateral spinal nucleus, superficial dorsal horn, and the dorsal commissure (DCN) (27, 28). Interestingly, these regions do not appear to differentiate between non-nociceptive and nociceptive mechanical stimuli and chemical stimuli. The major destination for bladder signals entering the spinal cord is the PAG (28), such that the degree of excitation within the PAG is closely linked to bladder volume, and thus the degree of afferent firing from the bladder. The PAG coordinates ascending excitatory input from the spinal cord with excitatory and inhibitory signals from the ACC, insula, and hypothalamus to provide an overview of the appropriateness to urinate. This is ultimately determined by the prefrontal cortex, allowing conscious control of urination. When a consensus is reached, subsequent activation of the pontine micturition center initiates the switch from a storage to voiding phase, and urination commences (28, 29). A number of studies have also shown that an important pelvic pain pathway may exist in the DCN, involving postsynaptic DCN neurons that project directly to the nucleus gracilis, before continuing on to activate regions of the thalamus and cortex contributing to pain sensation (30).
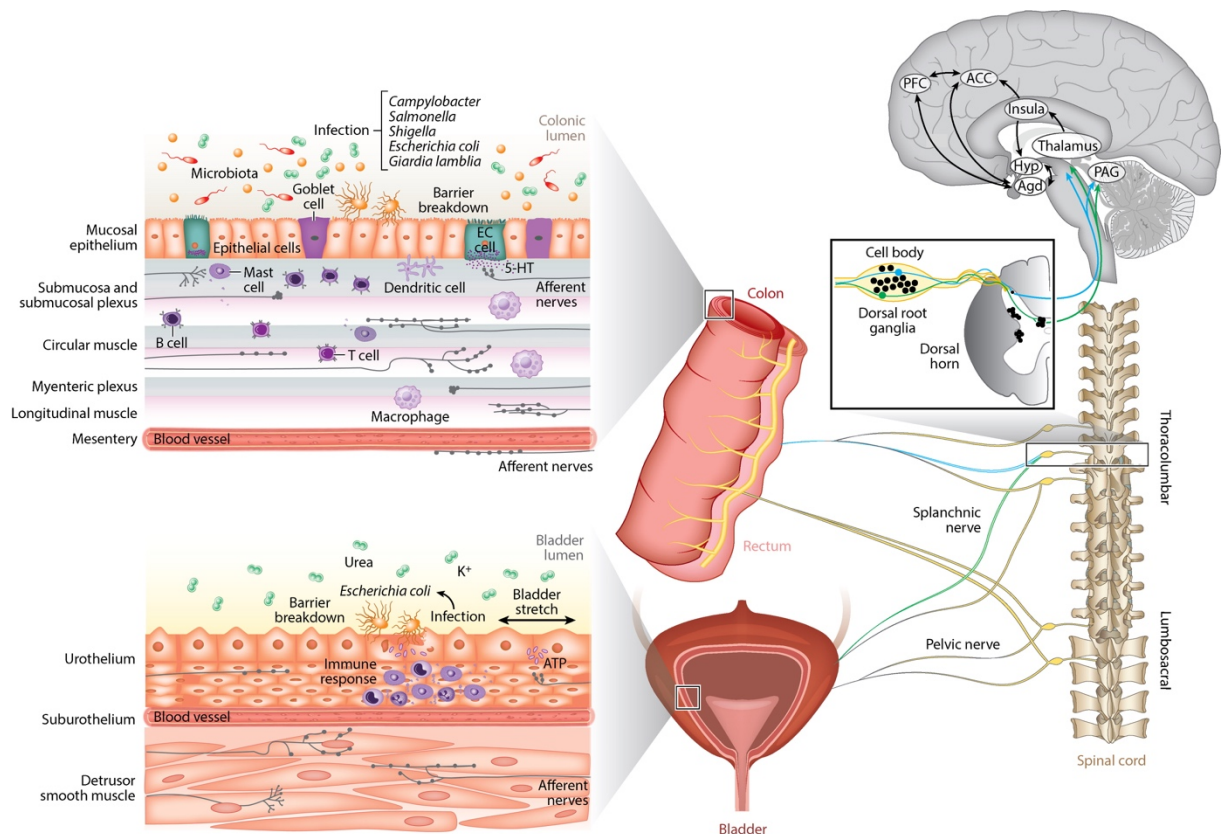
Figure 1.1. Schematic overview of the extrinsic sensory innervation of the colon/rectum and bladder. The colon and rectum are innervated by spinal afferents that follow the splanchnic and pelvic nerves. These afferents have cell bodies within the thoracolumbar and lumbosacral dorsal root ganglia, respectively. Their central axons terminate within the respective thoracolumbar and lumbosacral dorsal horn of the spinal cord, where they synapse onto second-order neurons. The peripheral projections of these afferents innervate the mucosa, myenteric/submucosal ganglia, and muscle; they also wrap around blood vessels within the submucosa and on the mesenteric attachment. This gives rise to distinct functional classes of afferents: muscular, mucosal, and vascular (splanchnic and pelvic pathway); and mesenteric (splanchnic only) and muscular/mucosal (pelvic only). Several populations of mechanically insensitive silent afferents also exist. Combined, these afferents allow detection of the full range of mechanical and chemical stimuli occurring within the colon and rectum. The bladder is also innervated by afferents from the pelvic and splanchnic pathways, with central projections to the thoracolumbar and lumbosacral dorsal horn of the spinal cord. Bladder afferents have specialized peripheral endings located within the urothelium, but predominantly within the detrusor smooth muscle. These afferents have both low- and high-mechanical activation thresholds to distension, allowing the full range of bladder distension and contraction to be detected. Populations of mechanically insensitive afferents also exist. Abbreviations: ACc, anterior cingulate cortex; Agd, amygdala; EC, enterochromaffin; Hyp, hypothalamus; PAG, periaqueductal gray; PFC, prefrontal cortex.

1.6 Afferent subtypes innervating the colon and bladder

Although the colon/rectum and bladder are innervated by spinal sensory afferents, their physiological properties and anatomical structures are distinct from those innervating the skin (**Figure 1.1**). Hence, the traditional nomenclature for subclassifying cutaneous afferents is not appropriate or relevant for visceral organs. Generally speaking, visceral afferents are predominantly peptidergic [calcitonin gene-related peptide (CGRP), NF200, and TRPV1 expressing] C-fibers that display polymodal characteristics to mechanical and chemical stimuli. These afferents express a wide variety of pro- and antinociceptive ion channels and receptors that dictate visceral afferent sensitivity and peripheral drive to the spinal cord (**Figure 1.2**). This balance can be dramatically shifted during inflammation, or in chronic visceral hypersensitivity (CVH) states, as discussed later in this review. The generalized nomenclature of visceral afferents therefore reflects their overall function, their mechanical responsiveness to a variety of stimuli, their mechanical activation thresholds, and the layer of gut or bladder they reside in.
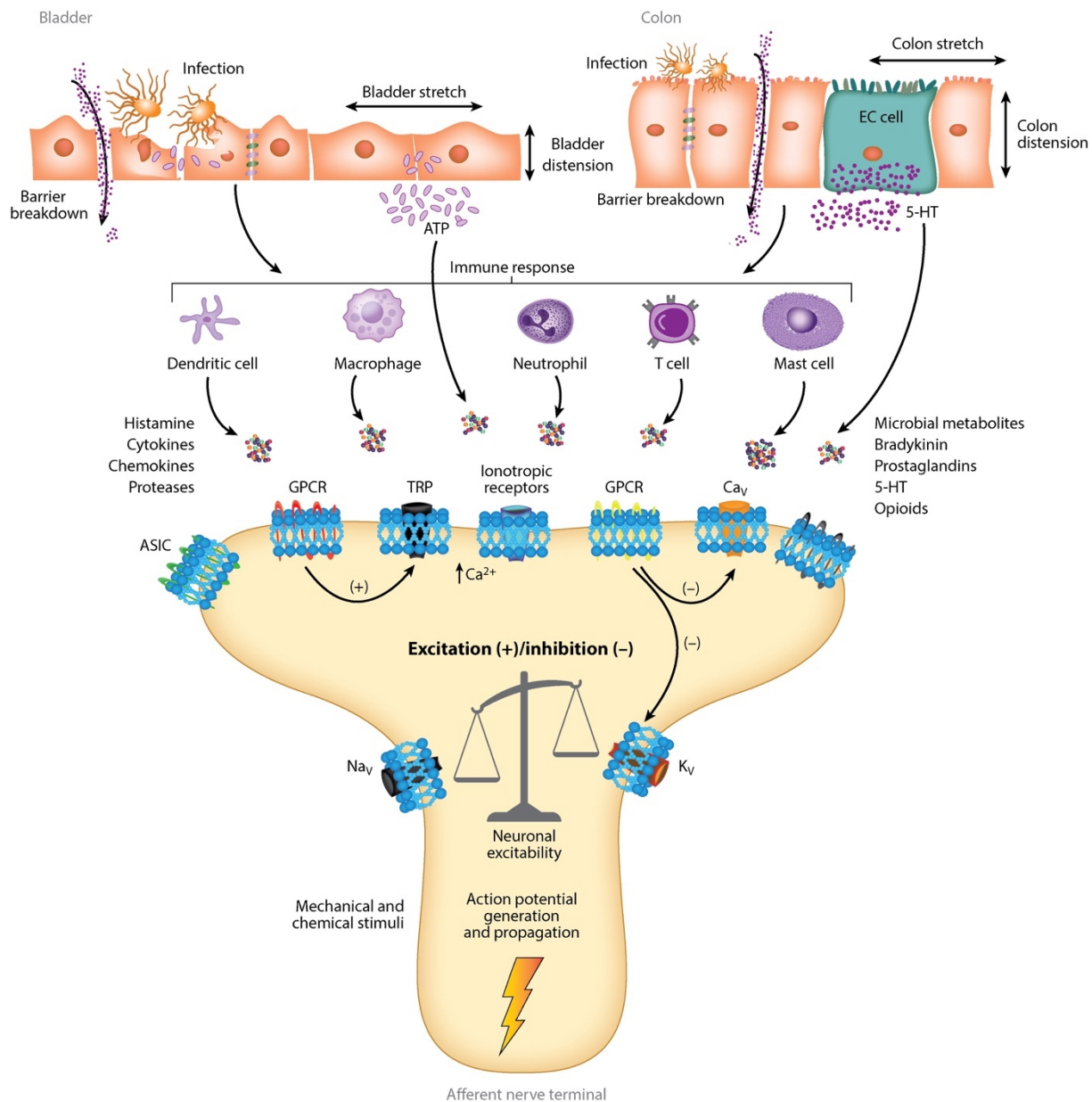
Figure 1.2. Schematic overview of the signaling mechanisms that affect visceral afferent sensitivity. The colon and bladder are highly dynamic signaling environments. Both undergo contraction and relaxation, providing direct mechanical activation of sensory afferents. Furthermore, specialized colonic EC cells can be activated by a range of endogenous mediators, including microbial metabolites, resulting in the release of 5-HT, which activates mucosal afferents via synaptic connections. In the bladder, release of ATP from urothelial cells results in subsequent activation of bladder afferents to modulate afferent sensitivity. Both the colon and bladder are susceptible to infection and inflammation resulting in barrier breakdown, allowing intraluminal mediators to access afferent nerve endings. Infection and inflammation also recruit distinct immune processes. These immune cells release a plethora of mediators that can activate and sensitize afferents via an arsenal of ion channels and receptors expressed by afferent nerve terminals. Some of these processes are excitatory (pronociceptive), while some are inhibitory (antinociceptive). The respective balance between the two processes regulates overall neuronal excitability and peripheral afferent drive to the central nervous system. Abbreviations: ATP, adenosine 5′-triphosphate; Ca$_v$, voltage-gated calcium channel; EC, enterochromaffin; GPCR, G protein–coupled receptor; K$_v$, voltage-gated potassium channel; Na$_v$, voltage-gated sodium channel; TRP, transient receptor potential channel.

6

1.6.1 Colon

The peripheral projections of spinal afferents innervate all layers of the colon/rectum wall, with 13 morphologically distinct endings identified to date (31). They include various types of mucosal endings, submucosal endings, intraganglionic laminar endings, intramuscular arrays, and afferents that wrap around blood vessels (32–34) (**Figure 1.1**). These endings correlate with eight different functional classes of afferents found within the splanchnic and pelvic innervations of the mouse colon. Importantly, the first five afferent classes discussed below have been confirmed in recordings from human colon (35–38).

1.6.1.1 Mucosal afferents

These have very low activation thresholds, are highly sensitive to distortion of the colonic mucosal epithelium, and likely play a crucial role in detecting the particle size of luminal contents (24, 39). These afferents are incredibly rare in the splanchnic nerve (1% of all afferents) but common in the pelvic nerve (15–25% of all afferents) (24, 39, 40). Pelvic mucosal afferents also communicate directly with enterochromaffin (EC) cells via 5-HT acting as an intermediary, whereby 5-HT is released from EC cells in response to norepinephrine acting on α2A-adrenoceptors (Adrα2A) or microbial metabolites, such as isovalerate, acting on Olfr558 receptors expressed on EC cells (41). Mucosal afferents also express TRPA1 and become mechanically hypersensitive during CVH states (39, 42).

1.6.1.2 Muscular afferents

Muscular afferents respond at low distension thresholds with a wide dynamic range. They represent 6–10% of the afferents in the splanchnic pathway and 16–25% of afferents in the pelvic pathway (24, 39, 40). Muscular afferents signal distension (and contraction) caused by fecal matter in the distal colon and rectum that provides information necessary for coordinating reflex loops and stimulating defecatory pathways (24, 39). These afferents also signal into the noxious range and likely contribute to nociception at high stimulus intensities. Antagonism of the voltage-gated sodium (Na_v) channel subtype $Na_v1.6$ reduces their action potential firing to stretch (43), whilst deletion of TRPV1 or ASIC3 also reduces their functional responsiveness (44).

1.6.1.3 Muscular/mucosal afferents

Muscular/mucosal afferents respond to both mucosal distortion and circular stretch, and contribute to 16–25% of the afferents within the pelvic pathway (24, 39, 40). Interestingly, these afferents have not been observed in the splanchnic innervation of the distal colon, suggesting they may play a key role in spinal defecatory circuits and conscious sensation of urge (24, 39). ASIC3 and TRPV1 contribute to their responsiveness to mechanosensory stimuli, and they can undergo long-term sensitization following zymosan treatment (44, 45). Muscular/mucosal afferents can be inhibited by $GABA_B$ receptor agonists or by µ-opioid receptor agonists (46, 47).

1.6.1.4 Vascular endings

These afferents wrap around blood vessels in the mesentery and submucosa and respond to high-threshold stimuli and a variety of inflammatory and immune mediators (24, 33, 39, 48). Vascular afferents also respond to noxious levels of distension and serve a role in signaling mechanically induced pain (24, 39, 42, 49). Afferents within the submucosa represent ~30% of afferents within both the splanchnic and pelvic pathways (24, 39, 40). Interestingly, mesenteric vascular afferents are exclusive to the splanchnic pathway (28–50% of all afferents) and respond to noxious distension of the colon and to changes in intramesenteric arterial pressure (49, 50). Overall, vascular afferents show the greatest similarity to traditional cutaneous nociceptors. Vascular afferents also display reduced activation thresholds and enhanced responsiveness during colitis and in models of CVH (39, 46, 51–55). Key targets include the Na_v channel isoforms $Na_v1.1$ (55, 56), $Na_v1.8$ (57), and $Na_v1.9$ (58); the voltage-gated calcium (Ca_v) channels $Ca_v2.2$ and $Ca_v2.3$ (46); the voltage-gated potassium (K_v) channel K_v7 (59); and the transient receptor potential channels TRPA1, TRPV1, and TRPV4 (42, 49, 60). In particular, $Na_v1.1$, $Ca_v2.2$, $Ca_v2.3$, TRPA1, and TRPV1 play key roles in contributing to CVH (48). Importantly, numerous inhibitory mechanisms have also been identified on subpopulations of these afferents, including TRPM8 (61) and the oxytocin (OTR) (53), $GABA_B$ (46, 51), κ-opioid (KOR) (54, 62), δ-opioid (63), and µ-opioid receptors

(63). For both OTR and KOR, these inhibitory effects only become apparent during inflammation or in CVH states (54, 62), perhaps as a compensatory mechanism in response to reduced abundance of their respective endogenous agonists.

1.6.1.5 Mechanically insensitive or silent afferents

These constitute ~25% of the afferents innervating the splanchnic and pelvic pathways (40). There are three different types of mechanically insensitive/silent afferents: those chemically activated by inflammatory or immune mediators [including histamine, 5-HT, bradykinin, capsaicin and adenosine 5'-triphosphate (ATP)] that do not subsequently develop mechanical sensitivity; those not chemically activated but mechanically sensitized; and those chemically activated and mechanically sensitized (40, 45, 60, 64). Interestingly, the silent afferents that develop mechanical sensitivity following inflammatory mediator application display the properties of high-threshold vascular afferents. In sensitized states, there is a decrease in the proportion of mechanically insensitive afferents but a corresponding increase in the proportion of mechanically sensitive high-threshold vascular afferents (40). These changes likely contribute to an increased afferent barrage from the periphery in response to distension and contraction, resulting in persistent pain states. Recent studies suggest that silent nociceptors are characterized by the expression of the nicotinic acetylcholine receptor subunit alpha 3 (CHRNA3) and that the mechanically gated ion channel PIEZO2 mediates nerve growth factor (NGF)-induced mechanosensitivity in these neurons (65).

Overall, these different afferent structures, combined with a differing arsenal of ion channels and receptors to regulate their neuronal excitability, underlie the vastly different sensory functions of these afferent classes (7, 48, 66) (Figure 2). Molecular expression profiles identified via RNAseq of colon-innervating DRG neurons suggest seven broad classes of colon-innervating afferents (67), which broadly accounts for the functional classes described above. This reflects the different stimuli transduced by these nerves and their overall function, including transmission of nociceptive information by the splanchnic nerves (but also the pelvic nerves) and encoding of defecatory reflexes by pelvic nerves. Therefore, these subclasses of afferents allow detection of non-noxious physiological stimuli, including luminal events, muscle stretch during organ distension and contraction, as well as noxious mechanical (bloating, intense distension/contraction) and chemical stimuli (7). These afferents are also activated and sensitized by inflammatory and immune mediators, including those acting via P2X (60), P2Y (35), 5-HT_3 (67), histamine 1 (68), PAR_1 (69), PAR_2 (70), bradykinin 1 (64), TNF-α (47), interleukin (IL)-β (47), IL-6 (47), and IL-2 (71) receptors. For further information regarding specific interactions between these ion channels and receptors, please see recent comprehensive reviews (48, 66, 72, 73).

1.6.2 Bladder

In the bladder, spinal afferents have specialized peripheral endings within the urothelium and three distinct types of ending, with branching, simple, or complex morphology in the detrusor smooth muscle (74). These endings broadly correlate with four broad functional classes of afferents found within the bladder.

1.6.2.1 Muscle mechanoreceptors

These respond to both contraction and distension, acting as tension receptors to accurately determine the degree of bladder stretch during urine accommodation. In the mouse, these afferents represent 30% of the splanchnic pathway and 63% of the pelvic pathway (75). In keeping with the role of these afferents in sensing bladder volume in the physiological range, most mechanosensitive afferents are active at low levels (3–15 mm Hg) of intravesical pressure, when the first sensations of bladder fullness in humans occur. A smaller population of afferents become active only when bladder pressures extend into the noxious range, including those that would induce sensations of urgency, discomfort, and eventually pain (28). Both low- and high-threshold muscle mechanoreceptors can be sensitized by inflammatory mediators (75). Electrophysiology recordings measuring conduction velocity reveal bladder afferents to be either myelinated (Aδ) or unmyelinated (C) fibers. However, in another break with somatic afferent properties, conduction velocity does not correlate with response threshold, with both fiber types demonstrating low or high thresholds to graded distension, as well as the majority of afferents expressing

`

CGRP, NF200, and TRPV1 (17, 76). Interestingly, more low-threshold afferents are capsaicin sensitive than the high-threshold afferents (77, 78). However, the high-threshold capsaicin-sensitive bladder afferents also coexpress TRPA1 (79), whereas TRPV4 is expressed by a population of TRPV1-negative, bladder-innervating neurons (80), suggesting subtype specialization. Therefore, although TRPV4 inhibition alone improves bladder function in cyclophosphamide-induced cystitis (81), coadministration of TRPV4 and TRPV1 antagonists has greater combined effects (80). P2X$_3$ receptor–mediated mechanisms also contribute to both non-nociceptive and nociceptive mechanosensory transduction, with populations of both low- and high-threshold muscular afferents responding to P2X$_3$ agonists (82). Correspondingly, their muscular bladder afferent responsiveness is reduced by P2X$_3$ antagonists (82). Similarly, onabotulinumtoxinA reduces both low- and high-threshold bladder afferent nerve firing (83), which may be a consequence of reduced ATP release from the urothelium.

1.6.2.2 Urothelial afferents
These are distension insensitive, but their position embedded within or in close proximity to the urothelium indicates a role as sentinels to rapidly detect urothelial breakdown, bladder infection, and inflammation through bidirectional communication with the urothelium and chemical environment. These urothelial afferents are activated by urothelial stroking and various chemical stimuli (75, 78, 84, 85). They have not been found in the splanchnic innervation of the bladder, but they represent ∼10% of the pelvic innervation (75).

1.6.2.3 Muscular/urothelial afferents
These are similar to muscular/mucosal afferents in the colon. They represent 3% of the splanchnic and 14% of the pelvic innervation of the bladder (75). They respond to lower threshold stimuli than bladder muscle mechanoreceptors and respond to both mechanical stretch and light stroking of the urothelium. These afferents can be activated by ATP (78), and thus their location close to the urothelium suggests that they might also respond to ATP released by urothelial distension (86).

1.6.2.4 Serosal afferents/mechanically insensitive silent afferents
Serosal afferents are distension-insensitive afferents that can be activated by punctate stimulation of their receptive fields. They represent 67% of the splanchnic innervation but only 14% of the pelvic innervation of the bladder (75). They are called serosal afferents, as their physiological properties resembled afferents recorded within the colon. However, in the colon at least, serosal afferents have been subsequently associated with blood vessels innervating the submucosa and termed vascular afferents (see above). Meanwhile, the anatomical structure of serosal afferents within the bladder remains unclear. Some serosal afferents have likely been termed mechanically insensitive silent afferents in a number of previous studies, because like those found in the colon, they are unresponsive to distension under normal conditions but become activated following irritation or inflammation (82). This includes activation and sensitization via P2X receptors (82).

1.6.3 Persistent Changes in Visceral Sensory Afferent Pathways
Overall, most colonic and bladder afferents show exquisite sensitivity for mechanical distension or luminal distortion, enabling them to detect physiologically relevant stimuli and provide the afferent component of spinal and extraspinal reflexes. High-threshold afferents provide further resolution between normal and nociceptive stimuli, which result in visceral sensations ranging from discomfort, urgency, and ultimately to pain. Sensitization of these afferents, particularly high-threshold, distension-sensitive and vascular afferents, plus the recruitment of mechanically insensitive afferents, leads to an increase in sensory signaling from the periphery to the spinal cord. In many situations this sensitization resolves following resolution of the initial pathology (inflammation or physical challenge) (7). However, in CVH, this sensitization does not resolve and can be exacerbated for months after the initial infectious or inflammatory insult. This leads to persistent neuroplasticity (synaptic or intrinsic changes of afferent endings) that may drive subsequent changes in downstream sensory pathways (7). For example, in the colon during CVH there is evidence of chronic afferent ending sensitization (39, 46, 51–55), hyperexcitability of colon-innervating DRG neurons (51), and increased activation of dorsal horn neurons

9

within the spinal cord in response to noxious distension (25). The latter is also accompanied by sprouting of the central terminals of colonic afferents, which normally reside predominantly within laminae I (LI) and V (LV) and project down the middle and lateral dorsal horn collateral pathways (25). However, during postinflammatory CVH, there is an increased density and more widespread distribution of terminals within LI, with terminals now also present within deeper laminae. Such changes are also accompanied by activation of dorsal horn neurons within deeper laminae of the spinal cord in response to noxious stimuli (25). A key driver of persistent changes following colitis is granulocyte colony–stimulating factor (G-CSF) signaling in spinal microglia, as ablating microglia or blocking the G-CSF receptor prevents colitis-induced sensitization (87).

In relation to the bladder, cyclophosphamide-induced cystitis causes hyperexcitability of bladder-innervating DRG neurons (88) and evokes bladder overactivity in addition to allodynia and hyperalgesia to bladder distension (89–91), thereby mimicking the symptoms of IC/BPS. Consequently, a key concept in visceral pain research is the switch from a healthy environment to a sensitized acute pain state and progression toward a recurrent sensitization and CVH state. We discuss the key contributing factors below (**Figure 1.3**).
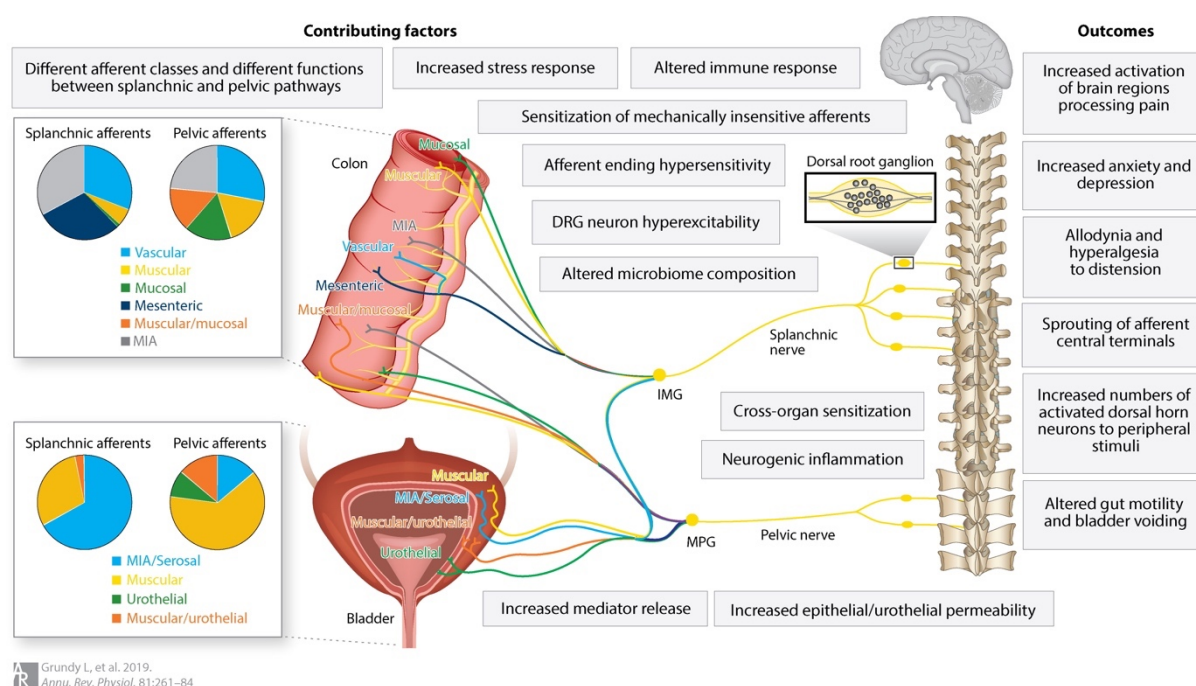
Figure 1.3. Schematic overview of the major factors contributing to chronic visceral pain from the colon and bladder. Many visceral pain disorders, such as irritable bowel syndrome or painful bladder syndrome, present without an obvious underlying cause, such as a pronounced epithelial/urothelial inflammation at the time of referral to generalist or specialist practitioners. The schematic highlights numerous contributing factors and their resultant outcomes that produce chronic abdominal and pelvic pain. For example, in some cases, inflammation or infection is the underlying trigger; however, following healing of the tissue, neuroplasticity in pain pathways exists for several years following the initial insult, resulting in chronic pain. In other cases, there is evidence for altered immune responses, while stress can trigger and also exacerbate symptoms. Cross-organ sensitization can allow alterations in neuronal signaling in one organ to subsequently alter the adjacent organ, due to their common neural innervations. Abbreviations: DRG, dorsal root ganglia; IMG, inferior mesenteric ganglion; MIA, mechanically insensitive afferent; MPG, major pelvic ganglion.

1.6.4 Neuroepithelial Interactions

The colon and bladder epithelia provide a key interface between luminal contents and the underlying sensory afferents. In the colon, a particular type of epithelial cell, called EC cells, are electrically excitable and act as sentinels of noxious chemical stimuli or other insults (41). EC cells are polymodal chemosensors that respond to specific mediators, including TRPA1 agonists; the microbial metabolites isovalerate, isobutyrate, and butyrate; and dopamine, epinephrine, and norepinephrine (41). This results

in the basolateral release of 5-HT, via a TRPC4-dependent mechanism. 5-HT then acts on 5-HT_3 receptors expressed on pelvic mucosal afferents, resulting in mechanical sensitization (41). Most 5-HT in the body is synthesized, stored, and released by these EC cells. Alterations in the fundamental properties of 5-HT signaling, including synthesis, release, or reuptake of 5-HT, may play a significant role in the development of visceral pain in IBD and IBS (92). Although effective, 5-HT_3 receptor antagonists, such as alosetron, are only approved for treating very specific cohorts of IBS patients, due to incidences of adverse effects, including ischemic colitis (93). Voltage-gated sodium currents generated by $Na_v1.3$ likely allow EC cells to respond to the detection of mechanical and chemical stimuli within the lumen of the colon (41, 94) and may provide a novel therapeutic target for treating pain symptoms.

The bladder urothelium expresses numerous receptors and ion channels, including TRPV4, TRPV2, and TRPM8 (95), and secretes a range of mediators that are capable of modulating sensory afferents and inflammatory cells. Under physiological conditions, the urothelium is not thought to come into direct contact with urine, as it is protected by the hydrophobic glycosaminoglycan (GAG) layer. However, under pathological conditions, such as bacterial infection, the urothelium is exposed and can provide input to autonomic reflexes regulating micturition. ATP has been the most extensively studied urothelial release factor, and there are several reports providing evidence of dysfunction in the urothelial/sensory afferent purinergic signaling complex. Knockout of $P2X_3$ and $P2X_{2/3}$ receptors in mice reduces bladder mechanosensitivity by limiting P2X activation on afferents in response to urothelial ATP release (96). Urothelial release of ATP from patients with IC/BPS is enhanced compared to controls, which may be a result of reduced ATP metabolism. As such, there has been significant interest in this pathway for the development of novel analgesics for IC/BPS patients (97); however, pharmacological exploitation of this pathway has not been forthcoming in clinical trials. An alternative therapeutic intervention is the intramural injection of botulinum toxin type A (BOTOX), which does show efficacy in treating visceral hyperalgesia and is the fourth-line treatment for IC/BPS (98, 99). BOTOX acts by preventing vesicular release of neurotransmitters and was originally proposed to act by blocking parasympathetic-mediated acetylcholine release at the neuromuscular junction. However, a recent study showed that BOTOX, instilled into the bladder during graded distension, significantly reduced bladder afferent mechanosensitivity and luminal ATP release without influencing bladder compliance (83). BOTOX administration also increased luminal release of nitric oxide, which acts as an inhibitory transmitter on bladder afferents (100).

1.6.5 Epithelial Breakdown

As the colon and bladder are responsible for storing and eliminating toxic waste metabolites from the body, the epithelial lining of these organs provides an essential barrier between luminal contents and the underlying interstitium. A leaky gut refers to increased permeability of the luminal epithelial layers of the intestinal mucosa, such that luminal content gains unregulated access to underlying tissues. Increased gut permeability can be caused by numerous factors, including high-fat or high-fructose diets, alcohol ingestion, vitamin A deficiency, and changes in the intestinal microbiome. A leaky gut can cause pain due to access of sensitizing agents from food consumption and substances released from the microbiome to afferents that innervate the tissue. Patients with IBD, IBS, and celiac disease have increased gut permeability, which may contribute to increased pain signaling (1, 7, 8). Although pharmacologically improved cell–cell adhesion of the intestinal epithelial layer can decrease permeability, further research on whether it can improve visceral pain is needed (101).

A key component of the urothelial barrier is the GAG mucus layer, composed of sulfated polysaccharides, that has hydrorepellent properties, which block the movement of small molecules and urine access to the underlying tissue. Upon histological examination, many, but not all, IC/BPS patients show a diminished urothelium or loss of umbrella cells and GAG layer. It remains to be determined if bladder permeability is part of the underlying pathology of visceral hypersensitivity or a downstream consequence of an inflammatory process. However, a positive response to the potassium sensitivity test, in which high potassium is infused into the bladder, is indicated by allodynia and hyperalgesia to bladder distention and is reported by >80% of IC/BPS patients, as well as patients diagnosed with chronic pelvic pain (102). The use of oral pentosane polysulphate therapy to repair the GAG layer is the only treatment for IC/BPS approved by the US Food and Drug Administration. Pentosane polysulphate induces broad anti-

inflammatory actions, including the inhibition of mast cell histamine release in the bladder (103, 104), which may provide an additional mechanism of action to alleviate IC/BPS symptoms.

1.6.6 Infection and Inflammation

The importance of visceral afferents in pain sensation and homeostatic regulation is exemplified during acute bacterial infections, whereby physiological responses enhance gastrointestinal motility and urinary frequency to rapidly eliminate the pathogen from the body. Inflammation manifests as a local influx of immune cells, release of proinflammatory mediators, edema, and pain sensation via sensitization of sensory neurons innervating the affected tissue. Inflammatory mediators, such as NGF, TNF-α, bradykinin, substance P, histamine, prostaglandins, and ATP, activate specific receptors on sensory afferents, which leads to a localized membrane depolarization (7, 17, 48). The change in membrane potential can be sufficient to activate voltage-gated ion channels, leading to action potential generation and transmission to the central nervous system (48, 66, 105). Recurring episodes of visceral inflammation can lead to long-term neuroplasticity within the peripheral and central nervous systems, which can contribute to development and maintenance of CVH (7, 17, 48).

1.6.7 Altered Immune Responses

Recent studies utilizing clinical samples show that subgroups of IBS patients display altered immunological function (47, 106–108). For example, colonic biopsies of IBS patients have increased numbers of CD3+ T cells and mast cells versus control biopsies (106, 109, 110). Colonic biopsies from IBS patients also display increased release of key mediators, including histamine, tryptase, trypsin-3, and the proinflammatory cytokine IL-1β, which can correlate with the severity and frequency of abdominal pain (109–111). Histamine, proteases, and IL-1β can all act on receptors expressed by colonic afferents to cause sensitization via TRPV1-, TRPV4-, and Na_v1.7-dependent mechanisms (47, 48, 68, 69). Correspondingly, supernatants from IBS patient biopsies, but not healthy controls, cause activation of colonic afferents (110). Immune changes in IBS patients are also apparent in peripheral blood mononuclear cells (PBMCs) (47, 107, 112). The proinflammatory cytokines, TNF-α, IL-1β, and IL-6, are all increased in PBMC supernatants from IBS-D patients, which correlates with symptoms of abdominal pain (47, 112). Conversely, immune-derived opioidergic inhibition is decreased in IBS patients, with monocyte-derived β-endorphin levels and colonic macrophage numbers lower in IBS patients than controls (107). The latter represents the loss of a key antinociceptive mechanism, as preclinical studies show that immune-derived endogenous opioids play a key role in modulating visceral hypersensitivity (113–115).

1.6.8 Neurogenic Inflammation

In addition to their sensory role, visceral afferents also exhibit an efferent function, as the vast majority of afferents innervating the colon and bladder are peptidergic. Accordingly, they produce and release neuropeptides such as substance P, CGRP, neurokinin A, and neurokinin B to enhance sensory fidelity. However, under the correct conditions, they promote local inflammation, termed neurogenic inflammation, which promotes vasodilatation and plasma extravasation, leading to immune cell infiltration. Although neurogenic inflammation can be a beneficial process during naïve states, neuronal hypersensitivity in CVH states may result in persistent neurogenic inflammation.

1.6.9 Stress and the Gut–Brain and Bladder–Brain Axes

As described above, the processing of sensory stimuli from visceral organs requires neural pathways linking autonomic afferent excitability with emotional and cognitive centers in the brain. These core neural circuits are also dependent on neuroendocrine, immune, and sensory afferent integration. Together, these processes undergo bidirectional communication to regulate visceral homeostasis via a brain–gut or brain–bladder axis. The evolutionary development of the fight or flight response relies on activation of the sympathomedullary axis and the hypothalamic–pituitary–adrenal (HPA) axis during stressful situations. Corticotrophin-releasing factor (CRF) initiates the HPA axis by binding to CRF_1 receptors (CRF_1Rs) in the anterior pituitary and leads to subsequent release of cortisol from the adrenal cortex in preparation for a physical or psychological challenge. However, CRF and CRF_1R are also widely distributed in various

brain regions, including those linked with anxiogenic and digestive behaviors (116). As such, a common human reflection on the physiological perception of acute stress or anxiety is the presence of butterflies in the stomach and the need to urinate (117).

However, maladaptive responses to physical or psychosocial stress represent a common risk factor for visceral pain disorders. In preclinical rodent studies employing acute and chronic stress, early life stress, and high anxiety, Wistar-Kyoto rats exhibit hyperalgesia to colorectal distension and altered micturition (117–119). Similarly, CRF injections induce allodynia and hyperalgesia to colorectal distension and bladder overactivity (120–122), while CRF_1R antagonism prevents visceral hyperalgesia induced by acute and chronic stress (123, 124). From a clinical point of view, symptoms of IBS, IBD, and IC/BPS patients are enhanced during periods of stress and exhibit significant overlap with psychiatric disorders such as anxiety and depression and posttraumatic stress disorder, as well as a history of early life stress/trauma (118, 125–128). In support of centrally mediated visceral pain mechanisms, translational studies identify altered brain activation patterns in response to nociceptive stimuli in IBS, IBD, and IC/BPS patients suggestive of central sensitization (129–132). These findings provide strong evidence that stress can cause or exacerbate visceral sensation. However, despite these obvious connections, there has been considerable translational failure of CRF_1R antagonists owing to persistent side effect profiles that are likely the result of ubiquitous expression of the CRF_1R throughout the body and brain (133).

1.6.10 Cross-Organ Sensitization Between the Colon and Bladder

Coordination of afferent signals between the bladder and colon is essential for efficient and synchronized bladder and bowel evacuation. However, it is now apparent that disease of one visceral organ can induce the development of pathology in an adjacent, otherwise unaffected organ (11). As such, this pathological occurrence is thought to underlie the comorbidity of a number of visceral pain disorders, including but not limited to IBS, IBD, and IC/PBS (134). Preclinical research has consistently implicated cross-organ sensitization of common afferent pathways as a key player in this phenomenon (11). This is because both bladder and colonic afferents innervate the same levels of the DRG and spinal cord. Several studies have shown that colitis can also induce hypersensitivity of bladder afferent pathways (135, 136), with up-regulation of brain-derived neurotrophic factor in the DRG being a key contributing factor (137). This phenomenon has classically been explained by viscero-visceral convergence of afferents within the DRG and spinal cord, such that sensitization of one axon induces sensitization of all convergent axons. However, the proportion of dichotomizing afferents within the DRG and convergent neurons within the spinal cord remains relatively small, approximately 10–20% of the total population of bladder or colonic afferents (11). Furthermore, lumbosacral DRG and spinal neurons with axons innervating only the bladder also display neuronal hypersensitivity following chemically induced colitis (135). These findings therefore suggest a more widespread sensitization of the entire visceral afferent network as a result of neuroplasticity. Because the central terminals of colonic afferents exhibit sprouting within the dorsal horn following recovery from colitis (25), an intriguing possibility exists that additional input onto convergent visceral axon terminals occurs in CVH states.

1.6.11 Gut Microbiome

One key factor that can potentially integrate the mechanisms described above is the gut microbiome, which comprises trillions of microbes from a wide diversity of species. Their potential influence in visceral pain is profound, as they and their metabolic products influence intestinal permeability, immune function, the gut–brain axis, and visceral pain responses (138, 139). Consequently, dysbiosis (alterations in intestinal microbial composition) has been linked to IBS and IBD, and more recently, to conditions outside of the gut, including, stress, anxiety, and cognition (140, 141).

Early indicators of the role the microbiome plays in colonic hypersensitivity arose from studies utilizing antibiotic and probiotic treatments. In these studies, mice treated with antibiotics had altered gut microbiome composition, increased inflammatory markers, and visceral hypersensitivity to colorectal distension (142). Treatment of these mice with the probiotic *Lactobacillus paracasei* normalized colonic hypersensitivity (142), while other studies have shown that *Lactobacillus acidophilus* reduces colonic hypersensitivity via opioid and cannabinoid receptor mechanisms (143). Furthermore, decreasing

13
`

Lactobacillus abundance and butyrate production also exacerbates colitis in mice (144). In terms of possible direct interactions between bacteria and afferent nerves, recent studies of cutaneous afferents demonstrate that *Staphylococcus aureus* can directly activate DRG neurons via the pore-forming toxin α-haemolysin (145). Other studies show that different bacterial species can suppress DRG neuron excitability through activation of PAR-4 (146). Similarly, a lipopeptide produced by the probiotic *E. coli* strain Nissle 1917 directly inhibits DRG neurons and reduces visceral pain by crossing the epithelial barrier and activating GABA$_B$ receptors expressed on afferents (147). Overall, these findings suggest that the microbiome can alter colonic afferent sensitivity via their roles in barrier function, immune responses, as well as metabolite-epithelial-neuronal, metabolite-neuronal, or bacterial-neuronal interactions. Microbial dysbiosis likely changes the balance of these mechanisms, resulting in persistent sensitization via a variety of mechanisms.

Numerous studies have associated symptoms in IBS patients to microbial dysbiosis, in particular, the decreased abundance of *Lactobacillus* and *Bifidobacterium* species and increases in Firmicutes and Bacteroidetes (139, 148, 149). Interestingly, changes in gut microbial composition correlate with differential activation of brain regions in IBS patients (149), which likely reflects altered emotional processing of sensory input. The relevance of the microbiome to these clinical conditions is also highlighted by recent studies transferring abnormal human phenotypes to mice, whereby transplantation of fecal microbiota from IBS-D patients into germ-free mice results in altered gastrointestinal transit, intestinal barrier dysfunction, innate immune activation, and anxiety-like behavior in the recipient mice (150). Hence, pre- and probiotics are of therapeutic interest in the treatment of IBS (141). However, recent studies also suggest that dysbiosis in IBS and IBD is not only limited to bacterial species but extends to both viral and fungal species (151, 152). Indeed, the correct composition of these respective organisms is deemed so important for gastrointestinal function that fecal microbiota transplantation to IBD patients with recurrent *Clostridium difficile* infection is offered as a genuine therapeutic option (153).

1.6.12 Bladder Microbiome
The recent identification of a bladder-specific microbiome has triggered links between the balance of bacteria in the bladder and the symptoms of IC/BPS (154, 155). Patients with bladder symptoms may have genuine infections but are misdiagnosed, as large numbers of bacteria are undetected by routine midstream urine cultures (156). Changes in bacterial species that make up the bladder microbiome have been associated with the presence and severity of IC/BPS (154, 157, 158). Recent studies have identified women with IC/BPS as having a less diverse microbiota than normal subjects (159, 160). Despite significant interpatient variability in bladder microbiomes, a decrease in *Lactobacillus* in IC/BPS patients compared to controls is a common finding (160), with an absence of *L. acidophilus* associated with higher pain scores and higher scores on the interstitial cystitis symptom index (159).

1.7 Conclusions
As discussed within this review, chronic visceral pain is an extremely common symptom experienced by >20% of the global population. Chronic visceral pain is debilitating for those afflicted individuals and has considerable economic burden, costing >$65 billion per annum in the United States for IBS, IBD, and IC/BPS. The mechanisms contributing to chronic visceral pain are incredibly complex and involve a range of processes from the level of the microbiome to the brain. The mechanisms and therefore the etiologies of these clinical conditions are further complicated by cross talk between adjacent visceral organs. Therefore, future studies will need to study underlying mechanisms and potential treatment strategies at a holistic level.

1.8 Disclosure statement

1.9 Acknowledgements

1.10 Literature cited

1. Enck P, Aziz Q, Barbara G, Farmer AD, Fukudo S, et al. 2016. Irritable bowel syndrome. *Nat. Rev. Dis. Primers* 2:16014
2. Natl. Inst. Health. 2009. Opportunities and challenges in digestive diseases research: recommendations of the national commission on digestive diseases. Rep. 08-6514, *Natl. Inst. Diabetes Dig. Kidney Dis.*, Natl. Inst. Health, Bethesda, MD
3. Sikandar S, Dickenson AH. 2012. Visceral pain: the ins and outs, the ups and downs. *Curr. Opin. Support Palliat. Care* 6:17–26
4. Farrell KE, Callister RJ, Keely S. 2014. Understanding and targeting centrally mediated visceral pain in inflammatory bowel disease. *Front. Pharmacol.* 5:27
5. Volkow ND, McLellan AT. 2016. Opioid abuse in chronic pain - misconceptions and mitigation strategies. *N. Engl. J. Med.* 374:1253–63
6. Kaplan GG. 2015. The global burden of IBD: from 2015 to 2025. *Nat. Rev. Gastroenterol. Hepatol.* 12:720–27
7. Brierley SM, Linden DR. 2014. Neuroplasticity and dysfunction after gastrointestinal inflammation. *Nat. Rev. Gastroenterol. Hepatol.* 11:611–27
8. Chey WD, Kurlander J, Eswaran S. 2015. Irritable bowel syndrome: a clinical review. *JAMA* 313:949–58
9. Spiller R, Garsed K. 2009. Postinfectious irritable bowel syndrome. *Gastroenterology* 136:1979–88
10. Marshall JK, Thabane M, Garg AX, Clark WF, Moayyedi P, et al. 2010. Eight year prognosis of postinfectious irritable bowel syndrome following waterborne bacterial dysentery. *Gut* 59:605–11
11. Grundy L, Brierley SM. 2018. Cross-organ sensitization between the colon and bladder: to pee or not to pee? *Am. J. Physiol. Gastrointest. Liver Physiol.* 314:G301–8
12. Lembo A. 2007. The clinical and economic burden of irritable bowel syndrome. *Pract. Gastroenterol.* 31:3–9
13. Berry SH, Elliott MN, Suttorp M, Bogart LM, Stoto MA, et al. 2011. Prevalence of symptoms of bladder pain syndrome/interstitial cystitis among adult females in the United States. *J. Urol.* 186:540–44
14. Suskind AM, Berry SH, Ewing BA, Elliott MN, Suttorp MJ, Clemens JQ. 2013. The prevalence and overlap of interstitial cystitis/bladder pain syndrome and chronic prostatitis/chronic pelvic pain syndrome in men: results of the RAND Interstitial Cystitis Epidemiology male study. *J. Urol.* 189:141–45
15. Pierce AN, Christianson JA. 2015. Stress and chronic pelvic pain. *Prog. Mol. Biol. Transl. Sci.* 131:509–35
16. Kim SH, Kim TB, Kim SW, Oh SJ. 2009. Urodynamic findings of the painful bladder syndrome/interstitial cystitis: a comparison with idiopathic overactive bladder. *J. Urol.* 181:2550–54
17. de Groat WC, Yoshimura N. 2009. Afferent nerve regulation of bladder function in health and disease. *Handb. Exp. Pharmacol.* 194:91–138
18. Burgmann T, Clara I, Graff L, Walker J, Lix L, et al. 2006. The Manitoba Inflammatory Bowel Disease Cohort Study: prolonged symptoms before diagnosis - how much is irritable bowel syndrome? *Clin. Gastroenterol. Hepatol.* 4:614–20
19. Ansari R, Attari F, Razjouyan H, Etemadi A, Amjadi H, et al. 2008. Ulcerative colitis and irritable bowel syndrome: relationships with quality of life. *Eur. J. Gastroenterol. Hepatol.* 20:46–50
20. Alagiri M, Chottiner S, Ratner V, Slade D, Hanno PM. 1997. Interstitial cystitis: unexplained associations with other chronic disease and pain syndromes. *Urology* 49:52–57
21. Whorwell PJ, Lupton EW, Erduran D, Wilson K. 1986. Bladder smooth muscle dysfunction in patients with irritable bowel syndrome. *Gut* 27:1014–17
22. Cukier JM, Cortina-Borja M, Brading AF. 1997. A case-control study to examine any association between idiopathic detrusor instability and gastrointestinal tract disorder, and between irritable bowel syndrome and urinary tract disorder. *Br. J. Urol. Int.* 79:865–78
23. Clemens JQ, Brown SO, Kozloff L, Calhoun EA. 2006. Predictors of symptom severity in patients with chronic prostatitis and interstitial cystitis. *J. Urol.* 175:963–66
24. Brierley SM, Jones RC 3rd, Gebhart GF, Blackshaw LA. 2004. Splanchnic and pelvic mechanosensory afferents signal different qualities of colonic stimuli in mice. *Gastroenterology* 127:166–78
25. Harrington AM, Brierley SM, Isaacs N, Hughes PA, Castro J, Blackshaw LA. 2012. Sprouting of colonic afferent central terminals and increased spinal mitogen-activated protein kinase

expression in a mouse model of chronic visceral hypersensitivity. *J. Comp. Neurol.* 520:2241–55

26. Todd AJ. 2010. Neuronal circuitry for pain processing in the dorsal horn. *Nat. Rev. Neurosci.* 11:823–36

27. de Groat WC, Yoshimura N. 2015. Anatomy and physiology of the lower urinary tract. *Handb. Clin. Neurol.* 130:61–108

28. Fowler CJ, Griffiths D, de Groat WC. 2008. The neural control of micturition. *Nat. Rev. Neurosci.* 9:453–66

29. Griffiths D. 2015. Neural control of micturition in humans: a working model. *Nat. Rev. Urol.* 12:695–705

30. Willis WD Jr. 2008. A novel visceral pain pathway in the posterior funiculus of the spinal cord. *J. Med. Sci.* 1:33–37

31. Spencer NJ, Kyloh M, Duffield M. 2014. Identification of different types of spinal afferent nerve endings that encode noxious and innocuous stimuli in the large intestine using a novel anterograde tracing technique. *PLOS ONE* 9:e112466

32. Brookes S, Chen N, Humenick A, Spencer NJ, Costa M. 2016. Extrinsic sensory innervation of the gut: structure and function. *Adv. Exp. Med. Biol.* 891:63–69

33. Brookes SJ, Spencer NJ, Costa M, Zagorodnyuk VP. 2013. Extrinsic primary afferent signalling in the gut. *Nat. Rev. Gastroenterol. Hepatol.* 10:286–96

34. Spencer NJ, Zagorodnyuk V, Brookes SJ, Hibberd T. 2016. Spinal afferent nerve endings in visceral organs: recent advances. *Am. J. Physiol. Gastrointest. Liver Physiol.* 311:G1056–63

35. Hockley JR, Tranter MM, McGuire C, Boundouki G, Cibert-Goton V, et al. 2016. P2Y receptors sensitize mouse and human colonic nociceptors. *J. Neurosci.* 36:2364–76

36. Jiang W, Adam IJ, Kitsanta P, Tiernan J, Hill C, et al. 2011. 'First-in-man': characterising the mechanosensitivity of human colonic afferents. *Gut* 60:281–82

37. McGuire C, Boundouki G, Hockley JRF, Reed D, Cibert-Goton V, et al. 2018. *Ex vivo* study of human visceral nociceptors. *Gut* 67:86–96

38. Peiris M, Bulmer DC, Baker MD, Boundouki G, Sinha S, et al. 2011. Human visceral afferent recordings: preliminary report. *Gut* 60:204–8

39. Hughes PA, Brierley SM, Martin CM, Brookes SJ, Linden DR, Blackshaw LA. 2009. Post-inflammatory colonic afferent sensitization: different subtypes, different pathways and different time courses. *Gut* 58:1333–41

40. Feng B, Gebhart GF. 2011. Characterization of silent afferents in the pelvic and splanchnic innervations of the mouse colorectum. *Am. J. Physiol. Gastrointest. Liver Physiol.* 300:G170–80

41. Bellono NW, Bayrer JR, Leitch DB, Castro J, Zhang C, et al. 2017. Enterochromaffin cells are gut chemosensors that couple to sensory neural pathways. *Cell* 170:185–98.e16

42. Brierley SM, Hughes PA, Page AJ, Kwan KY, Martin CM, et al. 2009. The ion channel TRPA1 is required for normal mechanosensation and is modulated by algesic stimuli. *Gastroenterology* 137:2084–95.e3

43. Feng B, Zhu Y, La JH, Wills ZP, Gebhart GF. 2015. Experimental and computational evidence for an essential role of $Na_v1.6$ in spike initiation at stretch-sensitive colorectal afferent endings. *J. Neurophysiol.* 113:2618–34

44. Jones RC 3rd, Xu L, Gebhart GF. 2005. The mechanosensitivity of mouse colon afferent fibers and their sensitization by inflammatory mediators require transient receptor potential vanilloid 1 and acid-sensing ion channel 3. *J. Neurosci.* 25:10981–89

45. Feng B, La JH, Schwartz ES, Tanaka T, McMurray TP, Gebhart GF. 2012. Long-term sensitization of mechanosensitive and -insensitive afferents in mice with persistent colorectal hypersensitivity. *Am. J. Physiol. Gastrointest. Liver Physiol.* 302:G676–83

46. Castro J, Harrington AM, Garcia-Caraballo S, Maddern J, Grundy L, et al. 2017. α-Conotoxin Vc1.1 inhibits human dorsal root ganglion neuroexcitability and mouse colonic nociception via GABA$_B$ receptors. *Gut* 66:1083–94

47. Hughes PA, Harrington AM, Castro J, Liebregts T, Adam B, et al. 2013. Sensory neuro-immune interactions differ between irritable bowel syndrome subtypes. *Gut* 62:1456–65

48. Sadeghi M, Erickson A, Castro J, Deiteren A, Harrington AM, et al. 2018. Contribution of membrane receptor signalling to chronic visceral pain. *Int. J. Biochem. Cell Biol*. 98:10–23

49. Brierley SM, Page AJ, Hughes PA, Adam B, Liebregts T, et al. 2008. Selective role for TRPV4 ion channels in visceral sensory pathways. *Gastroenterology* 134:2059–69

50. Humenick A, Chen BN, Wiklendt L, Spencer NJ, Zagorodnyuk VP, et al. 2015. Activation of intestinal spinal afferent endings by changes in intra-mesenteric arterial pressure. *J. Physiol.* 593:3693–709

51. Castro J, Grundy L, Deiteren A, Harrington AM, O'Donnell T, et al. 2017. Cyclic analogues of α-conotoxin Vc1.1 inhibit colonic nociceptors and provide analgesia in a mouse model of chronic abdominal pain. *Br. J. Pharmacol.* 175:2384–98

`

52. Castro J, Harrington AM, Hughes PA, Martin CM, Ge P, et al. 2013. Linaclotide inhibits colonic nociceptors and relieves abdominal pain via guanylate cyclase-C and extracellular cyclic guanosine 31,51- monophosphate. *Gastroenterology* 145:1334–46.e11

53. de Araujo AD, Mobli M, Castro J, Harrington AM, Vetter I, et al. 2014. Selenoether oxytocin analogues have analgesic properties in a mouse model of chronic abdominal pain. *Nat. Commun.* 5:3165

54. Hughes PA, Castro J, Harrington AM, Isaacs N, Moretta M, et al. 2014. Increased κ-opioid receptor expression and function during chronic visceral hypersensitivity. *Gut* 63:1199–200

55. Osteen JD, Herzig V, Gilchrist J, Emrick JJ, Zhang C, et al. 2016. Selective spider toxins reveal a role for the $Na_v1.1$ channel in mechanical pain. *Nature* 534:494–99

56. Salvatierra J, Castro J, Erickson A, Li Q, Braz J, et al. 2018. $Na_v1.1$ inhibition can reduce visceral hypersensitivity. *JCI Insight* 3:e121000

57. Inserra MC, Israel MR, Caldwell A, Castro J, Deuis JR, et al. 2017. Multiple sodium channel isoforms mediate the pathological effects of Pacific ciguatoxin-1. *Sci. Rep.* 7:42810

58. Hockley JR, Boundouki G, Cibert-Goton V, McGuire C, Yip PK, et al. 2014. Multiple roles for $Na_v1.9$ in the activation of visceral afferents by noxious inflammatory, mechanical, and human disease-derived stimuli. *Pain* 155:1962–75

59. Peiris M, Hockley JRF, Reed DE, Smith ESJ, Bulmer DC, Blackshaw LA. 2017. Peripheral K_v7 channels regulate visceral sensory function in mouse and human colon. *Mol. Pain* 13. https://doi.org/ 10.1177/1744806917709371

60. Brierley SM, Carter R, Jones W 3rd, Xu L, Robinson DR, et al. 2005. Differential chemosensory function and receptor expression of splanchnic and pelvic colonic afferents in mice. *J. Physiol.* 567:267–81

61. Harrington AM, Hughes PA, Martin CM, Yang J, Castro J, et al. 2011. A novel role for TRPM8 in visceral afferent function. *Pain* 152:1459–68

62. Brust A, Croker DE, Colless B, Ragnarsson L, Andersson A, et al. 2016. Conopeptide-derived κ-opioid agonists (conorphins): potent, selective, and metabolic stable dynorphin A mimetics with antinociceptive properties. *J. Med. Chem.* 59:2381–95

63. Guerrero-Alba R, Valdez-Morales EE, Jime´nez-Vargas NN, Bron R, Poole D, et al. 2018. Co-expression of μ and δ opioid receptors by mouse colonic nociceptors. *Br. J. Pharmacol.* 175:2622–34

64. Brierley SM, Jones RC 3rd, Xu L, Gebhart GF, Blackshaw LA. 2005. Activation of splanchnic and pelvic colonic afferents by bradykinin in mice. *Neurogastroenterol. Motil.* 17:854–62

65. Prato V, Taberner FJ, Hockley JRF, Callejo G, Arcourt A, et al. 2017. Functional and molecular characterization of mechanoinsensitive "silent" nociceptors. *Cell Rep.* 21:3102–15

66. Erickson A, Deiteren A, Harrington AM, Garcia-Caraballo S, Castro J, et al. 2018. Voltage-gated sodium channels: (Na_v)igating the field to determine their contribution to visceral nociception. *J. Physiol.* 596:785–807

67. Hockley JRF, Taylor TS, Callejo G, Wilbrey AL, Gutteridge A, et al. 2018. Single-cell RNAseq reveals seven classes of colonic sensory neuron. *Gut.* In press. https://doi.org/10.1136/gutjnl-2017-315631

68. Wouters MM, Balemans D, Van Wanrooy S, Dooley J, Cibert-Goton V, et al. 2016. Histamine receptor H1-mediated sensitization of TRPV1 mediates visceral hypersensitivity and symptoms in patients with irritable bowel syndrome. *Gastroenterology* 150:875–87.e9

69. Desormeaux C, Bautzova T, Garcia-Caraballo S, Rolland C, Barbaro MR, et al. 2018. Protease-activated receptor 1 is implicated in irritable bowel syndrome mediators-induced signalling to thoracic human sensory neurons. Pain 159:1257–67

70. Sipe WE, Brierley SM, Martin CM, Phillis BD, Cruz FB, et al. 2008. Transient receptor potential vanilloid 4 mediates protease activated receptor 2-induced sensitization of colonic afferent nerves and visceral hyperalgesia. *Am. J. Physiol. Gastrointest. Liver Physiol.* 294:G1288–98

71. Campaniello MA, Harrington AM, Martin CM, Ashley Blackshaw L, Brierley SM, Hughes PA. 2016. Activation of colorectal high-threshold afferent nerves by Interleukin-2 is tetrodotoxin-sensitive and upregulated in a mouse model of chronic visceral hypersensitivity. *Neurogastroenterol. Motil.* 28:54–63

72. Balemans D, Boeckxstaens GE, Talavera K, Wouters MM. 2017. Transient receptor potential ion channel function in sensory transduction and cellular signaling cascades underlying visceral hypersensitivity. *Am. J. Physiol. Gastrointest. Liver Physiol.* 312:G635–48

73. Hockley JR, Winchester WJ, Bulmer DC. 2016. The voltage-gated sodium channel $Na_v1.9$ in visceral pain. *Neurogastroenterol. Motil.* 28:316–26

74. Spencer NJ, Greenheigh S, Kyloh M, Hibberd TJ, Sharma H, et al. 2018. Identifying unique subtypes of spinal afferent nerve endings within the urinary bladder of mice. *J. Comp. Neurol.* 526:707–20

75. Xu L, Gebhart GF. 2008. Characterization of mouse lumbar splanchnic and pelvic nerve urinary bladder mechanosensory afferents. *J. Neurophysiol.* 99:244–53

17

76. Forrest SL, Osborne PB, Keast JR. 2013. Characterization of bladder sensory neurons in the context of myelination, receptors for pain modulators, and acute responses to bladder inflammation. *Front. Neurosci.* 7:206

77. Daly D, Rong W, Chess-Williams R, Chapple C, Grundy D. 2007. Bladder afferent sensitivity in wild-type and TRPV1 knockout mice. *J. Physiol.* 583:663–74

78. Zagorodnyuk VP, Gibbins IL, Costa M, Brookes SJ, Gregory SJ. 2007. Properties of the major classes of mechanoreceptors in the guinea pig bladder. *J. Physiol.* 585:147–63

79. Nicholas S, Yuan SY, Brookes SJ, Spencer NJ, Zagorodnyuk VP. 2017. Hydrogen peroxide preferentially activates capsaicin-sensitive high threshold afferents via TRPA1 channels in the guinea pig bladder. *Br. J. Pharmacol.* 174:126–38

80. Charrua A, Cruz CD, Jansen D, Rozenberg B, Heesakkers J, Cruz F. 2015. Co-administration of transient receptor potential vanilloid 4 (TRPV4) and TRPV1 antagonists potentiate the effect of each drug in a rat model of cystitis. *Br. J. Urol. Int.* 115:452–60

81. Everaerts W, Zhen X, Ghosh D, Vriens J, Gevaert T, et al. 2010. Inhibition of the cation channel TRPV4 improves bladder function in mice and rats with cyclophosphamide-induced cystitis. *PNAS* 107:19084–89

82. Rong W, Spyer KM, Burnstock G. 2002. Activation and sensitization of low and high threshold afferent fibres mediated by P2X receptors in the mouse urinary bladder. *J. Physiol.* 41:591–600

83. Collins VM, Daly DM, Liaskos M, McKay NG, Sellers D, et al. 2013. OnabotulinumtoxinA significantly attenuates bladder afferent nerve firing and inhibits ATP release from the urothelium. *Br. J. Urol. Int.* 112:1018–26

84. Zagorodnyuk VP, Costa M, Brookes SJ. 2006. Major classes of sensory neurons to the urinary bladder. *Auton. Neurosci.* 126–127:390–97

85. Zagorodnyuk VP, Brookes SJ, Spencer NJ, Gregory S. 2009. Mechanotransduction and chemosensitivity of two major classes of bladder afferents with endings in the vicinity to the urothelium. *J. Physiol.* 587:3523–38

86. Sadananda P, Kao FC, Liu L, Mansfield KJ, Burcher E. 2012. Acid and stretch, but not capsaicin, are effective stimuli for ATP release in the porcine bladder mucosa: Are ASIC and TRPV1 receptors involved? *Eur. J. Pharmacol.* 683:252–59

87. Basso L, Lapointe TK, Iftinca M, Marsters C, Hollenberg MD, et al. 2017. Granulocyte-colony-stimulating factor (G-CSF) signaling in spinal microglia drives visceral sensitization following colitis. *PNAS* 114:11235–40

88. Dang K, Lamb K, Cohen M, Bielefeldt K, Gebhart GF. 2008. Cyclophosphamide-induced bladder inflammation sensitizes and enhances P2X receptor function in rat bladder sensory neurons. *J. Neurophysiol.* 99:49–59

89. DeBerry JJ, Saloman JL, Dragoo BK, Albers KM, Davis BM. 2015. Artemin immunotherapy is effective in preventing and reversing cystitis-induced bladder hyperalgesia via TRPA1 regulation. *J. Pain* 16:628–36

90. DeBerry JJ, Schwartz ES, Davis BM. 2014. TRPA1 mediates bladder hyperalgesia in a mouse model of cystitis. *Pain* 155:1280–87

91. Lai HH, Qiu CS, Crock LW, Morales ME, Ness TJ, Gereau RW. 2011. Activation of spinal extracellular signal-regulated kinases (ERK) 1/2 is associated with the development of visceral hyperalgesia of the bladder. *Pain* 152:2117–24

92. Mawe GM, Hoffman JM. 2013. Serotonin signalling in the gut—functions, dysfunctions and therapeutic targets. *Nat. Rev. Gastroenterol. Hepatol.* 10:473–86

93. Zheng Y, Yu T, Tang Y, Xiong W, Shen X, et al. 2017. Efficacy and safety of 5-hydroxytryptamine 3 receptor antagonists in irritable bowel syndrome: a systematic review and meta-analysis of randomized controlled trials. *PLOS ONE* 12:e0172846

94. Strege PR, Knutson KR, Eggers SJ, Wang F, Li J, et al. 2017. SCN3A-encoded voltage-gated sodium channel $Na_v1.3$ is specifically expressed in human and mouse gastrointestinal enterochromaffin cells and is important for enterochromaffin cell excitability. *FASEB J.* 31:1007.40 (Abstr.)

95. Everaerts W, Vriens J, Owsianik G, Appendino G, Voets T, et al. 2010. Functional characterization of transient receptor potential channels in mouse urothelial cells. *Am. J. Physiol. Ren. Physiol.* 298:F692–701

96. Cockayne DA, Dunn PM, Zhong Y, Rong W, Hamilton SG, et al. 2005. $P2X_2$ knockout mice and $P2X_2/P2X_3$ double knockout mice reveal a role for the $P2X_2$ receptor subunit in mediating multiple sensory effects of ATP. *J. Physiol.* 567:621–39

97. Burnstock G. 2017. Purinergic signalling: therapeutic developments. Front. Pharmacol. 8:661

98. Rahnama'i MS, Marcelissen T, Apostolidis A, Veit-Rubin N, Schurch B, et al. 2018. The efficacy of botulinum toxin A and sacral neuromodulation in the management of interstitial cystitis (IC)/bladder pain syndrome (BPS), what do we know? *ICI-RS 2017 think tank, Bristol. Neurourol. Urodyn.* 37:S99–107

99. Eldred-Evans D, Sahai A. 2017. Medium- to long-term outcomes of botulinum toxin A for idiopathic overactive bladder. *Ther. Adv. Urol.* 9:3–10

`

100. Daly DM, Collins VM, Chapple CR, Grundy D. 2011. The afferent system and its role in lower urinary tract dysfunction. *Curr. Opin. Urol.* 21:268–74

101. Quigley EM. 2016. Leaky gut—concept or clinical entity? Curr. Opin. Gastroenterol. 32:74–79

102. Parsons CL, Greenberger M, Gabal L, Bidair M, Barme G. 1998. The role of urinary potassium in the pathogenesis and diagnosis of interstitial cystitis. *J. Urol.* 159:1862–66

103. Wu J, Guan TJ, Zheng S, Grosjean F, Liu W, et al. 2011. Inhibition of inflammation by pentosan polysulfate impedes the development and progression of severe diabetic nephropathy in aging C57B6 mice. *Lab. Investig. J. Tech. Methods Pathol.* 91:1459–71

104. Anderson VR, Perry CM. 2006. Pentosan polysulfate: a review of its use in the relief of bladder pain or discomfort in interstitial cystitis. *Drugs* 66:821–35

105. Brierley SM. 2016. Altered ion channel/receptor expression and function in extrinsic sensory neurons: the cause of and solution to chronic visceral pain? *Adv. Exp. Med. Biol.* 891:75–90

106. Bashashati M, Moossavi S, Cremon C, Barbaro MR, Moraveji S, et al. 2018. Colonic immune cells in irritable bowel syndrome: a systematic review and meta-analysis. *Neurogastroenterol. Motil.* 30:e13192

107. Hughes PA, Moretta M, Lim A, Grasby DJ, Bird D, et al. 2014. Immune derived opioidergic inhibition of viscerosensory afferents is decreased in Irritable Bowel Syndrome patients. *Brain Behav. Immun.* 42:191–203

108. Hughes PA, Zola H, Penttila IA, Blackshaw LA, Andrews JM, Krumbiegel D. 2013. Immune activation in irritable bowel syndrome: can neuroimmune interactions explain symptoms? *Am. J. Gastroenterol.* 108:1066–74

109. Barbara G, Stanghellini V, De Giorgio R, Cremon C, Cottrell GS, et al. 2004. Activated mast cells in proximity to colonic nerves correlate with abdominal pain in irritable bowel syndrome. *Gastroenterology* 126:693–702

110. Barbara G, Wang B, Stanghellini V, de Giorgio R, Cremon C, et al. 2007. Mast cell-dependent excitation of visceral-nociceptive sensory neurons in irritable bowel syndrome. *Gastroenterology* 132:26–37

111. Rolland-Fourcade C, Denadai-Souza A, Cirillo C, Lopez C, Jaramillo JO, et al. 2017. Epithelial expression and function of trypsin-3 in irritable bowel syndrome. *Gut* 66:1767–78

112. Liebregts T, Adam B, Bredack C, Roth A, Heinzel S, et al. 2007. Immune activation in patients with irritable bowel syndrome. *Gastroenterology* 132:913–20

113. Basso L, Boué J, Augé C, Deraison C, Blanpied C, et al. 2017. Mobilization of CD4+ T lymphocytes in inflamed mucosa reduces pain in colitis mice: toward a vaccinal strategy to alleviate inflammatory visceral pain. *Pain* 159:331–41

114. Basso L, Garnier L, Bessac A, Boué J, Blanpied C, et al. 2018. T-lymphocyte-derived enkephalins reduce Th1/Th17 colitis and associated pain in mice. *J. Gastroenterol.* 53:215–26

115. Boué J, Basso L, Cenac N, Blanpied C, Rolli-Derkinderen M, et al. 2014. Endogenous regulation of visceral pain via production of opioids by colitogenic CD4+ T cells in mice. *Gastroenterology* 146:166–75

116. Taché Y, Martinez V, Wang L, Million M. 2004. CRF1 receptor signaling pathways are involved in stress- related alterations of colonic function and viscerosensitivity: implications for irritable bowel syndrome. *Br. J. Pharmacol.* 141:1321–30

117. Pierce AN, Christianson JA. 2015. Stress and chronic pelvic pain. In Progress in Molecular Biology and Translational Science, ed. TJ Price, G Dussor, pp. 509–35. *New York: Academic*

118. Fuentes IM, Christianson JA. 2018. The influence of early life experience on visceral pain. *Front. Syst. Neurosci.* 12:2

119. Meerveld BG, Johnson AC. 2018. Mechanisms of stress-induced visceral pain. *J. Neurogastroenterol. Motil.* 24:7–18

120. Greenwood-Van Meerveld B, Johnson AC, Cochrane S, Schulkin J, Myers DA. 2005. Corticotropin-releasing factor 1 receptor-mediated mechanisms inhibit colonic hypersensitivity in rats. *Neurogastroenterol. Motil.* 17:415–22

121. Saito K, Kasai T, Nagura Y, Ito H, Kanazawa M, Fukudo S. 2005. Corticotropin-releasing hormone receptor 1 antagonist blocks brain-gut activation induced by colonic distention in rats. *Gastroenterology* 129:1533–43

122. Klausner AP, Streng T, Na YG, Raju J, Batts TW, et al. 2005. The role of corticotropin releasing factor and its antagonist, astressin, on micturition in the rat. *Auton. Neurosci.* 123:26–35

123. Larauche M, Kiank C, Taché Y. 2009. Corticotropin releasing factor signaling in colon and ileum: regulation by stress and pathophysiological implications. *J. Physiol. Pharmacol.* 60(Suppl. 7):33–46

124. Johnson AC, Tran L, Schulkin J, Greenwood-Van Meerveld B. 2012. Importance of stress receptor-mediated mechanisms in the amygdala on visceral pain perception in an intrinsically anxious rat. *Neurogastroenterol. Motil.* 24:479–86.e219

125. Lai H, Gardner V, Vetter J, Andriole GL. 2015. Correlation between psychological stress levels and the severity of overactive bladder symptoms. *BMC Urol.* 15:14

19

126. Lai HH, Morgan CD, Vetter J, Andriole GL. 2016. Impact of childhood and recent traumatic events on the clinical presentation of overactive bladder. *Neurourol. Urodyn.* 35:1017–23
127. Rothrock NE, Lutgendorf SK, Kreder KJ, Ratliff T, Zimmerman B. 2001. Stress and symptoms in patients with interstitial cystitis: a life stress model. *Urology* 57:422–27
128. Roohafza H, Bidaki EZ, Hasanzadeh-Keshteli A, Daghaghzade H, Afshar H, Adibi P. 2016. Anxiety, de- pression and distress among irritable bowel syndrome and their subtypes: an epidemiological population based study. *Adv. Biomed. Res.* 5:183
129. Agostini A, Filippini N, Cevolani D, Agati R, Leoni C, et al. 2011. Brain functional changes in patients with ulcerative colitis: a functional magnetic resonance imaging study on emotional processing. *Inflamm. Bowel Dis.* 17:1769–77
130. Deutsch G, Deshpande H, Frolich MA, Lai HH, Ness TJ. 2016. Bladder distension increases blood flow in pain related brain structures in subjects with interstitial cystitis. *J. Urol.* 196:902–10
131. Farmer MA, Huang L, Martucci K, Yang CC, Maravilla KR, et al. 2015. Brain white matter abnormalities in female interstitial cystitis/bladder pain syndrome: a MAPP network neuroimaging study. *J. Urol.* 194:118–26
132. Kairys AE, Schmidt-Wilcke T, Puiu T, Ichesco E, Labus JS, et al. 2015. Increased brain gray matter in the primary somatosensory cortex is associated with increased pain and mood disturbance in patients with interstitial cystitis/painful bladder syndrome. J. Urol. 193:131–37
133. Spierling SR, Zorrilla EP. 2017. Don't stress about CRF: assessing the translational failures of CRF_1 antagonists. *Psychopharmacology* 234:1467–81
134. Kaplan SA, Dmochowski R, Cash BD, Kopp ZS, Berriman SJ, Khullar V. 2013. Systematic review of the relationship between bladder and bowel function: implications for patient management. *Int. J. Clin. Pract.* 67:205–16
135. Qin C, Malykhina AP, Akbarali HI, Foreman RD. 2005. Cross-organ sensitization of lumbosacral spinal neurons receiving urinary bladder input in rats with inflamed colon. *Gastroenterology* 129:1967–78
136. Ustinova EE, Gutkin DW, Pezzone MA. 2007. Sensitization of pelvic nerve afferents and mast cell infiltration in the urinary bladder following chronic colonic irritation is mediated by neuropeptides. *Am. J. Physiol. Ren. Physiol.* 292:F123–30
137. Xia C, Shen S, Hashmi F, Qiao LY. 2016. Colitis-induced bladder afferent neuronal activation is regulated by BDNF through PLCγ pathway. *Exp. Neurol.* 285:126–35
138. Mayer EA, Savidge T, Shulman RJ. 2014. Brain-gut microbiome interactions and functional bowel disorders. Gastroenterology 146:1500–12
139. Mayer EA, Tillisch K, Gupta A. 2015. Gut/brain axis and the microbiota. *J. Clin. Investig.* 125:926–38
140. Mayer EA, Knight R, Mazmanian SK, Cryan JF, Tillisch K. 2014. Gut microbes and the brain: paradigm shift in neuroscience. *J. Neurosci.* 34:15490–96
141. Stern EK, Brenner DM. 2018. Gut microbiota-based therapies for irritable bowel syndrome. *Clin. Transl. Gastroenterol*. 9:e134
142. Verdu EF, Bercik P, Verma-Gandhu M, Huang XX, Blennerhassett P, et al. 2006. Specific probiotic therapy attenuates antibiotic induced visceral hypersensitivity in mice. Gut 55:182–90
143. Rousseaux C, Thuru X, Gelot A, Barnich N, Neut C, et al. 2007. *Lactobacillus acidophilus* modulates intestinal pain and induces opioid and cannabinoid receptors. *Nat. Med*. 13:35–37
144. Miranda PM, De Palma G, Serkis V, Lu J, Louis-Auguste MP, et al. 2018. High salt diet exacerbates colitis in mice by decreasing *Lactobacillus* levels and butyrate production. *Microbiome* 6:57
145. Chiu IM, Heesters BA, Ghasemlou N, Von Hehn CA, Zhao F, et al. 2013. Bacteria activate sensory neurons that modulate pain and inflammation. *Nature* 501:52–57
146. Sessenwein JL, Baker CC, Pradhananga S, Maitland ME, Petrof EO, et al. 2017. Protease-mediated suppression of DRG neuron excitability by commensal bacteria. *J. Neurosci.* 37:11758–68
147. Pe´rez-Berezo T, Pujo J, Martin P, Le Faouder P, Galano JM, et al. 2017. Identification of an analgesic lipopeptide produced by the probiotic Escherichia coli strain Nissle 1917. *Nat. Commun.* 8:1314
148. Chichlowski M, Rudolph C. 2015. Visceral pain and gastrointestinal microbiome. J. *Neurogastroenterol. Motil.* 21:172–81
149. Labus JS, Hollister EB, Jacobs J, Kirbach K, Oezguen N, et al. 2017. Differences in gut microbial composition correlate with regional brain volumes in irritable bowel syndrome. *Microbiome* 5:49
150. De Palma G, Lynch MD, Lu J, Dang VT, Deng Y, et al. 2017. Transplantation of fecal microbiota from patients with irritable bowel syndrome alters gut function and behavior in recipient mice. *Sci. Transl. Med*. 9:eaaf6397
151. Botschuijver S, Roeselers G, Levin E, Jonkers DM, Welting O, et al. 2017. Intestinal fungal dysbiosis is associated with visceral hypersensitivity in patients with irritable bowel syndrome and rats. *Gastroenterology* 153:1026–39
152. Norman JM, Handley SA, Baldridge MT, Droit L, Liu CY, et al. 2015. Disease-specific alterations in the enteric virome in inflammatory bowel disease. *Cell* 160:447–60

153. Khanna S, Shin A, Kelly CP. 2017. Management of Clostridium difficile infection in inflammatory bowel disease: expert review from the clinical practice updates committee of the AGA Institute. *Clin. Gastroen- terol. Hepatol.* 15:166–74

154. Balachandran AA, Wildman SS, Strutt M, Duckett J. 2016. Is chronic urinary infection a cause of overactive bladder? *Eur. J. Obstet. Gynecol. Reprod. Biol.* 201:108–12

155. Drake MJ, Morris N, Apostolidis A, Rahnama'i MS, Marchesi JR. 2017. The urinary microbiome and its contribution to lower urinary tract symptoms; ICI-RS 2015. *Neurourol. Urodyn.* 36:850-3

156. Khasriya R, Sathiananthamoorthy S, Ismail S, Kelsey M, Wilson M, et al. 2013. Spectrum of bacterial colonization associated with urothelial cells from patients with chronic lower urinary tract symptoms. *J. Clin. Microbiol.* 51:2054–62

157. Whiteside SA, Razvi H, Dave S, Reid G, Burton JP. 2015. The microbiome of the urinary tract–a role beyond infection. *Nat. Rev. Urol.* 12:81–90

158. Siddiqui H, Lagesen K, Nederbragt AJ, Jeansson SL, Jakobsen KS. 2012. Alterations of microbiota in urine from women with interstitial cystitis. *BMC Microbiol.* 12:205

159. Abernethy MG, Rosenfeld A, White JR, Mueller MG, Lewicky-Gaupp C, Kenton K. 2017. Urinary microbiome and cytokine levels in women with interstitial cystitis. *Obstet. Gynecol*. 129:500–6

160. Hilt EE, McKinley K, Pearce MM, Rosenfeld AB, Zilliox MJ, et al. 2014. Urine is not sterile: use of enhanced urine culture techniques to detect resident bacterial flora in the adult female bladder. *J. Clin. Microbiol.* 52:871–76

Statement of Authorship

Title of Paper	Voltage-gated sodium channels: (NaV)igating the field to determine their contribution to visceral nociception
Publication Status	☑ Published ☐ Accepted for Publication ☐ Submitted for Publication ☐ Unpublished and Unsubmitted work written in manuscript style
Publication Details	Erickson, A., Deiteren, A., Harrington, A. M., Garcia-Caraballo, S., Castro, J., Caldwell, A., Grundy, L. and Brierley, S. M. (2018). Voltage-gated sodium channels: (NaV)igating the field to determine their contribution to visceral nociception. J Physiol, 596(5), 785-807. doi:10.1113/jp273461

Principal Author

Name of Principal Author (Candidate)	Andelain Erickson
Contribution to the Paper	Planning, writing, generation of figures and editing of manuscript
Overall percentage (%)	70
Certification:	This paper reports on original research I conducted during the period of my Higher Degree by Research candidature and is not subject to any obligations or contractual agreements with a third party that would constrain its inclusion in this thesis. I am the primary author of this paper.
Signature		Date	15/1/2019

Co-Author Contributions

By signing the Statement of Authorship, each author certifies that:

i. the candidate's stated contribution to the publication is accurate (as detailed above);

ii. permission is granted for the candidate in include the publication in the thesis; and

iii. the sum of all co-author contributions is equal to 100% less the candidate's stated contribution.

Name of Co-Author	Annemie Deiteren
Contribution to the Paper	Editing of manuscript
Signature		Date	27-MAR-2019

Name of Co-Author	Andrea M. Harrington
Contribution to the Paper	Editing of manuscript
Signature		Date	14.3.2019

Name of Co-Author	Sonia Garcia-Caraballo		
Contribution to the Paper	editing the manuscript.		
Signature		Date	25/3/19

Name of Co-Author	Joel Castro		
Contribution to the Paper	EDITING THE MANUSCRIPT.		
Signature		Date	19.03.19

Name of Co-Author	Ashlee Caldwell		
Contribution to the Paper	writing the manuscript.		
Signature		Date	25.3.19

Name of Co-Author	Luke Grundy		
Contribution to the Paper	writing the manuscript		
Signature		Date	19-03.19

Name of Co-Author	Stuart M. Brierley (corresponding author)		
Contribution to the Paper	supervision, corresponding author, project head, writing/editing manuscript/finances.		
Signature		Date	14/3/2019.

23

Chapter 2 Voltage-gated sodium channels: (Nav)igating the field to determine their contribution to visceral nociception

Erickson A[1,2], Deiteren A[1,2], Harrington AM[1,2], Garcia-Caraballo S[1,2], Castro J[1,2], Caldwell A[1,2], Grundy L[1,2], Brierley SM[1,2].

[1]Visceral Pain Research Group, Human Physiology, Centre for Neuroscience, College of Medicine and Public Health, Flinders University, Bedford Park, South Australia, 5042, Australia. [2]Centre for Nutrition and Gastrointestinal Diseases, Discipline of Medicine, University of Adelaide, South Australian Health and Medical Research Institute (SAHMRI), North Terrace, Adelaide, South Australia 5000, Australia.

Edited by: Ole Petersen & Yasushi Okamura

2.1 Abstract

Chronic visceral pain, altered motility and bladder dysfunction are common, yet poorly managed symptoms of functional and inflammatory disorders of the gastrointestinal and urinary tracts. Recently, numerous human channelopathies of the voltage-gated sodium (Na_v) channel family have been identified, which induce either painful neuropathies, an insensitivity to pain, or alterations in smooth muscle function. The identification of these disorders, in addition to the recent utilisation of genetically modified Na_v mice and specific Na_v channel modulators, has shed new light on how Na_v channels contribute to the function of neuronal and non-neuronal tissues within the gastrointestinal tract and bladder. Here we review the current pre-clinical and clinical evidence to reveal how the nine Na_v channel family members ($Na_v1.1$–$Na_v1.9$) contribute to abdominal visceral function in normal and disease states.
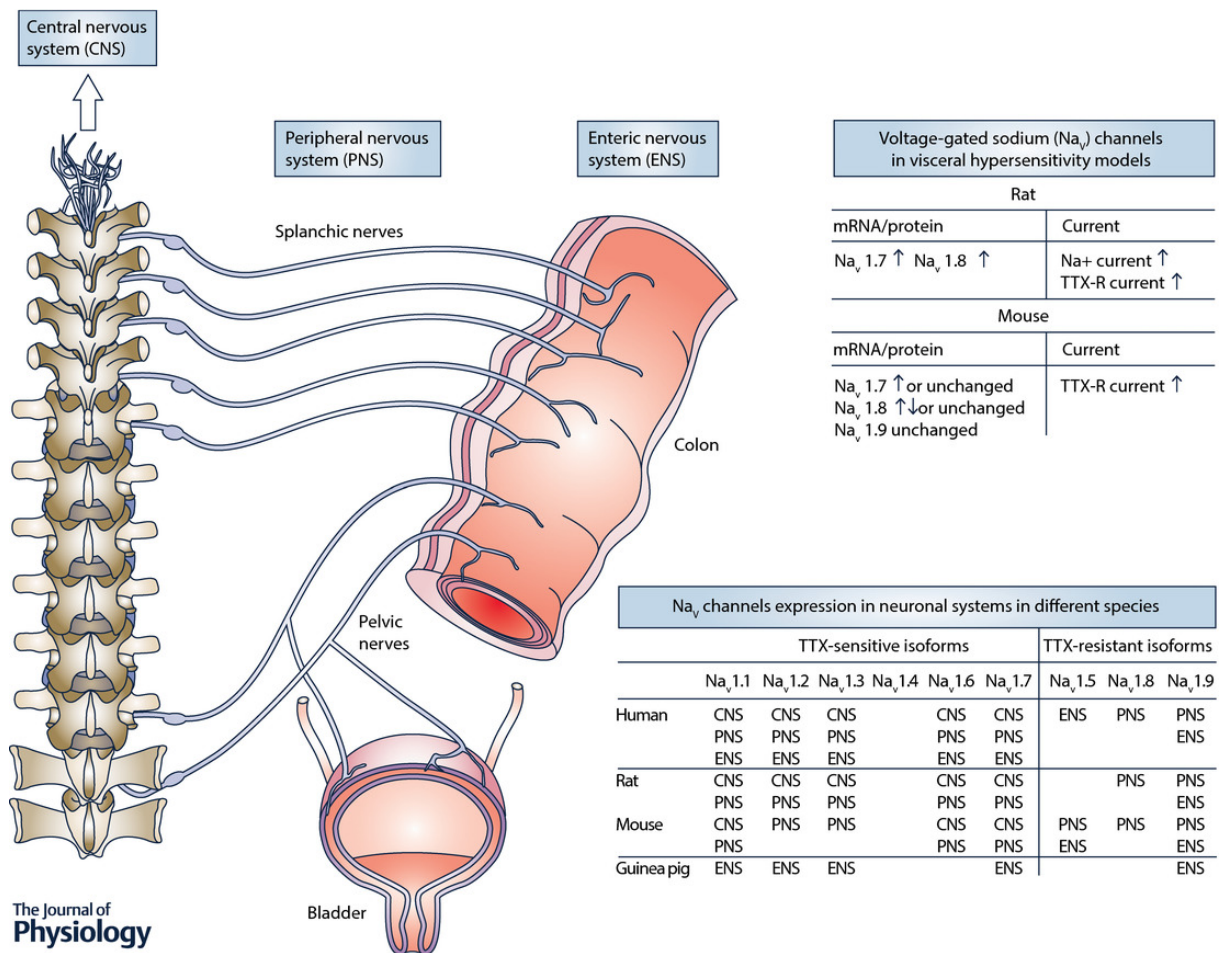
Figure 2.1 Abstract figure.

2.2 Introduction

Chronic visceral pain, altered intestinal motility and bladder dysfunction remain poorly managed symptoms of functional and inflammatory disorders of the gastrointestinal and urinary tracts. A lack of suitable treatments for these disorders is a major contributing factor to their debilitating nature and the large socio-economic cost accrued by patients, their families and society (NIH, 2009; Gaskin & Richard, 2012; Enck et al. 2016). Conventional analgesics, such as opioids and non-steroidal anti-inflammatory drugs (NSAIDs), are unsuitable for treating chronic pain originating in the gastrointestinal and lower urinary tract, as they are associated with severe side effects. This includes tolerance, a lack of efficacy and importantly for some inflammatory gastrointestinal disorders the potential to exacerbate the disease (Sikandar & Dickenson, 2012; Farrell et al. 2014). The colon, rectum and bladder are innervated by specialised sensory afferents travelling via the splanchnic and pelvic nerves that terminate within the dorsal horn of the thoracolumbar and lumbosacral spinal cord, respectively (Brierley et al. 2004; Harrington et al. 2012; Brierley & Linden, 2014). These neurons detect both non-noxious physiological stimuli, including muscle stretch during organ distension, and noxious mechanical and chemical stimuli such as bloating, intense distension/contraction, or the presence of inflammatory mediators (Brierley & Linden, 2014; Brierley, 2016). To encode for such wide-ranging stimuli, visceral organs rely on an array of stimuli-activated primary 'sentinel' transducers, including transient receptor potential (TRP) channels, acid-sensing ion channels (ASIC), mechanosensitive two-pore domain K (K2P) channels and Piezo channels (Grundy, 2002; Brierley, 2010; Christianson & Davis, 2010; La & Gebhart, 2011; Brierley, 2016; Alcaino et al. 2017). Furthermore, primary transducers and ion channels involved in sensory signalling can be modulated and controlled by G-protein coupled receptors (GPCRs) and regulators of GPCR signalling proteins, in response to endogenous mediators (Geppetti et al. 2015; Salaga et al. 2016).

Voltage-gated sodium (Na_v) channels are secondary in the neuronal response to non-noxious or noxious stimuli. They perform the crucial role of regulating neuronal excitability and the key function of amplifying cation influx generated by the primary transducers to generate and propagate action potentials (Catterall, 2012; King & Vetter, 2014). Voltage-gated potassium (K_v) channels repolarise the membrane potential following Na^+ influx and modulate firing frequency, and have been reported to contribute to visceral hypersensitivity in peripheral neurons in animal models (Hirano et al. 2007; Qian et al. 2009; Luo et al. 2011; Du & Gamper, 2013); however, this family of ion channels is not covered within the scope of this review.

The Na_v channel family contains nine isoforms (Na_v1.1–Na_v1.9), which are encoded by nine *SCN* genes (*SCN1A, SCN2A, SCN3A, SCN4A, SCN5A, SCN8A, SCN9A, SCN10A, SCN11A*). Functionally, these channels are historically categorised as either tetrodotoxin-sensitive (TTX-S: Na_v1.1-Na_v1.4, Na_v1.6 and Na_v1.7), or tetrodotoxin-resistant (TTX-R: Na_v1.5, Na_v1.8 and Na_v1.9). Anatomically, these channels display wide and diverse expression patterns across neuronal and smooth muscle cells throughout the body (**Table 2.1**), as well as cells of the immune system (including macrophages and mast cells) where they are involved in migration and phagocytosis (Bradding et al. 2003; Roselli et al. 2006; Carrithers et al. 2011; Black & Waxman, 2013). Na_v1.1, Na_v1.2, Na_v1.3 and Na_v1.6 are traditionally considered to be the predominant isoforms expressed in the brain and spinal cord, whilst Na_v1.7, Na_v1.8 and Na_v1.9 are preferentially expressed in the peripheral nervous system (PNS). Na_v1.4 is found predominantly within skeletal muscle and Na_v1.5 is the major isoform in cardiac myocytes (Catterall et al. 2005). Furthermore, Na_v channels are regulated by a range of enzymes and structural proteins, including auxiliary β-subunits (β1, β1$_B$, β2, β3, β4) (Qin et al. 2003; Tseng et al. 2007), kinases and ubiquitin-protein ligases (Feng et al. 2012; Savio-Galimberti et al. 2012; Laedermann et al. 2015), which collectively regulate Na_v channel biophysical properties and expression.

Table 2.1 Expression of Na$_v$ isoforms in neuronal and non-neuronal cells in different species relevant for visceral sensation and processing.

Na$_v$ isoform	Species	System or tissue	Found in	Not found in	Reference
Na$_v$1.1	Human	CNS	Cerebral cortex, cerebellum, hypothalamus, caudate, hippocampus, amygdala, C1 level spinal cord		GTEx Consortium et al. 2017)
	Rat	CNS	Hippocampus, cerebellum, spinal cord (dorsal horn, ventral horn, primarily grey matter restricted)	Embryonic brain and spinal cord	(Beckh et al. 1989; Westenbroek et al. 1989)
	Mouse	CNS	Cerebral cortex, cerebellum, hippocampus, thalamus, central grey, pons, medulla	Fimbria, corpus callosum	(Duflocq et al. 2008)
	Human	PNS	L3–L5		(Chang et al. 2018)
	Rat	PNS	L4–L5; L5		(Black et al. 1996; Fukuoka et al. 2008; Wang et al. 2011)
	Mouse	PNS	Colonic neurons in T10–L1 and L5–S1; T10–L1	L3–L6 dorsal and ventral roots	(Duflocq et al. 2008; Osteen et al. 2016; Hockley et al. 2017)
	Human	ENS	Colonic myenteric plexus		(Hetz et al. 2014)
	Guinea pig	ENS		Duodenal myenteric plexus	(Sage et al. 2007)
Na$_v$1.2	Human	CNS	Cerebral cortex, cerebellum, hypothalamus, caudate, hippocampus, amygdala, C1 level spinal cord		(GTEx Consortium et al. 2017)
	Rat, cat	CNS	Cortex, hippocampus, cerebellum, hypothalamus, spinal cord grey matter		(Jarnot & Corbett, 2006)
	Rat	CNS	Hippocampus and cerebellum; embryonic brain and spinal cord		(Beckh et al. 1989; Westenbroek et al. 1989)
	Human	PNS	L3–L5		(Chang et al. 2018)
	Rat	PNS	L4–L5; L5		(Black et al. 1996; Fukuoka et al. 2008)
	Mouse	PNS	Colonic neurons in T10–L1 and L5–S1		(Chang et al. 2018; Hockley et al. 2017)
	Human	ENS	Colonic myenteric plexus		(Hetz et al. 2014)
	Guinea pig	ENS		Duodenal myenteric plexus	(Sage et al. 2007)
Na$_v$1.3	Human	CNS	Caudate, cerebellum, cerebral cortex, hippocampus, hypothalamus, amygdala, C1 level spinal cord		(GTEx Consortium et al. 2017)
	Rat	CNS	Embryonic brain and spinal cord	Adult brain and spinal cord	(Beckh et al. 1989)
	Human	PNS	L3–L5		(Chang et al. 2018)
	Rat	PNS	L4–L5	L5	(Black et al. 1996; Fukuoka et al. 2008)
	Mouse	PNS	Colonic neurons in T10–L1 and L5–S1; DRG		(Chang et al. 2018; Hockley et al. 2017)
	Human	ENS	Colonic myenteric plexus		(Hetz et al. 2014)
	Guinea pig	ENS	Duodenal myenteric plexus		(Sage et al. 2007)
	Human, mouse	Neuro-endocrine	Jejunal and colonic enterochromaffin cells		(Bellono et al. 2017; Strege et al. 2017a,b)
Na$_v$1.4	Human	CNS		Brain	(GTEx Consortium et al. 2017)
	Rat	PNS		L5	(Fukuoka et al. 2008)
	Mouse	PNS		Colonic neurons in T10–L1 and L5–S1	(Hockley et al. 2017)
	Human	ENS		Colonic myenteric plexus	(Hetz et al. 2014)

	Human	Muscle	Oesophageal smooth muscle		(Deshpande et al. 2002)
Na$_v$1.5	Human	CNS		Brain	(GTEx Consortium et al. 2017)
	Mouse	PNS	Colonic neurons in T10–L1 and L5–S1		(Hockley et al. 2017)
	Human	ENS	Colonic myenteric plexus		(Hetz et al. 2014)
	Mouse	ENS	Duodenal myenteric plexus		(Osorio et al. 2014)
	Human	Interstitial cells	Jejunal interstitial cells of Cajal		(Strege et al. 2003)
	Human, dog, rat	Muscle	Jejunal circular smooth muscle		(Holm et al. 2002; Ou et al. 2002; Strege et al. 2007; Beyder et al. 2016)
	Human, rat	Muscle	Colonic circular smooth muscle		(Strege et al. 2003; Beyder et al. 2016)
	Human, mouse	Muscle		Jejunal longitudinal smooth muscle	(Ou et al. 2002; Strege et al. 2007)
	Pig, guinea pig	Muscle		Jejunal circular smooth muscle	(Strege et al. 2007)
	Human	Macro-phages	Macrophages		(Carrithers et al. 2007, 2011; Black & Waxman, 2013)
Na$_v$1.6	Human	CNS	Cerebral cortex, cerebellum, hypothalamus, caudate, hippocampus		(Whitaker et al. 1999; GTEx Consortium et al. 2017)
	Rat	CNS	Cerebellum, hippocampus, spinal cord (white and grey matter)		(Tzoumaka et al. 2000)
	Mouse	CNS	Spinal cord white and grey matter		(Duflocq et al. 2008)
	Human	PNS	L3–L5		(Chang et al. 2018)
	Rat	PNS	L4–L5; L5		(Tzoumaka et al. 2000; Fukuoka et al. 2008)
	Mouse	PNS	L3–L6 dorsal and ventral roots; DRG		(Duflocq et al. 2008; Chang et al. 2018)
	Mouse	PNS	Colonic neurons in T10–L1 and L5–S1; T10–L1; T9–T13; L6		(King et al. 2009; Feng et al. 2015; Hockley et al. 2017; Inserra et al. 2017)
	Human	ENS	Colonic myenteric plexus		(Hetz et al. 2014)
	Guinea pig	ENS		Duodenal myenteric plexus	(Sage et al. 2007)
	Human	Macro-phages	Macrophages		(Carrithers et al. 2007, 2011; Black & Waxman, 2013)
Na$_v$1.7	Human	CNS	Hypothalamus		(GTEx Consortium et al. 2017)
	Rat	CNS	Hypothalamus, subfornical organ, intermediolateral cell column	Cerebellum, cerebral cortex, hippocampus, striatum, septum, thalamic nuclei	(Morinville et al. 2007)
	Mouse	CNS	Hypothalamus		(Branco et al. 2016)
	Human	PNS	L3–L5; DRG		(Flegel et al. 2015; Chang et al. 2018)
	Rat	PNS	L5		(Fukuoka et al. 2008)
	Mouse	PNS	Colonic neurons in T10–L1 and L5–S1; T10–L1; L6		(Feng et al. 2015; Hockley et al. 2017; Inserra et al. 2017)
	Human	ENS	Colonic myenteric plexus		(Hetz et al. 2014)
	Guinea pig	ENS	Duodenal myenteric plexus		(Sage et al. 2007)

Na$_v$ isoform	Species	System			Citation
Na$_v$1.8	Human	CNS		Brain	(Flegel et al. 2015; GTEx Consortium et al. 2017)
	Human	PNS	L3–L5; DRG		(Flegel et al. 2015; Chang et al. 2018)
	Rat	PNS	Colonic neurons T13–L2		(Hu et al. 2013a, 2016; Lin et al. 2017)
	Mouse	PNS	Colonic neurons in T10–L1 and L5–S1; T10–L1; T9–T13; T9–L1; L6		(Beyak et al. 2004; Hillsley et al. 2006; King et al. 2009; Feng et al. 2015; Hockley et al. 2017; Inserra et al. 2017)
	Human	ENS		Colonic myenteric plexus	(Hetz et al. 2014)
	Mouse	ENS		Duodenal myenteric plexus	(Osorio et al. 2014)
Na$_v$1.9	Human	CNS		Brain	(GTEx Consortium et al. 2017)
	Human	PNS	L3–L5; DRG		(Flegel et al. 2015; Chang et al. 2018)
	Rat	PNS	L4–L5		(Dib-Hajj et al. 1998)
	Mouse	PNS	Colonic neurons T9–T13; trigeminal ganglia		(Beyak et al. 2004; Padilla et al. 2007; King et al. 2009)
	Human	ENS	Colonic submucosal and myenteric plexus		(Hetz et al. 2014; O'Donnell et al. 2016)
	Rat	ENS	Duodenal myenteric plexus		(Rugiero et al. 2003)
	Mouse	ENS	Sensory, Dogiel type II, myenteric and submucosal neurons		(Padilla et al. 2007; Osorio et al. 2014)
	Guinea pig	ENS	Duodenal intrinsic primary afferent neurons; duodenal myenteric plexus		(Rugiero et al. 2003; Copel et al. 2009)
	Human	Muscle	Colonic smooth muscle		(O'Donnell et al. 2016)
	Human	Mast cells	lung, skin and cord blood-derived mast cells		(Bradding et al. 2003)

Recently, numerous studies have reported Na$_v$ isoform channelopathies, including for Na$_v$1.7 (*SCN9A*), Na$_v$1.8 (*SCN10A*) and Na$_v$1.9 (*SCN11A*) as the primary cause of increased pain or loss of pain phenotypes in humans (Yang et al. 2004; Cox et al. 2006; Fertleman et al. 2006; Klein et al. 2013; Leipold et al. 2013; Huang et al. 2014, 2017; Waxman et al. 2014; Dib-Hajj et al. 2015; Han et al. 2015). Pharmacological modulation of Na$_v$ channels supports these genetic observations, including the finding that activation of all Na$_v$ channels by Pacific ciguatoxin 1 (P-CTX-1) or veratridine due to accidental consumption manifests as acute and severe gastrointestinal disturbances associated with abdominal pain in humans (Schep et al. 2006; Stewart et al. 2010). Intracolonic administration of purified P-CTX-1 also causes pain behaviour in mice (Inserra et al. 2017). On the other hand, TTX (which blocks Na$_v$1.1–Na$_v$1.4, Na$_v$1.6 and Na$_v$1.7) poisoning in humans is associated with paralysis rather than pain (Lago et al. 2015). Whilst potentially fatal upon consumption, administration of Na$_v$-selective agents such as TTX and neosaxitoxin has been shown to decrease pain responses in a range of pain modalities including visceral pain in humans (Hagen et al. 2011, 2017; Manriquez et al. 2015) and rodents (Marcil et al. 2006; Gonzalez-Cano et al. 2017). Similarly, intrarectal administration of lidocaine (lignocaine) in irritable bowel syndrome (IBS) patients reduces rectal sensitivity and abdominal pain, suggesting Na$_v$ channels and activation of peripheral afferent endings in the colon play key roles in the pathogenesis of chronic visceral pain in IBS patients (Verne et al. 2005).

Human genetic studies have triggered widespread investigation into the therapeutic potential of Na$_v$ channels in the treatment of acute and chronic pain and also prompted studies to identify the wider roles of these channels throughout the body. It is also clear from most studies utilising inflammatory, nematode or bacterial models that gut- and bladder-innervating neurons become hyperexcitable after the initial

insult, which involves changes in TTX-R and TTX-S Na$_v$ currents, amongst others. This is apparent in neurons innervating the stomach (Gebhart et al. 2002; Bielefeldt et al. 2002a, b; Dang et al. 2004), small intestine (Moore et al. 2002; Stewart et al. 2003; Hillsley et al. 2006; Keating et al. 2008), the colon (Beyak et al. 2004; Ibeakanma et al. 2009; King et al. 2009) and the bladder (Yoshimura & deGroat, 1997). This review presents recent evidence on the specific roles of Na$_v$1.1–Na$_v$1.9 in transmitting sensation and nociception from the distal gut and bladder in healthy and pathological states.

2.3 Na$_v$1.1

Na$_v$1.1 is predominantly expressed in cell bodies, axon initial segments and at the nodes of Ranvier in the central nervous system (CNS) (Westenbroek et al. 1989; Duflocq et al. 2008; Carithers et al. 2015; Uhlen et al. 2015; GTEx Consortium et al. 2017). It is also expressed in human, rat and mouse PNS (Fukuoka et al. 2008; Wang et al. 2011; Osteen et al. 2016; Chang et al. 2018), and in human, but not guinea pig, myenteric plexus (Sage et al. 2007; Hetz et al. 2014) (**Table 2.1**). In thoracolumbar (T10–L1) and lumbar (L5) dorsal root ganglia (DRG) neurons, which contain the cell bodies of sensory neurons innervating the colon, rectum, bladder and skin, Na$_v$1.1 is expressed in 15–35% of all neurons. Expression is predominantly in Tropomyosin-related kinase C (TrkC)- and Tropomyosin-related kinase A (TrkA)-expressing myelinated A-fibres of medium to large diameter and nearly absent in C-fibre small diameter neurons innervating the skin (Fukuoka et al. 2008; Wang et al. 2011; Osteen et al. 2016). However, Na$_v$1.1 mRNA transcript is detected in approximately half of thoracolumbar (T10–L1) and lumbosacral (L5–S1) mouse DRG neurons innervating the colon (Osteen et al. 2016; Hockley et al. 2017). As colonic afferents are predominantly peptidergic C-fibres, there are clearly key differences in the populations of afferent neurons expressing Na$_v$1.1 when comparing between the colon and the skin. In colon-innervating DRG neurons, Na$_v$1.1 is frequently co-localised with Na$_v$1.2, Na$_v$1.3, Na$_v$1.6, Na$_v$1.7, Na$_v$1.8 and Na$_v$1.9 (Osteen et al. 2016; Hockley et al. 2017). Functional studies of colonic afferents reveal that Na$_v$1.1 plays a crucial role in the signalling of mechanical pain from the colon (Osteen et al. 2016). Application of the selective Na$_v$1.1 agonist, δ-theraphotoxin-Hm1a (Hm1a), enhances mechanically evoked firing in a subpopulation of high-threshold colonic nociceptors. Notably, the mechanical hypersensitivity evoked by Hm1a was blocked by incubation with the Na$_v$1.1/Na$_v$1.3 antagonist ICA-121431 (**Table 2.2**) (Osteen et al. 2016). Furthermore, Hm1a also induces hyperexcitability of isolated colon-innervating DRG neurons from healthy control mice (Osteen et al. 2016). Notably, the percentage of colon-innervating afferents/neurons affected by Hm1a is similar to the percentage of colon-innervating DRG neurons expressing Na$_v$1.1, as determined by single cell PCR (Osteen et al. 2016; Hockley et al. 2017). Importantly, colon-innervating DRG neurons isolated from mice with chronic visceral hypersensitivity (CVH) show significantly enhanced responsiveness to Hm1a compared to healthy control mice, suggesting that Na$_v$1.1 may be essential for the development and maintenance of chronic visceral pain conditions (Osteen et al. 2016). As such, antagonism of Na$_v$1.1 may be a future target for the treatment of disorders accompanied by chronic visceral pain originating from the colon. There are currently no reports on the expression profile or function of Na$_v$1.1 in the bladder or bladder-innervating sensory neurons.

2.4 Na$_v$1.2

Na$_v$1.2 is extensively expressed in the CNS (Jarnot & Corbett, 2006) but has also been detected at low levels in small-diameter DRG neurons (Black et al. 1996; Fukuoka et al. 2008; Chang et al. 2018). Conversely, in colon-innervating DRG neurons of the mouse, Na$_v$1.2 mRNA transcript is present in 69% of thoracolumbar (T10–L1) neurons and at a similar level in lumbosacral (L5–S1) neurons (Hockley et al. 2017) (**Table 2.1**). Despite this mRNA expression, there is currently no functional data to support a role for Na$_v$1.2 in colonic sensory signalling or pain. Similarly, there are currently no reports on the expression profile or function of Na$_v$1.2 in the bladder or bladder-innervating sensory neurons.

2.5 Na$_v$1.3

Na$_v$1.3 is highly expressed in sensory neurons during embryogenesis in rats, but its expression traditionally subsides in fully developed neurons (Beckh et al. 1989). The major body of Na$_v$1.3 research in nociception focuses on its role in neuropathic pain, as Na$_v$1.3 is re-expressed following neuropathic

injury in large diameter, myelinated A-fibre neurons where it may contribute to ectopic discharge and painful neuropathy (Waxman et al. 1994; Zang et al. 2010). However, due to the limited expression of this channel in adult tissues and lack of channelopathy-associated pain syndromes, studies investigating the role of $Na_v1.3$ in other pain pathways are few. In relation to the viscera, $Na_v1.3$ mRNA is detected in adult guinea-pig enteric nervous system (ENS) neurons (Sage et al. 2007), but its functional role has yet to be determined. Initial experiments indicate that $Na_v1.3$ expression is low in rat lumbar (L5) DRG neurons (Fukuoka et al. 2008). However, $Na_v1.3$ mRNA transcripts are detected in approximately half of the colon-innervating thoracolumbar (T10–L1) and lumbosacral (L5–S1) DRG neurons in the mouse (Hockley et al. 2017) (**Table 2.1**). More recent studies show a key role for $Na_v1.3$ in non-neuronal tissues, specifically within enterochromaffin cells located within the epithelium from the small and large intestine of humans and mice (Bellono et al. 2017; Strege et al. 2017a,b). Voltage-gated sodium currents generated by $Na_v1.3$ likely allow enterochromaffin cells to respond to the detection of mechanical and chemical stimuli within the lumen of the intestine (Bellono et al. 2017; Strege et al. 2017b). In contrast, expression of the other eight Na_v isoforms is very low, or indeed lacking from both intestinal enterochromaffin cells and the wider population of intestinal epithelial cells (Bellono et al. 2017). There are currently no reports on the role of $Na_v1.3$ in the bladder or bladder-innervating sensory neurons.

2.6 $Na_v1.4$

$Na_v1.4$ is the predominant Na_v isoform in skeletal muscle (Trimmer et al. 1990) but is also found in human oesophageal smooth muscle tissue (Deshpande et al. 2002). In peripheral neurons, $Na_v1.4$ transcripts are nearly absent in rat lumbar (L5) DRG (Fukuoka et al. 2008) and in colon-innervating mouse DRG neurons (Hockley et al. 2017) (**Table 2.1**). In agreement with tissue distribution, $Na_v1.4$ channelopathies appear to exclusively involve deficits in skeletal muscle function, and to date no involvement in colon or bladder function has been shown.

2.7 $Na_v1.5$

$Na_v1.5$ channels have been identified in circular smooth muscle of the jejunum of human, dog, rat and mouse but are absent in pig and guinea pig. $Na_v1.5$ is also absent from human and mouse jejunal longitudinal smooth muscle (Holm et al. 2002; Ou et al. 2002; Strege et al. 2007; Beyder et al. 2016). $Na_v1.5$ has been found in colonic circular smooth muscle of human and rat (Strege et al. 2003), in jejunal interstitial cells of Cajal in human (Strege et al. 2003), and in myenteric plexuses of human and mouse (Hetz et al. 2014; Osorio et al. 2014). $Na_v1.5$ in circular smooth muscle may contribute to normal intestinal motility through modulation of slow-wave activity and muscle contractility (Ou et al. 2002; Strege et al. 2007). These findings are supported by data showing that ranolazine, a treatment for chronic angina, is able to inhibit $Na_v1.5$ currents in human colonic smooth muscle cells (Neshatian et al. 2015), which is likely to be responsible for the constipation seen during long-term ranolazine treatment (Nash & Nash, 2008). These data strongly point towards a primary role for $Na_v1.5$ channels in mediating gastrointestinal motility and transit (Beyder & Farrugia, 2016). Similarly, several loss-of-function mutations in *SCN5A*, the gene encoding $Na_v1.5$ channels, are associated with IBS and abdominal pain (Saito et al. 2009; Beyder et al. 2014; Strege et al. 2017c). Whether this is purely a consequence of reduced gastrointestinal contractility or whether $Na_v1.5$ channels also play a direct role in visceral sensation remains unclear, as $Na_v1.5$ mRNA transcripts are expressed in 18% of thoracolumbar and 51% of lumbosacral colon-innervating DRG neurons (Hockley et al. 2017) (**Table 2.1**). Whether this translates into channel expression and a functional role remains to be determined. There are currently no reports on the expression profile or function of $Na_v1.5$ in the bladder or bladder-innervating sensory neurons.

2.8 $Na_v1.6$

$Na_v1.6$ is extensively expressed within the CNS and PNS (Whitaker et al. 1999; Tzoumaka et al. 2000; Catterall et al. 2005; Catterall, 2012; Chang et al. 2018), commonly located in clusters at the nodes of Ranvier (Duflocq et al. 2008), indicating that $Na_v1.6$ may have a primary role in transmitting rather than initiating action potentials. In rat lumbar (L5) DRG neurons, $Na_v1.6$ transcripts are detected in a third of all neurons and selectively expressed in TrkC- and TrkA-expressing myelinated A-fibre nociceptors (Fukuoka et al. 2008). In colon-innervating mouse DRG neurons, $Na_v1.6$ mRNA transcript is present in

63–87% of thoracolumbar (T10–L1) neurons, and in 51% of lumbosacral (L5–S1) neurons (Hockley et al. 2017; Inserra et al. 2017). Immunohistochemical and western blot analysis show that Na_v1.6 protein is present in the cell bodies of sensory neurons and on sensory afferent nerve endings innervating the distal colon and rectum in mice (Feng et al. 2015) (**Table 2.1**). Antagonism of Na_v1.6 reduces action potential firing of stretch-sensitive colorectal afferents *in vitro* (Feng et al. 2015) (**Table 2.2**). Whether these effects are altered in animal models of inflammatory or chronic visceral pain remains to be investigated. It has, however, been reported that there is no change in Na_v1.6 expression in colon-innervating DRG neurons (T9–T13) during the acute inflammatory phase of the mouse model of trinitrobenzenesulphonic acid (TNBS)-induced colitis (King et al. 2009). This corresponds with the phase when colorectal afferent hypersensitivity also occurs (Hughes et al. 2009). Activation of low-threshold stretch-sensitive afferents is essential for normal physiological function of the colon (Brierley et al. 2004; Kyloh et al. 2011) and Na_v1.6 appears to play a key integrative role in this process. Whether Na_v1.6 contributes to aberrant colonic afferent sensory signalling during chronic visceral hypersensitivity remains to be determined. There are currently no reports on the expression profile or function of Na_v1.6 in the bladder or bladder-innervating sensory neurons.

2.9 Na_v1.7

Na_v1.7 has become a key target of interest as several human mutations in the *SCN9A* gene, which encodes Na_v1.7, lead to either a loss of pain or increased pain perception (Bennett & Woods, 2014). For example, a loss-of-function mutation of *SCN9A* results in a congenital insensitivity to pain (CIP) (Cox et al. 2006; Goldberg et al. 2007), whereas gain-of-function mutations produce distinct pain syndromes, such as erythromelalgia, small-fibre neuropathy and paroxysmal extreme pain disorder (Fertleman et al. 2006). Na_v1.7 is extensively expressed in sensory and sympathetic neurons of the PNS, as well as ENS neurons, and is highly restricted in the CNS (Klugbauer et al. 1995; Catterall et al. 2005; Morinville et al. 2007; Sage et al. 2007; Branco et al. 2016; Chang et al. 2018). In rat lumbar (L5) DRG neurons, Na_v1.7 transcripts are preferentially expressed in TrkA-expressing C-fibre neurons, and in a subset of A-fibre neurons (Fukuoka et al. 2008). Robust immunolabelling of Na_v1.7 is present within the peripheral endings of sensory nerves in the skin (Black et al. 2012).

From mouse knock-out studies, it appears that Na_v1.7 in Na_v1.8-expressing cells (Na_v1.7[Nav1.8]) does not contribute in the development of neuropathic pain, nor noxious cold or heat detection (Nassar et al. 2004, 2005; Minett et al. 2012, 2014; Hockley et al. 2017). However, Na_v1.7[Nav1.8] mice have significantly reduced behavioural responses to inflammatory mediators (formalin, complete Freund's adjuvant, carrageenan and nerve growth factor) when injected into the sole of the hind paw (Nassar et al. 2004) and impaired somatic noxious mechanosensation (Minett et al. 2012, 2014). Thus far, only the deletion of Na_v1.7 in sympathetic and sensory (Wnt1-expressing) neurons and the global Na_v1.7 knock-out have been able to significantly reduce pain responses to a range of stimuli and recapitulate the human *SCN9A*-associated CIP phenotype (Gingras et al. 2014; Minett et al. 2014). Recent studies also show that endogenous opioids contribute to pain insensitivity in both humans and mice lacking Na_v1.7, as the opioid antagonist naloxone reverses analgesia associated with the loss of Na_v1.7 expression (Minett et al. 2015). This suggests that Na_v1.7 channel blockers alone may not replicate the analgesic phenotypes of Na_v1.7 null mutants, but may be potentiated with exogenous opioids. Na_v1.7-selective inhibitors are currently in clinical trial for different types of pain (Pennington et al. 2017; Yekkirala et al. 2017).

In relation to visceral sensation, Na_v1.7 is highly abundant in human lumbar DRG, and is expressed in 100% of mouse colon-innervating thoracolumbar (T10–L1) DRG neurons, and in most colon-innervating lumbosacral (L5–S1) DRG neurons (Chang et al. 2018; Hockley et al. 2017; Inserra et al. 2017) (**Table 2.1**). Accordingly, Na_v1.7 constitutes the most prevalent TTX-S isoform within colon-innervating DRG neurons. It is of interest to note that 'paroxysmal extreme pain disorder', caused by the human gain of function *SCN9A* mutation, was originally called 'familial rectal pain syndrome'. As the name implies, this disorder is characterised by excruciating rectal and abdominal pain commonly associated with defecation (Fertleman et al. 2006), suggesting a key role for Na_v1.7 in visceral pain. Moreover, pain perception in a subset of patients with interstitial cystitis/bladder pain syndrome (IC/BPS) is shown to correlate with a

polymorphism in *SCN9A* (Reeder et al. 2013). IC/BPS patients treated with a bladder infiltration of neosaxitoxin, a blocker of TTX-S Na_v channels, resulted in significant analgesia and reduced bladder overactivity for 90 days after the treatment (Manriquez et al. 2015). Normal physiological function of the bladder, however, appears to be independent of Na_v1.7, as *SCN9A*-associated CIP individuals have normal bladder control, and no increased incidence of urinary infections, incontinence, or retention (Cox et al. 2006).

Despite these studies, the initial promise of Na_v1.7's contribution to visceral pain is somewhat tempered by experimental studies showing that Na_v1.7[Nav1.8] mice exhibit normal nocifensive responses to intracolonic administration of capsaicin (TRPV1 agonist) and mustard oil (TRPA1 agonist), indicating that Na_v1.7 is not crucial for acute visceral pain signalling (Hockley et al. 2017). Low-threshold stretch-sensitive pelvic afferents are unaffected by the Na_v1.7 antagonist ProTX-II (Feng et al. 2015) (**Table 2.2**). Similarly, *ex vivo* extracellular recordings of mesenteric afferents from resected human appendices show that peak firing before and after exposure to a novel Na_v1.7-selective antagonist, PF-5198007, is unchanged during repeat noxious ramp distensions (Hockley et al. 2017). Afferent responses in mouse *ex vivo* colorectal recordings are attenuated by application of TTX (Feng et al. 2015), indicating that TTX-S channels other than Na_v1.7 may be important in responding to innocuous and noxious mechanical stimuli. Accordingly, intracolonic co-administration of TTX and P-CTX-1 did not significantly alter the pain response induced by P-CTX-1 (Inserra et al. 2017).

Ex vivo extracellular recordings of splanchnic nerve activity from the distal colon of Na_v1.7[Nav1.8] mice show no difference in peak firing between Na_v1.7[Nav1.8] and littermate control afferents in the physiological and supraphysiological pressure range (0–80 mmHg) (Hockley et al. 2017). However, significantly less action potential firing in afferents from Na_v1.7[Nav1.8] mice at distension pressures in the supramaximal range (80–145 mmHg) is observed, suggesting that Na_v1.7 in Na_v1.8-positive colonic afferent neurons may be involved in transducing non-physiological extremes of pressure. This may be important and more relevant to chronic visceral pain states, when splanchnic afferents show mechanical hypersensitivity and decreased activation thresholds to mechanical stimuli (Hughes et al. 2009; Castro et al. 2013, 2017; de Araujo et al. 2014; Osteen et al. 2016). In the bladder, Na_v1.7[Nav1.8] mice have comparable levels of referred hyperalgesia in an acute cyclophosphamide-induced cystitis model compared to littermates (Hockley et al. 2017). Overall, these findings suggest that Na_v1.7 has a role in mediating acute inflammatory pain in somatic but not visceral pathways. While studies on visceral nociception using Na_v1.7[Nav1.8] mice have provided valuable insight, replication of these studies in mice with sensory neuron-specific deletion of Na_v1.7 (e.g. Na_v1.7[Advill]) will be beneficial to strengthen conclusions concerning Na_v1.7 in visceral pain signalling.

Diseases that have a significant visceral pain component are commonly chronic and have unmet needs in terms of clinical treatment. Therefore, further investigations into the role of Na_v1.7 in long term and chronic visceral pain models, which are more clinically relevant to pathological chronic visceral pain states, are critical. For example, significant up-regulation of Na_v1.7 mRNA occurs 4 weeks after induction of colitis in colon-innervating DRG (L6–S1) neurons (Campaniello et al. 2016). Similarly, rats with streptozotocin-induced diabetes show hypersensitivity to colonic distension, which corresponds with the up-regulation of Na_v1.7 protein in thoracolumbar (T13–L2) DRG neurons 4 weeks post-induction (Hu et al. 2016). In support of these findings, rat neonatal colitis-induced visceral hypersensitivity induces up-regulation of Na_v1.7 protein levels in DRG from higher spinal levels (T13–L2), but not lower spinal levels (L4–L5) at 6 weeks post-colitis compared to control animals (Qu et al. 2013). Taken together, these findings suggest that Na_v1.7 may have an acquired role during chronic visceral pain states. It is well documented that inflammation, tissue damage and healing of visceral organs can induce structural, synaptic or intrinsic neuroplasticity, altering neuronal and gastrointestinal function in the long term (Brierley & Linden, 2014). For example, rectal samples from patients with physiologically characterised rectal hypersensitivity show significantly increased numbers of Na_v1.7-immunoreactive nerve fibres in the mucosal, submucosal and muscle layers compared to control tissues (Yiangou et al. 2007). In addition to these findings, changes in the ratios of Na_v1.7 to a pan-neuronal structural marker, PGP9.5, indicate that

increased $Na_v1.7$ expression and nerve sprouting occurs in rectal mucosa, which may contribute to enhanced sensitivity in these patients (Yiangou et al. 2007).

Overall, the role of $Na_v1.7$ in pain sensation is complicated, and species differences in expression, assumed translatability of isoform-compound interaction, and effects of Na_v knock-out on other genes may confound overall conclusions. Furthermore, few studies using human tissue have been completed, and healthy tissue is often obtained from patients with colonic or rectal carcinoma (Yiangou et al. 2007; Hetz et al. 2014; Hockley et al. 2017). In addition to species-dependent differences in tissue distributions (**Table 2.1**), there are also differences in relative isoform distributions, for example, $Na_v1.7$ is the most abundant isoform in human lumbar DRG, whereas $Na_v1.8$ is more abundant in mouse (Chang et al. 2018). $Na_v1.7$ isoforms from different species can also have different compound selectivity in heterologous expression systems that should be carefully considered during experimental design. For example, human, monkey, dog and mouse $Na_v1.7$ isoforms were found to be largely insensitive to a small molecule inhibitor of $Na_v1.1/Na_v1.3$ (ICA-121431) and potently inhibited by a small molecule inhibitor of $Na_v1.7$ (PF-04856264), whereas rat $Na_v1.7$ was potently inhibited by ICA-121431, but largely insensitive to PF-04856264 (McCormack et al. 2013). A ProTxII analogue, JNJ63955918, on the other hand was equipotent at human and rat $Na_v1.7$ (Flinspach et al. 2017). Single cell studies have shown that Na_v channel expression is heterologous across cells, and there is high co-localisation of $Na_v1.7$ with $Na_v1.6$, $Na_v1.8$ and $Na_v1.9$ in colon-innervating thoracolumbar and lumbosacral neurons in mice (Hockley et al. 2017). However, functional relationships of co-expression and investigations of redundancy between Na_v channels are unclear. In knock-out models, deletion of one Na_v gene can lead to a change in expression levels of over 190 genes (Minett et al. 2015). Studies investigating Na_v channel contribution to pain signalling using knock-out models or pharmacological modification may benefit from collecting data on regulation of other Na_v family genes and auxiliary β-subunits in parallel, and other key genes where possible. Furthermore, inducible knock-out models offer the advantage of normal development and being able to compare Na_v channel contribution pre- and post-induction of visceral hypersensitivity in the adult, thereby increasing therapeutic potential of these findings.

2.10 $Na_v1.8$

$Na_v1.8$ mediates slowly inactivating TTX-R Na^+ currents and carries the majority of the current underlying the upstroke of the action potential in nociceptive neurons. Hence, they are considered to play an important role in action potential electrogenesis (Renganathan et al. 2001). $Na_v1.8$-null mice display reduced sensitivity to noxious mechanical stimuli (tail pressure) and noxious thermal stimuli (radiant heat), but normal sensitivity to acute noxious colonic distension by isotonic saline and intraperitoneal acetylcholine (Akopian et al. 1999; Laird et al. 2002). $Na_v1.8$ is the most abundant isoform expressed in mouse lumbar DRG (Chang et al. 2018) and is prevalently expressed in thoracolumbar (96%) and lumbosacral (91%) colonic sensory DRG neurons, with almost complete co-expression with $Na_v1.7$ (Hockley et al. 2017). Consistent with this, knock-down of $Na_v1.8$ in DRG neurons results in action potentials with reduced peak amplitude and slower rise times, but similar baseline excitability (Renganathan et al. 2001; Hillsley et al. 2006). Similarly, A-803467, a selective $Na_v1.8$ antagonist, does not significantly affect the frequency of action potential firing from low-threshold mechanosensitive colonic afferent nerve endings (Feng et al. 2015). Together, these data seem to suggest that $Na_v1.8$ channels do play a major role in mediating visceral sensations and pain under physiological conditions.

$Na_v1.8$ channels also have a major role in visceral signalling under pathophysiological conditions. Several studies support increased expression of $Na_v1.8$ protein in colon-innervating sensory DRG neurons in murine models of visceral hypersensitivity (Beyak et al. 2004; Hillsley et al. 2006; King et al. 2009; Qu et al. 2013; Hu et al. 2013a,b; Inserra et al. 2017; Lin et al. 2017) (**Table 2.2**). In most studies, increased channel expression correlates with enhanced TTX-R Na^+ current density in colon-innervating DRG neurons *in vitro*, and with visceral hypersensitivity *in vivo*, as the visceromotor response to noxious colonic distension in rats is significantly reduced following intraperitoneal administration of the $Na_v1.8$-specific antagonist A-803467 (Jarvis et al. 2007). Similarly, colonic co-administration of A-803467 with P-CTX-1 significantly reduces P-CTX-1-induced nocifensive behaviours in mice (Inserra et al. 2017). These

`

findings are consistent with studies in $Na_v1.8$-null mice, which do not develop visceral hypersensitivity after intracolonic administration of sensitising agents such as capsaicin (TRPV1 agonist) and mustard oil (TRPA1 agonist). Furthermore, unlike their wild-type littermates, DRG neurons from $Na_v1.8$-null mice do not display enhanced neuronal hyperexcitability following intestinal infection with *Nippostrongylus brasiliensis* (Laird et al. 2002; Hillsley et al. 2006).

Inflammatory mediators acting via GPCRs are powerful modulators of $Na_v1.8$ currents and are believed to underlie increased excitability of nociceptive DRG neurons and associated hyperalgesia (Beyak et al. 2004). In this regard, colon-innervating DRG neurons incubated with supernatant from colonic biopsies from patients with active ulcerative colitis (a chronic inflammatory bowel disease) show increased action potential discharge and enhanced $Na_v1.8$ currents (Ibeakanma & Vanner, 2010). These effects were replicated by incubation with tumour necrosis factor α (TNFα), whose levels are enhanced in the ulcerative colitis supernatant. Similar sensitising effects have been reported for prostaglandin E2 (PGE2), adenosine, serotonin (5-HT), ATP, as well as nerve growth factor (NGF), which may persist during and possibly after the inflammation as a result of increased expression of $Na_v1.8$ channels (Gold, 1999; Gold et al. 2002; Beyak et al. 2004). Recent data, however, indicate that these effects are not limited to inflammatory conditions, but may extend to non-inflammatory chronic pain states. Partial colonic obstruction is associated with an increase in $Na_v1.8$ mRNA expression, as well as enhanced TTX-R Na^+ currents and referred *in vivo* hyperalgesia, effects that were abolished by anti-NGF treatment (King et al. 2009; Ibeakanma & Vanner, 2010).

Decreased TTX-R currents occur in bladder-innervating DRG neurons from T8 spinal transected rats (Yoshimura & deGroat, 1997), which has since been attributed to a down-regulation of $Na_v1.8$ (Black et al. 2003). This change is only seen in bladder-innervating DRG neurons and is accompanied by an up-regulation of TTX-S current, which may also enhance the excitability of these afferent neurons. Knock-down of $Na_v1.8$ in rats at spinal levels L6–S1, known to contain the majority of bladder sensory terminals, does not have an effect on intercontraction intervals following cystometry with saline; however, intravesical acetic acid-induced hyper-reflexia is attenuated in knock-down rats (Yoshimura et al. 2001). $Na_v1.8$-null mice develop normal pain and inflammatory responses during cyclophosphamide-induced cystitis compared to littermates (Laird et al. 2002), and pain behaviours are sustained in rats with cyclophosphamide-induced cystitis following intraperitoneal administration of A-803467 (Jarvis et al. 2007).

Cross-organ sensitisation of the gastrointestinal and lower urinary tract is evident clinically and in animal models (Malykhina et al. 2004, 2012; Lei & Malykhina, 2012), highlighting the importance of understanding the mechanisms of viscero-visceral crosstalk. Several studies report increases in TTX-resistant Na^+ current in bladder-innervating DRG neurons following colitis, implicating some involvement of TTX-R channels in bladder pain as a consequence of gastrointestinal tract inflammation. C-fibre bladder-innervating DRG neurons, involved in the transduction of noxious stimuli signalling (Fowler et al. 2008), in the majority express TTX-R currents (Yoshimura & deGroat, 1997). Collectively, experimental findings to date indicate that $Na_v1.8$ is not crucial for visceral pain signalling from the bladder in response to several noxious stimuli, but it may have an important role during referred hyperalgesia and in response to certain irritants.

2.11 $Na_v1.9$

Several human $Na_v1.9$ channelopathies are associated with congenital episodic pain syndromes, painful neuropathy, and an insensitivity to pain (Huang et al. 2014, 2017). $Na_v1.9$ channels are preferentially expressed in small-diameter nociceptors (Dib-Hajj et al. 1998; Tate et al. 1998), and mediate ultraslow or persistent TTX-R Na^+ currents. Due to their kinetic properties, $Na_v1.9$ channels are unlikely to contribute to action potential generation, but instead regulate neuronal excitability by setting the resting membrane potential closer to threshold (Dib-Hajj et al. 1998, 2002; Tate et al. 1998). In colonic afferents, action potential firing in response to colonic ramp distension is reduced in $Na_v1.9^{-/-}$ mice and accompanied by a run-down of responses to repeated phasic distension (Hockley et al. 2014). Similar to $Na_v1.8$ channels,

several studies indicate that $Na_v1.9$ currents can be enhanced via GPCRs (Maingret et al. 2008; Ostman et al. 2008; Vanoye et al. 2013; Hockley et al. 2016b). Colonic afferent excitatory responses to the application of multiple inflammatory mediators (applied at once, either in the form of supernatants from chronically inflamed human bowel or as an experimental inflammatory soup containing ATP, PGE2, bradykinin, histamine and 5-HT) are significantly reduced in visceral afferents from $Na_v1.9^{-/-}$ mice (Hockley et al. 2014, 2016a) (**Table 2.2**).

$Na_v1.9^{-/-}$ mice have similar baseline visceromotor responses to colonic distension to wild-type littermates, but reduced visceral hypersensitivity *in vivo* after colonic inflammation induced by activation of toll-like receptor 7 (Martinez & Melgar, 2008). Neuronal hyperexcitability following *Nippostrongylus bransiliensis* infection is unchanged in $Na_v1.9^{-/-}$ mice compared to wild-type littermates, reporting similar action potential characteristics and excitability of colon-innervating DRG neurons (Hillsley et al. 2006). Likewise, others do not see changes in $Na_v1.9$ protein expression in colon-innervating DRG neurons, nor differences in either the numbers of neurons expressing persistent TTX-R ($Na_v1.9$) currents or the magnitude of these currents in acute TNBS-induced colitis (Beyak et al. 2004; King et al. 2009). It is unclear whether these discrepancies in the contribution of $Na_v1.9$ to neuronal (hyper)excitability relates to differences in knock-out constructs and mice strains, or to differences in the inflammatory insult studied. The latter may be of considerable importance as inflammatory mediators such as bradykinin, ATP, histamine, PGE2 and noradrenaline (norepinephrine), potentiate $Na_v1.9$ channel activity when applied conjointly, but fail to modulate $Na_v1.9$ currents when applied separately (Maingret et al. 2008).

$Na_v1.9$ channels are also present in myenteric plexus neurons in human, mouse, rat and guinea-pig (Rugiero et al. 2003; Padilla et al. 2007; Copel et al. 2009; Osorio et al. 2014) pointing towards an additional role in intestinal motor function. In line with this, colonic migrating motor complex patterns are altered in $Na_v1.9^{-/-}$ mice (Copel et al. 2013). Moreover, expression of $Na_v1.9$ channels is decreased in submucosal and myenteric plexus neurons (most likely intrinsic primary afferent neurons) in Hirschsprung's disease (O'Donnell et al. 2016). Interestingly, these findings apply not only to aganglionic bowel sections, but in some patients extend to those sections containing normal ganglia numbers, which could explain some of the post-surgery bowel dysmotility issues frequently encountered by these patients (O'Donnell et al. 2016). Conversely, a gain-of-function mutation (L811P) in the $Na_v1.9$ gene, *SCN11A*, identified in three unrelated individuals with congenital insensitivity to pain, is associated with severe gastrointestinal dysmotility, including alternating episodes of diarrhoea and constipation (Leipold et al. 2013; Woods et al. 2015). In contrast, other gain-of-function mutations are predominantly linked to chronic pain syndromes such as autosomal-dominant episodic pain and small-fibre neuropathy (Zhang et al. 2013; Huang et al. 2014; Han et al. 2015).

No difference is observed in basal urodynamics between wild-type and $Na_v1.9^{-/-}$ mice; however, the change of urodynamic parameters associated with cyclophosphamide-induced cystitis is absent in $Na_v1.9^{-/-}$ mice, as well as attenuation of PGE2-induced afferent excitability during bladder distension (Ritter et al. 2009). It remains to be investigated whether this involvement of $Na_v1.9$ in bladder nociception is due to functional up-regulation of $Na_v1.9$ in bladder afferents, or whether $Na_v1.9$ has a role in central processing of bladder nociceptive pathways.

Table 2.2 Predominant Na$_v$ isoforms contributing functionally to visceral sensation.

A. Healthy states ↓			
Species	**Test**	**Response**	**Reference**
Human	Appendix distension (*ex vivo* extracellular recordings of mesenteric afferents) before and after exposure to PF-5198007 (Na$_v$1.7 antagonist)	No difference in mesenteric afferent peak firing	(Hockley et al. 2017)
Mouse	Colonic mechanical stimulation (*ex vivo* extracellular recordings of colonic afferents in the splanchnic nerve) after Hm1a (highly selective Na$_v$1.1 agonist, mucosal application)	Increase in colonic nociceptor response to mechanical stimuli in a sub-population of afferents.	(Osteen et al. 2016)
	Colonic stretch (*ex vivo* extracellular recordings of colorectal afferents in the pelvic nerve) μ-conotoxin GIIIa, and μ-conotoxin PIIIa, serosal/mucosal application)	Reduced action potential firing of stretch-sensitive afferent response	(Feng et al. 2015)
	Colonic stretch (*ex vivo* extracellular recordings of colorectal afferents in the pelvic nerve) - ProTxII (Na$_v$1.7 antagonist, serosal/mucosal application)	No difference in stretch-sensitive afferent response	
	Ciguatoxin (pan-Na$_v$ agonist) (intracolonic)	Increased pain behavioural response	(Inserra et al. 2017)
	Colonic incubation with A-803467 (Na$_v$1.8 antagonist) (*ex vivo* extracellular recordings of colorectal nociceptors), followed by ciguatoxin	Inhibited afferent firing induced by ciguatoxin	
	Incubation with supernatant from colitis patients	Increased excitability of colonic DRG neurons associated with enhanced Na$_v$1.8 currents	(Ibeakanma & Vanner, 2010)
	Tumour necrosis factor-α incubation		

B. Knock-out and knock-down models ↓				
Model (species)	**Test**		**Response**	**Reference**
Na$_v$1.7$^{Nav1.8}$ (mouse)	Formalin (intraplantar)		Reduction in pain behavioural response in phase I and phase II of formalin response	(Nassar et al. 2004)
	Complete Freund's adjuvant (intraplantar)		Reduction in thermal hyperalgesia and mechanical allodynia from day 1 to day 10	
	Carrageenan (intraplantar)		Reduction in thermal hyperalgesia from 1 to 4 h	
	Nerve growth factor (intraplantar)		Absence of phase I thermal hyperalgesia and reduction in phase II	
	Colonic distension (*ex vivo* extracellular recordings of lumbar splanchnic nerve activity)		No difference in afferent firing in physiological range (0–80 mmHg)	(Hockley et al. 2017)
	Reduction in firing in supramaximal range (80–145 mmHg)			
	Capsaicin (intracolonic)		Normal pain behavioural response	
	Mustard oil (intracolonic)			
	Cyclophosphamide-induced cystitis		Normal level of referred mechanical hyperalgesia responses	
Na$_v$1.8$^{-/-}$ (mouse)	Whole-cell patch clamp		Reduced action potential amplitude in retrogradely labelled neurons projecting to the peritoneal cavity (DRG, T9–T13)	(Hillsley et al. 2006)
	Nippostrongylus brasiliensis post-infectious stage, whole-cell patch clamp		Absence of neuronal hyperexcitability 19–25 days post-infection in retrogradely labelled neurons projecting to the peritoneal cavity (DRG, T9–T13)	
	Acetylcholine (intraperitoneal injection)		Normal pain behavioural response	(Laird et al. 2002)
	Capsaicin (intracolonic)		Reduced pain behavioural response	
	Mustard oil (intracolonic)			
	Cyclophosphamide-induced cystitis		Normal pain and inflammatory responses	
Na$_v$1.8 knock-down (L6–S1) (rat)	Cystometry (saline)		No change in intercontraction intervals	(Yoshimura et al. 2001)
	Acetic acid (intravesical)		Hyper-reflexia attenuated	

		Whole-cell patch clamp	Normal excitability and action potential characteristics in colonic neurons (DRG T9–T13)		(Hillsley et al. 2006)
Na$_v$1.9$^{-/-}$ (mouse)		*Nippostrongylus brasiliensis* post-infectious stage, whole-cell patch clamp	No change in neuronal hyperexcitability 19–25 days post-infection in retrogradely labelled neurons projecting to the peritoneal cavity (DRG, T9–T13)		
		Colorectal distension	Normal pain behavioural response		(Martinez & Melgar, 2008)
		R-848 (toll-like receptor 7 activator)-induced colonic inflammation, colorectal distension	Reduced pain behavioural response		
		Colonic distension (*ex vivo* extracellular recordings of splanchnic nerve activity)	Reduced afferent discharge		(Hockley et al. 2014)
		Ex vivo extracellular recordings of lumbar splanchnic nerve activity following inflammatory soup (bradykinin, ATP, histamine, PGE2 and 5-HT), or inflammatory bowel disease patient colonic supernatant application	Reduced afferent fibre responses		
		Ex vivo extracellular recordings of lumbar splanchnic nerve activity following UTP (P2Y2 and P2Y4 agonist) or ADP (P2Y1, P2Y12 and P2Y13 agonist) application	Reduced afferent fibre responses		(Hockley et al. 2016a)
		Cystometry (saline)	No change in basal urodynamics		(Ritter et al. 2009)
		Cyclophosphamide-induced cystitis			
		Bladder distension (*ex vivo* extracellular recordings of bladder nerve activity) following PGE2 bladder infusion application	Reduced afferent excitability		

C. Inflammatory hypersensitivity models ↓					
Model/disease (species)	Test			Response	Reference
Neonatal induced colitis (rat)	Protein expression	Increase in Na$_v$1.7 and Na$_v$1.8 protein in colonic (DRG, T13–L2) neurons post-inflammation			(Qu et al. 2013)
	Whole-cell patch-clamp	Increase in Na$^+$ current in colonic neurons (DRG, T13–L2) 6 weeks post-inflammation			
		No change in Na$^+$ current in colonic neurons (DRG, T13–L2) 10 weeks post-inflammation			
		No change in Na$^+$ current in non-colonic neurons (DRG, L4–L5) 6 or 10 weeks post inflammation			
Acute TNBS-induced colitis (mouse)	Whole-cell patch clamp	Increased slow TTX-R Na$^+$ current in colonic neurons (DRG, T9–L1) 7-10 days post-induction			(Beyak et al. 2004)
		No change in persistent TTX-R Na$^+$ currents in colonic neurons (DRG, T9–L1) 7–10 days post-induction			
	Gene and protein expression	No change in Na$_v$1.7 mRNA or protein in retrogradely labelled colonic neurons (DRG, T9–T13) 1 week post-induction			(King et al. 2009)
	Gene expression	Tenfold reduction in Na$_v$1.8 mRNA 2–4 days post-induction, no change at day 7, in retrogradely labelled colonic neurons (DRG, T9–T13)			
	Protein expression	No change in Na$_v$1.8 protein 2–4 days post-induction, up-regulation at day 7, in retrogradely labelled colonic neurons (DRG, T9–T13) 1 week post-induction			
		No change in Na$_v$1.9 protein in colonic neurons (DRG, T9–T13) day 7 post-induction			
Post-TNBS-induced colitis (mouse)	Whole-cell patch clamp in the presence of Hm1a (Na$_v$1.7 agonist)	Pronounced increase in excitability of colonic DRG neurons: significant lowering of rheobase and a dramatic increase in the number of action potentials fired at 2-times rheobase			(Osteen et al. 2016)
	Gene expression	Up-regulation of Na$_v$1.7 mRNA in retrogradely labelled colonic neurons (DRG, L6–S1) 4 weeks post-induction			(Campaniello et al. 2016)

`

Nippostrongylus brasiliensis post-infectious stage (mouse)	Gene expression	No change in $Na_v1.8$ or $Na_v1.9$ mRNA 19–25 days post-infection in retrogradely labelled neurons projecting to the peritoneal cavity (DRG, T9–T13)	(Hillsley et al. 2006)
Interstitial cystitis/bladder pain syndrome (human)	Neosaxitoxin (blocker of TTX-S Na_v channels) (bladder infiltration)	Analgesia and reduced frequency lasting up to 90 days	(Manriquez et al. 2015)
Cyclophosphamide-induced cystitis (rat)	A-803467 administration (intraperitoneal)	No change in pain behavioural response	(Jarvis et al. 2007)

D. Non-inflammatory hypersensitivity models ↓			
Model/disease (species)	Test	Response	Reference
Clinical rectal hypersensitivity (human)	Protein expression (full thickness rectal biopsies)	Increased $Na_v1.7$-immunoreactive nerve fibres in mucosal, submucosal and muscle layers	(Yiangou et al. 2007)
Maternal separation model (visceral hypersensitivity) (rat)	Gene expression	No change in $Na_v1.8$ mRNA in colonic neurons (DRG, T13–L2)	(Hu et al. 2013a)
	Protein expression	Increase in $Na_v1.8$ protein in colonic neurons (DRG, T13–L2)	
	Whole-cell patch clamp	Increased TTX-R Na+ current in colonic neurons (DRG, T13–L2)	
Streptozotocin-induced diabetes (visceral hypersensitivity) (rat)	Protein expression	Increase in $Na_v1.7$ and $Na_v1.8$ protein in colonic neurons (DRG, T13–L2)	(Hu et al. 2016)
	Whole-cell patch clamp	Increased TTX-R Na+ current in colonic neurons (DRG, T13–L2)	
Partial colonic obstruction (visceral hypersensitivity) (rat)	Gene expression	Increase in $Na_v1.8$ mRNA in colonic neurons (DRG, T13–L2)	(Lin et al. 2017)
	Whole-cell patch clamp	Increased TTX-R Na+ current in colonic neurons (DRG, T13–L2)	
T8 spinal transection (rat)	Whole-cell patch clamp	Reduced TTX-R Na+ current in bladder neurons	(Yoshimura & deGroat, 1997)

2.12 Conclusion

Recent findings highlight the diversity in expression patterns of Na_v isoforms in abdominal visceral organs. This diversity extends across neurons (enteric, extrinsic sensory DRG innervating the intestine or bladder) and non-neuronal cells (intestinal enterochromaffin cells, intestinal smooth muscle cells, and interstitial cells of Cajal). Na_v channels have a range of functions in health and disease and we are only now, with the development of novel pharmacological and genetic tools, beginning to unpick their complex physiological and pathophysiological interactions. $Na_v1.1$, $Na_v1.6$, $Na_v1.8$ and $Na_v1.9$, contribute to visceral hypersensitivity, particularly within colonic pathways, and respond to inflammatory mediators in pathophysiological models (**Figure 2.2**).

Enterochromaffin cells

$Na_v1.3$

Colonic smooth muscle cells

$Na_v1.5$

Spinal cord

Splanchic nerves

Pelvic nerves

Colon

$Na_v1.1$

$Na_v1.6$

$Na_v1.8$

$Na_v1.9$

Colon innervating extrinsic
sensory afferent nerve terminal

Bladder

$Na_v1.8$

Bladder innervating extrinsic
sensory afferent nerve terminal
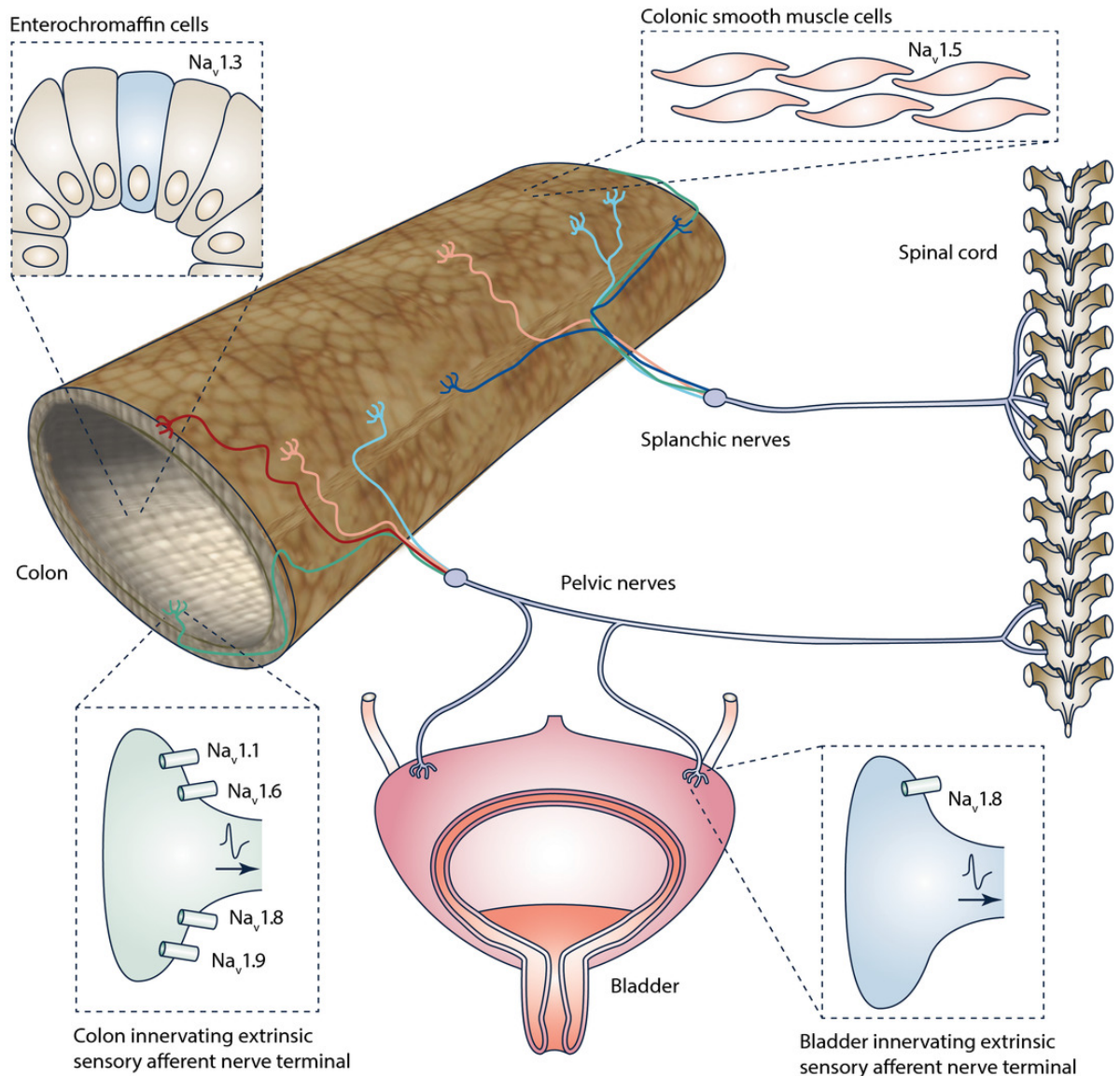
The Journal of
Physiology

Figure 2.2: Current understanding of how specific voltage-gated sodium channels (Na_v) contribute to the functioning of neurons and non-neuronal cells within visceral organs.

Whilst $Na_v1.3$ contributes to enterochromaffin cell function and $Na_v1.5$ contributes to intestinal smooth muscle cells and interstitial cells of Cajal function, there is currently no determined function in visceral afferents for $Na_v1.2$, $Na_v1.3$, $Na_v1.4$ or $Na_v1.5$, despite significant mRNA expression of $Na_v1.2$ and $Na_v1.5$ in visceral afferent pathways. $Na_v1.7$ is one of the most extensively expressed and studied Na_v channels, but a role in visceral pain, like that attributed to $Na_v1.7$ in somatic pain studies is currently unclear. Although many of these Na_v channels have been investigated under physiological conditions or in models of acute pain, chronic visceral pain models are necessary for the determination of a precise role in long term pathological visceral pain. Future studies would benefit from the further development of novel, specific agonists and antagonists, as we have seen with recent advances in the role of $Na_v1.1$ in mechanical pain. Likewise, selective Na_v modulators with low systemic uptake for *in vivo* studies will advance our understanding of Na_v channels in visceral pain signalling and the suitability of targeting Na_v channels in the treatment of pain originating in the distal gut and bladder.

2.13 Additional information

Competing interests: In relation to the content covered within this review, the authors have nothing to declare.

2.14 Author contributions

All authors contributed to searching the published literature and to writing the review. All authors approved the final version and agree to be accountable for all aspects of the work. All persons designated as authors qualify for authorship, and all those who qualify for authorship are listed.

2.15 Funding

2.16 Literature cited

Akopian AN, Souslova V, England S, Okuse K, Ogata N, Ure J, Smith A, Kerr BJ, McMahon SB, Boyce S, Hill R, Stanfa LC, Dickenson AH & Wood JN (1999). The tetrodotoxin-resistant sodium channel SNS has a specialized function in pain pathways. *Nat Neurosci* 2, 541–548.

Alcaino C, Farrugia G & Beyder A (2017). Mechanosensitive piezo channels in the gastrointestinal tract. *Curr Top Membr* 79, 219–244.

Beckh S, Noda M, Lübbert H & Numa S (1989). Differential regulation of three sodium channel messenger RNAs in the rat central nervous system during development. *EMBO J* 8, 3611–3616.

Bellono NW, Bayrer JR, Leitch DB, Castro J, Zhang C, O'Donnell TA, Brierley SM, Ingraham HA & Julius D (2017). Enterochromaffin cells are gut chemosensors that couple to sensory neural pathways. *Cell* 170, 185–198.e16.

Bennett DL & Woods CG (2014). Painful and painless channelopathies. *Lancet Neurol* 13, 587–599.

Beyak MJ, Ramji N, Krol KM, Kawaja MD & Vanner SJ (2004). Two TTX-resistant Na^+ currents in mouse colonic dorsal root ganglia neurons and their role in colitis-induced hyperexcitability. *Am J Physiol Gastrointest Liver Physiol* 287, G845–G855.

Beyder A & Farrugia G (2016). Ion channelopathies in functional GI disorders. *Am J Physiol Gastrointest Liver Physiol* 311, G581–G586.

Beyder A, Gibbons SJ, Mazzone A, Strege PR, Saravanaperumal SA, Sha L, Higgins S, Eisenman ST, Bernard CE, Geurts A, Kline CF, Mohler PJ & Farrugia G (2016). Expression and function of the *Scn5a*-encoded voltage-gated sodium channel $Na_v1.5$ in the rat jejunum. *Neurogastroenterol Motil* 28, 64–73.

Beyder A, Mazzone A, Strege PR, Tester DJ, Saito YA, Bernard CE, Enders FT, Ek WE, Schmidt PT, Dlugosz A, Lindberg G, Karling P, Ohlsson B, Gazouli M, Nardone G, Cuomo R, Usai-Satta P, Galeazzi F, Neri M, Portincasa P, Bellini M, Barbara G, Camilleri M, Locke GR III, Talley NJ, D'Amato M, Ackerman MJ & Farrugia G (2014). Loss-of-function of the voltage-gated sodium channel $Na_v1.5$ (channelopathies) in patients with irritable bowel syndrome. *Gastroenterology* 146, 1659–1668.

Bielefeldt K, Ozaki N & Gebhart GF (2002a). Experimental ulcers alter voltage-sensitive sodium currents in rat gastric sensory neurons. *Gastroenterology* 122, 394–405.

Bielefeldt K, Ozaki N & Gebhart GF (2002b). Mild gastritis alters voltage-sensitive sodium currents in gastric sensory neurons in rats. *Gastroenterology* 122, 752–761.

Black JA, Cummins TR, Yoshimura N, de Groat WC & Waxman SG (2003). Tetrodotoxin-resistant sodium channels $Na_v1.8$/SNS and $Na_v1.9$/NaN in afferent neurons innervating urinary bladder in control and spinal cord injured rats. *Brain Res* 963, 132–138.

Black JA, Dib-Hajj S, McNabola K, Jeste S, Rizzo MA, Kocsis JD & Waxman SG (1996). Spinal sensory neurons express multiple sodium channel alpha-subunit mRNAs. *Brain Res Mol Brain Res* 43, 117–131.

Black JA, Frezel N, Dib-Hajj SD & Waxman SG (2012). Expression of $Na_v1.7$ in DRG neurons extends from peripheral terminals in the skin to central preterminal branches and terminals in the dorsal horn. *Mol Pain* 8, 82.

Black JA & Waxman SG (2013). Noncanonical roles of voltage-gated sodium channels. *Neuron* 80, 280–291.

Bradding P, Okayama Y, Kambe N & Saito H (2003). Ion channel gene expression in human lung, skin, and cord blood-derived mast cells. *J Leukoc Biol* 73, 614–620.

Branco T, Tozer A, Magnus CJ, Sugino K, Tanaka S, Lee AK, Wood JN & Sternson SM (2016). Near-perfect synaptic integration by Na$_v$1.7 in hypothalamic neurons regulates body weight. *Cell* 165, 1749–1761.

Brierley SM (2010). Molecular basis of mechanosensitivity. *Auton Neurosci* 153, 58–68.

Brierley SM (2016). Altered ion channel/receptor expression and function in extrinsic sensory neurons: the cause of and solution to chronic visceral pain? *Adv Exp Med Biol* 891, 75–90.

Brierley SM, Jones RCW, Gebhart GF & Blackshaw LA (2004). Splanchnic and pelvic mechanosensory afferents signal different qualities of colonic stimuli in mice. *Gastroenterology* 127, 166–178.

Brierley SM & Linden DR (2014). Neuroplasticity and dysfunction after gastrointestinal inflammation. *Nat Rev Gastroenterol Hepatol* 11, 611–627.

Campaniello MA, Harrington AM, Martin CM, Ashley Blackshaw L, Brierley SM & Hughes PA (2016). Activation of colorectal high-threshold afferent nerves by interleukin-2 is tetrodotoxin-sensitive and upregulated in a mouse model of chronic visceral hypersensitivity. *Neurogastroenterol Motil* 28, 54–63.

Carithers LJ, Ardlie K, Barcus M, Branton PA, Britton A, Buia SA, Compton CC, DeLuca DS, Peter-Demchok J, Gelfand ET, Guan P, Korzeniewski GE, Lockhart NC, Rabiner CA, Rao AK, Robinson KL, Roche NV, Sawyer SJ, Segre AV, Shive CE, Smith AM, Sobin LH, Undale AH, Valentino KM, Vaught J, Young TR & Moore HM; GTEx Consortium (2015). A novel approach to high-quality postmortem tissue procurement: The GTEx Project. *Biopreserv Biobank* 13, 311–319.

Carrithers LM, Hulseberg P, Sandor M & Carrithers MD (2011). The human macrophage sodium channel Na$_v$1.5 regulates mycobacteria processing through organelle polarization and localized calcium oscillations. *FEMS Immunol Med Microbiol* 63, 319–327.

Carrithers MD, Dib-Hajj S, Carrithers LM, Tokmoulina G, Pypaert M, Jonas EA & Waxman SG (2007). Expression of the voltage-gated sodium channel Na$_v$1.5 in the macrophage late endosome regulates endosomal acidification. *J Immunol* 178, 7822–7832.

Castro J, Harrington AM, Garcia-Caraballo S, Maddern J, Grundy L, Zhang J, Page G, Miller PE, Craik DJ, Adams DJ & Brierley SM (2017). α-Conotoxin Vc1.1 inhibits human dorsal root ganglion neuroexcitability and mouse colonic nociception via GABA$_B$ receptors. *Gut* 66, 1083–1094.

Castro J, Harrington AM, Hughes PA, Martin CM, Ge P, Shea CM, Jin H, Jacobson S, Hannig G, Mann E, Cohen MB, MacDougall JE, Lavins BJ, Kurtz CB, Silos-Santiago I, Johnston JM, Currie MG, Blackshaw LA & Brierley SM (2013). Linaclotide inhibits colonic nociceptors and relieves abdominal pain via guanylate cyclase-C and extracellular cyclic guanosine 3′,5′-monophosphate. *Gastroenterology* 145, 1334–1346.

Catterall WA (2012). Voltage-gated sodium channels at 60: structure, function and pathophysiology. *J Physiol 590, 2577–2589.*

Catterall WA, Goldin AL & Waxman SG (2005). International Union of Pharmacology. XLVII. Nomenclature and structure-function relationships of voltage-gated sodium channels. *Pharmacol Rev* 57, 397–409.

Chang W, Berta T, Kim YH, Lee S, Lee S-Y & Ji R-R (2018). Expression and role of voltage-gated sodium channels in human dorsal root ganglion neurons with special focus on Na$_v$1.7, species differences, and regulation by paclitaxel. *Neurosci Bull* 34, 4–12.

Christianson JA & Davis BM (2010). The role of visceral afferents in disease In Translational Pain Research: From Mouse to Man, chap. 3, ed. Kruger L, editor; & Light AR, editor. CRC Press/Taylor & Francis, Boca Raton, FL, USA.

Copel C, Clerc N, Osorio N, Delmas P & Mazet B (2013). The Na$_v$1.9 channel regulates colonic motility in mice. *Front Neurosci* 7, 1–8.

Copel C, Osorio N, Crest M, Gola M, Delmas P & Clerc N (2009). Activation of neurokinin 3 receptor increases Na$_v$1.9 current in enteric neurons. *J Physiol* 587, 1461–1479.

Cox JJ, Reimann F, Nicholas AK, Thornton G, Roberts E, Springell K, Karbani G, Jafri H, Mannan J, Raashid Y, Al-Gazali L, Hamamy H, Valente EM, Gorman S, Williams R, McHale DP, Wood JN, Gribble FM & Woods CG (2006). An SCN9A channelopathy causes congenital inability to experience pain. *Nature* 444, 894–898.

Dang K, Bielefeldt K & Gebhart GF (2004). Gastric ulcers reduce A-type potassium currents in rat gastric sensory ganglion neurons. *Am J Physiol Gastrointest Liver Physiol* 286, G573–G579.

de Araujo AD, Mobli M, Castro J, Harrington AM, Vetter I, Dekan Z, Muttenthaler M, Wan J, Lewis RJ, King GF, Brierley SM & Alewood PF (2014). Selenoether oxytocin analogues have analgesic properties in a mouse model of chronic abdominal pain. *Nat Commun* 5, 1–12.

Deshpande MA, Wang J, Preiksaitis HG, Laurier LG & Sims SM (2002). Characterization of a voltage-dependent Na+ current in human esophageal smooth muscle. *Am J Physiol Cell Physiol* 283, C1045–C1055.

Dib-Hajj S, Black JA, Cummins TR & Waxman SG (2002). NaN/Na$_v$1.9: a sodium channel with unique properties. *Trends Neurosci* 25, 253–259.

`

Dib-Hajj SD, Black JA & Waxman SG (2015). Na$_v$1.9: a sodium channel linked to human pain. *Nat Rev Neurosci* 16, 511–519.

Dib-Hajj SD, Tyrrell L, Black JA & Waxman SG (1998). NaN, a novel voltage-gated Na channel, is expressed preferentially in peripheral sensory neurons and down-regulated after axotomy. *Proc Natl Acad Sci USA* 95, 8963–8968.

Du X & Gamper N (2013). Potassium channels in peripheral pain pathways: expression, function and therapeutic potential. *Curr Neuropharmacol* 11, 621–640.

Duflocq A, Le Bras B, Bullier E, Couraud F & Davenne M (2008). Na$_v$1.1 is predominantly expressed in nodes of Ranvier and axon initial segments. *Mol Cell Neurosci* 39, 180–192.

Enck P, Aziz Q, Barbara G, Farmer AD, Fukudo S, Mayer EA, Niesler B, Quigley EM, Rajilic-Stojanovic M, Schemann M, Schwille-Kiuntke J, Simren M, Zipfel S & Spiller RC (2016). Irritable bowel syndrome. *Nat Rev Dis Primers* 2, 16014.

Farrell KE, Callister RJ & Keely S (2014). Understanding and targeting centrally mediated visceral pain in inflammatory bowel disease. *Front Pharmacol* 5, 1–4.

Feng B, Zhu Y, La JH, Wills ZP & Gebhart GF (2015). Experimental and computational evidence for an essential role of Na$_v$1.6 in spike initiation at stretch-sensitive colorectal afferent endings. *J Neurophysiol* 113, 2618–2634.

Feng S, Pflueger M, Lin SX, Groveman BR, Su J & Yu XM (2012). Regulation of voltage-gated sodium current by endogenous Src family kinases in cochlear spiral ganglion neurons in culture. *Pflugers Arch* 463, 571–584.

Fertleman CR, Baker MD, Parker KA, Moffatt S, Elmslie FV, Abrahamsen B, Ostman J, Klugbauer N, Wood JN, Gardiner RM & Rees M (2006). *SCN9A* mutations in paroxysmal extreme pain disorder: allelic variants underlie distinct channel defects and phenotypes. *Neuron* 52, 767–774.

Flegel C, Schobel N, Altmuller J, Becker C, Tannapfel A, Hatt H & Gisselmann G (2015). RNA-Seq analysis of human trigeminal and dorsal root ganglia with a focus on chemoreceptors. *PLoS One* 10, e0128951.

Flinspach M, Xu Q, Piekarz AD, Fellows R, Hagan R, Gibbs A, Liu Y, Neff RA, Freedman J, Eckert WA, Zhou M, Bonesteel R, Pennington MW, Eddinger KA, Yaksh TL, Hunter M, Swanson RV & Wickenden AD (2017). Insensitivity to pain induced by a potent selective closed-state Na$_v$1.7 inhibitor. *Sci Rep* 7, 39662.

Fowler CJ, Griffiths D & de Groat WC (2008). The neural control of micturition. *Nat Rev Neurosci* 9, 453–466.

Fukuoka T, Kobayashi K, Yamanaka H, Obata K, Dai Y & Noguchi K (2008). Comparative study of the distribution of the α-subunits of voltage-gated sodium channels in normal and axotomized rat dorsal root ganglion neurons. *J Comp Neurol* 510, 188–206.

Gaskin DJ & Richard P (2012). The economic costs of pain in the United States. *J Pain* 13, 715–724.

Gebhart GF, Bielefeldt K & Ozaki N (2002). Gastric hyperalgesia and changes in voltage gated sodium channel function in the rat. *Gut* 51, i15.

Geppetti P, Veldhuis NA, Lieu T & Bunnett NW (2015). G protein-coupled receptors: dynamic machines for signaling pain and itch. *Neuron* 88, 635–649.

Gingras J, Smith S, Matson DJ, Johnson D, Nye K, Couture L, Feric E, Yin RY, Moyer BD, Peterson ML, Rottman JB, Beiler RJ, Malmberg AB & McDonough SI (2014). Global Na$_v$1.7 knockout mice recapitulate the phenotype of human congenital indifference to pain. *PLoS One* 9, e105895.

Gold MS (1999). Tetrodotoxin-resistant Na$^+$ currents and inflammatory hyperalgesia. *Proc Natl Acad Sci USA* 96, 7645–7649.

Gold MS, Zhang L, Wrigley DL & Traub RJ (2002). Prostaglandin E2 modulates TTX-R I$_{Na}$ in rat colonic sensory neurons. *J Neurophysiol* 88, 1512–1522.

Goldberg YP, MacFarlane J, MacDonald ML, Thompson J, Dube MP, Mattice M, Fraser R, Young C, Hossain S, Pape T, Payne B, Radomski C, Donaldson G, Ives E, Cox J, Younghusband HB, Green R, Duff A, Boltshauser E, Grinspan GA, Dimon JH, Sibley BG, Andria G, Toscano E, Kerdraon J, Bowsher D, Pimstone SN, Samuels ME, Sherrington R & Hayden MR (2007). Loss-of-function mutations in the Na$_v$1.7 gene underlie congenital indifference to pain in multiple human populations. *Clin Genet* 71, 311–319.

Gonzalez-Cano R, Tejada MA, Artacho-Cordon A, Nieto FR, Entrena JM, Wood JN & Cendan CM (2017). Effects of tetrodotoxin in mouse models of visceral pain. *Mar Drugs* 15, E188.

Grundy D (2002). Neuroanatomy of visceral nociception: vagal and splanchnic afferent. *Gut* 51 Suppl. 1, i2–5.

GTEx Consortium; Laboratory, Data Analysis &Coordinating Center (LDACC) – Analysis Working Group; Statistical Methods groups – Analysis Working Group; Enhancing GTEx (eGTEx) groups; NIH Common Fund; NIH/NCI; NIH/NHGRI; NIH/NIMH; NIH/NIDA; Biospecimen Collection Source Site – NDRI; Biospecimen Collection Source Site – RPCI; Biospecimen Core Resource – VARI; Brain Bank Repository – University of Miami Brain Endowment Bank; Leidos Biomedical – Project Management; ELSI Study; Genome Browser Data Integration

&Visualization – EBI; Genome Browser Data Integration &Visualization – UCSC Genomics Institute, University of California Santa Cruz; Lead analysts:; Laboratory, Data Analysis &Coordinating Center (LDACC):; NIH program management:; Biospecimen collection:; Pathology:; eQTL manuscript working group: Battle A, Brown CD, Engelhardt BE & Montgomery SB (2017). Genetic effects on gene expression across human tissues. *Nature* 550, 204–213.

Hagen NA, Cantin L, Constant J, Haller T, Blaise G, Ong-Lam M, du Souich P, Korz W & Lapointe B (2017). Tetrodotoxin for moderate to severe cancer-related pain: a multicentre, randomized, double-blind, placebo-controlled, parallel-design trial. *Pain Res Manag* 2017, 7212713.

Hagen NA, Lapointe B, Ong-Lam M, Dubuc B, Walde D, Gagnon B, Love R, Goel R, Hawley P, Ngoc AH & du Souich P (2011). A multicentre open-label safety and efficacy study of tetrodotoxin for cancer pain. *Curr Oncol* 18, e109–e116.

Han C, Yang Y, de Greef BT, Hoeijmakers JG, Gerrits MM, Verhamme C, Qu J, Lauria G, Merkies IS, Faber CG, Dib-Hajj SD & Waxman SG (2015). The domain II S4-S5 linker in Na$_v$1.9: a missense mutation enhances activation, impairs fast inactivation, and produces human painful neuropathy. *Neuromolecular Med* 17, 158–169.

Harrington AM, Brierley SM, Isaacs N, Hughes PA, Castro J & Blackshaw LA (2012). Sprouting of colonic afferent central terminals and increased spinal mitogen-activated protein kinase expression in a mouse model of chronic visceral hypersensitivity. *J Comp Neurol* 520, 2241–2255.

Hetz S, Acikgoez A, Moll C, Jahnke H-G, Robitzki AA, Metzger R & Metzger M (2014). Age-related gene expression analysis in enteric ganglia of human colon after laser microdissection. *Front Aging Neurosci* 6, 276.

Hillsley K, Lin JH, Stanisz A, Grundy D, Aerssens J, Peeters PJ, Moechars D, Coulie B & Stead RH (2006). Dissecting the role of sodium currents in visceral sensory neurons in a model of chronic hyperexcitability using Na$_v$1.8 and Na$_v$1.9 null mice. *J Physiol* 576, 257–267.

Hirano K, Kuratani K, Fujiyoshi M, Tashiro N, Hayashi E & Kinoshita M (2007). K$_v$7.2–7.5 voltage-gated potassium channel (KCNQ2–5) opener, retigabine, reduces capsaicin-induced visceral pain in mice. *Neurosci Lett* 413, 159–162.

Hockley JRF, Boundouki G, Cibert-Goton V, McGuire C, Yip PK, Chan C, Tranter M, Wood JN, Nassar MA, Blackshaw LA, Aziz Q, Michael GJ, Baker MD, Winchester WJ, Knowles CH & Bulmer DC (2014). Multiple roles for Na$_v$1.9 in the activation of visceral afferents by noxious inflammatory, mechanical, and human disease-derived stimuli. *Pain* 155, 1962–1975.

Hockley JRF, González-Cano R, McMurray S, Tejada-Giraldez MA, McGuire C, Torres A, Wilbrey AL, Cibert-Goton V, Nieto FR, Pitcher T, Knowles CH, Baeyens JM, Wood JN, Winchester WJ, Bulmer DC, Cendán CM & McMurray G (2017). Visceral and somatic pain modalities reveal Na$_v$1.7-independent visceral nociceptive pathways. *J Physiol* 595, 2661–2679.

Hockley JRF, Tranter MM, McGuire C, Boundouki G, Cibert-Goton V, Thaha MA, Blackshaw LA, Michael GJ, Baker MD, Knowles CH, Winchester WJ & Bulmer DC (2016a). P2Y receptors sensitize mouse and human colonic nociceptors. *J Neurosci* 36, 2364–2376.

Hockley JRF, Winchester WJ & Bulmer DC (2016b). The voltage-gated sodium channel Na$_v$1.9 in visceral pain. *Neurogastroenterol Motil* 28, 316–326.

Holm AN, Rich A, Miller SM, Strege P, Ou Y, Gibbons S, Sarr MG, Szurszewski JH, Rae JL & Farrugia G (2002). Sodium current in human jejunal circular smooth muscle cells. *Gastroenterology* 122, 178–187.

Hu J, Song Z-Y, Zhang H-H, Qin X, Hu S, Jiang X & Xu G-Y (2016). Colonic hypersensitivity and sensitization of voltage-gated sodium channels in primary sensory neurons in rats with diabetes. *J Neurogastroenterol Motil* 22, 129–140.

Hu S, Xiao Y, Zhu L, Li L, Hu CY, Jiang X & Xu GY (2013a). Neonatal maternal deprivation sensitizes voltage-gated sodium channel currents in colon-specific dorsal root ganglion neurons in rats. *Am J Physiol Gastrointest Liver Physiol* 304, G311–G321.

Hu S, Xu W, Miao X, Gao Y, Zhu L, Zhou Y, Xiao Y & Xu GY (2013b). Sensitization of sodium channels by cystathionine β-synthetase activation in colon sensory neurons in adult rats with neonatal maternal deprivation. *Exp Neurol* 248, 275–285.

Huang J, Han C, Estacion M, Vasylyev D, Hoeijmakers JGJ, Gerrits MM, Tyrrell L, Lauria G, Faber CG, Dib-Hajj SD, Merkies IS, Waxman SG & PROPANE Study Group (2014). Gain-of-function mutations in sodium channel Na$_v$1.9 in painful neuropathy. *Brain* 137, 1627–1642.

Huang J, Vanoye CG, Cutts A, Goldberg YP, Dib-Hajj SD, Cohen CJ, Waxman SG & George AL Jr (2017). Sodium channel Na$_v$1.9 mutations associated with insensitivity to pain dampen neuronal excitability. *J Clin Invest* 127, 2805–2814.

Hughes PA, Brierley SM, Martin CM, Brookes SJH, Linden DR & Blackshaw LA (2009). Post-inflammatory colonic afferent sensitisation: different subtypes, different pathways and different time courses. *Gut* 58, 1333–1341.

Ibeakanma C, Miranda-Morales M, Richards M, Bautista-Cruz F, Martin N, Hurlbut D & Vanner S (2009). Citrobacter rodentium colitis evokes post-infectious hyperexcitability of mouse nociceptive colonic dorsal root ganglion neurons. *J Physiol* 587, 3505–3521.

Ibeakanma C & Vanner S (2010). TNFα is a key mediator of the pronociceptive effects of mucosal supernatant from human ulcerative colitis on colonic DRG neurons. *Gut* 59, 612–621.

Inserra MC, Israel MR, Caldwell A, Castro J, Deuis JR, Harrington AM, Keramidas A, Garcia-Caraballo S, Maddern J, Erickson A, Grundy L, Rychkov GY, Zimmermann K, Lewis RJ, Brierley SM & Vetter I (2017). Multiple sodium channel isoforms mediate the pathological effects of Pacific ciguatoxin-1. *Sci Rep 7*, 42810.

Jarnot M & Corbett AM (2006). Immunolocalization of Na$_v$1.2 channel subtypes in rat and cat brain and spinal cord with high affinity antibodies. *Brain Res* 1107, 1–12.

Jarvis MF, Honore P, Shieh CC, Chapman M, Joshi S, Zhang XF, Kort M, Carroll W, Marron B, Atkinson R, Thomas J, Liu D, Krambis M, Liu Y, McGaraughty S, Chu K, Roeloffs R, Zhong C, Mikusa JP, Hernandez G, Gauvin D, Wade C, Zhu C, Pai M, Scanio M, Shi L, Drizin I, Gregg R, Matulenko M, Hakeem A, Gross M, Johnson M, Marsh K, Wagoner PK, Sullivan JP, Faltynek CR & Krafte DS (2007). A-803467, a potent and selective Na$_v$1.8 sodium channel blocker, attenuates neuropathic and inflammatory pain in the rat. *Proc Natl Acad Sci USA* 104, 8520–8525.

Keating C, Beyak M, Foley S, Singh G, Marsden C, Spiller R & Grundy D (2008). Afferent hypersensitivity in a mouse model of post-inflammatory gut dysfunction: role of altered serotonin metabolism. *J Physiol* 586, 4517–4530.

King DE, Macleod RJ & Vanner SJ (2009). Trinitrobenzenesulphonic acid colitis alters Na$_v$1.8 channel expression in mouse dorsal root ganglia neurons. *Neurogastroenterol Motil* 21, 880–e864.

King GF & Vetter I (2014). No gain, no pain: Na$_v$1.7 as an analgesic target. *ACS Chem Neurosci* 5, 749–751.

Klein CJ, Wu Y, Kilfoyle DH, Sandroni P, Davis MD, Gavrilova RH, Low PA & Dyck PJ (2013). Infrequent *SCN9A* mutations in congenital insensitivity to pain and erythromelalgia. *J Neurol Neurosurg Psychiatry* 84, 386–391.

Klugbauer N, Lacinova L, Flockerzi V & Hofmann F (1995). Structure and functional expression of a new member of the tetrodotoxin-sensitive voltage-activated sodium channel family from human neuroendocrine cells. *EMBO J* 14, 1084–1090.

Kyloh M, Nicholas S, Zagorodnyuk VP, Brookes SJ & Spencer NJ (2011). Identification of the visceral pain pathway activated by noxious colorectal distension in mice. *Front Neurosci* 5, 16.

La JH & Gebhart GF (2011). Colitis decreases mechanosensitive K2P channel expression and function in mouse colon sensory neurons. *Am J Physiol Gastrointest Liver Physiol* 301, G165–G174.

Laedermann CJ, Abriel H & Decosterd I (2015). Post-translational modifications of voltage-gated sodium channels in chronic pain syndromes. *Front Pharmacol* 6, 263.

Lago J, Rodríguez LP, Blanco L, Vieites JM & Cabado AG (2015). Tetrodotoxin, an extremely potent marine neurotoxin: distribution, toxicity, origin and therapeutical uses. *Mar Drugs* 13, 6384–6406.

Laird JM, Souslova V, Wood JN & Cervero F (2002). Deficits in visceral pain and referred hyperalgesia in Na$_v$1.8 (SNS/PN3)-null mice. *J Neurosci* 22, 8352–8356.

Lei Q & Malykhina AP (2012). Colonic inflammation up-regulates voltage-gated sodium channels in bladder sensory neurons via activation of peripheral transient potential vanilloid 1 receptors. *Neurogastroenterol Motil* 24, 575–e257.

Leipold E, Liebmann L, Korenke GC, Heinrich T, Giesselmann S, Baets J, Ebbinghaus M, Goral RO, Stodberg T, Hennings JC, Bergmann M, Altmueller J, Thiele H, Wetzel A, Nuernberg P, Timmerman V, De Jonghe P, Blum R, Schaible H-G, Weis J, Heinemann SH, Huebner CA & Kurth I (2013). A de novo gain-of-function mutation in *SCN11A* causes loss of pain perception. *Nat Genet* 45, 1399–1404.

Lin YM, Fu Y, Winston J, Radhakrishnan R, Sarna SK, Huang LM & Shi XZ (2017). Pathogenesis of abdominal pain in bowel obstruction: Role of mechanical stress-induced upregulation of nerve growth factor in gut smooth muscle cells. *Pain* 158, 583–592.

Luo JL, Qin HY, Wong CK, Tsang SY, Huang Y & Bian ZX (2011). Enhanced excitability and down-regulated voltage-gated potassium channels in colonic DRG neurons from neonatal maternal separation rats. *J Pain* 12, 600–609.

McCormack K, Santos S, Chapman ML, Krafte DS, Marron BE, West CW, Krambis MJ, Antonio BM, Zellmer SG, Printzenhoff D, Padilla KM, Lin Z, Wagoner PK, Swain NA, Stupple PA, de Groot M, Butt RP & Castle NA (2013). Voltage sensor interaction site for selective small molecule inhibitors of voltage-gated sodium channels. *Proc Natl Acad Sci USA* 110, E2724–E2732.

Maingret F, Coste B, Padilla F, Clerc N, Crest M, Korogod SM & Delmas P (2008). Inflammatory mediators increase Na$_v$1.9 current and excitability in nociceptors through a coincident detection mechanism. *J Gen Physiol* 131, 211–225.

Malykhina AP, Qin C, Foreman RD & Akbarali HI (2004). Colonic inflammation increases Na^+ currents in bladder sensory neurons. *Neuroreport* 15, 2601–2605.

Malykhina AP, Wyndaele J-J, Andersson K-E, De Wachter S & Dmochowski RR (2012). Do the urinary bladder and large bowel interact, in sickness or in health? *Neurourol Urodyn* 31, 352–358.

Manriquez V, Caperan DC, Guzman R, Naser M, Iglesia V & Lagos N (2015). First evidence of neosaxitoxin as a long-acting pain blocker in bladder pain syndrome. *Int Urogynecol J* 26, 853–858.

Marcil J, Walczak JS, Guindon J, Ngoc AH, Lu S & Beaulieu P (2006). Antinociceptive effects of tetrodotoxin (TTX) in rodents. *Br J Anaesth* 96, 761–768.

Martinez V & Melgar S (2008). Lack of colonic-inflammation-induced acute visceral hypersensitivity to colorectal distension in $Na_v1.9$ knockout mice. *Eur J Pain* 12, 934–944.

Minett MS, Eijkelkamp N & Wood JN (2014). Significant determinants of mouse pain behaviour. *PLoS One* 9, e104458.

Minett MS, Nassar MA, Clark AK, Passmore G, Dickenson AH, Wang F, Malcangio M & Wood JN (2012). Distinct $Na_v1.7$-dependent pain sensations require different sets of sensory and sympathetic neurons. *Nat Commun* 3, 791.

Minett MS, Pereira V, Sikandar S, Matsuyama A, Lolignier S, Kanellopoulos AH, Mancini F, Iannetti GD, Bogdanov YD, Santana-Varela S, Millet Q, Baskozos G, MacAllister R, Cox JJ, Zhao J & Wood JN (2015). Endogenous opioids contribute to insensitivity to pain in humans and mice lacking sodium channel $Na_v1.7$. *Nat Commun* 6, 8967.

Moore BA, Stewart TM, Hill C & Vanner SJ (2002). TNBS ileitis evokes hyperexcitability and changes in ionic membrane properties of nociceptive DRG neurons. *Am J Physiol Gastrointest Liver Physiol* 282, G1045–G1051.

Morinville A, Fundin B, Meury L, Juréus A, Sandberg K, Krupp J, Ahmad S & O'Donnell D (2007). Distribution of the voltage-gated sodium channel $Na_v1.7$ in the rat: Expression in the autonomic and endocrine systems. *J Comp Neurol* 504, 680–689.

Nash DT & Nash SD (2008). Ranolazine for chronic stable angina. *Lancet* 372, 1335–1341.

Nassar MA, Levato A, Stirling LC & Wood JN (2005). Neuropathic pain develops normally in mice lacking both $Na_v1.7$ and $Na_v1.8$. *Mol Pain* 1, 1–9.

Nassar MA, Stirling LC, Forlani G, Baker MD, Matthews EA, Dickenson AH & Wood JN (2004). Nociceptor-specific gene deletion reveals a major role for $Na_v1.7$ (PN1) in acute and inflammatory pain. *Proc Natl Acad Sci USA* 101, 12706–12711.

Neshatian L, Strege PR, Rhee PL, Kraichely RE, Mazzone A, Bernard CE, Cima RR, Larson DW, Dozois EJ, Kline CF, Mohler PJ, Beyder A & Farrugia G (2015). Ranolazine inhibits voltage-gated mechanosensitive sodium channels in human colon circular smooth muscle cells. *Am J Physiol Gastrointest Liver Physiol* 309, G506–G512.

NIH (2009). Opportunities & Challenges in Digestive Diseases Research: Recommendations of the National Commission on Digestive Diseases. United States Department of Health & Human Services, National Institute of Diabetes and Digestive and Kidney Diseases, *NIH Publication* No. 08–6514, Bethesda, MD, USA.

O'Donnell AM, Coyle D & Puri P (2016). Decreased $Na_v1.9$ channel expression in Hirschsprung's disease. *J Pediatr Surg* 51, 1458–1461.

Osorio N, Korogod S & Delmas P (2014). Specialized functions of $Na_v1.5$ and $Na_v1.9$ channels in electrogenesis of myenteric neurons in intact mouse ganglia. *J Neurosci* 34, 5233–5244.

Osteen JD, Herzig V, Gilchrist J, Emrick JJ, Zhang C, Wang X, Castro J, Garcia-Caraballo S, Grundy L, Rychkov GY, Weyer AD, Dekan Z, Undheim EAB, Alewood P, Stucky CL, Brierley SM, Basbaum AI, Bosmans F, King GF & Julius D (2016). Selective spider toxins reveal a role for the $Na_v1.1$ channel in mechanical pain. *Nature* 534, 494–499.

Ostman JA, Nassar MA, Wood JN & Baker MD (2008). GTP up-regulated persistent Na^+ current and enhanced nociceptor excitability require $Na_v1.9$. *J Physiol* 586, 1077–1087.

Ou Y, Gibbons SJ, Miller SM, Strege PR, Rich A, Distad MA, Ackerman MJ, Rae JL, Szurszewski JH & Farrugia G (2002). *SCN5A* is expressed in human jejunal circular smooth muscle cells. *Neurogastroenterol Motil* 14, 477–486.

Padilla F, Couble M-L, Coste B, Maingret F, Clerc N, Crest M, Ritter AM, Magloire H & Delmas P (2007). Expression and localization of the $Na_v1.9$ sodium channel in enteric neurons and in trigeminal sensory endings: Implication for intestinal reflex function and orofacial pain. *Mol Cell Neurosci* 35, 138–152.

Pennington MW, Czerwinski A & Norton RS (2017). Peptide therapeutics from venom: Current status and potential. *Bioorg Med Chem;* doi: 10.1016/j.bmc.2017.09.029

Qian AH, Liu XQ, Yao WY, Wang HY, Sun J, Zhou L & Yuan YZ (2009). Voltage-gated potassium channels in IB4-positive colonic sensory neurons mediate visceral hypersensitivity in the rat. *Am J Gastroenterol* 104, 2014–2027.

Qin N, D'Andrea MR, Lubin ML, Shafaee N, Codd EE & Correa AM (2003). Molecular cloning and functional expression of the human sodium channel $\beta1_B$ subunit, a novel splicing variant of the $\beta1$ subunit. *Eur J Biochem* 270, 4762–4770.

Qu R, Tao J, Wang Y, Zhou Y, Wu G, Xiao Y, Hu C-Y, Jiang X & Xu G-Y (2013). Neonatal colonic inflammation sensitizes voltage-gated Na^+ channels via upregulation of cystathionine β-synthetase expression in rat primary sensory neurons. *Am J Physiol Gastrointest Liver Physiol* 304, G763–G772.

Reeder JE, Byler TK, Foster DC, Landas SK, Okafor H, Stearns G, Wood RW, Zhang Y & Mayer RD (2013). Polymorphism in the *SCN9A* voltage-gated sodium channel gene associated with interstitial cystitis/bladder pain syndrome. *Urology* 81, 210e1–210e4.

Renganathan M, Cummins TR & Waxman SG (2001). Contribution of $Na_v1.8$ sodium channels to action potential electrogenesis in DRG neurons. *J Neurophysiol* 86, 629–640.

Ritter AM, Martin WJ & Thorneloe KS (2009). The voltage-gated sodium channel $Na_v1.9$ is required for inflammation-based urinary bladder dysfunction. *Neurosci Lett* 452, 28–32.

Roselli F, Livrea P & Jirillo E (2006). Voltage-gated sodium channel blockers as immunomodulators. *Recent Pat CNS Drug Discov* 1, 83–91.

Rugiero F, Mistry M, Sage D, Black JA, Waxman SG, Crest M, Clerc N, Delmas P & Gola M (2003). Selective expression of a persistent tetrodotoxin-resistant Na^+ current and $Na_v1.9$ subunit in myenteric sensory neurons. *J Neurosci* 23, 2715–2725.

Sage D, Salin P, Alcaraz G, Castets F, Giraud P, Crest M, Mazet B & Clerc N (2007). $Na_v1.7$ and $Na_v1.3$ are the only tetrodotoxin-sensitive sodium channels expressed by the adult guinea pig enteric nervous system. *J Comp Neurol* 504, 363–378.

Saito YA, Strege PR, Tester DJ, Locke GR, Talley NJ, Bernard CE, Rae JL, Makielski JC, Ackerman MJ & Farrugia G (2009). Sodium channel mutation in irritable bowel syndrome: evidence for an ion channelopathy. *Am J Physiol Gastrointest Liver Physiol* 296, G211–G218.

Salaga M, Storr M, Martemyanov KA & Fichna J (2016). RGS proteins as targets in the treatment of intestinal inflammation and visceral pain: New insights and future perspectives. *Bioessays* 38, 344–354.

Savio-Galimberti E, Gollob MH & Darbar D (2012). Voltage-gated sodium channels: biophysics, pharmacology, and related channelopathies. *Front Pharmacol* 3, 124.

Schep LJ, Schmierer DM & Fountain JS (2006). Veratrum poisoning. *Toxicol Rev* 25, 73–78.

Sikandar S & Dickenson AH (2012). Visceral pain – the Ins and Outs, the Ups and Downs. *Curr Opin Support Palliat Care* 6, 17–26.

Stewart I, Lewis RJ, Eaglesham GK, Graham GC, Poole S & Craig SB (2010). Emerging tropical diseases in Australia. Part 2. Ciguatera fish poisoning. *Ann Trop Med Parasitol* 104, 557–571.

Stewart T, Beyak MJ & Vanner S (2003). Ileitis modulates potassium and sodium currents in guinea pig dorsal root ganglia sensory neurons. *J Physiol* 552, 797–807.

Strege PR, Knutson K, Eggers SJ, Li JH, Wang F, Linden D, Szurszewski JH, Milescu L, Leiter AB, Farrugia G & Beyder A (2017a). Sodium channel $Na_v1.3$ is important for enterochromaffin cell excitability and serotonin release. *Sci Rep* 7, 15650.

Strege PR, Knutson KR, Eggers SJ, Wang F, Li J, Leiter A, Farrugia G & Beyder A (2017b). *SCN3A*-encoded voltage-gated sodium channel $Na_v1.3$ is specifically expressed in human and mouse gastrointestinal enterochromaffin cells and is important for enterochromaffin cell excitability. *FASEB J* 31, 1007–1040.

Strege PR, Mazzone A, Bernard CE, Neshatian L, Gibbons SJ, Saito YA, Tester DJ, Calvert ML, Mayer EA, Chang L, Ackerman MJ, Beyder A & Farrugia G (2017c). Irritable bowel syndrome (IBS) patients have *SCN5A* channelopathies that lead to decreased $Na_v1.5$ current and mechanosensitivity. *Am J Physiol Gastrointest Liver Physio*l; doi 10.1152/ajpgi.00016.2017

Strege PR, Mazzone A, Kraichely RE, Sha L, Holm AN, Ou Y, Lim I, Gibbons SJ, Sarr MG & Farrugia G (2007). Species dependent expression of intestinal smooth muscle mechanosensitive sodium channels. *Neurogastroenterol Motil* 19, 135–143.

Strege PR, Ou YJ, Sha L, Rich A, Gibbons SJ, Szurszewski JH, Sarr MG & Farrugia G (2003). Sodium current in human intestinal interstitial cells of Cajal. *Am J Physiol Gastrointest Liver Physiol* 285, G1111–G1121.

Tate S, Benn S, Hick C, Trezise D, John V, Mannion RJ, Costigan M, Plumpton C, Grose D, Gladwell Z, Kendall G, Dale K, Bountra C & Woolf CJ (1998). Two sodium channels contribute to the TTX-R sodium current in primary sensory neurons. *Nat Neurosci* 1, 653–655.

Trimmer JS, Cooperman SS, Agnew WS & Mandel G (1990). Regulation of muscle sodium channel transcripts during development and in response to denervation. *Dev Biol* 142, 360–367.

Tseng TT, McMahon AM, Johnson VT, Mangubat EZ, Zahm RJ, Pacold ME & Jakobsson E (2007). Sodium channel auxiliary subunits. *J Mol Microbiol Biotechnol* 12, 249–262.

Tzoumaka E, Tischler AC, Sangameswaran L, Eglen RM, Hunter JC & Novakovic SD (2000). Differential distribution of the tetrodotoxin-sensitive rPN4/NaCh6/*Scn8a* sodium channel in the nervous system. *J Neurosci Res* 60, 37–44.

`

Uhlen M, Fagerberg L, Hallstrom BM, Lindskog C, Oksvold P, Mardinoglu A, Sivertsson A, Kampf C, Sjostedt E, Asplund A, Olsson I, Edlund K, Lundberg E, Navani S, Szigyarto CA, Odeberg J, Djureinovic D, Takanen JO, Hober S, Alm T, Edqvist PH, Berling H, Tegel H, Mulder J, Rockberg J, Nilsson P, Schwenk JM, Hamsten M, von Feilitzen K, Forsberg M, Persson L, Johansson F, Zwahlen M, von Heijne G, Nielsen J & Ponten F (2015). Proteomics. Tissue-based map of the human proteome. *Science* 347, 1260419.

Vanoye CG, Kunic JD, Ehring GR & George AL Jr (2013). Mechanism of sodium channel Na$_v$1.9 potentiation by G-protein signaling. *J Gen Physiol* 141, 193–202.

Verne GN, Sen A & Price DD (2005). Intrarectal lidocaine is an effective treatment for abdominal pain associated with diarrhea-predominant irritable bowel syndrome. *J Pain* 6, 493–496.

Wang W, Gu J, Li Y-Q & Tao Y-X (2011). Are voltage-gated sodium channels on the dorsal root ganglion involved in the development of neuropathic pain? *Mol Pain* 7, 1–9.

Waxman SG, Kocsis JD & Black JA (1994). Type III sodium channel mRNA is expressed in embryonic but not adult spinal sensory neurons and is reexpressed following axotomy. *J Neurophysiol* 72, 466–470.

Waxman SG, Merkies IS, Gerrits MM, Dib-Hajj SD, Lauria G, Cox JJ, Wood JN, Woods CG, Drenth JP & Faber CG (2014). Sodium channel genes in pain-related disorders: phenotype-genotype associations and recommendations for clinical use. *Lancet Neurol* 13, 1152–1160.

Westenbroek RE, Merrick DK & Catterall WA (1989). Differential subcellular localization of the RI and RII Na$^+$ channel subtypes in central neurons. *Neuron* 3, 695–704.

Whitaker W, Faull R, Waldvogel H, Plumpton C, Burbidge S, Emson P & Clare J (1999). Localization of the type VI voltage-gated sodium channel protein in human CNS. *Neuroreport* 10, 3703–3709.

Woods CG, Babiker MOE, Horrocks I, Tolmie J & Kurth I (2015). The phenotype of congenital insensitivity to pain due to the Na$_v$1.9 variant p.L811P. *Eur J Hum Genet* 23, 561–563.

Yang Y, Wang Y, Li S, Xu Z, Li H, Ma L, Fan J, Bu D, Liu B, Fan Z, Wu G, Jin J, Ding B, Zhu X & Shen Y (2004). Mutations in *SCN9A*, encoding a sodium channel alpha subunit, in patients with primary erythermalgia. *J Med Genet* 41, 171–174.

Yekkirala AS, Roberson DP, Bean BP & Woolf CJ (2017). Breaking barriers to novel analgesic drug development. *Nat Rev Drug Discov* 16, 545–564.

Yiangou Y, Facer P, Chessell IP, Bountra C, Chan C, Fertleman C, Smith V & Anand P (2007). Voltage-gated ion channel Na$_v$1.7 innervation in patients with idiopathic rectal hypersensitivity and paroxysmal extreme pain disorder (familial rectal pain). *Neurosci Lett* 427, 77–82.

Yoshimura N & deGroat WC (1997). Plasticity of Na$^+$ channels in afferent neurones innervating rat urinary bladder following spinal cord injury. *J Physiol* 503, 269–276.

Yoshimura N, Seki S, Novakovic SD, Tzoumaka E, Erickson VL, Erickson KA, Chancellor MB & de Groat WC (2001). The involvement of the tetrodotoxin-resistant sodium channel Na$_v$1.8 (PN3/SNS) in a rat model of visceral pain. *J Neurosci* 21, 8690–8696.

Zang Y, He XH, Xin WJ, Pang RP, Wei XH, Zhou LJ, Li YY & Liu XG (2010). Inhibition of NF-kappaB prevents mechanical allodynia induced by spinal ventral root transection and suppresses the re-expression of Na$_v$1.3 in DRG neurons *in vivo* and *in vitro*. *Brain Res* 1363, 151–158.

Zhang XY, Wen J, Yang W, Wang C, Gao L, Zheng LH, Wang T, Ran K, Li Y, Li X, Xu M, Luo J, Feng S, Ma X, Ma H, Chai Z, Zhou Z, Yao J, Zhang X & Liu JY (2013). Gain-of-function mutations in *SCN11A* cause familial episodic pain. *Am J Hum Genet* 93, 957–966.

Chapter 3 Domain organization, gating mechanisms, and neurotoxin binding sites of mammalian voltage-gated sodium channels

A significant component of our current understanding of the contribution of Na_v channels to active electrophysiological properties in neurons in physiological and pathological conditions comes from studies using Na_v-selective modulators. This chapter will provide a brief description of Na_v channel domain organization, activation and fast inactivation (gating) mechanisms, and sites of pharmacological interaction with relevance to electrophysiological methods and pharmacological modulators described in this thesis. Slow inactivation, albeit an important property of Na_v channels, has not been evaluated electrophysiologically or pharmacologically in this study and will therefore not be discussed in this chapter.

3.1 Pore-forming α-subunit and auxiliary β-subunits

Na_v channels are comprised of a pore-forming α-subunit, of which nine isoforms have been identified (Na_v1.1-Na_v1.9), and auxiliary β-subunits, of which four main isoforms (β1-β4) and one splice variant ($β1_B$) have been identified (Qin et al. 2003; Tseng et al. 2007; Yu et al. 2003). The α-subunit is composed of four homologous domains denoted I–IV, each of which is made up of six α-helical transmembrane domains denoted S1–S6 (**Figure 3.1**) (Dib-Hajj et al. 2013; Goldin 2003). The term 'Na$_v$ isoform' refers to the specific α-subunit. While α-subunits can form fully functional sodium conducting channels on their own, they are believed to be associated with one or more auxiliary β-subunits. The β-subunits have been shown to modify gating properties and regulate transcription levels and membrane recruitment of the α-subunits (Isom 2001; Zhu et al. 2017). The α-subunits have a very high sequence identity (> 50%), greater than that of voltage-gated potassium and voltage-gated calcium channels (Catterall et al. 2005), which has made isoform-selective targeting challenging. Nevertheless, α-subunits exhibit subtle differences in gating kinetics, which can be used to distinguish the channels using electrophysiological approaches.

3.2 Mechanism of voltage-dependent activation

Voltage-gated sodium channels open, inactivate, and close, in response to voltage. Voltage-dependent activation is conferred by changes in the strength of interaction between positively charged residues in the S4 segments of each domain and the cellular membrane (**Figure 3.1**). The S4 segments are positively charged due to a conserved repeated motif containing a basic residue at every third position (Catterall 2014), and are referred to as the voltage sensors of the voltage-sensing domain (S1-S4). At the resting membrane potential, the S4 segments are stabilized in the membrane by ionic interactions with residues in the S1, S2 and/or S3 segments, and the channel is closed (Catterall 2000, 2010). As the membrane becomes depolarized, the strength of these ionic interactions decreases and the S4 segments traverse through the membrane towards the extracellular side (Kontis, Rounaghi & Goldin 1997; Stuhmer et al. 1989; Yang, George & Horn 1996; Yang & Horn 1995). At a threshold membrane potential, the S4 segments have altered conformation of the channel pore sufficiently to accommodate influx of sodium ions along the concentration gradient (Catterall 2014).
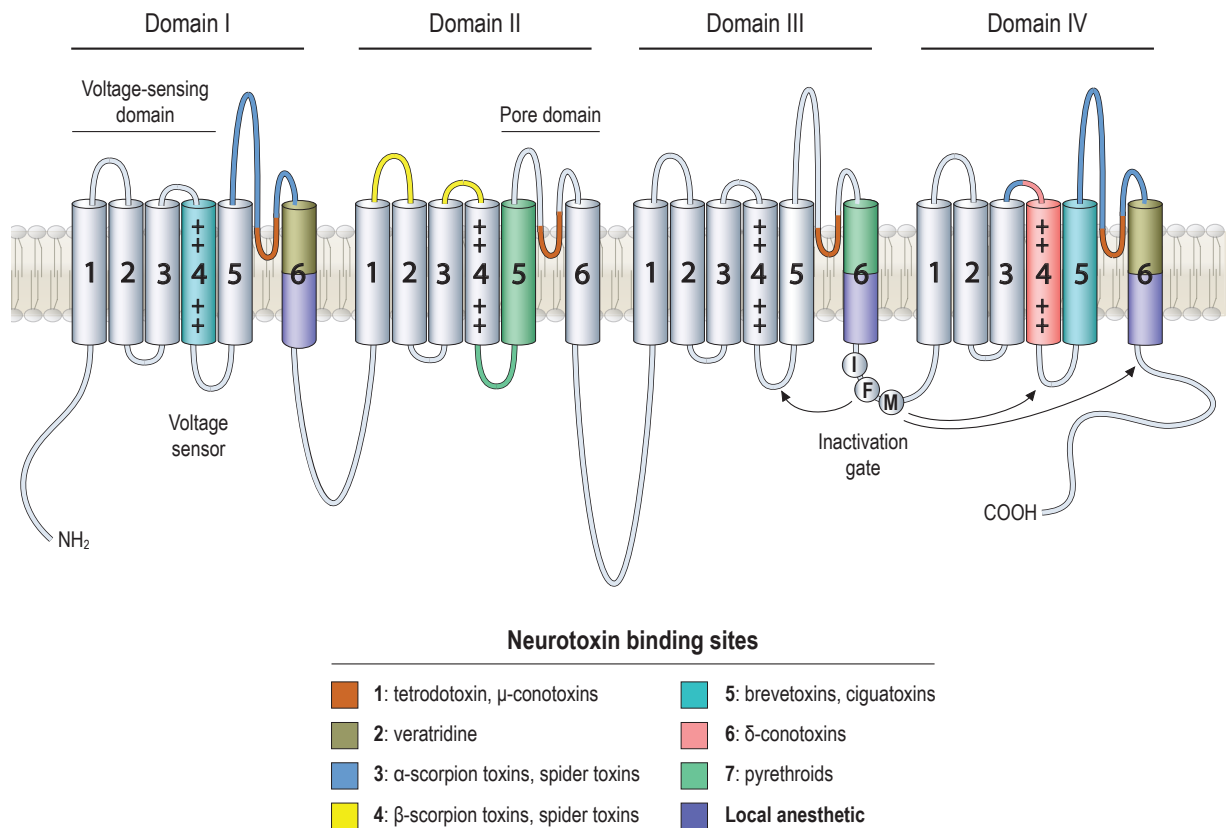
Figure 3.1: Domain organization of Na$_v$ α-subunits with neurotoxin binding sites highlighted. The α-subunit contains four homologous domains, I-IV, each of which contains six transmembrane segments, S1-S6. S1-S4 from each domain form the voltage sensing domain and S4 forms the voltage sensor. The interactions between positively charged residues in S4 with S1-S3 and between S1-S4 and the cellular membrane facilitate voltage-dependent closed and open conformations of Na$_v$ channels. The pore is composed of S5-S6 from each domain, with the selectivity filter conferred by charged residues in the re-entrant loops close to the S6 segments. The intracellular loop between domain III S6 and domain IV S1 contains a highly conserved three amino acid sequence (I-F-M), which functions as a fast inactivation gate. Immediately following activation, the residues in the inactivation gate are believed to interact with residues in nearby loop regions (indicated by arrows) to alter channel conformation and disable sodium influx. A range of bacterial toxins, marine toxins, plant alkaloids, arachnid toxins, and insecticides act on Na$_v$ channels via the neurotoxin binding sites highlighted.

3.3 Mechanism of fast inactivation

Voltage-dependent activation is coupled to fast inactivation, which occurs within milliseconds of activation (Catterall 2014). The inactivation loop is formed by the IIIS6-IVS1 intracellular loop, which contains a highly conserved three amino acid sequence (Ile-Phe-Met) (**Figure 3.1**). Hydrophobic interactions within the inactivation loop project the phenylalanine into the pore where it and other residues of the inactivation loop are stabilized through interactions with linker regions S4–S5 in domains III and IV, and the cytoplasmic terminal of the IVS6 segment (Nicholson & Little 2005; Rohl et al. 1999). This is believed to physically occlude the pore of the channel. The positive membrane potential induced by Na$^+$ influx activates voltage-gated potassium channels, which causes repolarization of the membrane. The repolarization enables movement of S4 segments to the closed Na$_v$ channel conformation.

3.4 Na$_v$ channel neurotoxin binding sites

There are several pharmacologically distinct binding sites on Na$_v$ channels, eight of which are listed in **Table 3.1** and highlighted in **Figure 3.1**. Na$_v$ channels can be modulated by toxins and venom peptides from diverse sources, including spiders, scorpions, cone snails, bacteria, plants, planktons, and frogs (**Table 3.1**). The mechanisms of modulation and their respective outcomes are varied, ranging from complete block of sodium conductance to increasing the probability of sodium influx. Na$_v$ modulators have specific, but overlapping, selectivity across Na$_v$ isoforms, and have been used to understand how these channels contribute to signaling in all excitable cells under physiological and pathological conditions.

49

Table 3.1: Overview of Na$_v$ channel neurotoxin binding sites in terms of composition, site-specific toxins, and modulatory effect of toxin interaction.

Neurotoxin binding site	Binding site composition	Toxins	Outcome of toxin binding
1	IS5-S6, IIS5-S6, IIIS5-S6 and IVS5-S6[a]	Tetrodotoxin, Saxitoxin[f], μ-Conotoxins[g]	Physical pore occlusion and blockage of sodium conductance[a]
2	IS6, IVS6, some contribution by IIS6 and IIIS6[a]	Batrachotoxin (Phyllobates aurotaenia), Grayanotoxins (Ericaceae), Veratridine (Liliaceae)[a]	Hyperpolarizing shift in voltage-dependence of activation and prevention or slowing down rate of channel inactivation[a]
3	IS5-S6 and IVS5-S6, IVS3-S4 loop[b]	Sea anemone toxins, α-scorpion toxins[h], δ-atracotoxins, Tx4 and Magi 4, β-PMTX[a]	Stabilization of activated IVS4, fast inactivation impairment, enhancement of channel recovery from inactivation[a]
4	IIS1-S2, IIS3-S4[a], possibly IIIS4[c]	β-scorpion toxins, μ-O-Conotoxins, Magi 5, δ-palutoxins, curtatoxins, μ-agatoxins and β/δ-agatoxins[a]	Immobilization of activated IIS4, hyperpolarizing shift in voltage-dependence of activation[a]
5	IS4 and IVS5[a]	Brevetoxins and ciguatoxins (marine dinoflagellates)[a]	Hyperpolarizing shift of voltage-dependence of activation, increase in open configuration duration, decrease in rate of inactivation[a]
6	IVS3-S4 and IVS4[a]	δ-Conotoxins[a]	Slowing down of inactivation independent of voltage[a]
7 (pyrethroid binding site)	IIS4-S5, IIS5, IIIS6[d]	Pyrethroids deltamethrin and DDT[a]	Slowing down of inactivation[a]
Local anesthetic binding site	IS6, IIIS6 and IVS6[e]	Local anesthetics, anticonvulsants, antiarrhythmics	Binding impedes ion permeation and blocks sodium conductance[i]

[a]Stevens, Peigneur and Tytgat (2011), [b]Cestele and Catterall (2000), [c]Song et al. (2011), [d]Davies et al. (2007), [e]Scholz (2002), [f]Hackett et al. (2013), [g]Stephan, Potts and Agnew (1994), [h]Bosmans and Tytgat (2007), [i]Lipkind and Fozzard (2005)

3.5 Literature cited

Bosmans, F & Tytgat, J 2007, 'Voltage-gated sodium channel modulation by scorpion α-toxins', *Toxicon*, vol. 49, no. 2, Feb, pp. 142-158.

Catterall, WA 2000, 'From ionic currents to molecular mechanisms: The structure and function of voltage-gated sodium channels', *Neuron*, vol. 26, no. 1, Apr, pp. 13-25.

Catterall, WA 2010, 'Ion Channel Voltage Sensors: Structure, Function, and Pathophysiology', *Neuron*, vol. 67, no. 6, Sep, pp. 915-928.

Catterall, WA 2014, 'Structure and function of voltage-gated sodium channels at atomic resolution', *Experimental Physiology*, vol. 99, no. 1, Jan, pp. 35-51.

Catterall, WA, Perez-Reyes, E, Snutch, TP & Striessnig, J 2005, 'International Union of Pharmacology. XLVIII. Nomenclature and structure-function relationships of voltage-gated calcium channels', *Pharmacological Reviews*, vol. 57, no. 4, Dec, pp. 411-425.

Cestele, S & Catterall, WA 2000, 'Molecular mechanisms of neurotoxin action on voltage-gated sodium channels', *Biochimie*, vol. 82, no. 9-10, Sep-Oct, pp. 883-892.

Davies, TG, Field, LM, Usherwood, PN & Williamson, MS 2007, 'DDT, pyrethrins, pyrethroids and insect sodium channels', *IUBMB Life*, vol. 59, no. 3, Mar, pp. 151-162.

Dib-Hajj, SD, Yang, Y, Black, JA & Waxman, SG 2013, 'The Na$_v$1.7 sodium channel: from molecule to man', *Nature Reviews Neuroscience*, vol. 14, no. 1, Jan, pp. 49-62.

Goldin, AL 2003, 'Mechanisms of sodium channel inactivation', *Current Opinion in Neurobiology*, vol. 13, no. 3, Jun, pp. 284-290.

Hackett, JD, Wisecaver, JH, Brosnahan, ML, Kulis, DM, Anderson, DM, Bhattacharya, D, Plumley, FG & Erdner, DL 2013, 'Evolution of saxitoxin synthesis in cyanobacteria and dinoflagellates', *Molecular Biology and Evolution*, vol. 30, no. 1, Jan, pp. 70-78.

Isom, LL 2001, 'Sodium channel β-subunits: Anything but auxiliary', *Neuroscientist*, vol. 7, no. 1, Feb, pp. 42-54.

Kontis, KJ, Rounaghi, A & Goldin, AL 1997, 'Sodium channel activation gating is affected by substitutions of voltage sensor positive charges in all four domains', *Journal of General Physiology*, vol. 110, no. 4, Oct, pp. 391-401.

Lipkind, GM & Fozzard, HA 2005, 'Molecular modeling of local anesthetic drug binding by voltage-gated sodium channels', *Molecular Pharmacology*, vol. 68, no. 6, Dec, pp. 1611-1622.

Nicholson, GM & Little, MJ 2005, 'Spider Neurotoxins Targeting Voltage-Gated Sodium Channels', *Toxin Reviews*, vol. 24, no. 3-4, 2005/01/01, pp. 313-343.

Qin, N, D'Andrea, MR, Lubin, ML, Shafaee, N, Codd, EE & Correa, AM 2003, 'Molecular cloning and functional expression of the human sodium channel β1 subunit, a novel splicing variant of the β1 subunit', *European Journal of Biochemistry*, vol. 270, no. 23, Dec, pp. 4762-4770.

Rohl, CA, Boeckman, FA, Baker, C, Scheuer, T, Catterall, WA & Klevit, RE 1999, 'Solution structure of the sodium channel inactivation gate', *Biochemistry*, vol. 38, no. 3, Jan, pp. 855-861.

Scholz, A 2002, 'Mechanisms of (local) anaesthetics on voltage-gated sodium and other ion channels', *British Journal of Anaesthesia*, vol. 89, no. 1, Jul, pp. 52-61.

Song, WZ, Du, YZ, Liu, ZQ, Luo, NG, Turkov, M, Gordon, D, Gurevitz, M, Goldin, AL & Dong, K 2011, 'Substitutions in the Domain III Voltage-sensing Module Enhance the Sensitivity of an Insect Sodium Channel to a Scorpion β-Toxin', *Journal of Biological Chemistry*, vol. 286, no. 18, May.

Stephan, MM, Potts, JF & Agnew, WS 1994, 'The μ-skeletal muscle sodium-channel - mutation E403Q eliminates sensititivy to tetrodotoxin but not to μ-conotoxins GIIIA and GIIIB', *Journal of Membrane Biology*, vol. 137, no. 1, Jan, pp. 1-8.

Stevens, M, Peigneur, S & Tytgat, J 2011, 'Neurotoxins and their binding areas on voltage-gated sodium channels', *Frontiers in pharmacology*, vol. 2, 2011.

Stuhmer, W, Conti, F, Suzuki, H, Wang, XD, Noda, M, Yahagi, N, Kubo, H & Numa, S 1989, 'Structural parts involved in activation and inactivation of the sodium-channel', *Nature*, vol. 339, no. 6226, Jun, pp. 597-603.

Tseng, TT, McMahon, AM, Johnson, VT, Mangubat, EZ, Zahm, RJ, Pacold, ME & Jakobsson, E 2007, 'Sodium channel auxiliary subunits', *Journal of Molecular Microbiology and Biotechnology*, vol. 12, no. 3-4, pp. 249-262.

Yang, NB, George, AL & Horn, R 1996, 'Molecular basis of charge movement in voltage-gated sodium channels', *Neuron*, vol. 16, no. 1, Jan, pp. 113-122.

Yang, NB & Horn, R 1995, 'Evidence for voltage-dependent S4 movement in sodium channels', *Neuron*, vol. 15, no. 1, Jul, pp. 213-218.

Yu, FH, Westenbroek, RE, Silos-Santiago, I, McCormick, KA, Lawson, D, Ge, P, Ferriera, H, Lilly, J, DiStefano, PS, Catterall, WA, Scheuer, T & Curtis, R 2003, 'Sodium channel β4, a new disulfide-linked auxiliary subunit with similarity to β2', *Journal of Neuroscience*, vol. 23, no. 20, Aug, pp. 7577-7585.

Zhu, W, Voelker, TL, Varga, Z, Schubert, AR, Nerbonne, JM & Silva, JR 2017, 'Mechanisms of noncovalent β subunit regulation of Na_v channel gating', *The Journal of General Physiology*, vol. 149, no. 8, pp. 813-831.

Aims

Aim 1

Determine the expression profile of voltage-gated sodium (Na_v) channels in colon-innervating dorsal root ganglia neurons from healthy mice and how this differs in a model of chronic visceral hypersensitivity.

Aim 2

Assess the electrophysiological properties of colon-innervating dorsal root ganglia neurons in healthy and chronic visceral hypersensitivity states.

Aim 3

Assess the effect of Na_v channel modulators on active electrophysiological properties in visceral-innervating dorsal root ganglia neurons to gain insight into Na_v channel function.

`

Chapter 4 Methods

4.1 Animals and chronic visceral hypersensitivity model

All experiments were approved by the Animal Ethics Committee of the University of Adelaide and the South Australian Health and Medical Research Institute (SAHMRI), under ethics codes SAM110 and SAM195. Age-matched C57BL/6J male mice from the SAHMRI Bioresources rodent facility and Jackson (JAX) Laboratories were assigned into two groups: healthy control (HC) and trinitrobenzenesulfonic acid (TNBS) treated. The number and age of mice used in electrophysiology experiments from each group are reported in **Table 4.1.**

Table 4.1 Summary statistics for mice used in electrophysiology experiments according to line and treatment group.

Group	SAHMRI line		JAX line		Age (weeks, mean ± SD)
	N	% of mice	N	% of mice	
Healthy control	23	(67)	11	(33)	16 ± 2
TNBS treatment	15	(65)	8	(35)	16 ± 1

Mice in the TNBS treatment group were fasted overnight prior to treatment, then anesthetized and administered an intracolonic enema of 0.1 mL TNBS (3.8 mg per mouse in 30% EtOH) via a polyethylene catheter as previously described (Hughes et al. 2009). This treatment causes inflammation of the colonic epithelium and mucosa, which spontaneously heals within 28 days. Following recovery from colitis, histological signs of inflammation are absent, whereas *in vivo* and *ex vivo* indicators of visceral hypersensitivity are present (Castro et al. 2017; Feng et al. 2012; Hughes et al. 2009). TNBS-treated mice were individually housed following treatment and monitored until reaching a positive percentage body weight change compared to the post-fasted weight and had a clinical record score of zero (lack of blood in stools, diarrhea, constipation, ruffled coat, and hunched posture), in accordance with approved project ethics. All mice in the TNBS-treated group exhibited weight loss for an extended time period (**Table 4.2**).

Table 4.2: Summary statistics for clinical scores of mice in TNBS-treated group according to line.

Group	Weight change (% of post-fast weight)			Days on negative weight		
	Average ± SD	Minimum	Maximum	Average ± SD	Minimum	Maximum
SAHMRI	-8.1 ± 2.2	-4.0	-19.2	3.6 ± 1.8	1	13
JAX	-8.6 ± 3.9	-5.6	-17.0	4.9 ± 3.0	1	7

TNBS-treated mice were used to model chronic visceral hypersensitivity (CVH) 28 days following induction of colitis. Treated mice from the same cohorts as mice used in this thesis have been confirmed to exhibit histological signs of acute inflammation following treatment, absence of inflammation following 28 days of recovery, enhanced colonic afferent nerve activity *ex vivo*, and enhanced visceral hypersensitivity to colorectal distension *in vivo* (Grundy et al. 2018; Salvatierra et al. 2018).

4.2 Retrograde labeling of colon-innervating neurons and dissociated dorsal root ganglia cell culture

Colon-innervating neurons were labeled as described (Salvatierra et al. 2018). Briefly, mice were anesthetized, a midline laparotomy was performed, and 10 µL (5 µg/µL) cholera toxin subunit B (CTB) conjugated to AlexaFluor-488 (Thermofisher, cat # C22841) (CTB-488) was injected into the serosa of the distal colonic wall. CTB binds ganglioside GM_1 on the cell membrane of neurons and is retrogradely transported to the endoplasmic reticulum (Aureli et al. 2016; Jobling et al. 2012), enabling visualization of neuronal cell bodies once dissociated (**Figure 4.1**). Mice were culled by CO_2 inhalation 3-5 days following tracer injection, and dorsal root ganglia (DRG) from thoracolumbar (TL, T10-L1) and lumbosacral (LS, L5-S1) spinal levels were surgically removed, dissociated using 4.7 mg/mL Dispase II (ThermoFisher, cat # 17105041) and 3.3 mg/mL Collagenase Type II (ThermoFisher, cat # 17101015) in HBSS (ThermoFisher, cat # 14170161), and plated on coverslips coated with 800 µg/mL poly-D-lysine hydrobromide (ThermoFisher, cat # P7886) and 20 µg/mL laminin (Sigma-Aldrich, cat # L2020) as described (Salvatierra et al. 2018). Neurons were placed in an incubator at 37°C in 5% CO_2 for 2 hrs following plating to allow

adherence to the coated surface before addition of media. Neurons were maintained in Dulbecco's Modified Eagle Medium (DMEM) (ThermoFisher, cat # 11995065), supplemented with 10% Fetal Calf Serum (FCS) (ThermoFisher, cat # 26170043), 2 mM L-glutamine (ThermoFisher, cat # 35050061), 100 µM Minimum Essential Medium (MEM) nonessential amino acids (ThermoFisher, cat # 11140050), 0.1 µg/mL nerve growth factor-7S (ThermoFisher, cat # 13290010), and 100 mg/mL penicillin/streptomycin (ThermoFisher, cat #15140122) in an incubator at 37°C in 5% CO_2.
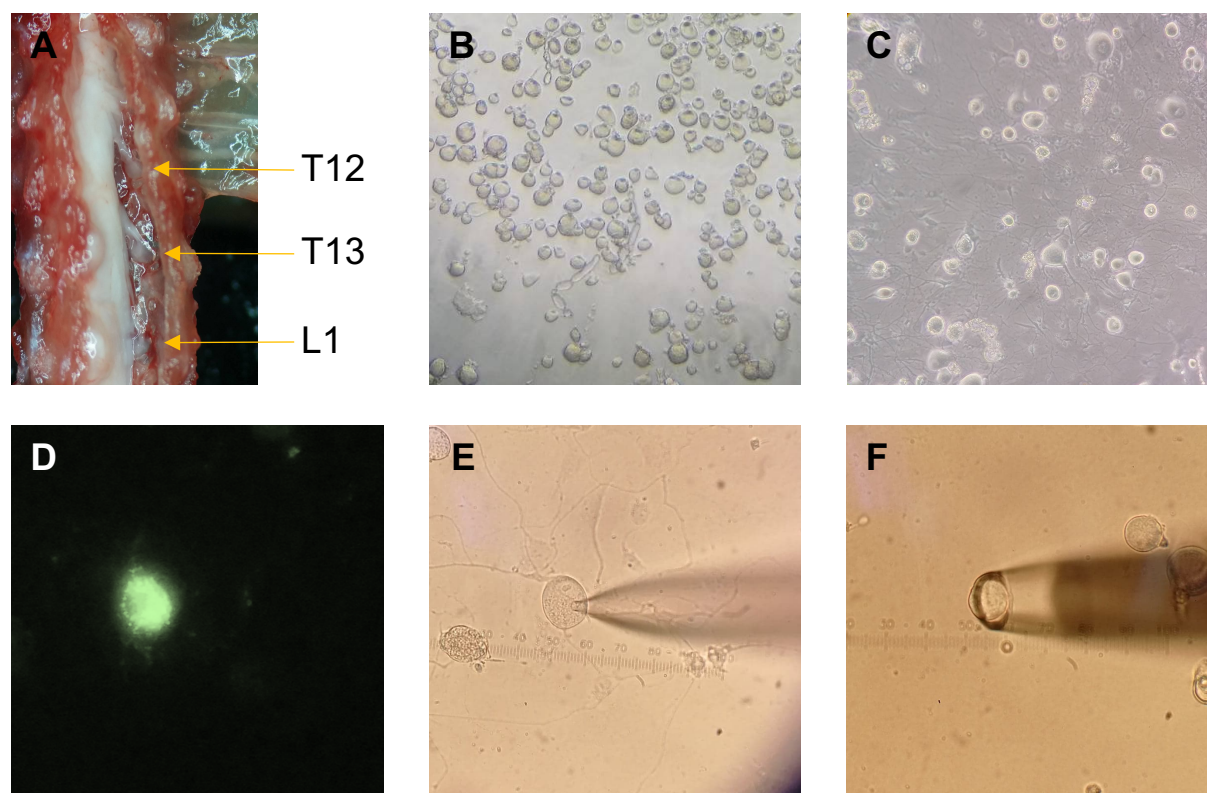
Figure 4.1: Dorsal root ganglia isolation and dissociated neurons, whole-cell patch-clamp electrophysiology and single-cell picking. A) Dorsal view of open vertebral column showing the spinal column, dorsal roots, and thoracic dorsal root ganglia T12, T13, and lumbar ganglion L1. **B)** Recently dissociated dorsal root ganglia neurons (< 2 hrs). Neurons appear round and without neuronal processes on the day of culture. **C)** Dissociated neurons on day 2 post culture (< 48 hrs). Neurons appear asymmetric and attached to the coated surface, with extensive networks of neuronal processes. **D)** A dissociated colon-innervating dorsal root ganglia neuron is identified by green fluorescence emission (retrogradely traced from the distal colon with CTB-488). **E)** Formation of GΩ seal for whole-cell patch-clamp electrophysiology using a 1 MΩ pipette. **F)** Single-cell picking of a dissociated neuron using an air-filled glass pipette for subsequent single-cell qRT-PCR.

4.3 RNA extraction and reverse-transcription quantitative polymerase chain reaction of whole dorsal root ganglia

Mice were culled by CO_2 inhalation and DRG pairs at spinal levels T10-L1 and L5-S1 were surgically isolated from 7 healthy and 6 CVH mice and trimmed for roots and connective tissue in phosphate-buffered saline (PBS) on ice. Cleaned DRG pairs were suspended in 20 µL sterile filtered PBS, placed on dry ice and stored at -80°C until RNA extraction. RNA was extracted from DRG pairs using the PureLink® RNA Micro Scale Kit (ThermoFisher, cat # 12183016) followed by DNAse treatment (ThermoFisher, cat #12185010) according to the manufacturer's instructions. Quantitative reverse-transcription polymerase chain reaction (qRT-PCR) was performed using EXPRESS One-Step SuperScript® qRT-PCR SuperMix Kit (ThermoFisher, cat # 1178101K) with commercially available hydrolysis probes (ThermoFisher, Taqman®, see **Table 4.3** for details) and RNAse-free water. For each reaction, 10 µL of qPCR SuperMix, 1 µL of TaqMan primer, 4 µL of water, and 5 µL RNA from each sample was tested in duplicate for each target. β-Actin was used as an endogenous control. Each assay plate contained RNA from one DRG pair from a healthy mouse and RNA from one DRG pair from a CVH mouse at the same spinal level to reduce batch effects. Assays were run for 45 cycles on a 7500 Fast Real-Time PCR System (Applied Biosystems) machine, using 7500 Fast software, v2.0.6. Duplicate C_t values were averaged, and expression levels

`

were quantified according to the ΔC_t method: relative expression $= 2^{[Ct\ of\ target\ gene - Ct\ of\ housekeeping\ gene]} = 2^{\Delta Ct}$.

Table 4.3 Taqman® primers used for qRT-PCR and single-cell RT-PCR.

Gene name	Gene target	Assay ID
β-Actin	*Actb*	Mm00607939_s1
Na$_v$1.1	*Scn1a*	Mm00450580_m1
Na$_v$1.2	*Scn2a1*	Mm01270359_m1
Na$_v$1.3	*Scn3a*	Mm00658167_m1
Na$_v$1.4	*Scn4a*	Mm00500103_m1
Na$_v$1.5	*Scn5a*	Mm01342518_m1
Na$_v$1.6	*Scn8a*	Mm00488110_m1
Na$_v$1.7	*Scn9a*	Mm00450762_s1
Na$_v$1.8	*Scn10a*	Mm00501467_m1
Na$_v$1.9	*Scn11a*	Mm00449367_m1
β1	*Scn1b*	Mm00441210_m1
β2	*Scn2b*	Mm01179204_g1
β3	*Scn3b*	Mm00463369_m1
β4	*Scn4b*	Mm01175562_m1
Tubulin, β 3 class III	*Tubb3*	Mm00727586_s1
glial fibrillary acidic protein	*Gfap*	Mm01253033_m1

4.4 Single-cell quantitative polymerase chain reaction of colon-innervating dorsal root ganglia neurons

Dissociated DRG neurons retrogradely labeled from the colon of healthy and CVH mice were perfused with sterile PBS and collected into the end of an air-filled wide aperture borosilicate glass pipette fabricated in the P-97 (Sutter Instruments) pipette puller (**Figure 4.1**, **F)**. For expression studies on *scn1a-scn11a*, neurons were collected < 12 hrs post dissociation. For expression studies on *scn1b-scn4b*, neurons were collected following patch-clamp electrophysiology experiments. Single-cell collection and qPCR on unpatched neurons were performed by Dr Sonia Garcia-Caraballo (Visceral Pain Research Group, Flinders University), and permission was obtained to analyze and include the results in this thesis. A separate pipette was used to sample bath solution to assess RNA contamination. The end of the glass pipette containing the collected neuron was broken into a sterile Eppendorf tube containing 10 µL of lysis buffer with DNase (ThermoFisher, TaqMan Gene Expression Cells-to-CT Kit, cat # AM1728). Incubation with lysis buffer occurred for 5-10 min at room temperature, followed by addition of 1 µL DNase stop solution and incubation for a further 5-10 min at room temperature. Lysates were frozen on dry ice and stored at -80°C until cDNA synthesis was performed. cDNA synthesis was performed using the SuperScript VILO IV EzDNase (ThermoFisher, cat #11766050) kit according to manufacturer's instructions. Each cDNA synthesis batch included one reverse transcriptase (RT) negative control to assess genomic DNA contamination. Synthesized cDNA was stored at -20°C until qPCR was performed. For each qPCR reaction, 10 µL of qPCR Master mix, 0.5 µL of each TaqMan primer, 8 µL of water, and 1.6 µL cDNA from each sample was tested in singlicate for each target. *Tubb3* was used as a neuronal marker and *Gfap* was used as a glial marker. RT controls, bath controls, negative controls (water instead of cDNA) were routinely included in qPCR reactions, and a positive control test was performed for each primer using cDNA synthesized from whole DRG RNA. Assays were run for 50 cycles on a 7500 Fast Real-Time PCR System (Applied Biosystems) machine, using 7500 Fast software, v2.0.6. Genes were considered expressed if a complete amplification curve was obtained within 50 cycles.

4.5 Whole-cell current-clamp electrophysiology of colon-innervating dorsal root ganglia neurons

Neurons: Dissociated DRG neurons isolated from colon-traced healthy and CVH mice were recorded on day 1 and day 2 post culturing (20-48 hrs). Neurons were not recorded if the resting membrane potential was more depolarized than -40 mV as this is an indicator of poor cell health. To determine average neuron diameter, the smallest and largest width of the neuronal soma was measured using the microscope eyepiece reticle calibrated with a stage micrometer and averaged. Solutions: Intracellular solution contained (in mM): 135 KCl; 2 MgCl$_2$; 2 MgATP; 5 EGTA-Na; 10 HEPES-Na; adjusted to pH 7.3, 275 mOsm. Extracellular (bath) solution contained (in mM): 140 NaCl; 4 KCl; 2 MgCl$_2$; 2 CaCl$_2$; 10 HEPES; 5

glucose; adjusted to pH 7.4, 285 mOsm. <u>Compounds and application</u>: Cells were continually perfused with solution by a gravity driven multi-barrel perfusion system positioned within 1 mm of the neuron under investigation. Compounds used in this thesis included tetrodotoxin (TTX) citrate (Alomone Labs, cat # T-550), veratridine (ApexBio, cat # B7219), A-803467 (Sigma-Aldrich, cat # A3109), ICA-121341 (Sigma-Aldrich, cat # SML1035), Compound B (1-benzyl-5-methyl-1H-1,2,3-triazole-4-carboxamide; Sigma-Aldrich, cat # CDS016890), Hs1a (provided by Prof Glenn King's lab, the Institute for Molecular Biology, the University of Queensland), and OD1 (provided by A/Prof Irina Vetter's lab, the Institute for Molecular Biology, the University of Queensland). All compounds, except for A-803467, were dissolved in MilliQ H_2O at 1000x final concentration and stored at -20°C. A-803467 was dissolved in DMSO (Sigma-Aldrich, cat # 41639) at 1000x final concentration and aliquots were filled with nitrogen to minimize oxidation during storage at -20°C. Baseline responses were recorded in bath solution using the protocol described below. Responses to compounds were recorded 1-2 minutes after perfusion. Hs1a at 100 and 500 nM were tested in series, and TTX was also incubated following Hs1a, compound B, or ICA-121341. <u>Pipettes</u>: Standard wall borosilicate glass pipettes (OD x ID x length: 1.5 mm x 0.86 mm x 7.5 cm, Harvard, cat # 64-0792) were pulled and fire-polished to 4 - 10 MΩ using a P-97 (Sutter Instruments) pipette puller. <u>Protocols</u>: In current-clamp mode, neurons were held at -70 mV for 15 ms, hyperpolarized by a -20 pA current injection for 475 ms, then held at -70 mV for 100 ms. Stepwise depolarizing pulses in increments of 10, 25, or 50 pA (475 ms) were applied from holding potential of -70 mV with 2 sec repetition intervals to determine the rheobase (minimum amount of current required to fire an action potential) and number of action potentials at 2-times rheobase. For studies comparing action potential half-width, half-width was defined as the duration (in ms) of the first action potential at half-maximal amplitude. Half-maximal amplitude was measured as 0.5(maximum mV – baseline mV). For studies comparing action potential overshoot, overshoot was defined as the peak positive membrane potential during an action potential. <u>Data acquisition and analysis</u>: Recordings were amplified with Axopatch 200A, digitized with Digidata 1322A, sampled at 20 kHz, filtered at 5 kHz, recorded with pCLAMP 9 software (Molecular Devices), and analyzed in Clampfit 10.3.2 (Molecular Devices), Prism v8.0.0 (GraphPad), and IBM SPSS Statistics v25.

4.6 Whole-cell voltage-clamp electrophysiology of colon-innervating dorsal root ganglia neurons

<u>Neurons</u>: Dissociated DRG neurons isolated from colon-traced healthy and CVH mice were recorded on day 1 and day 2 post culturing (20-48 hrs). Neurons were not used for analysis if the voltage error was greater than 10%. To determine average neuron diameter, the smallest and largest width of the neuronal soma was measured using the microscope eyepiece reticle calibrated with a stage micrometer and averaged <u>Solutions</u>: Voltage-clamp intracellular solution contained (mM): 60 CsF; 45 CsCl; 2 $MgCl_2$; 5 EGTA-Na; 10 HEPES-Cs; 30 TEA-Cl; 2 MgATP; adjusted to pH 7.2 with CsOH, 280 mOsm. Extracellular (bath) solution contained (mM): 70 NaCl; 50 NMDG; 40 TEA-Cl; 4 CsCl; 2 $MgCl_2$; 2 $CaCl_2$; 10 HEPES; 5 Glucose; adjusted to pH 7.4, approximately 300 mOsm. <u>Compounds and application</u>: Same as above section 4.5. <u>Pipettes</u>: Standard wall borosilicate glass pipettes (OD x ID x length: 1.5 mm x 0.86 mm x 7.5 cm, Harvard, cat # 64-0792) were pulled and fire-polished to 0.7 - 3 MΩ using a P-97 (Sutter Instruments) pipette puller. <u>Protocols</u>: Current-voltage (I_{Na}-V) relationships were determined by application of a pre-pulse to -100 mV (100 ms), followed by a series of step pulses from -65 mV to +60 mV (5 mV increments (100 ms)), before returning to hold at -70 mV (repetition interval of 3 sec, P/8 leak subtraction). Voltage dependence of steady-state fast inactivation was determined by application of a series of pre-pulses from -110 to +2.5 mV (7.5 mV increments (100 ms)), then a pulse at -30 mV, followed by hold at -70 mV (50 ms) (3 sec repetition interval) for bath and all compounds except for TTX, for which a pulse at -10 mV was applied (**Figure 4.2**).

A

B
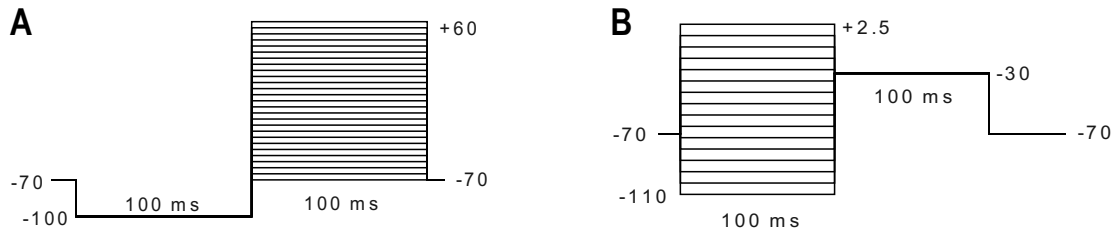
Figure 4.2: Voltage-clamp protocols used in whole-cell patch-clamp experiments. A) Current-voltage protocol. **B)** Steady-state fast inactivation protocol.

Data acquisition and analysis: Recordings were amplified with Axopatch 200A, digitized with Digidata 1322A, sampled at 20 kHz, filtered at 5 kHz, recorded with pCLAMP 9 software (Molecular Devices), and analyzed in Clampfit 10.3.2 (Molecular Devices), Prism v8.0.0 (GraphPad), and IBM SPSS Statistics v25. Peak sodium currents were normalized to the cell capacitance to account for differences in cell size. The estimated conductance (G) was calculated from the measured current (I) ($I/(V_{cmd} - V_{rev})$, where V_{cmd} is the command voltage and V_{rev} is the reversal potential for sodium under the experimental conditions (50 mV), and normalized to the maximum conductance (G_{max}). G/G_{max} was fitted with a Boltzmann sigmoidal curve in steady-state activation plots. For steady-state fast inactivation, peak inward currents were normalized to the maximal inward current (I_{max}) and fitted using a Boltzmann equation: $I/I_{max} = 1/(1+\exp((V_{50} - V_m)/k))$, where V_{50} is the half-maximal sodium current, V_m is the pre-conditioning potential, and k is the slope factor.

4.7 Literature cited

Aureli, M, Mauri, L, Ciampa, MG, Prinetti, A, Toffano, G, Secchieri, C & Sonnino, S 2016, 'GM1 Ganglioside: Past Studies and Future Potential', *Molecular Neurobiology*, vol. 53, no. 3, 2016/04/01, pp. 1824-1842.

Castro, J, Harrington, AM, Garcia-Caraballo, S, Maddern, J, Grundy, L, Zhang, J, Page, G, Miller, PE, Craik, DJ, Adams, DJ & Brierley, SM 2017, 'alpha-Conotoxin Vc1.1 inhibits human dorsal root ganglion neuroexcitability and mouse colonic nociception via GABA_B receptors', *Gut*, vol. 66, no. 6, Jun, pp. 1083-1094.

Feng, B, La, J-H, Tanaka, T, Schwartz, ES, McMurray, TP & Gebhart, GF 2012, 'Altered colorectal afferent function associated with TNBS-induced visceral hypersensitivity in mice', *American journal of physiology. Gastrointestinal and liver physiology*, vol. 303, no. 7, pp. G817-G824.

Grundy, L, Harrington, AM, Castro, J, Garcia-Caraballo, S, Deiteren, A, Maddern, J, Rychkov, GY, Ge, P, Peters, S, Feil, R, Miller, P, Ghetti, A, Hannig, G, Kurtz, CB, Silos-Santiago, I & Brierley, SM 2018, 'Chronic linaclotide treatment reduces colitis-induced neuroplasticity and reverses persistent bladder dysfunction', *JCI Insight*, vol. 3, no. 19, p. e121841.

Hughes, PA, Brierley, SM, Martin, CM, Brookes, SJ, Linden, DR & Blackshaw, LA 2009, 'Post-inflammatory colonic afferent sensitisation: different subtypes, different pathways and different time courses', *Gut*, vol. 58, no. 10, Oct, pp. 1333-1341.

Jobling, MG, Yang, Z, Kam, WR, Lencer, WI & Holmes, RK 2012, 'A single native ganglioside GM1-binding site is sufficient for cholera toxin to bind to cells and complete the intoxication pathway', *mBio*, vol. 3, no. 6, pp. e00401-00412.

Salvatierra, J, Castro, J, Erickson, A, Li, Q, Braz, J, Gilchrist, J, Grundy, L, Rychkov, GY, Deiteren, A, Rais, R, King, GF, Slusher, BS, Basbaum, A, Pasricha, PJ, Brierley, SM & Bosmans, F 2018, 'Na_v1.1 inhibition can reduce visceral hypersensitivity', *JCI Insight*, vol. 3, no. 11, Jun 7.

Chapter 5 Active electrophysiological properties of colon-innervating dorsal root ganglia neurons from healthy mice and TNBS-treated mice

In this section, gene expression of voltage-gated sodium (Na_v) channels in thoracolumbar (TL) and lumbosacral (LS) dorsal root ganglia (DRG), and in neurons retrogradely labeled from the colon, was investigated in samples from healthy control (HC) and TNBS-treated (CVH) mice. The first hypothesis for this part of the study was that Na_v channel expression, particularly of $Na_v1.7$ and $Na_v1.8$, would be altered in the disease state, as shown by others using similar visceral hypersensitivity models (King, Macleod & Vanner 2009; Qu et al. 2013). Electrophysiological properties of TL and LS colon-innervating DRG neurons from healthy and CVH mice were measured and compared. The second hypothesis for this section was that colon-innervating DRG neurons from CVH mice would display one or more signs of enhanced excitability: 1) reduced rheobase, 2) increased number of action potentials at 2-times rheobase, and 3) increased peak sodium current density (Hillsley et al. 2006; R Abdrakhmanova et al. 2010).

5.1 Thoracolumbar and lumbosacral dorsal root ganglia from healthy mice and TNBS-treated mice have similar expression levels of $Na_v1.1$-$Na_v1.9$ (*scn1a-scn11a*) and β-subunits β1-β4 (*scn1b-scn4b*)

DRG at spinal levels T10-L1 and L5-S1, which contain the cell bodies of sensory neurons that innervate the colon (Kyloh et al. 2011), were isolated from age-matched healthy and CVH adult male mice. qPCR was performed on RNA extracted from individual DRG pairs for the nine Na_v isoforms, *scn1a* ($Na_v1.1$), *Scn2a* ($Na_v1.2$), *Scn3a* ($Na_v1.3$), *Scn4a* ($Na_v1.4$), *Scn5a* ($Na_v1.5$), *Scn8a* ($Na_v1.6$), *scn9a* ($Na_v1.7$), *Scn10a* ($Na_v1.8$), *scn11a* ($Na_v1.9$), and the four β-subunits, *scn1b* (β1), *Scn2b* (β2), *Scn3b* (β3) and *scn4b* (β4). Expression data was separated into TL (T10-L1) (**Table 5.1**) and lumbosacral (L5-S1) (**Table 5.2**), and is shown in **Figure 5.1**.
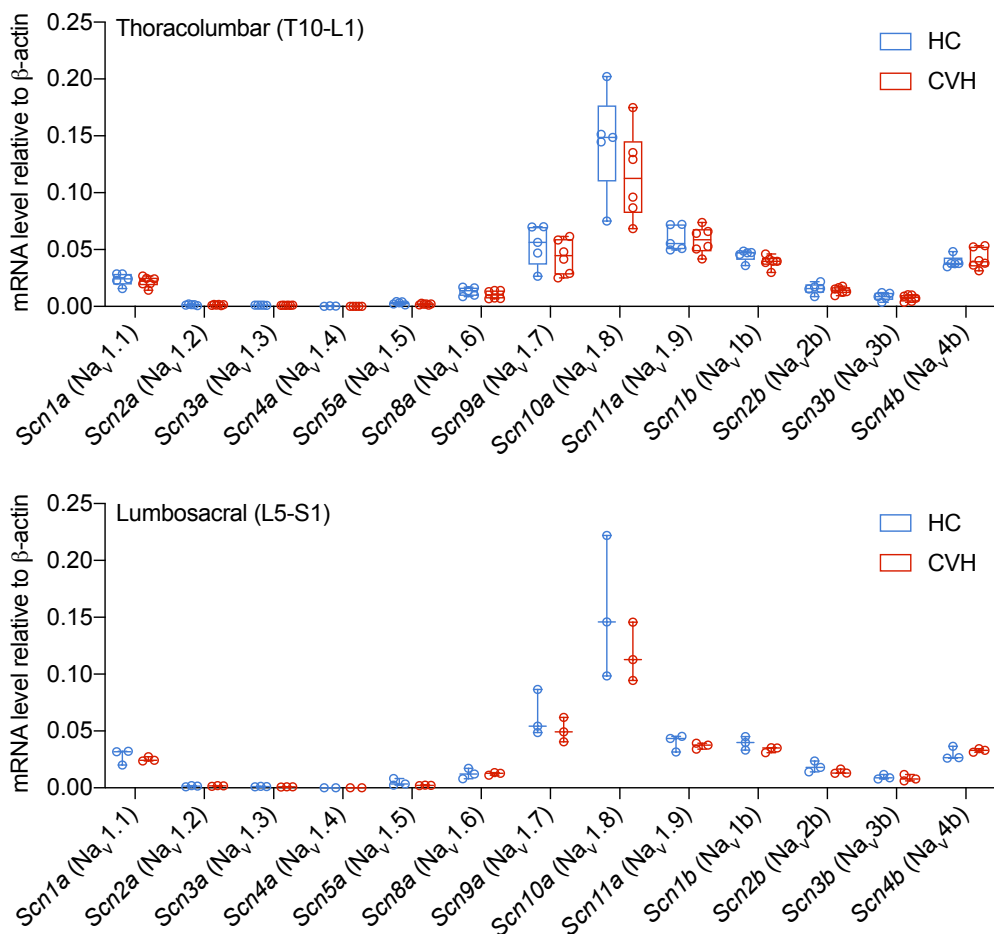
Figure 5.1: Pooled mRNA expression of *scn1a-scn11a* and *scn1b-scn4b* in dorsal root ganglia from healthy control (HC) and TNBS-treated (CVH) mice. Top: Expression of *scn1a-scn11a* and *scn1b-scn4b* in thoracolumbar (T10-L1) ganglia from healthy control (blue) and TNBS-treated (red) mice. Bottom: Expression of *scn1a-scn11a* and *scn1b-scn4b* in lumbosacral (L5-S1) ganglia from healthy control (blue) and TNBS-treated (red) mice. Expression of each gene was normalized to β-actin and is represented as Tukey box and whiskers plots where the middle line shows the median, upper and lower box limits show 1st and 3rd quartiles and whisker length is 1.5 inter-quartile distances.

Table 5.1: Average mRNA expression of *scn1a-scn11a* and *scn1b-scn4b* normalized to β-actin for thoracolumbar (T10-L1) dorsal root ganglia from healthy control (HC) and TNBS-treated (CVH) mice.

Gene	Average mRNA expression normalized to β-actin ± SD		Independent samples t-test				
	HC (N = 5)	CVH (N = 6)	Mean difference	95%CI Lower	95%CI Upper	t	p-value
Scn1a	0.0240 ± 0.0054	0.0217 ± 0.004	0.0023	-0.0044	0.0090	0.778	0.457
Scn2a	0.0014 ± 0.0005	0.0013 ± 0.0005	0.0001	-0.0006	0.0008	0.433	0.675
Scn3a	0.0011 ± 0.0001	0.0010 ± 0.0001	< 0.0000	-0.0002	0.0002	0.46	0.657
Scn4a	0.0003 ± 0.0002	< 0.0000	/	/	/	/	/
Scn5a	0.0030 ± 0.0012	0.0019 ± 0.006	0.0011	-0.0002	0.0024	1.956	0.082
Scn8a	0.0131 ± 0.0037	0.0104 ± 0.0037	0.0027	-0.0023	0.0078	1.23	0.250
Scn9a	0.0540 ± 0.0181	0.0439 ± 0.0150	0.0101	-0.0124	0.0326	1.012	0.338
Scn10a	0.1444 ± 0.0453	0.1151 ± 0.0388	0.0293	-0.0281	0.0866	1.155	0.278
Scn11a	0.0600 ± 0.0112	0.0582 ± 0.0118	0.0018	-0.0140	0.0176	0.259	0.802
Scn1b	0.0450 ± 0.0052	0.0393 ± 0.0053	0.0057	-0.0014	0.0129	1.809	0.104
Scn2b	0.0157 ± 0.0047	0.0142 ± 0.0030	0.0015	-0.0037	0.0068	0.661	0.525
Scn3b	0.0088 ± 0.0035	0.0074 ± 0.0028	0.0014	-0.0029	0.0056	0.713	0.494
Scn4b	0.0393 ± 0.0052	0.0420 ± 0.0090	-0.0027	-0.0130	0.0076	-0.591	0.569

Table 5.2: Average mRNA expression of *scn1a-scn11a* and *scn1b-scn4b* normalized to β-actin for lumbosacral (L5-S1) dorsal root ganglia from healthy control (HC) and TNBS-treated (CVH) mice.

Gene	Average mRNA expression normalized to β-actin ± SD		Independent samples t-test				
	HC (N = 3)	CVH (N = 3)	Mean difference	95%CI Lower	95%CI Upper	t	p-value
Scn1a	0.0281 ± 0.0068	0.0251 ± 0.0020	0.0029	-0.0085	0.0143	0.709	0.518
Scn2a	0.0015 ± 0.006	0.0016 ± 0.0003	-0.0001	-0.0011	0.0009	-0.257	0.810
Scn3a	0.0011 ± 0.0001	0.0009 ± 0.0001	0.0002	< 0.0000	0.0005	2.69	0.055
Scn4a	< 0.0000	< 0.0000	/	/	/	/	/
Scn5a	0.0047 ± 0.0030	0.0021 ± 0.0002	0.0025	-0.0023	0.0074	1.454	0.220
Scn8a	0.0125 ± 0.0046	0.0124 ± 0.0012	0.0001	-0.0075	0.0076	0.023	0.983
Scn9a	0.0631 ± 0.0205	0.0506 ± 0.0108	0.0125	-0.0246	0.0496	0.937	0.402
Scn10a	0.1555 ± 0.0623	0.1177 ± 0.0260	0.0378	-0.0705	0.1461	0.969	0.387
Scn11a	0.0401 ± 0.0075	0.0369 ± 0.0026	0.0031	-0.0096	0.0159	0.682	0.532
Scn1b	0.0394 ± 0.0060	0.0338 ± 0.0026	0.0056	-0.0048	0.0160	1.498	0.209
Scn2b	0.0186 ± 0.0048	0.0141 ± 0.0022	0.0045	-0.0039	0.0129	1.479	0.213
Scn3b	0.0095 ± 0.0021	0.0085 ± 0.0028	0.0009	-0.0048	0.0066	0.455	0.672
Scn4b	0.0297 ± 0.0059	0.0329 ± 0.0016	-0.0032	-0.0130	0.0067	-0.892	0.423

Scn9a (Na$_v$1.7) *Scn10a* (Na$_v$1.8) and *scn11a* (Na$_v$1.9) were the most abundant Na$_v$ isoforms in TL and LS DRG from healthy and CVH mice. *Scn1a* (Na$_v$1.1) and *Scn8a* (Na$_v$1.6) had moderate expression levels, *Scn2a* (Na$_v$1.2), *Scn3a* (Na$_v$1.3), and *Scn5a* (Na$_v$1.5) had low expression levels, whereas *Scn4a* (Na$_v$1.4) was not detected in most samples. All β subunits were detected, with *scn1b* (β1) and *scn4b* (β4) having the highest expression levels, followed by *Scn2b* (β2) and finally *Scn3b* (β3). A series of independent samples t-tests were run on *scn1a-scn11a* and *scn1b-scn4b* expression from TL DRG from 5 healthy and 6 CVH mice, and from lumbosacral DRG from 3 healthy and 3 CVH mice. There was insufficient evidence ($p > 0.05$) to reject the null hypothesis that expression level of any gene differed between healthy and CVH samples within each spinal level (see **Table 5.1** and **Table 5.2** for statistics).

5.2 Thoracolumbar colon-innervating dorsal root ganglia from healthy mice and TNBS-treated mice have comparable expression of Na$_v$1.1-Na$_v$1.9 (*scn1a-scn11a*) at the single-cell level

Colon-innervating DRG neurons comprise a minority of the total number of neurons in TL and LS DRG, and labeling methods are often applied to be able to measure this population specifically (Beyak et al. 2004; Grundy et al. 2018). To be able to identify colon-innervating neurons, a retrogradely transported fluorescent compound was injected into the serosa of the distal colon of mice, and DRG neurons were isolated 3-5 days following this procedure. TL and LS DRG cultures were examined, and fluorescent neurons were collected by a single cell picking method. Single-cell PCR was performed on 24 colon-innervating TL DRG neurons from healthy mice and 30 neurons from CVH mice to assess expression of Na$_v$ isoforms Na$_v$1.1-Na$_v$1.9 (*scn1a-scn11a*). The results are summarized in **Table 5.3** and displayed in **Figure 5.2**.

Table 5.3: Number and percentage of thoracolumbar neurons from healthy control (HC) and TNBS-treated (CVH) mice that expressed *scn1a-scn11a* mRNA.

Gene	HC (n = 24)		CVH (n = 30)		Fisher's Exact Test p-value
	n	%	n	%	
Scn1a	8	(33)	14	(47)	0.407
Scn2a	16	(67)	21	(70)	1.000
Scn3a	14	(58)	18	(60)	1.000
Scn4a	3	(13)	3	(10)	1.000
Scn5a	10	(42)	17	(57)	0.412
Scn8a	15	(63)	17	(57)	0.783
Scn9a	24	(100)	28	(93)	0.497
Scn10a	21	(88)	25	(83)	0.720
Scn11a	24	(100)	29	(97)	1.000
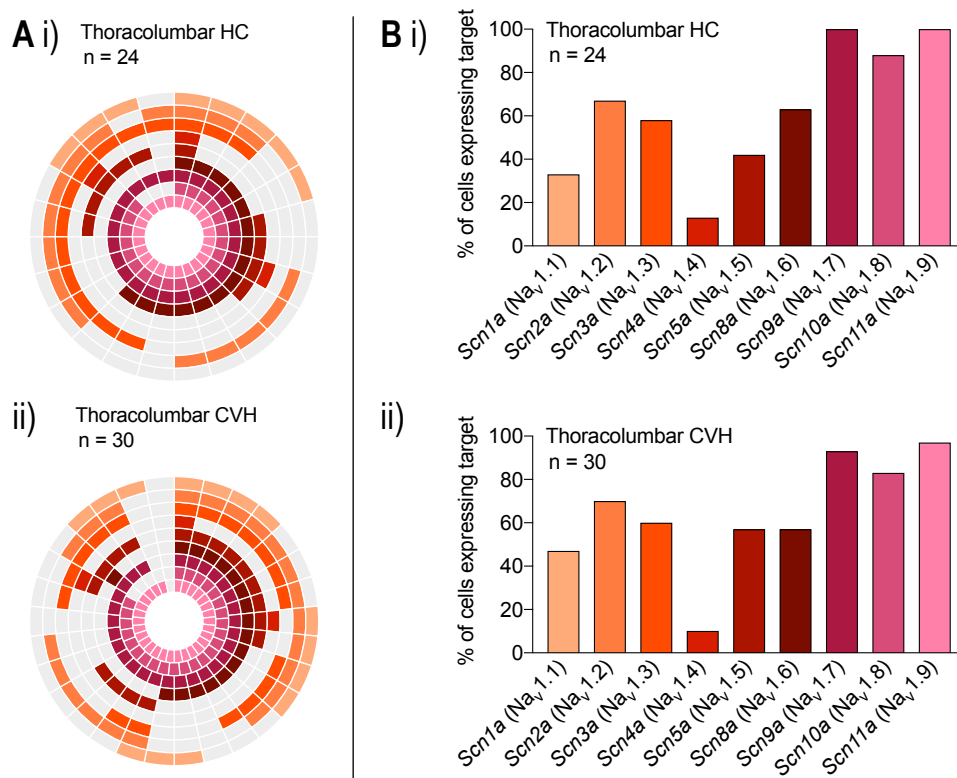
Figure 5.2: Single-cell mRNA expression of *scn1a-scn11a* in colon-innervating thoracolumbar dorsal root ganglia (T10-L1) from healthy control (HC) and TNBS-treated (CVH) mice. Donut plot of detected (bold colors) and not detected (grey) Na$_v$ isoforms in **i)** healthy and **ii)** TNBS-treated neurons. Each wedge represents one neuron. The innermost circle represents expression of *scn11a* (Na$_v$1.9), and the outermost circle represents expression of *scn1a* (Na$_v$1.1), with color coding consistent with bar graph labels in (**B**). **B)** Percentage of neurons where each target gene was detected in **i)** healthy and **ii)** TNBS-treated samples.

Fisher's Exact Test was used to test for an association between health status (HC or CVH) and the number of neurons that expressed each of the Na$_v$ channel genes. This test was used as the expected cell counts were small (<5). There was insufficient evidence to reject the null hypothesis that there is no association between the number of neurons that express each of the genes and health status (p > 0.05) (see **Table 5.3** for details).

5.3 Thoracolumbar and lumbosacral colon-innervating dorsal root ganglia from healthy mice express β-subunits β1-β4 (*scn1b-scn4b*) at the single-cell level

Single-cell PCR was performed on 33 colon-innervating TL DRG neurons and 31 colon-innervating LS DRG neurons from healthy mice following patch-clamp experiments to assess expression of the β-subunits β1-β4 (*scn1b-scn4b*). The results are summarized in **Table 5.4** and displayed in **Figure 5.3**.

Table 5.4: Number and percentage of thoracolumbar and lumbosacral neurons from healthy mice that expressed *scn1b-scn4b* mRNA.

Gene	Thoracolumbar (n = 33)		Lumbosacral (n = 31)	
	n	%	n	%
Scn1b	29	(88)	28	(90)
Scn2b	24	(73)	25	(81)
Scn3b	26	(79)	27	(87)
Scn4b	10	(30)	7	(23)
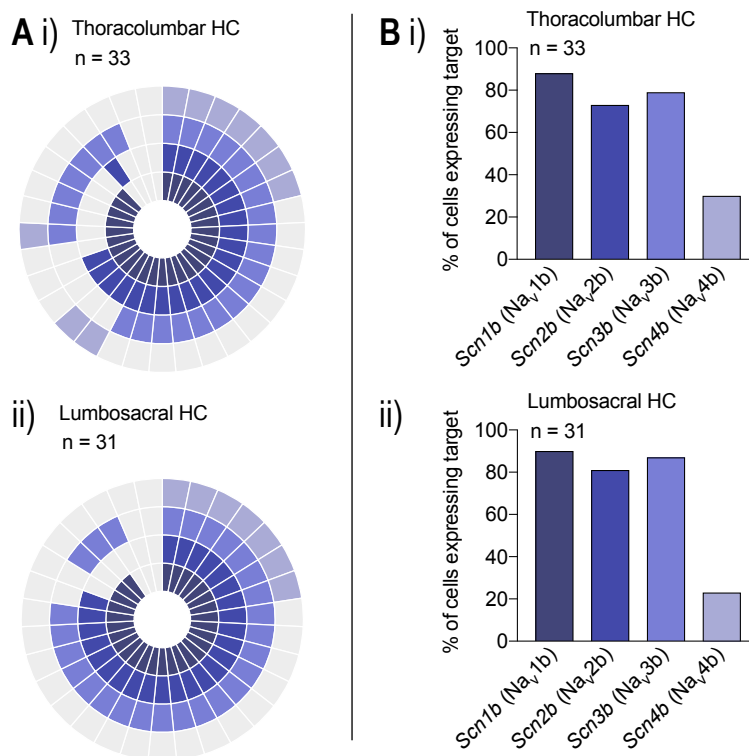
Figure 5.3: Single-cell mRNA expression of *scn1b-scn4b* in colon-innervating thoracolumbar and lumbosacral dorsal root ganglia from healthy control (HC) mice. Donut plot of detected (bold colors) and not detected (grey) Na$_v$ β-subunits in **i)** thoracolumbar and **ii)** lumbosacral neurons. Each wedge represents one neuron. The innermost circle represents expression of *scn1b* (β1), and the outermost circle represents expression of *scn4b* (β4), with color coding consistent with bar graph labels in **(B)**. **B)** Percentage of neurons where each target gene was detected in **i)** thoracolumbar and **ii)** lumbosacral samples. Note that neurons were used in patch-clamp electrophysiology experiments prior to collection, which may lead to an underrepresentation of transcript detection due to dilution of RNA.

`

Transcripts for the four main Na$_v$ β-subunits were detected in colon-innervating TL and LS neurons from healthy mice. β1, β2, and β3 were detected in the majority of neurons (> 70%), whereas β4 was detected in a smaller set of neurons (23-30%). While the single-cell expression dataset presented in section 5.2 was based on transcribed RNA from unpatched neurons < 12 hrs following culture, the Na$_v$ β-subunit expression dataset is based on transcribed RNA from patched neurons 24 – 48 hrs following culture, due to experimental limitations. This may lead to an underrepresentation of the number of neurons that express each isoform due to perfusion of cytoplasm during patch-clamp electrophysiology and is subject to expression changes due to longer exposure to culture conditions.

5.4 Baseline rheobase in colon-innervating dorsal root ganglia neurons is affected by spinal origin, number of days in culture, soma diameter, and resting membrane potential, but not TNBS treatment

The number of colon-innervating DRG neurons recorded for each of four groups defined by spinal level (TL or LS) and health status (HC or CVH) as well as summary statistics (mean ± SEM) for rheobase and the natural log transformed value, ln(rheobase), are reported for each group in **Table 5.5**, along with data on resting membrane potential and soma diameter. In addition, the number of neurons recorded on day 1 and day 2 post culturing is listed in **Table 5.6**.

Table 5.5: Summary statistics for rheobase, ln(rheobase), resting membrane potential and average diameter according to spinal level (thoracolumbar (TL) and lumbosacral (LS)) and health status (healthy control (HC) and TNBS-treated (CVH)).

Group	n	Average rheobase (pA) ± SEM	Average ln(rheobase) ± SEM	Average resting membrane potential (pA) ± SEM	Average diameter (µm) ± SEM
TL neurons					
HC	132	326.6 ± 29.3	5.3 ± 0.1	-52.9 ± 0.7	29 ± 1
CVH	59	392.2 ± 57.7	5.4 ± 0.2	-51.9 ± 1.0	30 ± 1
LS neurons					
HC	48	120.6 ± 14.4	4.5 ± 0.1	-48.4 ± 1.1	30 ± 1
CVH	50	87.2 ± 12.7	4.2 ± 0.1	-49.8 ± 1.1	31 ± 1

Table 5.6: Summary statistics for recordings made on day 1 and day 2 post culturing according to spinal level (thoracolumbar (TL) and lumbosacral (LS)) and health status (healthy control (HC) and TNBS-treated (CVH)).

Group	Day 1		Day 1	
	n	% of neurons	n	% of neurons
TL neurons				
HC (n=132)	63	(48)	69	(52)
CVH (n=59)	22	(37)	37	(63)
LS neurons				
HC (n=48)	20	(42)	28	(58)
CVH (n=50)	34	(68)	16	(32)

Multivariable regression was used to investigate whether health status could explain baseline rheobase in colon-innervating TL and LS DRG neurons. This approach allowed controlling for potentially confounding variables that may be associated with neuronal excitability, including the resting membrane potential of the neuron before recording, the average diameter of the soma, and whether the neuron was recorded on day 1 (16-28 hrs) or day 2 (38-48 hrs) post culturing. Rheobase as the dependent variable did not satisfy the assumption of equal variance of residuals and was transformed to the natural log of the rheobase values, ln(rheobase), which satisfied this assumption. Visual inspection of scatterplots indicated approximately linear relationships between the predictor variables and the outcome variable ln(rheobase). Variable box plots indicated there were no major outliers. Regression model adequacy was assessed via visual inspection of the residuals plot, and independence of residuals was assessed using the Durbin-Watson statistic. Multivariable regression coefficients are shown in **Table 5.7** with coded entries for categorical variables listed in **Table 5.8**.

Table 5.7: Linear regression coefficients for multivariable regression with dependent variable ln(rheobase) and independent variables health status, spinal level, day post culture, diameter, and resting membrane potential.

Regression variable	Unstandardized coefficients		t	P-value	95% Confidence Interval for B	
	B	Std. Error			Lower bound	Upper bound
Health status (HC/CVH)	-0.134	0.129	-1.035	0.3021	-0.389	0.121
Spinal level (TL/LS)	-0.912	0.137	-6.648	<0.0001	-1.183	-0.641
Day post culture (D1/D2)	0.590	0.125	4.717	<0.0001	0.343	0.837
Diameter	0.058	0.009	6.341	<0.0001	0.040	0.076
Resting membrane potential	-0.032	0.009	-3.604	0.0004	-0.050	-0.015

Table 5.8: Values of categorical variables in regression.

	Health status		Spinal level		Day post culture	
	HC	CVH	TL	LS	D1	D2
Code value	0	1	0	1	0	1

The regression model yielded R^2 = 0.445, $F(5, 174)$ = 27.848, $p < 0.0001$, indicating that the regression model accounts for approximately 44.5% of the variance in ln(rheobase). No issues with multicollinearity were observed (VIF statistic range 1.03 – 1.13, collinearity indices < 30).

The final regression model was: Ln(rheobase) = 1.672 – 0.134(health status) – 0.912(spinal level) + 0.590(day post culture) + 0.058(diameter) – 0.032(resting membrane potential)

In summary, linear regression was used to assess whether rheobase in colon-innervating DRG neurons from CVH mice differed to colon-innervating DRG neurons from healthy mice. 289 neurons were included in the analysis, and potentially confounding variables, such as spinal level, number of days in culture, average soma diameter, and resting membrane potential were controlled for. There was insufficient evidence to reject the null hypothesis that health status has no effect on rheobase levels (95% CI -0.389 to 0.121, p = 0.302). With all other variables held constant, LS neurons had, on average, ln(rheobase) levels that were 0.912 units lower than TL neurons (95% CI -1.183 to -0.641, $p < 0.0001$). Neurons recorded on day 2 had, on average, ln(rheobase) levels that were 0.590 units higher compared to neurons recorded on day 1 (95% CI 0.343 to 0.837, $p < 0.0001$). There was a significant positive effect of neuron diameter on ln(rheobase), with every 1 μm increase in neuron diameter associated with an average increase in ln(rheobase) of 0.058 units (95% CI 0.040 to 0.076, $p < 0.0001$). Resting membrane potential was negatively associated with ln(rheobase), with every 1 mV depolarization of resting membrane potential associated with a 0.032 unit decrease in ln(rheobase) (95% CI -0.050 to -0.015, p = 0.0004).

5.5 Colon-innervating dorsal root ganglia neurons from TNBS-treated mice do not display a higher number of action potentials at 2-times rheobase compared to neurons from healthy mice

The number of colon-innervating DRG neurons in each of four groups defined by spinal level (TL or LS) and health status (HC or CVH) that fired a single or multiple action potential(s) at 2-times rheobase is summarized in **Table 5.9**.

Table 5.9: Summary statistics for number of neurons that fired either a single or multiple action potential(s) according to spinal level (thoracolumbar (TL) and lumbosacral (LS)) and health status (healthy control (HC) and TNBS-treated (CVH)).

Group	Single		Multiple		Fisher's Exact Test
	n	% of neurons	n	% of neurons	p-value
TL neurons					
HC (n=101)	71	(70)	30	(30)	0.076
CVH (n=50)	42	(84)	8	(16)	
LS neurons					
HC (n=46)	38	(83)	8	(17)	0.045
CVH (n=50)	48	(96)	2	(4)	

Fisher's exact test was used to investigate whether a population of neurons defined by health status from each spinal level was more or less likely to elicit multiple action potentials at 2-times rheobase. This test was used as the expected cell counts were small (<5). 113 TL neurons and 86 LS neurons were included in the analysis. For TL neurons, there was insufficient evidence to reject the null hypothesis that there is no association between action potential frequency at 2-times rheobase and health status (p = 0.076). In the LS dataset, neurons from healthy mice were more likely to elicit multiple action potentials at 2-times rheobase compared to neurons from CVH mice (p = 0.045).

5.6 Baseline peak sodium current density in colon-innervating dorsal root ganglia neurons is affected by number of days in culture, but not health status or spinal origin

The number of colon-innervating DRG neurons recorded for each of four groups defined by spinal level (TL or LS) and health status (HC or CVH) as well as summary statistics (mean ± SEM) for peak sodium current and peak sodium current density, are reported for each group in **Table 5.10** and shown in **Figure 5.4**. In addition to the response variable peak sodium current density, the number of neurons recorded on day 1 and day 2 post culturing was recorded and is reported in **Table 5.11**.

Table 5.10: Summary statistics for peak sodium current and peak sodium current density according to spinal level (thoracolumbar (TL) and lumbosacral (LS)) and health status (healthy control (HC) and TNBS-treated (CVH)).

Group	n	Average peak current (pA) ± SEM	Average peak current density (pA/pF) ± SEM
TL neurons			
HC	35	-6564 ± 622	-193 ± 14
CVH	12	-6029 ± 1184	-196 ± 31
LS neurons			
HC	13	-5292 ± 830	-171 ± 24
CVH	18	-4588 ± 611	-162 ± 16

Table 5.11: Summary statistics for recordings made on day 1 and day 2 post culture according to spinal level (thoracolumbar (TL) and lumbosacral (LS)) and health status (healthy control (HC) and TNBS-treated (CVH)).

Group	Day 1		Day 1	
	n	% of neurons	n	% of neurons
TL neurons				
HC (n=35)	17	(49)	18	(51)
CVH (n=12)	8	(67)	4	(33)
LS neurons				
HC (n=13)	9	(69)	4	(31)
CVH (n=18)	10	(56)	8	(44)
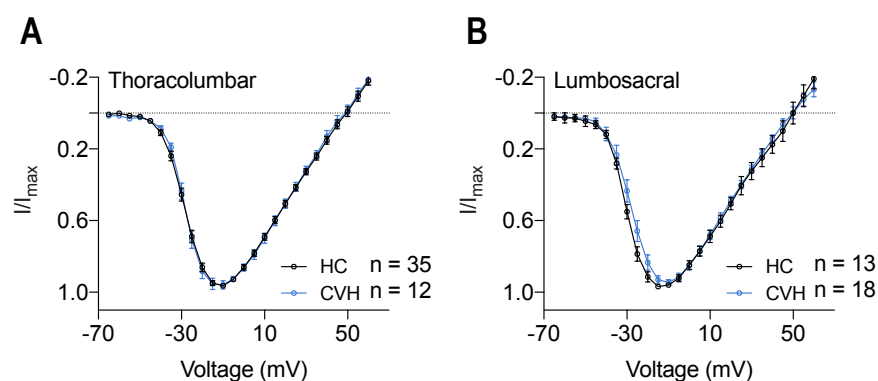
Figure 5.4: Voltage-dependent sodium current density in colon-innervating thoracolumbar and lumbosacral dorsal root ganglia neurons from healthy control (HC) and TNBS-treated (CVH) mice. Current-voltage relationship in **A**) thoracolumbar neurons from healthy (black) and TNBS-treated (blue) mice and **B**) lumbosacral neurons from healthy (black) and TNBS-treated (blue) mice. The measured current (I) at each voltage was normalized to the peak current (I_{max}), and each data point shown here is the averaged I/I_{max} ± SEM.

Multivariable regression was used to investigate whether health status was associated with baseline peak sodium current density in colon-innervating TL and LS DRG neurons. This approach allowed controlling for potentially confounding variables that may be associated with neuronal excitability, including whether the neuron was recorded on day 1 (16-28 hrs) or day 2 (38-48 hrs) post culturing. Visual inspection of scatterplots indicated approximately linear relationships between the predictor variables and the outcome variable peak sodium current density. Variable box plots indicated there were no major outliers. Regression model adequacy was assessed via visual inspection of the residuals plot, and independence of residuals was assessed using the Durbin-Watson statistic. Multivariable regression coefficients are shown in **Table 5.12** with coded entries for categorical variables listed in **Table 5.13**.

Table 5.12: Linear regression coefficients for multivariable regression with dependent variable peak sodium current density and independent variables health status, spinal level, and day post culture.

Regression variable	Unstandardized coefficients		t	p-value	95% Confidence Interval for B	
	B	Std. Error			Lower bound	Upper bound
Health status (HC/CVH)	0.303	19.954	0.015	0.9879	-39.456	40.063
Spinal level (TL/LS)	23.450	19.868	1.180	0.2417	-16.139	63.038
Day post culture (D1/D2)	-51.535	18.558	-2.777	0.0069	-88.514	-14.557

Table 5.13: Values of categorical variables in regression.

	Health status		Spinal level		Day post culture	
	HC	CVH	TL	LS	D1	D2
Code value	0	1	0	1	0	1

$R^2 = 0.118$ was obtained for the regression model, $F(3, 74) = 3.304$, $p = 0.025$, indicating that the regression model accounts for approximately 11.8% of the variance in peak sodium current density. No issues with multicollinearity were observed (VIF statistic range 1.01 – 1.12, collinearity indices < 5).

The final regression model was: Peak sodium current density (pA/pF) = -169.504 + 0.303(health status) + 23.450(spinal level) – 51.535(day post culture)

In summary, multivariable regression was used to assess whether peak sodium current density in colon-innervating DRG neurons from CVH mice differed compared to colon-innervating DRG neurons from healthy mice. 78 neurons were included in the analysis and the potentially confounding variables spinal level and number of days in culture were controlled for. There was insufficient evidence to reject the null hypothesis that health status has no effect on peak sodium current density (95% CI -39.456 to 40.063, p = 0.988). Spinal level was also not significantly associated with peak sodium current density (95% CI -16.139 to 63.038, p = 0.242). With all other variables held constant, neurons recorded on day 2 had, on average, 51.535 pA/pF greater peak sodium current density compared to neurons recorded on day 1 (95% CI -88.514 to -14.557 pA/pF, p = 0.007).

5.7 Literature cited

Beyak, MJ, Ramji, N, Krol, KM, Kawaja, MD & Vanner, SJ 2004, 'Two TTX-resistant Na⁺ currents in mouse colonic dorsal root ganglia neurons and their role in colitis-induced hyperexcitability', *Am. J. Physiol. GI. Liver Physiol.*, vol. 287, no. 4, Oct, pp. G845-855.

Grundy, L, Harrington, AM, Castro, J, Garcia-Caraballo, S, Deiteren, A, Maddern, J, Rychkov, GY, Ge, P, Peters, S, Feil, R, Miller, P, Ghetti, A, Hannig, G, Kurtz, CB, Silos-Santiago, I & Brierley, SM 2018, 'Chronic linaclotide treatment reduces colitis-induced neuroplasticity and reverses persistent bladder dysfunction', *JCI Insight*, vol. 3, no. 19, p. e121841.

Hillsley, K, Lin, JH, Stanisz, A, Grundy, D, Aerssens, J, Peeters, PJ, Moechars, D, Coulie, B & Stead, RH 2006, 'Dissecting the role of sodium currents in visceral sensory neurons in a model of chronic hyperexcitability using Na$_v$1.8 and Na$_v$1.9 null mice', *J. Physiol.*, vol. 576, no. Pt 1, Oct 1, pp. 257-267.

King, DE, Macleod, RJ & Vanner, SJ 2009, 'Trinitrobenzenesulphonic acid colitis alters Na$_v$1.8 channel expression in mouse dorsal root ganglia neurons', *Neurogastroenterology & Motility*, vol. 21, no. 8, pp. 880-e864.

Kyloh, M, Nicholas, S, Zagorodnyuk, VP, Brookes, SJ & Spencer, NJ 2011, 'Identification of the visceral pain pathway activated by noxious colorectal distension in mice', *Frontiers in Neuroscience*, vol. 5, 2011.

Qu, R, Tao, J, Wang, Y, Zhou, Y, Wu, G, Xiao, Y, Hu, C-Y, Jiang, X & Xu, G-Y 2013, 'Neonatal colonic inflammation sensitizes voltage-gated Na^+ channels via upregulation of cystathionine beta-synthetase expression in rat primary sensory neurons', *American Journal of Physiology-Gastrointestinal and Liver Physiology*, vol. 304, no. 9, May, pp. G763-G772.

R Abdrakhmanova, G, Alsharari, S, Kang, M, Imad Damaj, M & Akbarali, H 2010, *7-nAChR-mediated suppression of hyperexcitability of colonic dorsal root ganglia neurons in experimental colitis*, vol. 299.

`

Chapter 6 The effect of Na$_v$ channel agonists on electrophysiological properties of colon-innervating dorsal root ganglia neurons

Modulation of Na$_v$ channels has been researched extensively as an alternative approach to treating neuropathic pain, inflammatory pain, trigeminal neuralgia, chemotherapy-related pain (Bagal et al. 2014), and visceral pain (Bennett et al. 2019). In Chapter 6 - Chapter 9, the effects of several Na$_v$ modulators on colon-innervating dorsal root ganglia (DRG) neurons from mice were evaluated to gain insight into the functional contribution of different Na$_v$ isoforms and the potential use of Na$_v$ modulators on colon-specific pain signaling pathways.

In this chapter, the effect of Na$_v$ channel activation in colon-innervating DRG neurons from healthy control (HC) mice was evaluated using two Na$_v$ channel agonists with different Na$_v$-selectivity; veratridine, which targets all Na$_v$ isoforms, and OD1, which targets Na$_v$1.4, Na$_v$1.6, and Na$_v$1.7.

6.1 The effect of veratridine on rheobase in colon-innervating dorsal root ganglia neurons from healthy mice

Veratridine is a plant alkaloid toxin that activates Na$_v$ channels using neurotoxin site 2 (**Table 3.1**), and does not discriminate between isoforms of the Na$_v$ channel family (Catterall, Goldin & Waxman 2005). In this section, the effects of veratridine on variables involved in action potential generation were evaluated.

6.1.1 Veratridine at 50 µM reduces rheobase, depolarizes membrane potential following action potential generation, decreases action potential overshoot and increases action potential half-width in colon-innervating dorsal root ganglia neurons

Action potential generation in colon-innervating TL and LS neurons from healthy mice were recorded prior to and following incubation with veratridine. It was assessed whether incubation with veratridine at 50 µM is associated with a reduction in average rheobase (analyzed as natural log values to meet assumptions for statistical testing), membrane potential, action potential overshoot, and action potential half-width relative to baseline in these neurons. Summary statistics for these variables are shown in **Table 6.1**, **Table 6.2**, and **Figure 6.1**.

Table 6.1: Summary statistics for rheobase and ln(rheobase) at baseline and in the presence of veratridine (50 µM) in thoracolumbar (TL) and lumbosacral (LS) neurons from healthy mice.

Group	n	Average rheobase (pA) ± SEM		Average ln(rheobase) ± SEM		Average fold change in rheobase ± SEM
		Baseline	Veratridine	Baseline	Veratridine	
TL neurons	8	220.6 ± 35.0	180.0 ± 37.2	5.3 ± 0.2	5.1 ± 0.2	0.82 ± 0.09
LS neurons	13	139.6 ± 47.7	95.0 ± 26.0	4.4 ± 0.3	4.1 ± 0.5	0.91 ± 0.15

Table 6.2: Summary statistics for average membrane potential at holding current, action potential overshoot and action potential half-width at baseline and in the presence of veratridine (50 µM) in thoracolumbar (TL) and lumbosacral (LS) neurons from healthy mice.

Group	n	Average membrane potential at holding current (mV) ± SEM		Average action potential overshoot (mV) ± SEM		Average action potential half-width (ms) ± SEM	
		Baseline	Veratridine	Baseline	Veratridine	Baseline	Veratridine
TL neurons	8	-72.2 ± 1.4	-30.2 ± 3.8	73.1 ± 2.9	67.7 ± 2.1	2.4 ± 0.3	2.7 ± 0.4
LS neurons	13	-70.7 ± 0.5	-23.6 ± 4.8	71.5 ± 3.7	51.9 ± 3.9	2.5 ± 0.3	3.8 ± 0.4
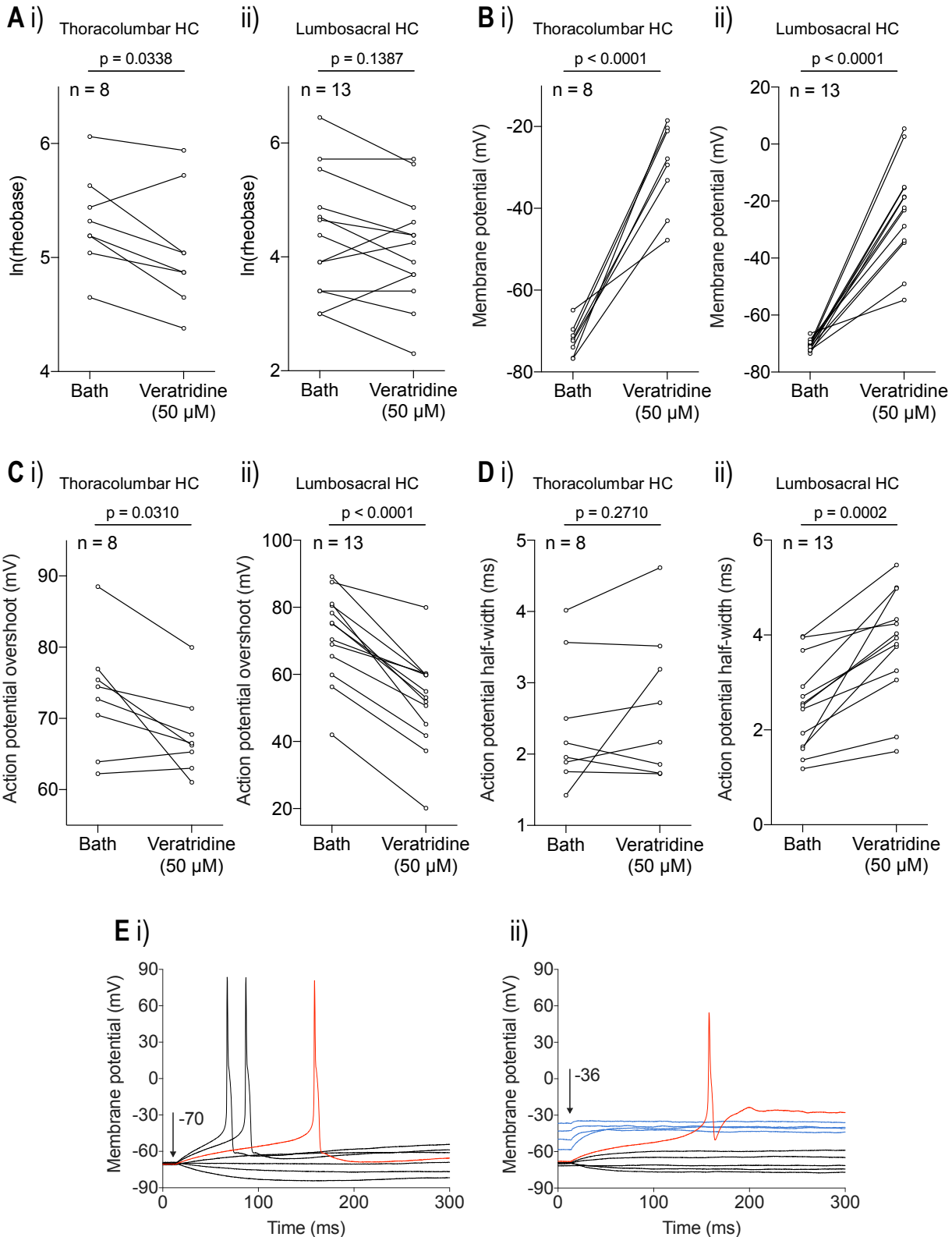
Figure 6.1: Veratridine (50 µM) reduces rheobase, depolarizes resting membrane potential, decreases action potential overshoot and increases action potential half-width in colon-innervating thoracolumbar and lumbosacral dorsal root ganglia neurons from healthy control (HC) mice. **A)** Ln(rheobase) at baseline and following incubation with 50 µM veratridine for 1-2 minutes in **i)** thoracolumbar and **ii)** lumbosacral neurons from healthy mice. Veratridine decreased mean ln(rheobase) compared to baseline in the thoracolumbar dataset (paired t-test, $p < 0.05$), but not in the lumbosacral dataset (paired t-test, $p > 0.05$). **B)** Membrane potential in response to holding current at baseline and following incubation with 50 µM veratridine for 1-2 minutes in **i)** thoracolumbar and **ii)** lumbosacral neurons from healthy mice. Veratridine increased mean membrane potential compared to baseline in both datasets (paired t-test, $p < 0.0001$). **C)** Action potential overshoot at baseline and following incubation with 50 µM veratridine for 1-2 minutes in **i)** thoracolumbar and **ii)** lumbosacral neurons from healthy mice. Veratridine decreased mean overshoot compared to baseline in both

datasets (paired t-test, p < 0.05). **D)** Action potential half-width at baseline and following incubation with 50 µM veratridine for 1-2 minutes in **i)** thoracolumbar and **ii)** lumbosacral neurons from healthy mice. Veratridine increased half-width in lumbosacral neurons (paired t-test, p < 0.05), but not in thoracolumbar neurons (paired t-test, p > 0.05). **E)** Raw traces of membrane potential measured at increasing current injections (10 pA increments starting at -20 pA) in a lumbosacral neuron. A depolarization of the membrane potential at holding current (during 0 - 10 ms) and a reduction in action potential overshoot after incubation with **ii)** veratridine compared to **i)** baseline was observed following the first action potential. The membrane repolarizes stepwise following the first action potential in the presence of veratridine (blue traces).

A series of paired t-tests were carried out on samples of 8 TL neurons and 13 LS neurons from healthy mice to assess the effect of veratridine (50 µM) on ln(rheobase), membrane potential, action potential overshoot, and action potential half-width.

<u>TL neurons.</u> TL neurons from healthy mice had a significantly lower mean ln(rheobase) in the presence of veratridine (5.1 ± 0.5) compared to baseline (5.3 ± 0.4). The estimated average difference was 0.2531 (95% CI -0.4791 to -0.0270, t(7) = -2.647, p = 0.033). TL neurons from healthy mice had a significantly depolarized mean membrane potential following the first action potential in the presence of veratridine (-30.2 ± 10.7 mV) compared to baseline (-72.2 ± 3.9 mV). The estimated average difference was 42.0 mV (95% CI 31.6 to 52.4 mV, t(7) = 9.518, p < 0.0001). The average action potential overshoot was significantly lower in the presence of veratridine (67.7 ± 5.9 mV) compared to baseline (73.1 ± 8.2 mV) (mean difference = -5.421 mV, 95% CI -10.18 to -0.6599 mV, t(7) = 2.692, p = 0.0310). Action potential half-width was not statistically different in the presence of veratridine (2.7 ± 1.0 ms) compared to baseline (2.4 ± 0.9 ms) (mean difference = 0.2818 ms, 95% CI -0.2759 to 0.8394 ms, t(7) = 1.195, p = 0.2710).

<u>LS neurons</u>. The average ln(rheobase) in LS neurons from healthy mice in the presence of veratridine (4.1 ± 1.0) was not statistically different to baseline (4.4 ± 1.1) (mean difference = 0.2384; 95% CI -0.5649 to 0.0881, t(12) = -1.591, p = 0.138). LS neurons from healthy mice had a significantly depolarized mean membrane potential following the first action potential in the presence of veratridine (-23.6 ± 17.3 mV) compared to baseline (-70.7 ± 1.8 mV). The estimated mean difference was 47.2 mV (95% CI 36.4 to 57.9 mV, t(12) = 9.545, p < 0.0001). The average action potential overshoot was significantly lower in the presence of veratridine (51.9 ± 14.2 mV) compared to baseline (71.5 ± 13.2 mV) (mean difference = -19.64 mV, 95% CI -24.54 to -14.74 mV, t(12) = 8.727, p < 0.0001). Action potential half-width was significantly higher in the presence of veratridine (3.8 ± 1.6 ms) compared to baseline (2.5 ± 1.0 ms) (mean difference = 1.291 ms, 95% CI 0.7683 to 1.814 ms, t(12) = 5.379, p = 0.0002).

In summary, veratridine at 50 µM significantly reduced rheobase, membrane potential following action potential generation, action potential overshoot and action potential half-width in colon-innervating DRG neurons from healthy mice. The change in rheobase induced by veratridine was a 0.82-fold reduction on average in TL neurons. A decrease in rheobase was also observed in LS neurons, but less consistently across neurons. The change in membrane potential following action potential generation was a depolarization of +42 mV on average in TL neurons and +47 mV on average in LS neurons. The change in action potential overshoot was a 10% reduction on average in TL neurons and a 30% reduction on average in LS neurons. The change in action potential half-width was a 1.5-fold increase on average in LS neurons. An increase was also observed in the TL neurons, however, less consistently across neurons.

6.2 The effect of OD1 on rheobase in colon-innervating dorsal root ganglia neurons from healthy mice

Action potential generation in colon-innervating DRG neurons in the presence of an agonist with higher selectivity, compared to veratridine, was investigated. OD1 is a scorpion venom peptide that exhibits characteristics of both α-scorpion (neurotoxin site 3) and β-scorpion (neurotoxin site 4) properties in the interaction with Na$_v$ channels **(Table 3.1)**. OD1 has high potency for Na$_v$1.4, Na$_v$1.6, and Na$_v$1.7, where it acts as an agonist by impairing inactivation (Durek et al. 2013). In this section, the effects of OD1 on

69

variables involved in action potential generation in colon-innervating TL and LS neurons from healthy mice were evaluated.

6.2.1 OD1 at 30 nM reduces rheobase and increases action potential half-width in colon-innervating dorsal root ganglia neurons

Action potential generation in colon-innervating TL and LS neurons from healthy mice were recorded prior to and following incubation with OD1. It was assessed whether incubation with OD1 at 30 nM is associated with a reduction in average rheobase (analyzed as natural log values to meet assumptions for statistical testing), action potential overshoot and action potential half-width relative to baseline in these neurons. Summary statistics for these variables are shown in **Table 6.3**, **Table 6.4**, and **Figure 6.2**.

Table 6.3: Summary statistics for rheobase and ln(rheobase) at baseline and in the presence of OD1 (30 nM) in thoracolumbar (TL) and lumbosacral (LS) neurons from healthy mice.

Group	n	Average rheobase (pA) ± SEM		Average ln(rheobase) ± SEM		Average fold change in rheobase ± SEM
		Baseline	OD1	Baseline	OD1	
TL neurons	7	258.6 ± 41.0	187.1 ± 43.2	5.5 ± 0.2	5.1 ± 0.2	0.72 ± 0.07
LS neurons	15	205 ± 56.8	161.0 ± 42.5	4.8 ± 0.3	4.4 ± 0.4	0.75 ± 0.05

Table 6.4: Summary statistics for average action potential overshoot and half-width in the presence of OD1 (30 nM) in thoracolumbar (TL) and lumbosacral (LS) neurons from healthy mice.

Group	n	Average action potential overshoot (mV) ± SEM		Average action potential half-width (ms) ± SEM	
		Baseline	OD1	Baseline	OD1
TL neurons	7	73.0 ± 6.0	71.3 ± 7.9	2.3 ± 0.3	4.4 ± 0.6
LS neurons	15	69.2 ± 13.6	68.0 ± 13.6	2.7 ± 0.3	4.9 ± 0.6
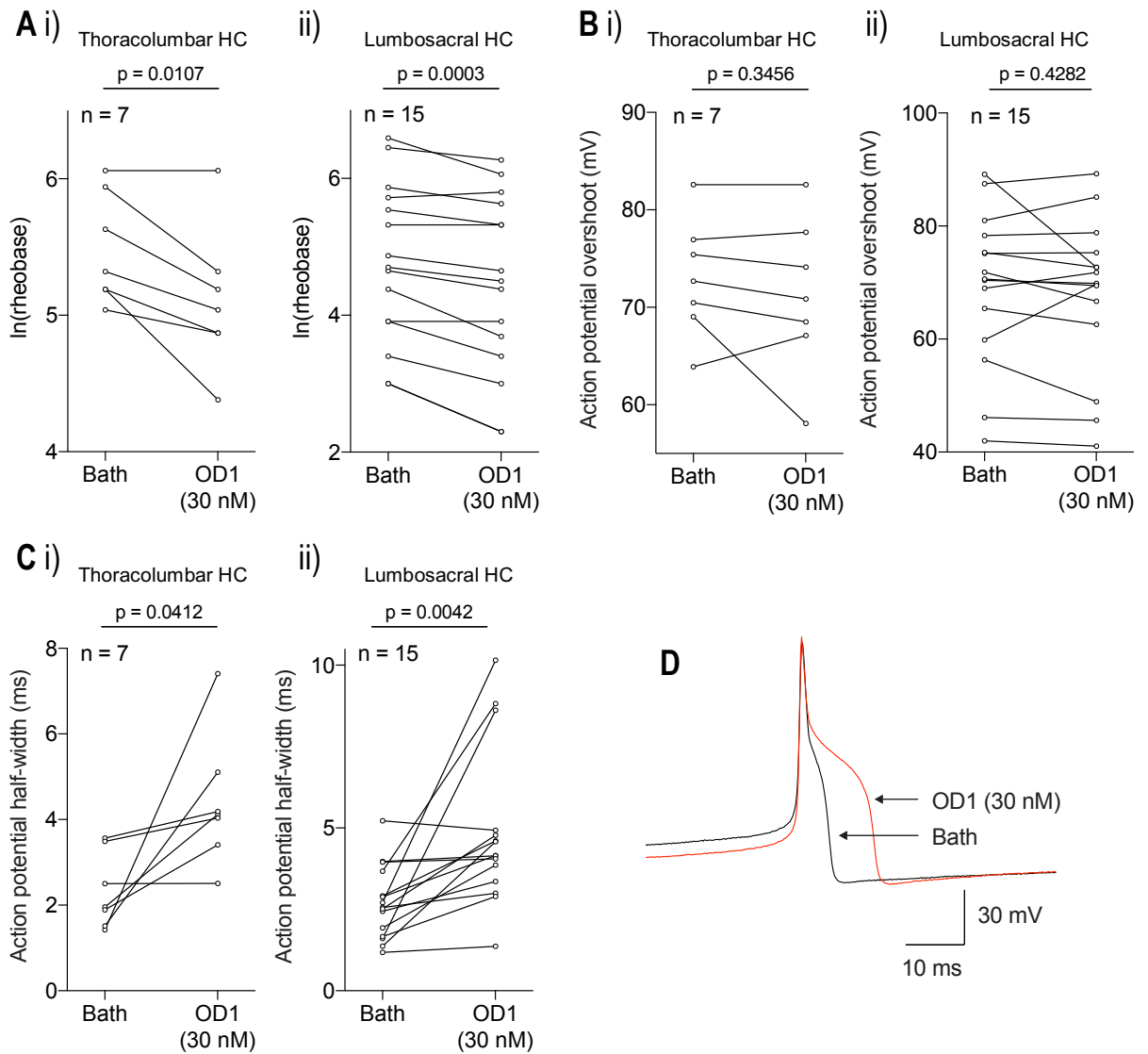
Figure 6.2: OD1 (30 nM) significantly reduces mean ln(rheobase) and increases action potential half-width in colon-innervating dorsal root ganglia neurons from healthy mice. A) Ln(rheobase) at baseline and following incubation with 30 nM OD1 for 1-2 minutes in **i)** thoracolumbar neurons and **ii)** lumbosacral neurons from healthy mice. OD1 decreased mean ln(rheobase) compared to baseline in both datasets (paired t-test, p < 0.05). **B**) Action potential overshoot at baseline and following incubation with OD1 in **i)** thoracolumbar neurons and **ii)** lumbosacral neurons from healthy mice. OD1 did not alter overshoot in either dataset (paired t-test, p > 0.05). **C)** Action potential half-width at baseline and following incubation with 30 nM OD1 for 1-2 minutes in **i)** thoracolumbar neurons and **ii)** lumbosacral neurons from healthy mice. OD1 increased mean action potential half-width compared to baseline in both datasets (paired t-test, p < 0.05). **D)** Overlaid raw traces of an action potential measured at rheobase in a lumbosacral neuron at baseline (black trace) and following incubation with OD1 (red trace), showing an increase in action potential half-width in the presence of OD1.

A series of paired t-tests were carried out on samples of 7 TL neurons and 15 LS neurons from healthy mice to assess the effect of OD1 (30 nM) on ln(rheobase), action potential half-width, and action potential overshoot.

<u>TL neurons.</u> TL neurons from healthy mice had a significantly lower mean ln(rheobase) in the presence of OD1 (5.1 ± 0.5) compared to baseline (5.5 ± 0.4). The estimated average difference was 0.4 (95% CI -0.6 to -0.1, t(6) = -3.679, p = 0.010). TL neurons from healthy mice had a significantly higher mean action potential half-width in the presence of OD1 (4.4 ± 1.5 ms) compared to baseline (2.3 ± 0.9 ms). The estimated average difference was 2.1 ms (95% CI 0.1 to 4.0 ms, t(6) = 2.590, p = 0.041). Action potential overshoot in the presence of OD1 (71.3 ± 7.9 mV) was not statistically different to baseline (73.0 ± 6.0 mV) in TL neurons (mean difference = -1.722 mV, 95% CI -5.840 to 2.396 mV, t(6) = 1.023, p = 0.3456).

<u>LS neurons</u>. LS neurons from healthy mice had a significantly lower mean ln(rheobase) in the presence of OD1 (4.4 ± 1.3) compared to baseline (4.8 ± 1.2). The estimated average difference was 0.3 (95% CI, -0.5 to -0.2, t(14) = -4.755, p = 0.0003). LS neurons from healthy mice had a significantly higher mean action potential half-width in the presence of OD1 (4.9 ± 2.4 ms) compared to baseline (2.7 ± 1.1 ms). The estimated average difference was 2.2 ms (95% CI 0.8 to 3.6 ms, t(14) = 3.409, p = 0.004). Action potential overshoot in the presence of OD1 (68.0 ± 13.6 mV) was not statistically different to baseline (69.2 ± 13.6 mV) in LS neurons (mean difference = -1.223 mV, 95% CI -4.437 to 1.991 mV, t(14) = 0.8160, p = 0.4282).

In summary, OD1 at 30 nM significantly reduced rheobase and increased action potential half-width in colon-innervating DRG neurons from healthy mice. The change in rheobase induced by OD1 was a reduction of 0.72-fold on average in LS neurons and a reduction of 0.75-fold on average in LS neurons. The change in action potential half-width was a 1.9-fold increase on average in TL neurons and a 1.8-fold increase on average in LS neurons. No effects on action potential overshoot were observed.

6.3 Literature cited

Bagal, SK, Chapman, ML, Marron, BE, Prime, R, Storer, RI & Swain, NA 2014, 'Recent progress in sodium channel modulators for pain', *Bioorganic & Medicinal Chemistry Letters*, vol. 24, no. 16, 2014/08/15/, pp. 3690-3699.

Bennett, DL, Clark, AJ, Huang, J, Waxman, SG & Dib-Hajj, SD 2019, 'The Role of Voltage-Gated Sodium Channels in Pain Signaling', *Physiological Reviews*, vol. 99, no. 2, 2019/04/01, pp. 1079-1151.

Catterall, WA, Goldin, AL & Waxman, SG 2005, 'International Union of Pharmacology. XLVII. Nomenclature and Structure-Function Relationships of Voltage-Gated Sodium Channels', *Pharmacological Reviews*, vol. 57, no. 4, pp. 397-409.

Durek, T, Vetter, I, Wang, C-IA, Motin, L, Knapp, O, Adams, DJ, Lewis, RJ & Alewood, PF 2013, 'Chemical Engineering and Structural and Pharmacological Characterization of the α-Scorpion Toxin OD1', *ACS Chemical Biology,* vol. 8, no. 6, 2013/06/21, pp. 1215-1222.

Chapter 7 The effect of tetrodotoxin on electrophysiological properties of colon-innervating dorsal root ganglia neurons from healthy mice and TNBS-treated mice

Tetrodotoxin (TTX) is a pore blocker of $Na_v1.1$, $Na_v1.2$, $Na_v1.3$, $Na_v1.4$, $Na_v1.6$ and $Na_v1.7$ (Catterall, Goldin & Waxman 2005), and inhibits sodium conductance by binding to the pore region of these channels (**Table 3.1**). TTX has historically been used to separate two populations of Na_v channels; TTX-sensitive and TTX-resistant ($Na_v1.5$, $Na_v1.8$ and $Na_v1.9$), and has been used to uncover changes in sodium current properties in colon-innervating dorsal root ganglia (DRG) neurons from visceral pain models (Hu, J et al. 2016; Hu, S et al. 2013; Lin et al. 2017). In addition to the use of TTX as a pharmacological tool, preclinical and clinical studies have shown promise with localized delivery of TTX in pain management (González-Cano et al. 2017; Hagen, Neil A. et al. 2017; Hagen, N. A. et al. 2011; Manriquez et al. 2015). To build on this, the effect of TTX on active electrophysiological properties in colon-innervating DRG neurons from healthy control (HC) mice and TNBS-treated (CVH) mice was investigated.

7.1 Tetrodotoxin increases rheobase in colon-innervating dorsal root ganglia neurons

Rheobase in colon-innervating thoracolumbar (TL) and lumbosacral (LS) neurons from healthy and CVH mice were recorded prior to and following incubation with TTX. It was assessed whether incubation with TTX at 100 nM is associated with an increase in average rheobase (analyzed as natural log values to meet assumptions for statistical testing), relative to baseline in these neurons. Summary statistics for rheobase and ln(rheobase) are shown in **Table 7.1** and **Figure 7.1**.

Table 7.1: Summary statistics for rheobase and ln(rheobase) at baseline and in the presence of tetrodotoxin (TTX) in thoracolumbar (TL) and lumbosacral (LS) neurons from healthy control (HC) and TNBS-treated (CVH) mice.

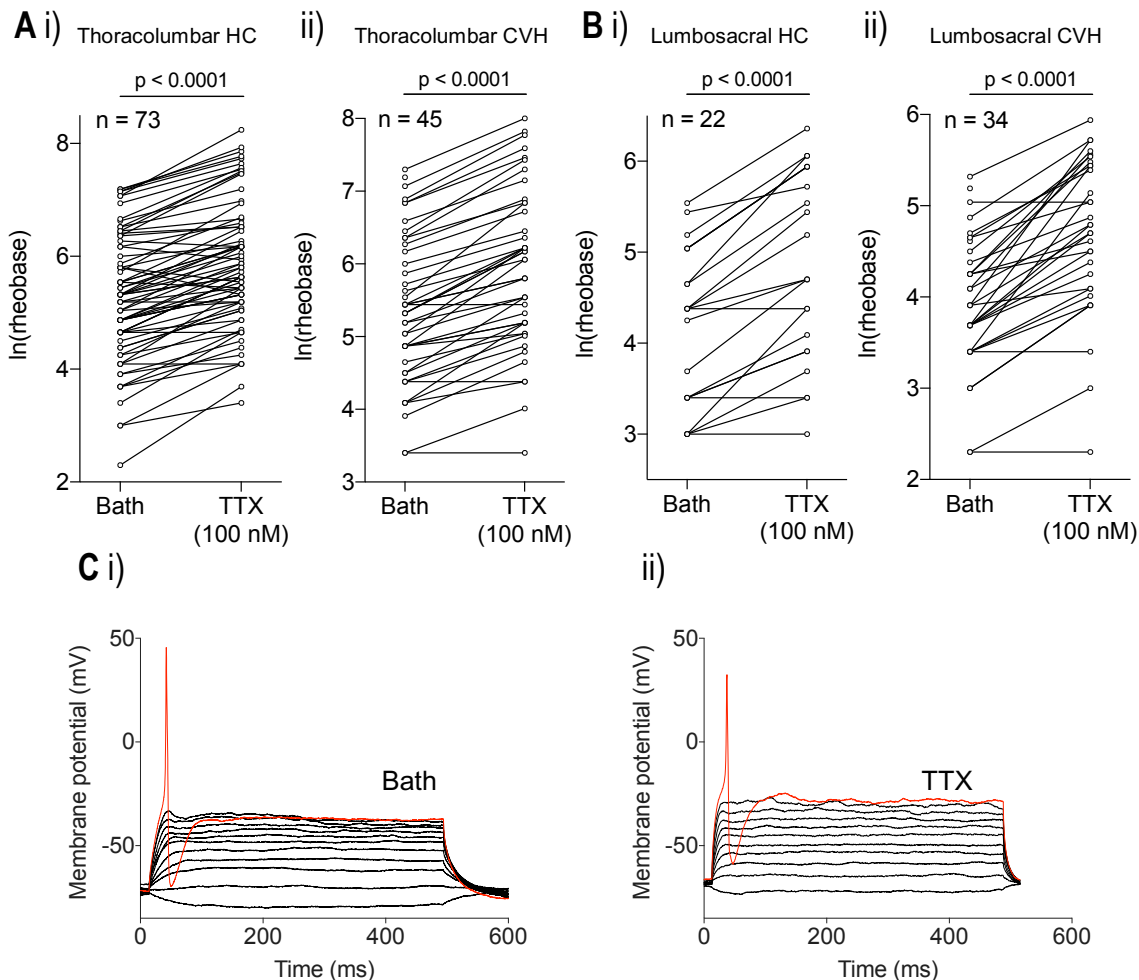| Group	n	Average rheobase (pA) ± SEM		Average ln(rheobase) ± SEM		Average fold change in rheobase ± SEM
		Baseline	TTX (100 nM)	Baseline	TTX (100 nM)	
TL neurons						
HC	73	331.5 ± 41.5	633.9 ± 90.5	5.3 ± 0.1	5.9 ± 0.1	2.00 ± 0.09
CVH	45	347.3 ± 54.4	708.0 ± 120.3	5.4 ± 0.2	6.0 ± 0.2	1.94 ± 0.09
LS neurons						
HC	22	89.6 ± 15.1	196.4 ± 35.9	4.2 ± 0.2	4.8 ± 0.2	2.15 ± 0.18
CVH	34	66.5 ± 8.1	165.2 ± 22.3	4.0 ± 0.1	4.8 ± 0.2	2.56 ± 0.24

Figure 7.1: Tetrodotoxin (TTX) (100 nM) significantly increases mean ln(rheobase) in colon-innervating dorsal root ganglia neurons from healthy control (HC) and TNBS-treated (CVH) mice. **A)** Ln(rheobase) at baseline and following incubation with tetrodotoxin for 1-2 minutes in thoracolumbar neurons from **i)** healthy and **ii)** TNBS-treated mice, and **B)** in lumbosacral neurons from **i)** healthy and **ii)** TNBS-treated mice. Tetrodotoxin increased mean ln(rheobase) compared to baseline in all data sets (paired t-test, p < 0.0001). **C)** Raw traces of membrane potential measured at increasing current injections (in increments of 25 pA for bath and 50 pA for tetrodotoxin) in a thoracolumbar neuron from a healthy mouse. An increase in the minimum current injection after incubation with **ii)** 100 nM tetrodotoxin (480 pA, red trace) compared to **i)** baseline (255 pA, red trace) was observed.

A series of paired t-tests were carried out on samples of 73 TL neurons from healthy mice, 45 TL neurons from CVH mice, 22 LS neurons from healthy mice, and 34 LS neurons from CVH mice, to assess the effect of TTX (100 nM) on ln(rheobase).

<u>TL neurons.</u> TL neurons from healthy mice had significantly higher mean ln(rheobase) in the presence of TTX (5.9 ± 1.1) compared to baseline (5.3 ± 1.1). The estimated average difference was 0.5957 (95% CI 0.5024 to 0.6890), t(72) = 12.727, p < 0.0001). TL neurons from CVH mice also had a higher mean ln(rheobase) in the presence of TTX (6.0 ± 1.1) compared to baseline (5.4 ± 1.0). This average increase of 0.6165 was statistically significant (95% CI 0.5232 to 0.7097, t(44) = 13.327, p < 0.0001).

<u>LS neurons.</u> There was a statistically significant increase of 0.6732 in mean ln(rheobase) in the presence of TTX (4.8 ± 1.0) compared to baseline (4.2 ± 0.9) among LS neurons from healthy mice (95% CI 0.4948 to 0.8516, t(21) = 7.847, p < 0.0001). LS neurons from CVH mice also had a significantly higher mean ln(rheobase) in the presence of TTX (5.6 ± 1.2) compared to baseline (5.0 ± 1.2). The average increase in the presence of TTX was 0.8143 (95% CI 0.6416 to 0.9870, t(33) = 9.594, p < 0.0001).

In summary, TTX (100 nM) significantly increased rheobase levels in TL and LS colon-innervating DRG neurons from healthy and CVH mice. The change in rheobase induced by TTX was a 2.0-fold increase in TL neurons and 2.4-fold increase in LS neurons.

74

7.2 Tetrodotoxin reduces peak sodium current density in colon-innervating dorsal root ganglia neurons

Peak sodium current density in colon-innervating TL and LS neurons from healthy and CVH mice were recorded prior to and following incubation with TTX. It was assessed whether incubation with TTX at 100 nM is associated with a reduction in average peak sodium current density relative to baseline in these neurons. Summary statistics for peak sodium current density are shown in **Table 7.2** and current-voltage plots are shown in **Figure 7.2**.

Table 7.2: Summary statistics for peak sodium current density at baseline and following exposure to tetrodotoxin (TTX) in thoracolumbar (TL) and lumbosacral (LS) neurons from healthy control (HC) and TNBS-treated (CVH) mice.

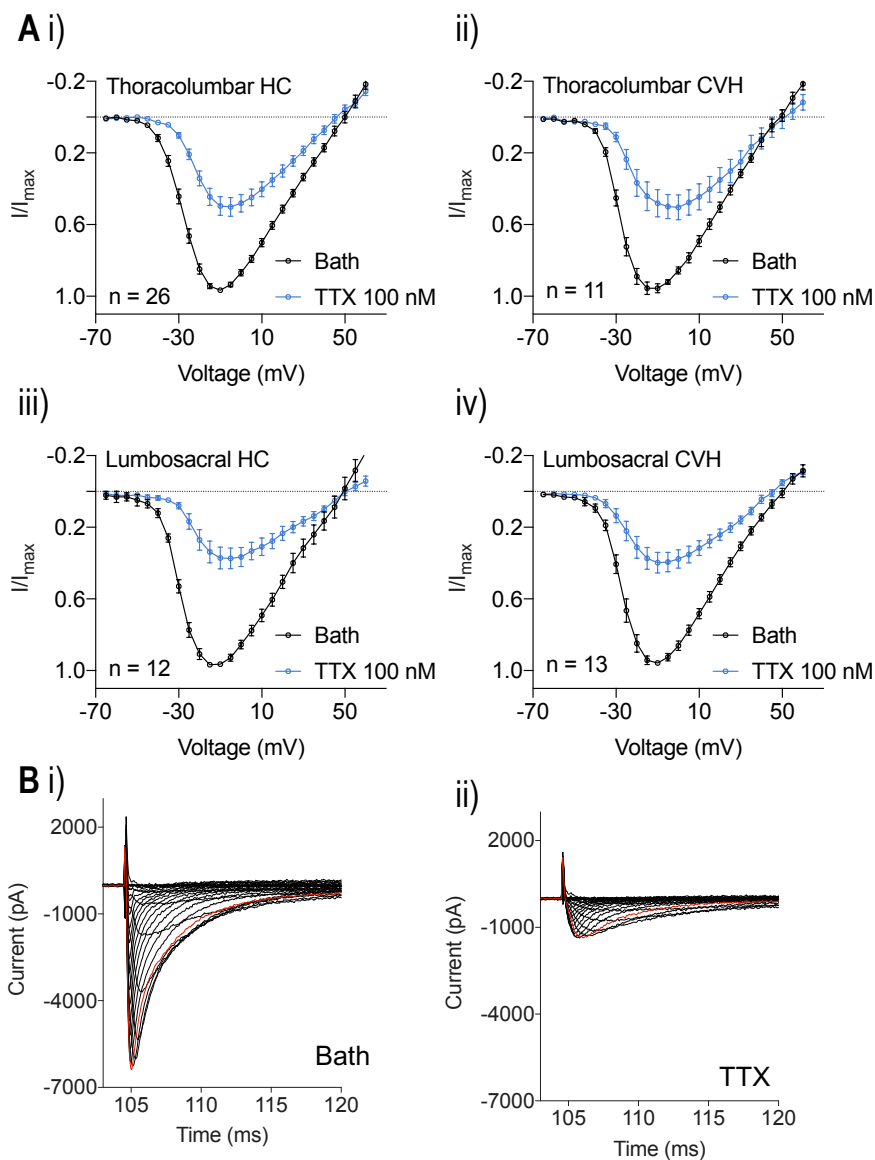| Group	n	Average peak sodium current density (pA/pF) ± SEM		Average fraction TTX-S current ± SEM
		Baseline	TTX (100 nM)	
TL neurons				
HC	26	-182.5 ± 17.4	-90.9 ± 13.0	0.48 ± 0.05
CVH	11	-206.7 ± 32.3	-118.8 ± 27.4	0.44 ± 0.08
LS neurons				
HC	12	-163.8 ± 24.7	-60.6 ± 14.9	0.61 ± 0.06
CVH	13	-167.6 ± 17.7	-73.3 ± 16.9	0.59 ± 0.06

Figure 7.2: Tetrodotoxin (TTX) at 100 nM reduces peak sodium current density in colon-innervating dorsal root ganglia neurons from healthy control (HC) and TNBS-treated (CVH) mice. A) Current-voltage relationship at baseline (black) and following incubation with 100 nM tetrodotoxin for 1-2 minutes (blue) in thoracolumbar neurons from **i)** healthy and **ii)** TNBS-treated mice, and in

lumbosacral neurons from **iii)** healthy and **iv)** TNBS-treated mice. The measured current (I) at each voltage was normalized to the peak current (I$_{max}$), and each data point shown here is the averaged I/I$_{max}$ ± SEM. **B)** Raw traces of peak currents obtained using the current-voltage protocol (5 mV increments from -70 mV to +60 mV) in a lumbosacral neuron. A reduction in magnitude and sharpness of maximum peak current (red trace) after incubation with **ii)** 100 nM tetrodotoxin compared to **i)** baseline was observed.

A series of paired t-tests were carried out on samples of 26 colon-innervating TL neurons from healthy mice, 11 TL neurons from CVH mice, 12 LS neurons from healthy mice, and 13 LS neurons from CVH mice, to assess the effect of inhibiting Na$_v$1.1, Na$_v$1.2, Na$_v$1.3, Na$_v$1.4, Na$_v$1.6 and Na$_v$1.7 on peak sodium current density using TTX (100 nM).

<u>TL neurons.</u> TL neurons from healthy mice had significantly reduced mean peak sodium current density in the presence of TTX (-90.9 ± 66.3 pA/pF) compared to baseline (-182.5 ± 88.8 pA/pF). The estimated average difference was 91.560 (95% CI 58.8690 to 124.2510 pA/pF, $t(25) = 5.768$, $p < 0.0001$). TL neurons from CVH mice also had a reduced mean peak sodium current density in the presence of TTX (-118.8 ± 91.0 pA/pF) compared to baseline (-206.7 ± 107.0 pA/pF). This average reduction of 87.9309 was statistically significant (95% CI 42.6282 to 133.2336 pA/pF, $t(10) = 4.325$, $p = 0.002$).

<u>LS neurons.</u> LS neurons from healthy mice had significantly reduced mean peak sodium current density in the presence of TTX (-60.6 ± 51.6 pA/pF) compared to baseline (163.8 ± 85.7 pA/pF). The estimated average difference was 103.2260 (95% CI 64.3892 to 142.0625 pA/pF, $t(11) = 5.850$, $p < 0.0001$). LS neurons from CVH mice also had a reduced mean peak sodium current density in the presence of TTX (-73.3 ± 60.9 pA/pF) compared to baseline (-167.6 ± 63.8 pA/pF). This average reduction of 94.2662 was statistically significant (95% CI 69.3978 to 119.1345 pA/pF, $t(12) = 8.259$, $p < 0.0001$).

In summary, TTX (100 nM) significantly reduced peak sodium current density in TL and LS colon-innervating DRG neurons from healthy and CVH mice. The average TTX-sensitive component of total peak sodium current was estimated to be 47% in TL neurons and 60% in LS neurons.

7.3 Tetrodotoxin shifts the conductance-voltage relationship rightward in colon-innervating dorsal root ganglia neurons

Steady-state activation was estimated from the current-voltage relationship (**Figure 7.2**) at baseline and in the presence of TTX in colon-innervating TL and LS DRG neurons. It was assessed whether incubation with TTX at 100 nM is associated with a shift in the conductance-voltage relationship in these neurons. A Boltzmann sigmoidal curve was fitted to each dataset, with voltage of half-maximal activation (V$_{50}$) and slope (k) listed in **Table 7.3**, and conductance-voltage plots shown in **Figure 7.3**.

Table 7.3: Summary statistics for the voltage of half-maximal activation (V$_{50}$) and slope factor (k) calculated by nonlinear regression of the current-voltage relationship obtained from a voltage-dependence of activation protocol following exposure to tetrodotoxin (TTX) in thoracolumbar (TL) and lumbosacral (LS) neurons from healthy control (HC) and TNBS-treated (CVH) mice.

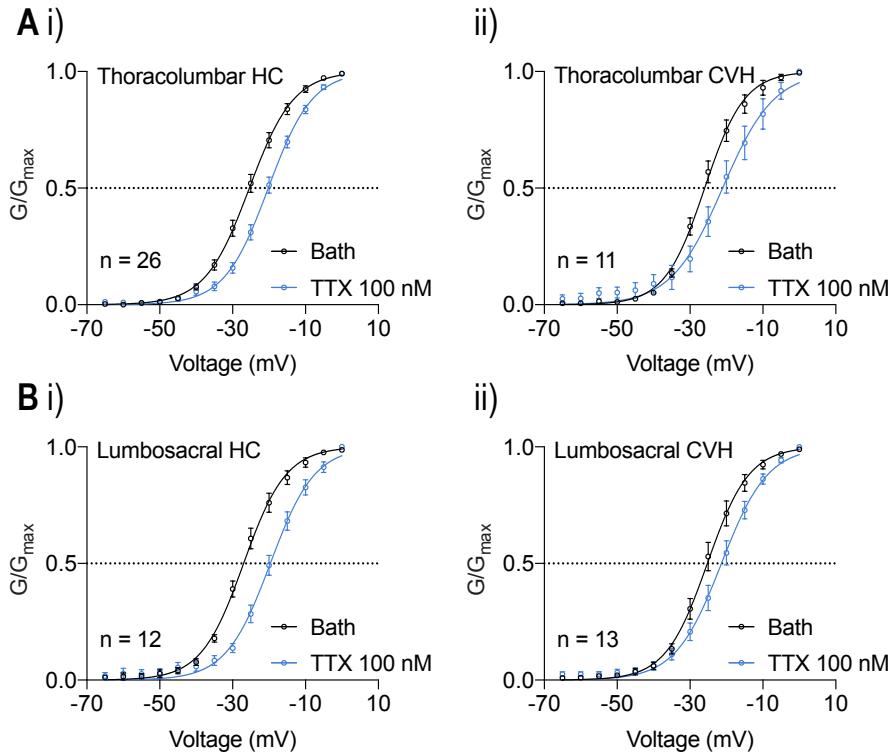| Group | n | V$_{50}$ (mV) | | | k | |
		Baseline	TTX (100 nM)	Sum-of-squares F-test p-value	Baseline	TTX (100 nM)
TL neurons						
HC	26	-25.41	-20.21	<0.0001	6.085	6.037
CVH	11	-25.98	-21.05	<0.0001	5.455	7.054
LS neurons						
HC	12	-26.98	-19.65	<0.0001	5.832	6.080
CVH	13	-25.25	-21.37	<0.0001	5.722	6.341

`

Figure 7.3: Tetrodotoxin (TTX) at 100 nM shifts the conductance-voltage relationship rightward in colon-innervating dorsal root ganglia neurons from healthy control (HC) and TNBS-treated (CVH) mice. A) Steady-state activation curves at baseline (black) and following incubation with 100 nM tetrodotoxin for 1-2 minutes (blue) in thoracolumbar neurons from **i)** healthy and **ii)** TNBS-treated mice, and in **B)** lumbosacral neurons from **i)** healthy and **ii)** TNBS-treated mice. The estimated conductance (G) was calculated from the measured current (I) ($I/(V_{cmd} - V_{rev})$, where V_{cmd} is the command voltage and V_{rev} is the reversal potential for sodium under the experimental conditions, and normalized to the maximum conductance (G_{max}). Each data point shows the mean $G/G_{max} \pm$ SEM and each data set has been fitted with a Boltzmann sigmoidal curve. A shift in V_{50} (at $G/G_{max} = 0.5$) was observed in the presence of tetrodotoxin compared to baseline in all cases.

A series of sum-of-squares F-tests were carried out on samples of 13 HC and 6 CVH colon-innervating TL neurons, and 12 HC and 13 CVH colon-innervating LS neurons to assess the effect of TTX (100 nM) on steady-state activation.

TL neurons. Steady-state activation was positively shifted in the presence of TTX in TL neurons from healthy mice (V_{50} = -20.21 mV; 95% CI -20.69 to -19.72 mV) compared to baseline (V_{50} = -25.41 mV; 95% CI -25.91 to -24.90 mV), a statistically significant shift in V_{50}, $F_{(1,752)}$ = 210.7, p < 0.0001. Steady-state activation was positively shifted in the presence of TTX in TL neurons from CVH mice (V_{50} = -21.05 mV; 95% CI -22.35 to -19.76 mV) compared to baseline (V_{50} = -25.98 mV; 95% CI -26.60 to -25.36 mV), a statistically significant shift in V_{50}, $F_{(1,304)}$ = 48.06, p < 0.0001.

LS neurons. Steady-state activation was positively shifted in the presence of TTX in LS neurons from healthy mice (V_{50} = -19.65; 95% CI -20.34 to -18.97 mV) compared to baseline (V_{50} = -26.98; 95% CI -27.58 to -26.38 mV), a statistically significant shift in V_{50}, $F_{(1,332)}$ = 243.6, p < 0.0001. Steady-state activation was positively shifted in the presence of TTX in LS neurons from CVH mice (V_{50} = -21.37 mV; 95% CI -22.11 to -20.64 mV) compared to baseline (V_{50} = -25.25 mV; 95% CI -25.97 to -24.54 mV), a statistically significant shift in V_{50}, $F_{(1,388)}$ = 54.51, p < 0.0001.

In summary, TTX (100 nM) induced a depolarizing shift in the conductance-voltage relationship in TL and LS colon-innervating DRG neurons from healthy and CVH mice. The voltage of half-maximal activation was shifted by on average +5.1 mV in TL neurons and +5.6 mV in LS neurons.

7.4 Tetrodotoxin shifts steady-state fast inactivation rightward in colon-innervating dorsal root ganglia neurons

Peak sodium current during fast inactivation voltage protocols in colon-innervating TL neurons from healthy and CVH mice were recorded prior to and following incubation with TTX. It was assessed whether incubation with TTX at 100 nM is associated with a shift in steady-state fast inactivation in these neurons. Summary statistics for the voltage of half-maximal inactivation (V_{50}) and the slope factor (k) of the steady-state fast inactivation at baseline and following exposure to TTX are reported for each group in **Table 7.4**. V_{50} and k were obtained by normalizing the peak inward currents (I) to the maximal inward current (I_{max}) and fitting the relationship between I/I_{max} and applied voltage with a Boltzmann equation: $I/I_{max} = 1/(1+exp((V_{50} - V_m)/k))$. Fitted steady-state fast inactivation curves at baseline and following exposure to TTX are shown in **Figure 7.4**.

Table 7.4: Summary statistics for the voltage of half-maximal inactivation (V_{50}) and slope factor (k) calculated by nonlinear regression of the current-voltage relationship obtained from steady-state fast inactivation protocols following exposure to tetrodotoxin (TTX) in thoracolumbar (TL) neurons from healthy control (HC) and TNBS-treated (CVH) mice.

Group	n	V_{50} (mV)			k	
		Baseline	TTX (100 nM)	Sum-of-squares F-test p-value	Baseline	TTX (100 nM)
TL neurons						
HC	13	-69.99	-37.07	<0.0001	-13.69	-4.93
CVH	6	-57.69	-32.95	<0.0001	-17.63	-7.86
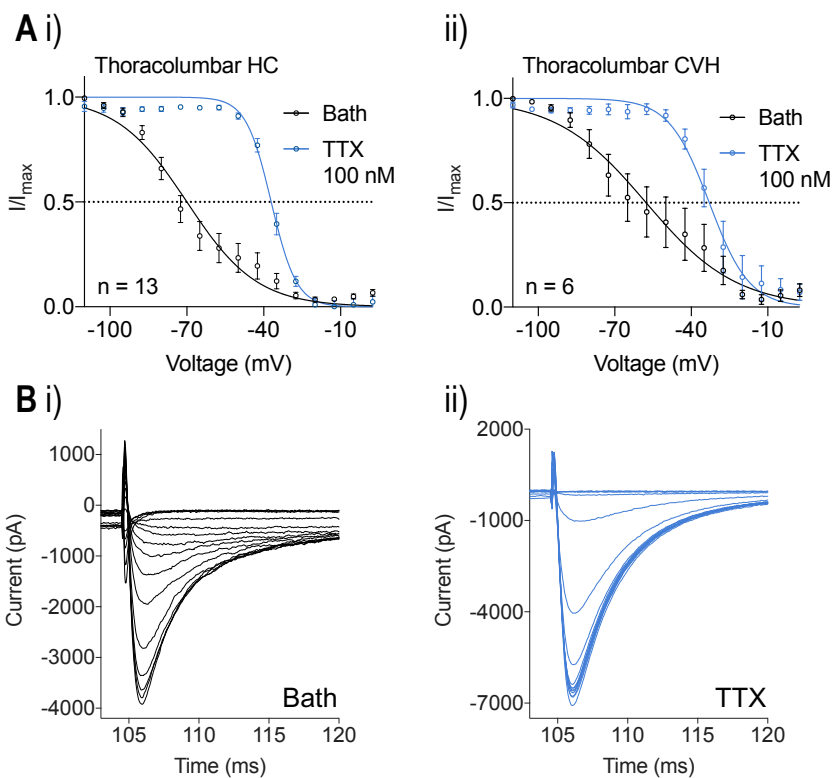
Figure 7.4: Tetrodotoxin (TTX) at 100 nM positively shifts steady-state fast inactivation in colon-innervating lumbosacral neurons from healthy control (HC) and TNBS-treated (CVH) mice. A) Steady-state fast inactivation curves at baseline (black) and following incubation with tetrodotoxin for 1-2 minutes (blue) in neurons from **i)** healthy and **ii)** TNBS-treated mice. The measured current (I) at each voltage was normalized to the peak current (I_{max}). Each data point shows the mean I/I_{max} ± SEM and each data set has been fitted with a Boltzmann sigmoidal curve. A positive shift in V_{50} (at I/I_{max} = 0.5) is observed in the presence of TTX in healthy **i)** and TNBS-treated **ii)** mice. **B)** Raw traces of peak currents obtained using the current-voltage protocol (measured at -30 mV (baseline) and -10 mV (tetrodotoxin) following 7.5 mV increments from -110 mV to +2.5 mV) in a thoracolumbar neuron from a healthy mouse. Peak currents at different voltage steps are evenly distributed at **i)** baseline compared to **ii)** tetrodotoxin, where peak currents are similar in the first half of test voltages (approximately -110 to -50 mV), indicating

that fast inactivation of Na_v channels that are sensitive to voltages < -50 mV has occurred in the presence of tetrodotoxin.

A series of sum-of-squares F-tests were carried out on samples of 13 HC and 6 CVH colon-innervating TL neurons to assess the effect of TTX (100 nM) on steady-state fast inactivation.

Steady-state fast inactivation was positively shifted in the presence of TTX in TL neurons from healthy mice (V_{50} = -37.07 mV; 95% CI -37.83 to -36.31 mV) compared to baseline (V_{50} = -69.99 mV; 95% CI, -72.14 to -67.81 mV), a statistically significant shift in V_{50}, $F(1,412)$ = 758.0, $p < 0.0001$. Steady-state fast inactivation was positively shifted in the presence of TTX in TL neurons from CVH mice (V_{50} = -32.95 mV; 95% CI -35.00 to -30.87 mV) compared to baseline (V_{50} = -57.69 mV; 95% CI, -61.83 to -53.51 mV), a statistically significant shift in V_{50}, $F(1,188)$ = 114.1, $p < 0.0001$.

In summary, TTX (100 nM) induced a depolarizing shift in the steady-state fast inactivation curve in TL colon-innervating DRG neurons from healthy and CVH mice. The voltage of half-maximal inactivation was shifted by on average +28.8 mV.

7.5 The tetrodotoxin-sensitive fraction of total current is greater in lumbosacral neurons compared to thoracolumbar neurons and is not associated with TNBS treatment

Previous studies have reported changes in the component of total sodium current that is blocked by TTX in colon-innervating DRG in visceral pain models (Hu, J et al. 2016; Hu, S et al. 2013; Lin et al. 2017). A multivariable regression with fraction of TTX-S current as the dependent variable and spinal level (TL or LS) and health status (HC or CVH) did not satisfy the assumption of linearity between dependent and independent variables as no linearity was observed between fraction of TTX-S current and health status. Instead, an independent samples t-test was run on a sample of 37 TL neurons (HC and CVH) and 25 LS neurons (HC and CVH) to compare the fraction of TTX-S current. LS neurons had a statistically higher mean fraction of TTX-S current (0.60 ± 0.2) compared to TL neurons (0.47 ± 0.3). The estimated average difference was 0.1333 ((95% CI, 0.0061 to 0.2604); $t(60)$ = 2.096, $p = 0.040$).

In summary, no association between the TTX-sensitive component of peak sodium current and health status (HC vs CVH) in colon-innervating TL and LS DRG neurons was observed. However, there was a significantly higher component of TTX-sensitive current in LS neurons compared to TL neurons.

7.6 Increase in rheobase in the presence of tetrodotoxin is greater in lumbosacral neurons compared to thoracolumbar neurons and is not affected by TNBS treatment

In section 7.5 on peak sodium current density, there was insufficient evidence to support an association between health status (HC vs CVH) and TTX-sensitivity, however, there was an association between spinal level (TL vs LS) and TTX-sensitivity. In this section, an evaluation of whether these associations were reflected in the rheobase levels was conducted.

The number of colon-innervating DRG neurons recorded for each of four groups defined by spinal level (TL or LS) and health status (HC or CVH) as well as summary statistics (mean ± SEM) for rheobase and the natural log transformed value, ln(rheobase), at baseline and in the presence of TTX are reported for each group in **Table 7.1**. Visual inspection of scatterplots indicated approximately linear relationships between the predictor variables and the outcome fold-change in rheobase in the presence of TTX. A box plot of fold change indicated there were no major outliers. Regression model adequacy was assessed via visual inspection of the residuals plot, and independence of residuals was assessed using the Durbin-Watson statistic. Multivariable regression coefficients are shown in **Table 7.5**.

79

Table 7.5: Linear regression coefficients for multivariable regression with dependent variable fold-change in rheobase in the presence of TTX and independent variables health status (healthy control (HC) vs TNBS-treated (CVH)) and spinal level (thoracolumbar (TL) vs lumbosacral (LS)).

Regression variable	Unstandardized coefficients		t	p-value	95% Confidence Interval for B	
	B	Std. Error			Lower bound	Upper bound
Health status (HC/CVH)	0.134	0.140	0.955	0.341	-0.143	0.411
Spinal level (TL/LS)	0.402	0.149	2.691	0.008	0.107	0.697

R^2 = 0.054 was obtained for the regression model, $F(2, 171)$ = 4.840, p = 0.009, indicating that the regression model accounts for approximately 5.4% of the variance in fold-change. No issues with multicollinearity were observed (VIF statistics 1.047, collinearity indices < 5).

The final regression model was: Fold change = 1.9 + 0.134(health status) + 0.402(spinal level)

In summary, linear regression was used to assess whether fold change in rheobase in the presence of TTX in colon-innervating neurons differed between neurons depending on spinal level. 174 neurons were included in the analysis. LS neurons had, on average, 0.402 greater fold change in the presence of TTX compared to TL neurons (95% CI, 0.107 to 0.697, p = 0.008). There was insufficient evidence to reject the null hypothesis that health status has no effect on fold change of rheobase (95% CI, -0.143 to 0.411, p = 0.341).

Taken together, these results support the hypothesis that inhibition of rheobase in the presence of TTX is greater in colon-innervating LS DRG neurons compared to TL DRG neurons. Furthermore, there was insufficient support for an association between health status (HC vs CVH) and TTX-sensitivity.

7.7 Literature cited

Catterall, WA, Goldin, AL & Waxman, SG 2005, 'International Union of Pharmacology. XLVII. Nomenclature and Structure-Function Relationships of Voltage-Gated Sodium Channels', *Pharmacological Reviews*, vol. 57, no. 4, pp. 397-409.

González-Cano, R, Tejada, MÁ, Artacho-Cordón, A, Nieto, FR, Entrena, JM, Wood, JN & Cendán, CM 2017, 'Effects of Tetrodotoxin in Mouse Models of Visceral Pain', *Marine Drugs*, vol. 15, no. 6, p. 188.

Hagen, NA, Cantin, L, Constant, J, Haller, T, Blaise, G, Ong-Lam, M, du Souich, P, Korz, W & Lapointe, B 2017, 'Tetrodotoxin for Moderate to Severe Cancer-Related Pain: A Multicentre, Randomized, Double-Blind, Placebo-Controlled, Parallel-Design Trial', *Pain Research & Management*, vol. 2017, pp. 7212713-7212713.

Hagen, NA, Lapointe, B, Ong–Lam, M, Dubuc, B, Walde, D, Gagnon, B, Love, R, Goel, R, Hawley, P, Ngoc, AH & du Souich, P 2011, 'A multicentre open-label safety and efficacy study of tetrodotoxin for cancer pain', *Current Oncology*, vol. 18, no. 3, pp. e109-e116.

Hu, J, Song, Z-Y, Zhang, H-H, Qin, X, Hu, S, Jiang, X & Xu, G-Y 2016, 'Colonic Hypersensitivity and Sensitization of Voltage-gated Sodium Channels in Primary Sensory Neurons in Rats with Diabetes', *Journal of Neurogastroenterology and Motility*, vol. 22, no. 1, pp. 129-140.

Hu, S, Xiao, Y, Zhu, L, Li, L, Hu, CY, Jiang, X & Xu, GY 2013, 'Neonatal maternal deprivation sensitizes voltage-gated sodium channel currents in colon-specific dorsal root ganglion neurons in rats', *American Journal of Physiology - Gastrointestinal and Liver Physiology*, vol. 304, no. 4, Feb 15, pp. G311-321.

Lin, YM, Fu, Y, Winston, J, Radhakrishnan, R, Sarna, SK, Huang, LM & Shi, XZ 2017, 'Pathogenesis of abdominal pain in bowel obstruction: Role of mechanical stress-induced upregulation of nerve growth factor in gut smooth muscle cells', *Pain*, Jan 06.

Manriquez, V, Castro Caperan, D, Guzman, R, Naser, M, Iglesia, V & Lagos, N 2015, 'First evidence of neosaxitoxin as a long-acting pain blocker in bladder pain syndrome', *Int Urogynecol J*, vol. 26, no. 6, Jun, pp. 853-858.

Chapter 8 The effect of Hs1a on electrophysiological properties of colon-innervating dorsal root ganglia neurons from healthy mice and TNBS-treated mice

Hs1a is a novel tarantula peptide, and a potent inhibitor of $Na_v1.1$, $Na_v1.7$, $Na_v1.2$, $Na_v1.3$, $Na_v1.6$ and has a potentiating effect on $Na_v1.8$, based on preliminary selectivity assays. Na_v-selective tarantula peptides commonly interact with Na_v channels in neurotoxin site 4, which reduces sodium conductance through the pore and hyperpolarizes steady-state activation (**Table 3.1**). As Hs1a exhibited a more selective profile of Na_v channels compared to tetrodotoxin, the effect of this compound on active electrophysiological properties in colon-innervating thoracolumbar (TL) dorsal root ganglia neurons (DRG) from healthy control (HC) mice and TNBS-treated (CVH) mice was investigated.

8.1 Hs1a at 500 nM, but not 100 nM, increases rheobase in colon-innervating dorsal root ganglia neurons

Rheobase in colon-innervating TL neurons from healthy and CVH mice were recorded prior to and following incubation with Hs1a. It was assessed whether incubation with Hs1a at 100 nM and 500 nM is associated with a reduction in average rheobase (analyzed as natural log values to meet assumptions for statistical testing), relative to baseline in these neurons. Summary statistics for rheobase and ln(rheobase) are shown in **Table 8.1** and **Figure 8.1**.

Table 8.1: Summary statistics for rheobase and ln(rheobase) at baseline and in the presence of Hs1a (100 nM and 500 nM) in thoracolumbar neurons from healthy control (HC) and TNBS-treated (CVH) mice.

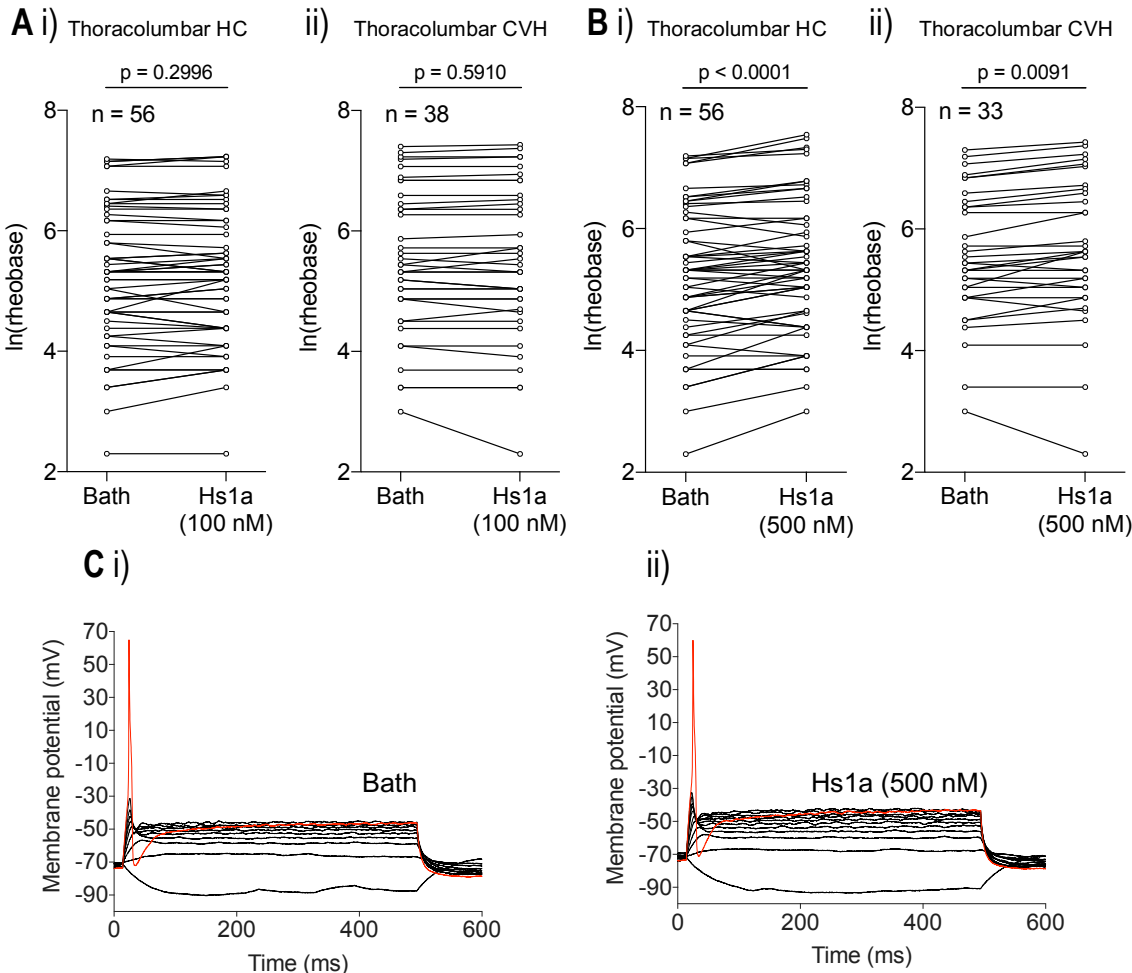| Group	n	Average rheobase (pA) ± SEM		Average ln(rheobase) ± SEM		Average fold change in rheobase ± SEM
		Baseline	Hs1a	Baseline	Hs1a	
Hs1a (100 nM)						
HC	56	325.9 ± 47.2	333.6 ± 49.6	5.2 ± 0.2	5.3 ± 0.2	1.04 ± 0.03
CVH	38	440.0 ± 75.1	449.9 ± 77.6	5.5 ± 0.2	5.5 ± 0.2	1.00 ± 0.02
Hs1a (500 nM)						
HC	56	325.9 ± 47.2	384.0 ± 60.5	5.2 ± 0.2	5.4 ± 0.2	1.21 ± 0.04
CVH	33	411.5 ± 72.3	484.6 ± 83.7	5.5 ± 0.2	5.6 ± 0.2	1.14 ± 0.04

Figure 8.1: Hs1a at 500 nM, but not 100 nM, significantly increases mean ln(rheobase) in colon-innervating neurons from healthy control (HC) and TNBS-treated (CVH) mice. A) Ln(rheobase) at baseline and following incubation with 100 nM Hs1a for 2 minutes in thoracolumbar neurons from **i)** healthy and **ii)** TNBS-treated mice, and **B)** following incubation with 500 nM Hs1a in thoracolumbar neurons from **i)** healthy and **ii)** TNBS-treated mice. Hs1a at 500 nM increased mean ln(rheobase) compared to baseline in healthy and TNBS-treated data sets (paired t-test, p < 0.01), whereas Hs1a at 100 nM did not significantly alter mean ln(rheobase) (paired t-test, p > 0.05). **C)** Raw traces of membrane potential measured at increasing current injections (25 pA increments starting at -20 pA) in a thoracolumbar neuron from a healthy mouse. An increase in the minimum current injection after incubation with **ii)** 500 nM Hs1a (255 pA, red trace) compared to **i)** baseline (205 pA, red trace) was observed.

A series of paired t-tests were carried out on samples of 56 TL neurons from healthy mice and 38 TL neurons from CVH mice to assess the effect of 100 nM of Hs1a on ln(rheobase), and 56 TL neurons from healthy mice and 33 TL neurons from CVH mice to assess the effect of 500 nM of Hs1a on ln(rheobase).

Hs1a (100 nM): The average ln(rheobase) in TL neurons from healthy mice in the presence of Hs1a (5.3 ± 1.1) was not statistically different to baseline (5.2 ± 1.1) (mean difference = 0.02453; 95% CI -0.0213 to 0.0704, t(55) = 1.073, p = 0.288). The average ln(rheobase) in TL neurons from CVH mice in the presence of Hs1a (5.5 ± 1.3) was not statistically different to baseline (5.5 ± 1.2) (mean difference = 0.01305, 95% CI -0.0618 to 0.0357), t(37) = -0.542, p = 0.591).

Hs1a (500 nM): TL neurons from healthy mice had a significantly higher mean ln(rheobase) in the presence of Hs1a (500 nM) (5.4 ± 1.1) compared to baseline (5.2 ± 1.1). The estimated average difference was 0.1538 (95% CI 0.0824 to 0.2252, t(55) = 4.317, p < 0.0001). TL neurons from CVH mice also had a higher mean ln(rheobase) in the presence of Hs1a (500 nM) (5.6 ± 1.2) compared to baseline (5.5 ± 1.1). This average increase of 0.1071 was statistically significant (95% CI 0.0293 to 0.1848, t(32) = 2.806, p = 0.008).

In summary, Hs1a (500 nM) significantly increased rheobase in TL colon-innervating DRG neurons from healthy and CVH mice. The change in rheobase induced by Hs1a was a 1.2-fold increase in these neurons. No effects were observed in the presence of Hs1a at 100 nM.

8.2 Hs1a at 500 nM, but not 100 nM, reduces peak sodium current density in colon-innervating dorsal root ganglia neurons

Peak sodium current density in colon-innervating TL neurons from healthy and CVH mice were recorded prior to and following incubation with Hs1a. It was assessed whether incubation with Hs1a at 100 nM and 500 nM is associated with a reduction in average peak sodium current density relative to baseline in these neurons. Summary statistics for peak sodium current density are shown in **Table 8.2** and current-voltage plots are shown in **Figure 8.2**.

Table 8.2: Summary statistics for peak sodium current density at baseline and following exposure to Hs1a in thoracolumbar neurons from healthy control (HC) and TNBS-treated (CVH) mice.

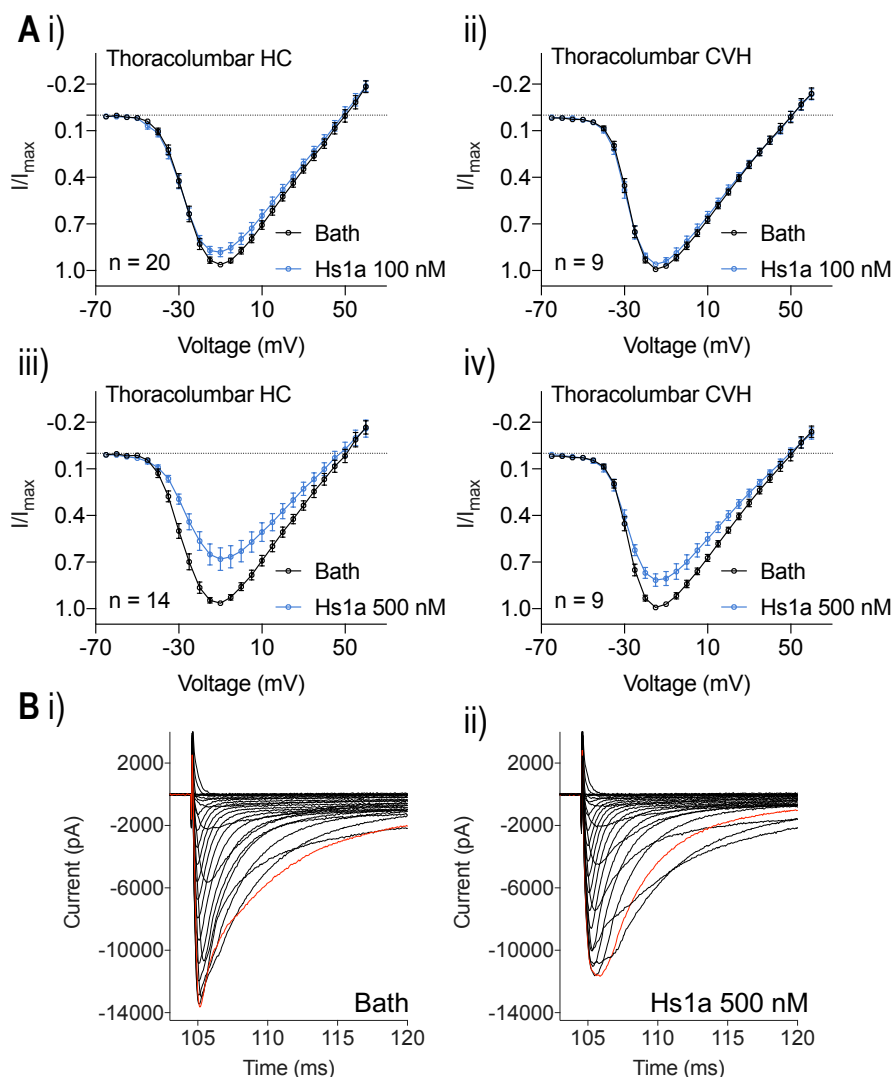| Group	n	Average peak sodium current density (pA/pF) ± SEM		Average fraction Hs1a-sensitive current ± SEM
		Baseline	Hs1a	
Hs1a (100 nM)				
HC	20	-175.7 ± 20.2	-156.3 ± 15.9	0.09 ± 0.02
CVH	9	-243.7 ± 27.5	-236.5 ± 25.5	0.03 ± 0.02
Hs1a (500 nM)				
HC	14	-181.3 ± 19.7	-126.8 ± 22.3	0.31 ± 0.07
CVH	9	-243.7 ± 27.5	-199.8 ± 21.8	0.17 ± 0.04

Figure 8.2: Hs1a at 500 nM, but not 100 nM, reduces sodium current in colon-innervating thoracolumbar neurons from healthy control (HC) and TNBS-treated (CVH) mice. A) Current-

voltage relationship at baseline (black) and following incubation with 100 nM Hs1a for 2 minutes (blue) in neurons from **i)** healthy and **ii)** TNBS-treated mice, and following incubation with 500 nM Hs1a for 2 minutes (blue) in neurons from **iii)** healthy and **iv)** TNBS-treated mice. The measured current (I) at each voltage was normalized to the peak current (I_{max}), and each data point shown here is the averaged I/I_{max} ± SEM. **B)** Raw traces of peak currents obtained using the current-voltage protocol (5 mV increments from -70 mV to +60 mV) in a thoracolumbar neuron. A reduction in magnitude and sharpness of maximum peak current (red trace) after incubation with **ii)** 500 nM Hs1a compared to **i)** baseline was observed.

A series of paired t-tests were carried out on samples of 20 TL neurons from healthy mice and 9 TL neurons from CVH mice to assess the effect of 100 nM of Hs1a on peak sodium current density, and 14 TL neurons from healthy mice and 9 TL neurons from CVH mice to assess the effect of 500 nM of Hs1a on peak sodium current density.

Hs1a (100 nM): TL neurons from healthy mice had a significantly reduced average peak sodium current density in the presence of Hs1a (-156.3 ± 71.1 pA/pF) compared to baseline (-175.7 ± 90.4 pA/pF). The estimated average difference was 19.3905 pA/pF (95% CI 4.0851 to 34.6960 pA/pF, t(19) = 2.652, p = 0.016). The average peak sodium current density in TL neurons from CVH mice in the presence of Hs1a (-236.5 ± 76.6 pA/pF) was not statistically different to baseline (-243.7 ± 82.4 pA/pF) (mean difference = 7.1622 pA/pF; 95% CI -2.5370 to 16.8615 pA/pF, t(8) = 1.703, p = 0.127).

Hs1a (500 nM): TL neurons from healthy mice had a significantly reduced average peak sodium current density in the presence of Hs1a (-126.8 ± 83.3 pA/pF) compared to baseline (-181.3 ± 73.6 pA/pF). The estimated average difference was 54.4907 pA/pF (95% CI 17.1958 to 91.7860 pA/pF, t(13) = 3.156, p = 0.008). TL neurons from CVH mice also had a reduced mean peak sodium current density in the presence of Hs1a (-199.8 ± 65.3 pA/pF) compared to baseline (-243.7 ± 82.4 pA/pF). This average reduction of 43.8344 was statistically significant (95% CI 13.0218 to 74.6407 pA/pF, t(8) = 3.281, p = 0.011).

In summary, Hs1a (500 nM) significantly reduced peak sodium current density in TL colon-innervating DRG neurons from healthy and CVH mice. The average Hs1a-sensitive component of total peak sodium current was estimated to be 24% in these neurons. A modest effect of Hs1a at 100 nM was observed in neurons from healthy animals, where the average Hs1a-sensitive component of total peak sodium current was estimated to be 9%.

8.3 Hs1a at 100 nM and 500 nM exerts modest effects on steady-state activation in colon-innervating thoracolumbar dorsal root ganglia neurons

Steady-state activation was estimated from the current-voltage relationship (**Figure 8.2**) at baseline and in the presence of Hs1a in colon-innervating TL DRG neurons. It was assessed whether incubation with Hs1a at 100 nM and 500 nM is associated with a shift in the conductance-voltage relationship in these neurons. A Boltzmann sigmoidal curve was fitted to each dataset, with voltage of half-maximal activation (V_{50}) and slope (k) listed in **Table 8.3**, and conductance-voltage plots shown in **Figure 8.3**.

Table 8.3: Summary statistics for the voltage of half-maximal activation (V_{50}) and slope factor (k) calculated by nonlinear regression of the current-voltage relationship obtained from a voltage-dependence of activation protocol following exposure to Hs1a in thoracolumbar neurons from healthy control (HC) and TNBS-treated (CVH) mice.

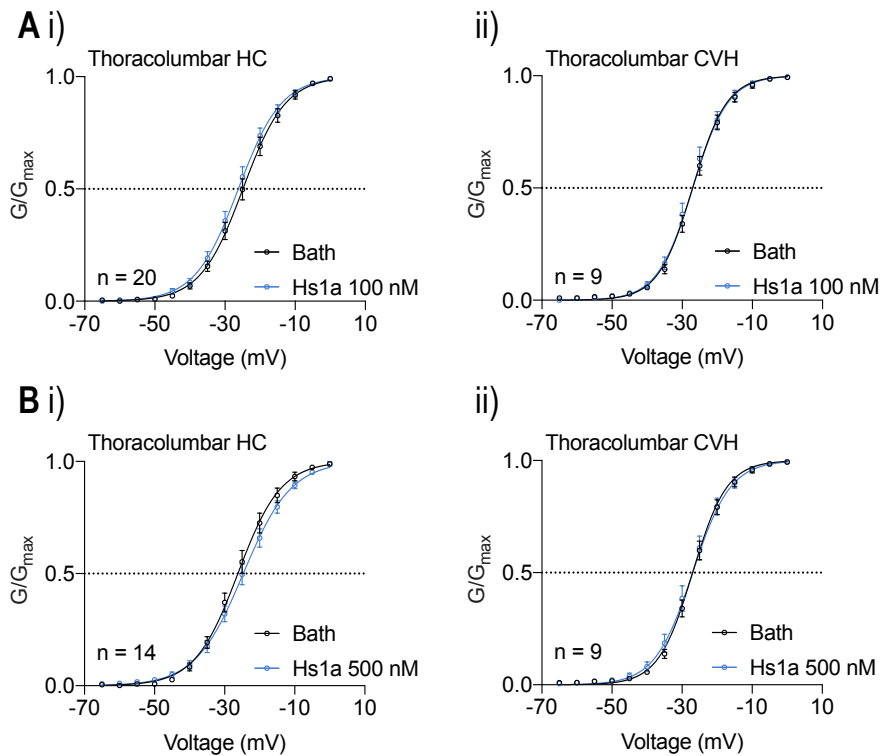| Group	n	V_{50} (mV)			k	
		Baseline	Hs1a	Sum-of-squares F-test p-value	Baseline	Hs1a
Hs1a (100 nM)						
HC	20	-24.90	-26.20	0.0026	6.06	6.15
CVH	9	-26.68	-27.39	0.0557	4.90	5.05
Hs1a (500 nM)						
HC	14	-26.22	-24.68	0.0011	6.16	6.85
CVH	9	-26.68	-27.32	0.1128	4.90	5.40

`

Figure 8.3: Hs1a (100 and 500 nM) modestly shifts the conductance-voltage relationship in colon-innervating thoracolumbar neurons from healthy control (HC) and TNBS-treated (CVH) mice. A) Steady-state activation curves at baseline (black) and following incubation with Hs1a (100 nM) for 2 minutes (blue) in neurons from **i)** healthy and **ii)** TNBS-treated mice, and **B)** following incubation with Hs1a (500 nM) in neurons from **i)** healthy and **ii)** TNBS-treated mice. The estimated conductance (G) was calculated from the measured current (I) ($I/(V_{cmd} - V_{rev})$, where V_{cmd} is the command voltage and V_{rev} is the reversal potential for sodium under the experimental conditions) and normalized to the maximum conductance (G_{max}). Each data point shows the mean G/G_{max} ± SEM and each data set has been fitted with a Boltzmann sigmoidal curve. A positive shift in V_{50} (at G/G_{max} = 0.5) is observed in the presence of 100 nM Hs1a in healthy neurons (**A, i**), a negative shift in V_{50} is observed in the presence of 500 nM Hs1a in healthy neuron (**B, i**) and no change in V_{50} is observed in the presence of 100 or 500 nM Hs1a in TNBS-treated neurons (**A, ii; B, ii**).

A series of sum-of-squares F-tests were carried out on samples of 20 healthy and 9 CVH colon-innervating TL neurons to assess the effect of Hs1a (100 nM) on steady-state activation, and on 14 healthy and 9 CVH colon-innervating TL neurons to assess the effect of Hs1a (500 nM) on steady-state activation.

<u>Hs1a (100 nM):</u> Steady-state activation was negatively shifted in the presence of Hs1a in TL neurons from healthy mice (V_{50} = -26.20 mV; 95% CI -26.80 to -25.60 mV) compared to baseline (V_{50} = -24.90 mV; 95% CI -25.50 to -24.30 mV), a statistically significant shift in V_{50}, $F_{(1, 556)}$ = 9.129, p = 0.003. Steady-state activation was not significantly shifted in TL neurons from CVH mice in the presence of Hs1a (V_{50} = -27.39 mV; 95% CI -27.97 to -26.82 mV) compared to baseline (V_{50} = -26.68 mV; 95% CI -27.14 to -26.22 mV), $F_{(1, 248)}$ = 3.694, p = 0.056.

<u>Hs1a (500 nM):</u> Steady-state activation was positively shifted in the presence of Hs1a in TL neurons from healthy mice (V_{50} = -24.68 mV; 95% CI -25.32 to -24.04 mV) compared to baseline (V_{50} = -26.22 mV; 95% CI -26.68 to -25.56 mV), a statistically significant shift in V_{50}, $F_{(1, 388)}$ = 10.82, p = 0.001. Steady-state activation was not significantly shifted in TL neurons from CVH mice in the presence of Hs1a (V_{50} = -27.32 mV; 95% CI -27.98 to -26.66 mV) compared to baseline (V_{50} = -26.68 mV; 95% CI -27.14 to -26.22 mV), $F_{(1, 248)}$ = 2.533, p = 0.113.

In summary, Hs1a (100 nM and 500 nM) induced marginal shifts on steady-state activation in colon-innervating TL DRG neurons from healthy mice, with a shift in the average voltage of half-maximal

activation of -1.3 mV in the presence of 100 nM, and +1.5 mV in the presence of 500 nM Hs1a. No effects on the steady-state activation in colon-innervating TL DRG neurons from CVH mice were observed.

8.4 Hs1a at 100 and 500 nM does not shift steady-state fast inactivation in colon-innervating thoracolumbar dorsal root ganglia neurons

Peak sodium current during fast inactivation voltage protocols in colon-innervating TL neurons from healthy and CVH mice were recorded prior to and following incubation with Hs1a. It was assessed whether incubation with Hs1a at 100 nM and 500 nM is associated with a shift in steady-state fast inactivation in these neurons. Summary statistics for the voltage of half-maximal inactivation (V_{50}) and the slope factor (k) of the steady-state fast inactivation at baseline and following exposure to Hs1a are reported for each group in **Table 8.4**. V_{50} and k were obtained by normalizing the peak inward currents (I) to the maximal inward current (I_{max}) and fitting the relationship between I/I_{max} and applied voltage with a Boltzmann equation: $I/I_{max} = 1/(1+\exp((V_{50} - V_m)/k))$. Fitted steady-state fast inactivation curves at baseline and following exposure to Hs1a are shown in **Figure 8.4**.

Table 8.4: Summary statistics for the voltage of half-maximal inactivation (V_{50}) and slope factor (k) calculated by nonlinear regression of the current-voltage relationship obtained from steady-state fast inactivation protocols following exposure to Hs1a in thoracolumbar neurons from healthy control (HC) and TNBS-treated (CVH) mice.

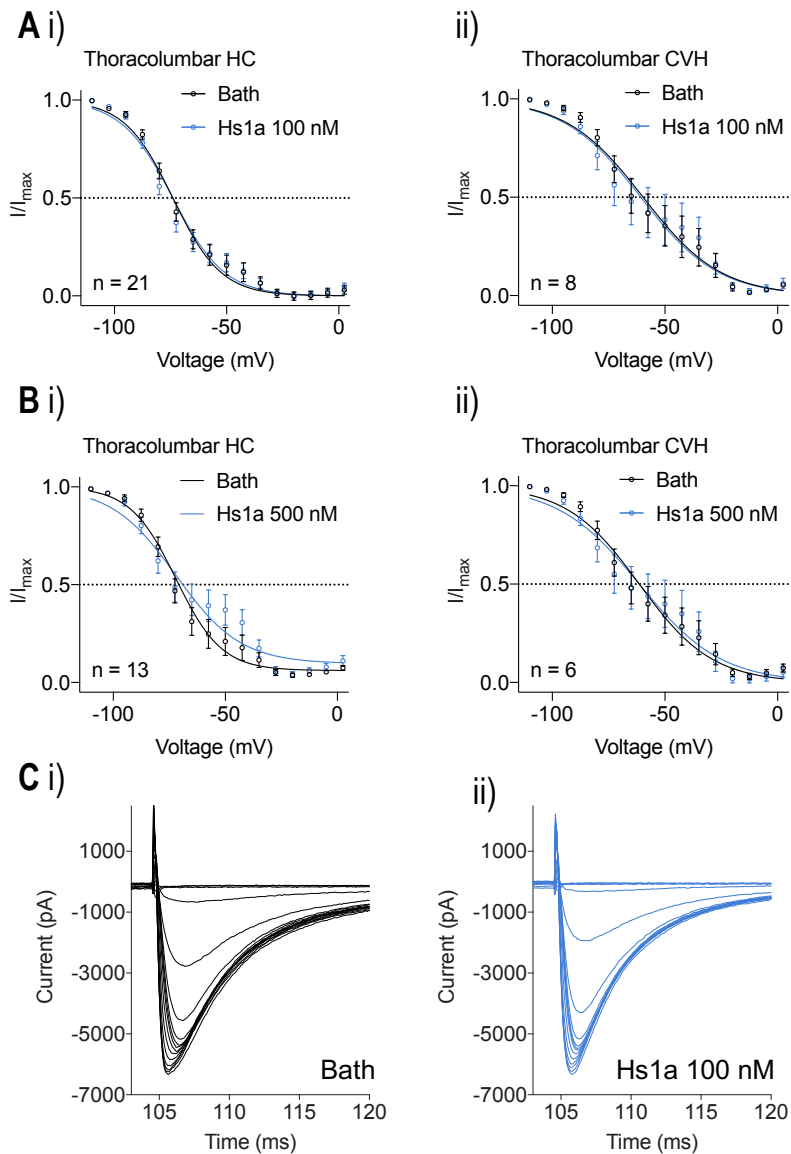| Group	n	V_{50} (mV)			k	
		Baseline	Hs1a	Sum-of-squares F-test p-value	Baseline	Hs1a
Hs1a (100 nM)						
HC	21	-73.13	-74,84	0.1057	-10.86	-11.42
CVH	8	-59.79	-60.60	0.2797	-15.92	-18.43
Hs1a (500 nM)						
HC	13	-73.36	-69.06	0.0733	-9.70	-15.60
CVH	6	-61.21	-61.55	0.8964	-16.14	-18.11

`

Figure 8.4: Hs1a at 100 and 500 nM did not alter parameters of steady-state fast inactivation in colon-innervating thoracolumbar neurons from healthy control (HC) mice. A) Steady-state fast inactivation curves at baseline (black) and following incubation with Hs1a (100 nM) for 2 minutes (blue) in neurons from **i)** healthy and **ii)** TNBS-treated (CVH) mice, and **B)** following incubation with Hs1a (500 nM) in neurons from **i)** healthy and **ii)** TNBS-treated mice. The measured current (I) at each voltage was normalized to the peak current (I_{max}). Each data point shows the mean I/I_{max} ± SEM and each data set has been fitted with a Boltzmann sigmoidal curve. V_{50} was unchanged in the presence of 100 nM Hs1a in healthy neurons (**A, i**), TNBS-treated neurons (**A, ii**), and in the presence of 500 nM Hs1a in healthy neurons (**B, i**), and in TNBS-treated neurons (**B, ii**). **C)** Raw traces of peak currents obtained using the current-voltage protocol (measured at -30 mV following 7.5 mV increments from -110 mV to +2.5 mV) in a thoracolumbar neuron from a healthy mouse. No changes in distribution of traces after incubation with 100 nM Hs1a (**ii**) compared to baseline (**i**) were observed.

A series of sum-of-squares F-tests were carried out on samples of 21 healthy and 8 CVH colon-innervating TL neurons to assess the effect of Hs1a (100 nM) on steady-state fast inactivation, and on 13 healthy and 6 CVH colon-innervating TL neurons to assess the effect of Hs1a (500 nM) on steady-state fast inactivation.

<u>Hs1a (100 nM):</u> Steady-state fast inactivation was not significantly shifted in TL neurons from healthy mice in the presence of Hs1a (V_{50} = -76.28 mV; 95% CI -76.28 to -73.38 mV) compared to baseline (V_{50} = -73.13 mV; 95% CI -74.60 to -71.65 mV), $F_{(1, 668)}$ = 2.624, p = 0.106. Steady-state fast inactivation was not significantly shifted in TL neurons from CVH mice in the presence of Hs1a (V_{50} = -60.60 mV; 95%

CI -64.97 to -56.18 mV) compared to baseline (V_{50} = -59.79 mV; 95% CI -62.97 to -56.56 mV), $F_{(1, 252)}$ = 1.173, p = 0.280.

Hs1a (500 nM): Steady-state fast inactivation was not significantly shifted in the presence of Hs1a in TL neurons from healthy mice (V_{50} = -69.06 mV; 95% CI -73.29 to -64.35 mV) compared to baseline (V_{50} = -73.36 mV; 95% CI -75.62 to -70.97 mV), $F_{(1, 410)}$ = 3.225, p = 0.0733, or in TL neurons from CVH mice, (V_{50} = -61.55 mV; 95% CI -65.64 to -57.44 mV) compared to baseline (V_{50} = -61.21 mV; 95% CI -64.22 to -58.17 mV), $F_{(1, 284)}$ = 0.01699, p = 0.900.

In summary, Hs1a (100 and 500 nM) did not alter parameters of steady-state fast inactivation in TL neurons from healthy or CVH mice.

8.5 Increase in rheobase and reduction in peak sodium current density in the presence of Hs1a (500 nM) is not different between neurons from healthy and TNBS-treated mice

In Chapter 7, no association between health status (HC vs CVH) and the effect of TTX on rheobase (section 7.6) and peak sodium current (section 7.5) was obtained. To assess whether this was also the case in responses to 500 nM Hs1a, a series of Welch-Satterthwaite tests were run on samples of healthy and CVH TL neurons to compare fold change in rheobase in the presence of Hs1a, and the Hs1a-sensitive component.

Fold-change in rheobase. TL neurons from healthy mice had a higher (1.2 ± 0.3) fold change in rheobase compared to TL neurons from CVH mice (1.1 ± 0.2), a difference of 0.0701 (95% CI -0.0576 to 0.1979), which was not found to be statistically significant, t(83.885), = 1.190, p = 0.237.

Hs1a-sensitive component of current. The difference in the average Hs1a-sensitive fraction of current between healthy neurons (0.31 ± 0.27) and CVH neurons (0.17 ± 0.12) was not statistically significant (mean difference = 0.1348; 95% CI -0.0396 to 0.3092, t(19.500) = 1.615, p = 0.122).

In summary, there was no association between health status (HC vs CVH) and the magnitude of inhibition by 500 nM Hs1a in terms of rheobase or peak sodium current density in colon-innervating TL DRG neurons.

Chapter 9 The effect of compound B, ICA-121341, and A-803467 on electrophysiological properties of colon-innervating dorsal root ganglia neurons from healthy mice

In this chapter, the effect of Na_v inhibition on action potential generation in colon-innervating dorsal root ganglia (DRG) neurons from healthy control (HC) mice was investigated using inhibitors with a narrower selectivity range compared to tetrodotoxin (Chapter 7) and Hs1a (Chapter 8). Inhibition of $Na_v1.1$ was investigated using Compound B, inhibition of $Na_v1.1$-$Na_v1.3$ was investigated using ICA-121341, and inhibition of $Na_v1.8$ was investigated using A-803467. Both thoracolumbar (TL) and lumbosacral (LS) neuron responses were investigated, however, differences between TL and LS neuron responses are not investigated in this chapter.

9.1 The effect of Compound B on rheobase in colon-innervating dorsal root ganglia neurons from healthy mice

$Na_v1.1$ was recently shown to have a role in mechanosensation in visceral afferents, and may be a novel pharmaceutical target for visceral pain (Osteen et al. 2016). To build on these results, the effect of Compound B, a $Na_v1.1$-selective inhibitor (Gilchrist et al. 2014), on active electrophysiological properties in colon-innervating DRG neurons was investigated. The effect of Compound B on peak sodium current density in colon-innervating DRG neurons is reported in Chapter 10 as part of a publication titled '$Na_v1.1$ inhibition can reduce visceral hypersensitivity', which also evaluates the effect of Compound B on mechanosensitive colonic afferents *ex vivo* and the visceromotor response to colorectal distension *in vivo*. Following reporting of these findings, the effect of Compound B on rheobase in colon-innervating DRG neurons from healthy mice was also investigated and is described below.

9.1.1 Compound B at 100 µM increases rheobase in colon-innervating dorsal root ganglia neurons

Rheobase in colon-innervating TL neurons from healthy mice were recorded prior to and following incubation with Compound B (100 µM). It was assessed whether incubation with Compound B is associated with an increase in average ln(rheobase) relative to baseline ln(rheobase) in these neurons. Summary statistics for rheobase and ln(rheobase) are shown in **Table 9.1** and **Figure 9.1**.

Table 9.1: Summary statistics for rheobase and ln(rheobase) at baseline and in the presence of Compound B (100 µM) in thoracolumbar neurons from healthy mice.

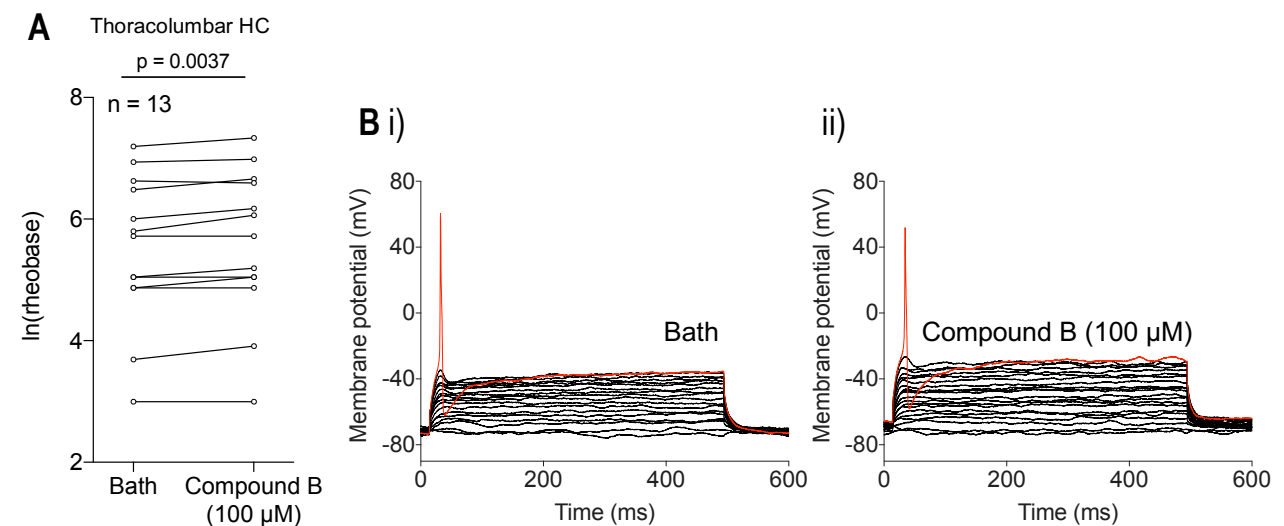| Group	n	Average rheobase (pA) ± SEM		Average ln(rheobase) ± SEM		Average fold change in rheobase ± SEM
		Baseline	Compound B	Baseline	Compound B	
TL neurons	13	418.5 ± 113.3	463.5 ± 125.7	5.5 ± 0.4	5.6 ± 0.04	1.11 ± 0.03

89

Figure 9.1: Compound B (100 µM) significantly increases mean ln(rheobase) in colon-innervating thoracolumbar neurons from healthy control (HC) mice. **A)** Ln(rheobase) at baseline and following incubation with 100 µM Compound B for 2 minutes in thoracolumbar neurons healthy mice. Compound B at 100 µM increased mean ln(rheobase) compared to baseline (paired t-test, p < 0.01). **B)** Raw traces of membrane potential measured at increasing current injections (25 pA increments starting at -20 pA) in a thoracolumbar neuron from a healthy mouse. An increase in the minimum current injection after incubation with **i)** 100 µM Compound B (480 pA, red trace) compared to **ii)** baseline (405 pA, red trace) was observed.

A paired t-test was run on a sample of 13 TL neurons from healthy mice to assess the effect of Compound B (100 µM) on ln(rheobase). TL neurons from healthy mice had a significantly higher mean ln(rheobase) in the presence of compound B (100 µM) (5.6 ± 1.2) compared to baseline (5.5 ± 1.2). The estimated average difference was 0.1010 (95% CI 0.0397 to 0.1621, t(12) = 3.590, p = 0.004).

In summary, Compound B (100 µM) significantly increased rheobase in TL colon-innervating DRG neurons from healthy mice. The change in rheobase induced by Compound B was a 1.1-fold increase in these neurons.

9.2 The effect of ICA-121341 on rheobase in colon-innervating dorsal root ganglia neurons from healthy mice

Following the finding that Compound B, a $Na_v1.1$-selective inhibitor, increased rheobase levels in colon-innervating DRG neurons (section 9.1), a less selective $Na_v1.1$ inhibitor was assessed. ICA-121341 is a potent inhibitor of $Na_v1.1$, $Na_v1.2$, and $Na_v1.3$ (McCormack et al. 2013), with highest potency for $Na_v1.1$ and $Na_v1.3$. The effect of ICA-121341 at three concentrations on rheobase in colon-innervating TL and LS neurons from healthy mice is described below.

9.2.1 ICA-121341 at 500 nM, but not 50 or 200 nM, increases rheobase in colon-innervating dorsal root ganglia neurons

Rheobase in colon-innervating TL and LS neurons from healthy mice were recorded prior to and following incubation with ICA-121341. It was assessed whether incubation with ICA-121341 at 50, 200, and 500 nM is associated with a reduction in average ln(rheobase) relative to baseline ln(rheobase) in these neurons. Summary statistics for rheobase and ln(rheobase) are shown in **Table 9.2** and **Figure 9.2**.

Table 9.2: Summary statistics for rheobase and ln(rheobase) at baseline and in the presence of ICA-121341 (50, 200, 500 nM) in thoracolumbar (TL) and lumbosacral (LS) neurons from healthy mice.

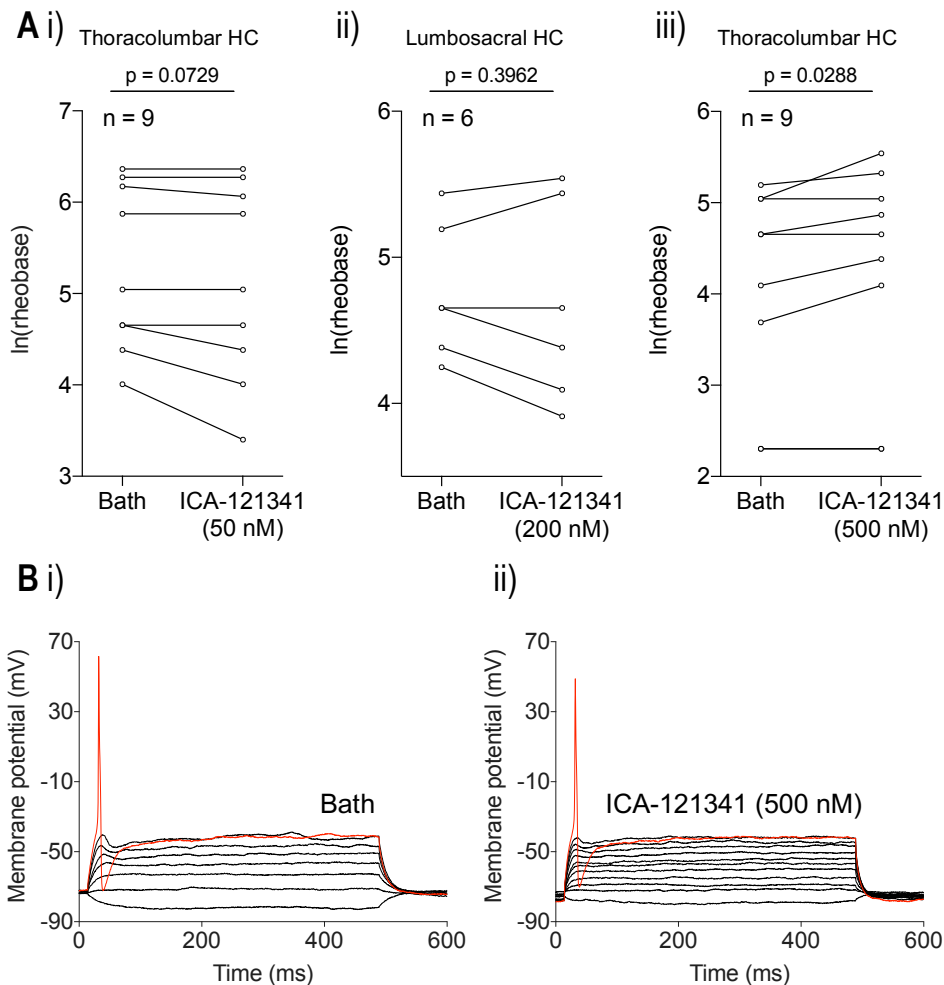| Group	n	Average rheobase (pA) ± SEM		Average ln(rheobase) ± SEM		Average fold change in rheobase ± SEM
		Baseline	ICA-121341	Baseline	ICA-121341	
ICA-121341 (50 nM)						
TL neurons	9	271.7 ± 71.2	257.8 ± 72.2	5.3 ± 0.3	5.1 ± 0.4	0.88 ± 0.06
ICA-121341 (200 nM)						
LS neurons	6	128.3 ± 25.7	130.0 ± 36.5	4.7 ± 0.2	4.7 ± 0.3	0.94 ± 0.09
ICA-121341 (500 nM)						
TL neurons	9	91.1 ± 21.5	112.2 ± 27.9	4.1 ± 0.4	4.3 ± 0.4	1.21 ± 0.08

Figure 9.2: ICA-121341 at 500 nM, but not 50 or 200 nM, significantly increases ln(rheobase) in colon-innervating neurons from healthy control (HC) mice. **A)** Ln(rheobase) at baseline and following a 2-minute incubation with **i)** 50 nM ICA-121341 in thoracolumbar neurons, **ii)** 200 nM ICA-121341 in lumbosacral neurons, and **ii)** 500 nM ICA-121341 in thoracolumbar neurons. ICA-121341 at 500 nM increased mean ln(rheobase) compared to baseline (paired t-test, p < 0.05), but not at 50 or 200 nM (paired t-test, p > 0.05). **B)** Raw traces of membrane potential measured at increasing current injections (25 pA increments starting at -20 pA) in a thoracolumbar neuron from a healthy mouse. An increase in the minimum current injection after incubation with **ii)** 500 nM ICA-121341 (255 pA, red trace) compared to **i)** baseline (155 pA, red trace) was observed.

A series of paired t-tests were carried out on samples of 9 TL neurons to assess the effect of 50 nM ICA-121341 on ln(rheobase), 6 LS neurons to assess the effect of 200 nM ICA-121341 on ln(rheobase), and 9 TL neurons to assess the effect of 500 nM ICA-121341.

ICA-121341 (50 nM). The average ln(rheobase) in TL neurons from healthy mice in the presence of ICA-121341 (5.1 ± 1.1) was not statistically different to baseline (5.3 ± 0.9) (mean difference = 0.1514; 95% CI -0.3206 to 0.0178, t(8) = 2.064, p = 0.0729).

ICA-121341 (200 nM). The average ln(rheobase) in LS neurons from healthy mice in the presence of ICA-121341 (4.7 ± 0.7) was not statistically different to baseline (4.7 ± 0.5) (mean difference = 0.0913; 95% CI -0.3443 to 0.1617, t(5) = 0.9275, p = 0.3962)

ICA-121341 (500 nM). TL neurons from healthy mice had a significantly higher mean ln(rheobase) in the presence of ICA-121341 (4.3 ± 1.2) compared to baseline (4.1 ± 1.1). The estimated average difference was 0.1705 (95% CI 0.0227 to 0.3183, t(8) = 2.660, p = 0.0288).

In summary, ICA-121341 at 500 nM significantly increased rheobase levels in colon-innervating TL DRG neurons from healthy mice. The change in rheobase induced by ICA-121341 was a 1.2-fold increase in these neurons. ICA-121341 at 50 nM and 200 nM did not affect rheobase levels.

9.3 The effect of A-803467 on rheobase in colon-innervating dorsal root ganglia neurons from healthy mice

$Na_v1.8$ is an isoform of considerable interest due to its implication in pain signaling (**Table 2.2**) and preferential expression in the peripheral nervous system (**Table 2.1**). In this section, the effects of A-803467, a local anesthetic derivative with high potency for $Na_v1.8$ over other isoforms (Jarvis et al. 2007), on action potential generation in colon-innervating LS DRG neurons from healthy mice was evaluated.

9.3.1 A-803467 at 500 nM, but not 250 nM, increases rheobase in colon-innervating dorsal root ganglia neurons

Rheobase in colon-innervating LS neurons from healthy mice were recorded prior to and following incubation with A-803467. It was assessed whether incubation with A-803467 at 250 nM and 500 nM is associated with a reduction in average ln(rheobase) and action potential overshoot relative to baseline in these neurons. Summary statistics for rheobase, ln(rheobase), and action potential overshoot, are shown in **Table 9.3, Table 9.4**, and **Figure 9.3**.

Table 9.3: Summary statistics for rheobase and ln(rheobase) at baseline and in the presence of A-803467 (250 and 500 nM) in lumbosacral (LS) neurons from healthy mice.

Group	n	Average rheobase (pA) ± SEM		Average ln(rheobase) ± SEM		Average fold change in rheobase ± SEM
		Baseline	A-803467	Baseline	A-803467	
A-803467 (250 nM)						
LS neurons	11	108.2 ± 10.9	111.8 ± 10.3	4.3 ± 0.1	4.3 ± 0.1	1.09 ± 0.04
A-803467 (500 nM)						
LS neurons	12	95.0 ± 9.7	113.6 ± 15.1	4.1 ± 0.1	4.4 ± 0.1	1.40 ± 0.04

Table 9.4: Summary statistics for action potential overshoot at baseline and in the presence of A-803467 (250 and 500 nM) in lumbosacral (LS) neurons from healthy mice.

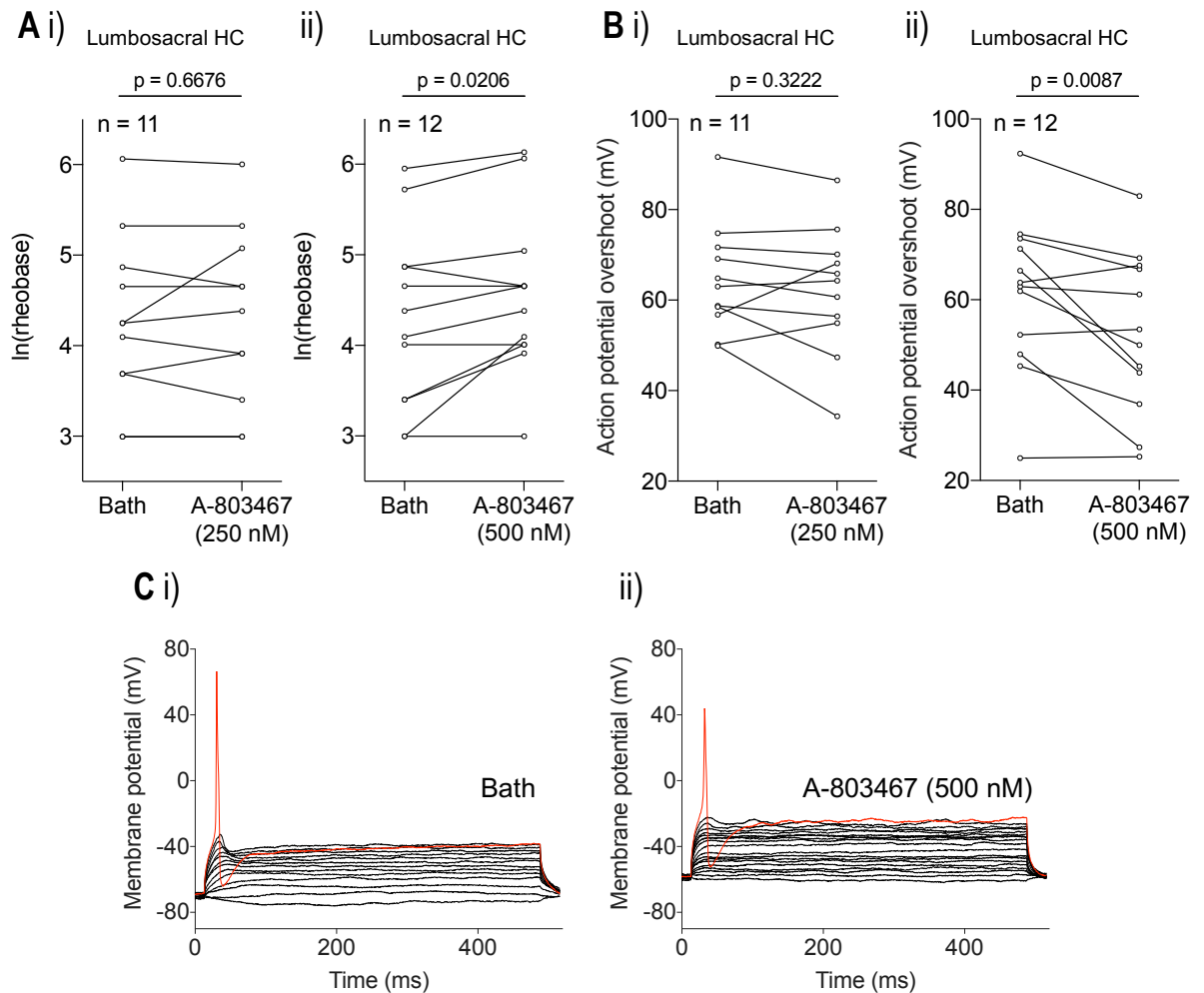| Group	n	Average action potential overshoot (mV) ± SEM		Average reduction in overshoot ± SEM
		Baseline	A-803467	
A-803467 (250 nM)				
LS neurons	11	64.5 ± 1.1	62.19 ± 1.3	0.04 ± 0.04
A-803467 (500 nM)				
LS neurons	12	61.4 ± 1.4	52.5 ± 1.5	0.14 ± 0.05

Figure 9.3: A-803467 at 500 nM, but not 250 nM, significantly increases ln(rheobase) and decreases action potential overshoot in colon-innervating lumbosacral neurons from healthy control (HC) mice. **A)** Ln(rheobase) at baseline and following a 1-2 minute incubation with **i)** 250 nM A-803467 and **ii)** 500 nM A-803467 in lumbosacral neurons. A-803467 at 500 nM increased mean ln(rheobase) compared to baseline (paired t-test, $p < 0.05$), but not at 250 nM (paired t-test, $p > 0.05$). Action potential overshoot at baseline and following incubation a 1-2 minute incubation with **i)** 250 nM A-803467 and **ii)** 500 nM A-803467 in lumbosacral neurons. A-803467 decreased mean overshoot compared to baseline in the 500 nM dataset (paired t-test, $p < 0.05$), but not the 250 nM dataset (paired t-test, $p > 0.05$). **C)** Raw traces of membrane potential measured at increasing current injections (10 pA increments starting at -20 pA). An increase in the minimum current injection after incubation with **ii)** 500 nM A-803467 (70 pA, red trace) compared to **i)** baseline (50 pA, red trace) was observed.

A series of paired t-tests were carried out on samples of 11 LS neurons to assess the effect of 250 nM A-803467 on ln(rheobase) and action potential overshoot, and 12 LS neurons to assess the effect of 500 nM A-803467 on ln(rheobase) and action potential overshoot.

A-803467 (250 nM). The average ln(rheobase) in LS neurons from healthy mice in the presence of A-803467 (4.3 ± 1.0) was not statistically different to baseline (4.3 ± 0.9) (mean difference = 0.0400; 95% CI -0.1614 to 0.2412, t(10) = 0.4424, p = 0.6676). The average action potential overshoot in LS neurons from healthy mice in the presence of A-803467 (62.19 ± 14.0 mV) was not statistically different to baseline (64.5 ± 12.1 mV) (mean difference = -2.275 mV; 95% CI -7.143 to 2.593 mV, t(10) = 1.041, p = 0.3222).

A-803467 (500 nM). LS neurons from healthy mice had a significantly higher mean ln(rheobase) in the presence of A-803467 (4.4 ± 0.8) compared to baseline (4.1 ± 0.9). The estimated average difference was 0.2716 (95% CI 0.0504 to 0.4928, t(11) = 2.702, p = 0.0206). The average action potential overshoot in LS neurons from healthy mice in the presence of A-803467 (52.5 ± 17.8 mV) was significantly lower than at baseline (61.4 ± 17.2 mV). The estimated average difference was -8.944 mV (95% CI -15.13 to -2.760 mV, t(11) = 3.183, p = 0.0087).

93

In summary, A-803467 at 500 nM significantly increased rheobase and reduced action potential overshoot in colon-innervating DRG neurons from healthy mice. The change in rheobase induced by A-803467 was a 1.4-fold increase on average in these neurons. The change in action potential overshoot was a 14% reduction on average in these neurons. No significant effects were observed with A-803467 at 250 nM.

9.4 Summary

In this chapter, the effect of pharmacological inhibition of $Na_v1.1$ using Compound B, $Na_v1.1$-$Na_v1.3$ using ICA-121341, and $Na_v1.8$ using A-803467 on action potential generation in colon-innervating TL and LS DRG neurons from healthy mice was investigated. Compound B increased rheobase at a concentration where it is believed to be selective for $Na_v1.1$ (100 μM), whereas ICA-121341 increased rheobase at a concentration where it is targeting $Na_v1.1$-$Na_v1.3$ (500 nM), as opposed to a concentration where it is more selective for $Na_v1.1$ and $Na_v1.3$ (50 and 200 nM). A-803467 increased rheobase at 500 nM, but not 250 nM, however, the higher concentration is believed to retain selectivity towards $Na_v1.8$.

9.5 Literature cited

Gilchrist, J, Dutton, S, Diaz-Bustamante, M, McPherson, A, Olivares, N, Kalia, J, Escayg, A & Bosmans, F 2014, '$Na_v1.1$ Modulation by a Novel Triazole Compound Attenuates Epileptic Seizures in Rodents', *ACS Chemical Biology*, vol. 9, no. 5, 2014/05/16, pp. 1204-1212.

Jarvis, MF, Honore, P, Shieh, CC, Chapman, M, Joshi, S, Zhang, XF, Kort, M, Carroll, W, Marron, B, Atkinson, R, Thomas, J, Liu, D, Krambis, M, Liu, Y, McGaraughty, S, Chu, K, Roeloffs, R, Zhong, C, Mikusa, JP, Hernandez, G, Gauvin, D, Wade, C, Zhu, C, Pai, M, Scanio, M, Shi, L, Drizin, I, Gregg, R, Matulenko, M, Hakeem, A, Gross, M, Johnson, M, Marsh, K, Wagoner, PK, Sullivan, JP, Faltynek, CR & Krafte, DS 2007, 'A-803467, a potent and selective $Na_v1.8$ sodium channel blocker, attenuates neuropathic and inflammatory pain in the rat', *Proceedings of the National Academy of Sciences of the United States of America*, vol. 104.

McCormack, K, Santos, S, Chapman, ML, Krafte, DS, Marron, BE, West, CW, Krambis, MJ, Antonio, BM, Zellmer, SG, Printzenhoff, D, Padilla, KM, Lin, Z, Wagoner, PK, Swain, NA, Stupple, PA, de Groot, M, Butt, RP & Castle, NA 2013, 'Voltage sensor interaction site for selective small molecule inhibitors of voltage-gated sodium channels', *Proceedings of the National Academy of Sciences of the United States of America*, vol. 110, no. 29, 07/01, pp. E2724-E2732.

Osteen, JD, Herzig, V, Gilchrist, J, Emrick, JJ, Zhang, C, Wang, X, Castro, J, Garcia-Caraballo, S, Grundy, L, Rychkov, GY, Weyer, AD, Dekan, Z, Undheim, EAB, Alewood, P, Stucky, CL, Brierley, SM, Basbaum, AI, Bosmans, F, King, GF & Julius, D 2016, 'Selective spider toxins reveal a role for the $Na_v1.1$ channel in mechanical pain', *Nature*, vol. 534, no. 7608, 06/23/print, pp. 494-499.

Statement of Authorship

Title of Paper	Nav1.1 inhibition can reduce visceral hypersensitivity
Publication Status	☑ Published ☐ Accepted for Publication ☐ Submitted for Publication ☐ Unpublished and Unsubmitted work written in manuscript style
Publication Details	Salvatierra, J., Castro, J., Erickson, A., Li, Q., Braz, J., Gilchrist, J., Grundy, L., Rychkov, G. Y., Deiteren, A., Rais, R, King, G. F., Slusher, B. S., Basbaum, A., Pasricha, P. J., Brierley, S. M. and Bosmans, F. (2018). NaV1.1 inhibition can reduce visceral hypersensitivity. JCI Insight, 3(11). doi:10.1172/jci.insight.121000

Principal Author

Name of Principal Author (Candidate)	Andelain Erickson (equal first author)
Contribution to the Paper	Retrograde labeling, DRG culture, whole-cell patch-clamp lectrophysiology and analysis, editing of manuscript
Overall percentage (%)	20
Certification:	This paper reports on original research I conducted during the period of my Higher Degree by Research candidature and is not subject to any obligations or contractual agreements with a third party that would constrain its inclusion in this thesis. I am the primary author of this paper.
Signature	Date 15/1/2019

Co-Author Contributions

By signing the Statement of Authorship, each author certifies that:

i. the candidate's stated contribution to the publication is accurate (as detailed above);

ii. permission is granted for the candidate in include the publication in the thesis; and

iii. the sum of all co-author contributions is equal to 100% less the candidate's stated contribution.

Name of Co-Author	Juan Salvatierra (equal first author)
Contribution to the Paper	two-electrode voltage clamp electrophysiology and analysis, editing manuscript.
Signature	Date 4/5/19

Name of Co-Author	Joel Castro (equal first author)
Contribution to the Paper	VMR TO CRD EXPERIMENTS AND INVITRO AFFERENT RECORDINGS EXPERIMENTS DATA ANALYSIS, FIGURE GENERATION AND EDITING OF MANUSCRIPT
Signature	Date 14.03.19

Name of Co-Author	Qian Li
Contribution to the Paper	VMR to CRD in IBS mouse model.
Signature		Date	4 2-19

Name of Co-Author	Joao Braz
Contribution to the Paper	Behavioral experiments
Signature		Date	4/24/19

Name of Co-Author	John Gilchrist
Contribution to the Paper	electrophysiology
Signature		Date	5 Apr 19

Name of Co-Author	Luke Grundy
Contribution to the Paper	Editing of manuscript, experimental design.
Signature		Date	19.3.19

Name of Co-Author	Grigori Y. Rychkov
Contribution to the Paper	Supervision of patch clamping and data analysis, editing of manuscripts
Signature		Date	14.03.2019

Name of Co-Author	Annemie Deiteren
Contribution to the Paper	VMR to CRD experiments, approved final manuscript
Signature		Date	27-MAR-2019

96

Name of Co-Author	Rana Rais
Contribution to the Paper	Drug Metabolism & Pk portion of compound B.
Signature	Date: April 3ʳᵈ 2019

Name of Co-Author	Glenn F. King
Contribution to the Paper	PROVIDED Hm1a PEPTIDE.
Signature	Date: 03/04/19

Name of Co-Author	Barbara S. Slusher
Contribution to the Paper	Drug Metabolism & Pk portion of compound B.
Signature	Date: 2 APRIL 2019

Name of Co-Author	Allan Basbaum
Contribution to the Paper	Experimental design - manuscript writing
Signature	Date: 4-3-19

Name of Co-Author	Pankaj J. Pasricha (corresponding author)
Contribution to the Paper	Designed study for VMR to CRD in IL3 smice
Signature	Date: 4-2-19

Name of Co-Author	Stuart M. Brierley (corresponding author)
Contribution to the Paper	SUPERVISION, PROJECT LEAD IN OVERSIGHT MANUSCRIPT WRITING + DRAFTING + FIGURES
Signature	Date: 14/3/2019

97

Name of Co-Author	Frank Bosmans (corresponding author)
Contribution to the Paper	Compound studies
Signature	Date 5/8/13

Compound studies

Chapter 10 Na$_v$1.1 inhibition can reduce visceral hypersensitivity

Juan Salvatierra,[1] Joel Castro,[2,3] Andelain Erickson,[2,3] Qian Li,[4] Joao Braz,[5] John Gilchrist,[1] Luke Grundy,[2,3] Grigori Y. Rychkov,[2,3] Annemie Deiteren,[2,3] Rana Rais,[6] Glenn F. King,[7] Barbara S. Slusher,[6] Allan Basbaum,[5] Pankaj J. Pasricha,[4] Stuart M. Brierley,[2,3] and Frank Bosmans (corresponding author)[1,8]

[1]Department of Physiology, Johns Hopkins University School of Medicine, Baltimore, Maryland, USA. [2]Visceral Pain Research Group, Human Physiology, Centre for Neuroscience, College of Medicine and Public Health, Flinders University, Australia. [3]Centre for Nutrition and Gastrointestinal Diseases, Discipline of Medicine, University of Adelaide, South Australian Health and Medical Research Institute, Adelaide, Australia. [4]Division of Gastroenterology and Hepatology, Johns Hopkins University School of Medicine, Baltimore, Maryland, USA. [5]Department of Anatomy, UCSF, California, USA. [6]Johns Hopkins Drug Discovery and Department of Neurology, Johns Hopkins University School of Medicine, Baltimore, Maryland, USA. [7]Institute for Molecular Bioscience, the University of Queensland, Brisbane, Australia. [8]Solomon H. Snyder Department of Neuroscience, Johns Hopkins University School of Medicine, Baltimore, Maryland, USA.

10.1 Abstract

Functional bowel disorder patients can suffer from chronic abdominal pain, likely due to visceral hypersensitivity to mechanical stimuli. As there is only a limited understanding of the basis of chronic visceral hypersensitivity (CVH), drug-based management strategies are ill defined, vary considerably, and include NSAIDs, opioids, and even anticonvulsants. We previously reported that the 1.1 subtype of the voltage-gated sodium (Na$_v$; Na$_v$1.1) channel family regulates the excitability of sensory nerve fibers that transmit a mechanical pain message to the spinal cord. Herein, we investigated whether this channel subtype also underlies the abdominal pain that occurs with CVH. We demonstrate that Na$_v$1.1 is functionally upregulated under CVH conditions and that inhibiting channel function reduces mechanical pain in 3 mechanistically distinct mouse models of chronic pain. In particular, we use a small molecule to show that selective Na$_v$1.1 inhibition (a) decreases sodium currents in colon-innervating dorsal root ganglion neurons, (b) reduces colonic nociceptor mechanical responses, and (c) normalizes the enhanced visceromotor response to distension observed in 2 mouse models of irritable bowel syndrome. These results provide support for a relationship between Na$_v$1.1 and chronic abdominal pain associated with functional bowel disorders.

10.2 Introduction

Functional bowel disorders (FBDs) such as irritable bowel syndrome (IBS), constipation, diarrhea, and abdominal bloating occur worldwide, and effective treatment is a major unmet clinical need in gastroenterology (1). Typically, FBDs are associated with alterations in bowel habits that result in a substantially decreased quality of life. Because of their prevalence, they are also a considerable drain on health care resources (2). People suffering from FBDs can have an array of symptoms. In particular, most common and observed in ≥40% of the IBS patient population (3) is chronic abdominal pain. A prominent hypothesis for the etiology of this abdominal pain is mechanical hypersensitivity of sensory fibers that innervate the gut (4–8). Although a range of channels and receptors have been implicated (9–20), our understanding of chronic visceral hypersensitivity (CVH) is still poor. Not surprisingly, therefore, pharmacological management of chronic abdominal pain is nonspecific and ranges from NSAIDs to opioids, without or with adjuvant analgesics (21). Anticonvulsants such as gabapentin and pregabalin show promise to treat CVH, but there is insufficient data to support their effectiveness in FBD patients, and all use is considered off-label (22).

Cell membrane–embedded voltage-gated sodium (Na$_v$) channels regulate cellular excitability and initiate action potentials in the peripheral, central, and enteric nervous systems (23–27). A subset of the 9 Na$_v$ channel subtypes is expressed in the enteric nervous system, and mutations can lead to gastrointestinal disorders, including constipation and diarrhea (10, 28). The discovery that Na$_v$1.1 can regulate the

excitability of sensory nerve fibers that mediate mechanical pain (29) led to our hypothesis that this channel subtype may also underlie the development of abdominal pain in FBD states. In our previous studies, consistent with this, a spider toxin (Hm1a) that activates $Na_v1.1$ increased mechanically evoked spiking in high-threshold colonic nociceptors in gut-nerve preparations from healthy control mice (29). Furthermore, baseline mechanosensory responses of colonic afferents from CVH mice were significantly increased compared with healthy control mice, and application of Hm1a enhanced mechanically evoked spiking beyond this already elevated level. Finally, in contrast to healthy control animals, toxin application evoked a pronounced increase in the electrical excitability of colonic dorsal root ganglion (DRG) neurons from CVH mice, suggesting that $Na_v1.1$ channels are functionally upregulated in CVH states (29). Taken together, these experiments suggest that inhibiting $Na_v1.1$ function could reduce chronic abdominal pain related to FBDs. This hypothesis remains to be tested, since we previously employed a nonspecific Na_v channel inhibitor in isolated mouse colonic afferents, not in behavioral experiments (29).

Here, we administered a selective $Na_v1.1$ inhibitor— 1-(phenylmethyl)-1H-1,2,3-triazole-4-carboxamide-5-methyl (Compound **B)** (30) — in a mouse model for peripheral afferent–mediated mechanical pain and 2 CVH paradigms in order to test whether mechanical hypersensitivity can be alleviated. We demonstrate that $Na_v1.1$ inhibition significantly reduces mechanical pain in CVH states, thereby substantiating an important contribution of this Na_v channel subtype to FBD-associated chronic abdominal pain.

10.3 Results

10.3.1 Pharmacological target screen

Compound B (100 μM) was previously shown to inhibit $Na_v1.1$ opening by depolarizing its conductance-voltage (G-V) relationship, whereas other channel gating properties were unaffected (30). Here, we tested compound susceptibility of additional Na_v channel subtypes that have also been found in gut nerves (10, 18, 31). When applying 100 μM Compound B to $Na_v1.5$, $Na_v1.7$, and $Na_v1.8$, none of the channels showed an altered G-V relationship (**Figure 10.7**). At 1 μM, Compound B still inhibited $Na_v1.1$ activation similar to 100 μM, which is likely to be a saturating concentration. To further investigate potential nonspecific activity of Compound B at 100 μM, we carried out a compound safety screen on 44 commonly tested targets (**Table 10.1**). With 1 exception, Compound B did not interact with any of the receptors, ion channels, or transporters. Of the enzymes, only phosphodiesterase 4D isoform 2 (PDE4D2) shows a mildly significant inhibitory response to 100 μM Compound B. This protein has 3',5'-cyclic-AMP phosphodiesterase activity and degrades cAMP, a signal transduction molecule in various cell types. PDE4 inhibitors are known to possess procognitive, neuroprotective, and antiinflammatory effects. Emetic effects caused by PDE4 inhibition have also been reported (32) but were not observed in our experiments.

10.3.2 Pharmacokinetic profile of Compound B

To make optimal use of our animal models, we determined the pharmacokinetic (PK) profile of Compound B. We found that the molecule was metabolically stable in mouse and human plasma over a period of 60 minutes (**Figure 10.8**). Additionally, in both mouse and human liver microsomal incubations fortified with NADPH, the compound was stable (>95% remaining), suggesting a resistance to CYP-450–dependent oxidation. A positive control with testosterone was completely metabolized, confirming assay validity (**Figure 10.8**).

We next examined the plasma PK, brain, and CSF distribution of Compound B in male C57BL/6J mice. Following a single i.v. administration, Compound B (10 mg/kg) showed low plasma clearance (~11 ml/min/kg) with an elimination half-life of ~1.5 hours (**Figure 10.9** and **Table 10.2**). The brain/plasma concentration ratio ranged between 0.6 and 1.7, and the CSF/plasma concentration ratio ranged between 0.3 and 0.5. After a single i.p. dose administration of Compound B (10 mg/kg), plasma, CSF, and brain concentrations were detected up to 24 hours with a time at maximum (T_{max}) of 0.5 hours. The brain/plasma concentration ratio ranged from 0.8–1.8, and the CSF/plasma concentration ratio fluctuated between 0.3 and 0.8. A single s.c. dose administration allowed detection of Compound B in plasma, CSF, and brain concentrations up to 8 hours with a T_{max} of 1 hour. The brain/plasma ratio ranged between 0.8 and 1.2,

and the CSF/plasma ratio was found to be between 0.3 and 0.5. Following a single per os (p.o.) administration of the compound, plasma, CSF, and brain concentrations were detected up to 8 hours with a T_{max} of 0.5 hours in plasma and 0.25 hours in the brain and CSF. The brain/plasma ratio ranged between 0.8 and 1.2, whereas the CSF/plasma ratio oscillated between 0.1 and 0.7. The oral solution bioavailability was 79%.

10.3.3 Toxicity

To examine the possibility of adverse side effects interfering with the interpretation of our animal model experiments, we performed a comprehensive toxicity study. In Phase A, single i.v. doses of 10, 25, 50, or 100 mg/kg Compound B were well tolerated in male and female Sprague Dawley rats. There were no treatment-related effects on survival or clinical signs such as body/organ weight changes, food consumption discrepancies, or visible inflammation. In Phase B, daily i.v. doses of 25, 50, or 100 mg/kg Compound B over the course of 7 days were well tolerated in male and female Sprague Dawley rats. There were no consistent or treatment-related effects on endpoints, including survival, clinical signs, body weight, clinical chemistry, blood chemistry, hematology, urinalysis parameters, absolute or relative organ weights, or histopathology.

10.3.4 Compound B reduces peripheral nerve injury–induced mechanical hypersensitivity

We previously demonstrated that spider toxin–mediated (Hm1a-mediated) activation of $Na_v1.1$ in peripheral sensory neurons elicits robust pain behaviors (29). Interestingly, profound mechanical but not thermal hypersensitivity was produced by Hm1a without neurogenic inflammation, indicating that Hm1a does not target unmyelinated peptidergic nociceptors (29). Conversely, partially eliminating $Na_v1.1$ from sensory neurons using a genetic approach significantly attenuated the toxin-evoked pain behaviors, indicating that this channel subtype regulates the excitability of primary afferent fibers that mediate mechanical pain. Before embarking on FBD mouse model trials, we sought to corroborate the contribution of $Na_v1.1$ to peripheral afferent-mediated mechanical pain. In these studies, we tested whether inhibiting $Na_v1.1$ with Compound B can ameliorate the hypersensitivity that occurs in a mouse model of neuropathic pain. For this, we used the spared nerve injury (SNI) model in which 2 of 3 branches of the sciatic nerve are transected. SNI mice rapidly exhibited profound and long-lasting mechanical hypersensitivity in response to von Frey hairs (vfh; see Methods). As expected, 3 days after SNI, we recorded a significant reduction (~57%) of the mechanical thresholds leading to mechanical hypersensitivity, ipsilateral to the injury side (**Figure 10.1**). At 7 days, this mechanical hypersensitivity was significantly reduced 30 minutes after systemic injection of a single dose of Compound B (i.p., 60 mg/kg). Contralateral mechanical thresholds were unaffected by the compound. One month after SNI, mice received another single dose of Compound B, and again, we recorded a significant reduction in mechanical hypersensitivity ipsilateral to the injury side (i.p., 60 mg/kg; **Figure 10.1**). Importantly, the same dose did not affect baseline thresholds, nor did it impair motor functions in naive mice, despite the compound penetrating the blood-brain barrier (**Figure 10.10**; rotarod test). Taken together, these results show that $Na_v1.1$ contributes, at least in part, to the mechanical hypersensitivity that develops after peripheral nerve injury.
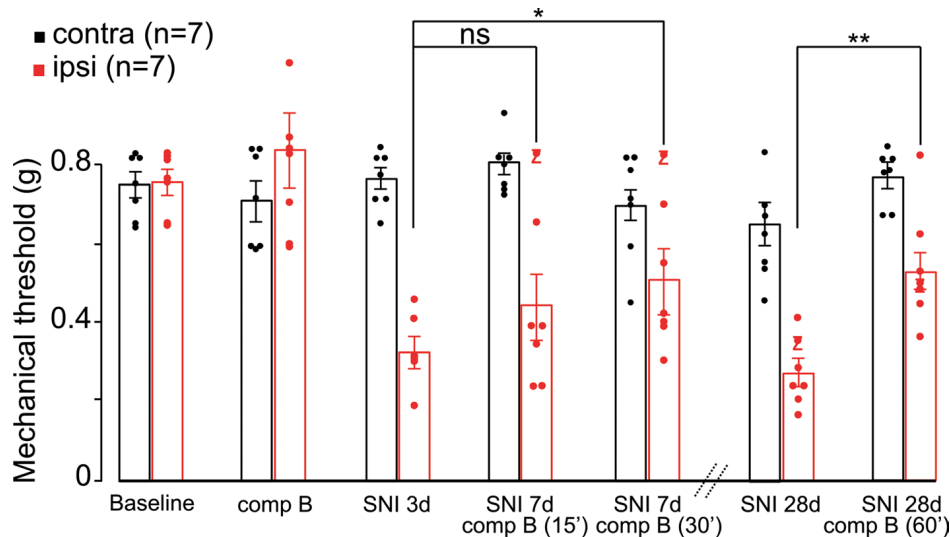
Figure 10.1: Pharmacological blockade of Na$_v$1.1 is antinociceptive. Systemic administration of Compound B (comp B; 60 mg/kg) has no effect on baseline mechanical thresholds of naive mice (baseline, 0.760 ± 0.03 g, vs. Compound B, 0.836 ± 0.105 g, 2-way ANOVA, P = 0.501, n = 7). Three days after spared nerve injury (SNI), mice exhibit mechanical hypersensitivity (~57%) ipsilateral to the injury (baseline, 0.760 ± 0.03 g, vs. SNI, 0.330 ± 0.034 g, 2-way ANOVA, P = 0.0001). A systemic injection of a single dose of Compound B (i.p., 60 mg/kg) significantly reduces mechanical hypersensitivity 30 minutes (i.p., 60 mg/kg; 0.515 ± 0.072 g, 2-way ANOVA, P = 0.039, n = 7), but not 15 minutes after injection. Contralateral mechanical thresholds were unaffected by the compound (0.703 ± 0.051 **G)**. One month after SNI, mice still exhibited mechanical hypersensitivity ipsilateral to the injury. Again, a single dose of Compound B (i.p., 60 mg/kg) significantly reduced mechanical hypersensitivity (60 minutes; SNI baseline, 0.277 ± 0.031 g, vs. Compound B, 0.530 ± 0.061 g, 2-way ANOVA, P = 0.003, n = 7). Data are presented as mean ± SEM with *P ≤ 0.05 and **P ≤ 0.005.

10.3.5 Sodium current recordings in colon-innervating DRG neurons

In addition to eliciting behaviors indicative of pain, Hm1a-induced activation of Na$_v$1.1 also evokes neuronal hypersensitivity in a subpopulation of retrograde-labeled colon-innervating DRG neurons (29). Here, we determined if the inhibitory effect of Compound B on Na$_v$1.1 reduces peak sodium current density in subpopulations of these neurons (**Figure 10.2** and **Figure 10.11**). We found that Compound B inhibited sodium currents from 17 of 39 (44%) colonic-innervating DRG neurons tested and caused an overall ~23% decrease in peak sodium currents in affected neurons, likely originating from inhibiting the Na$_v$1.1 current component, whereas other Na$_v$ channel subtypes are unaffected.
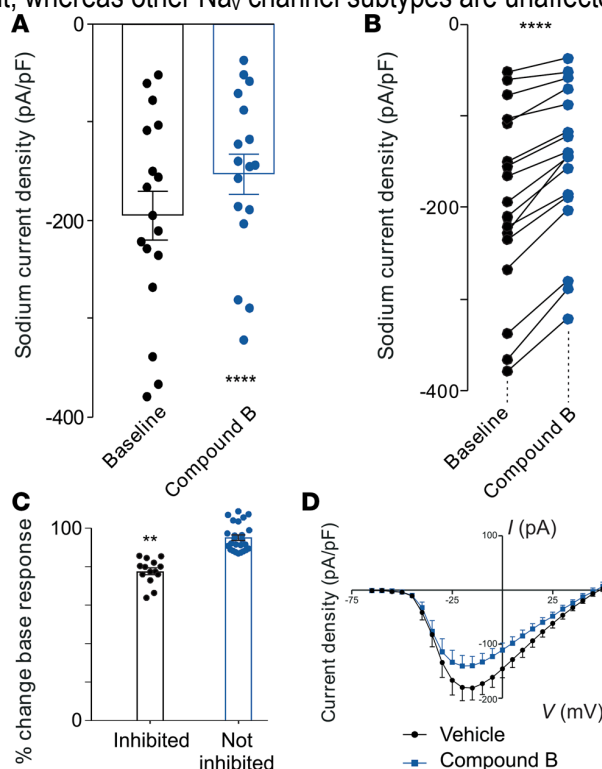
Figure 10.2: Compound B reduces sodium currents in colon-innervating DRG neurons. (A) Group data showing that sodium current density (pA/pF) in a population of colon-innervating DRG neurons was reduced when applying Compound B (100 μM). ****$P < 0.0001$, n = 14 neurons, paired t test. (B) Individual data from that the group data presented in A. ****$P < 0.0001$, n = 17 neurons, paired t test. (C) Compound B caused ~23% decrease in peak sodium currents in affected neurons (**$P < 0.001$, Mann Whitney U test). (D) Current-voltage (I-V) plots of sodium current density before (vehicle; black) and after (blue) Compound B application (100 μM) in inhibited colon-innervating DRG neurons. Data represent ± SEM.

10.3.6 Colonic nociceptor recordings

We showed that the Na$_v$1.1 activator Hm1a also induces mechanical hypersensitivity of colonic nociceptive afferents, an effect that is enhanced in a mouse model of IBS induced by intracolonic (i.c.) administration of trinitrobenzenesulfonic acid (TNBS) (29). Therefore, we tested whether Na$_v$1.1 inhibition by Compound B reduces colonic nociceptor mechanical responses in both healthy and CVH states (**Figure 10.3**). A substantial population of colonic nociceptors (6 of 9) from healthy mice was inhibited by application of Compound B, reducing responses by ~25% relative to baseline responses in affected afferents (**Figure 10.3** and **Figure 10.12**). In CVH mice, 75% of colonic nociceptors were inhibited by Compound B, and their response was reduced by ~35% relative to CVH baseline responses. In both control and CVH mice, Hm1a (100 nM) was unable to overcome Compound B inhibition of colonic nociceptor mechanical responses (**Figure 10.13**). Based on these findings, we next asked whether Na$_v$1.1 inhibition also reduces behavioral measures of mechanical hypersensitivity in representative FBD animal models.
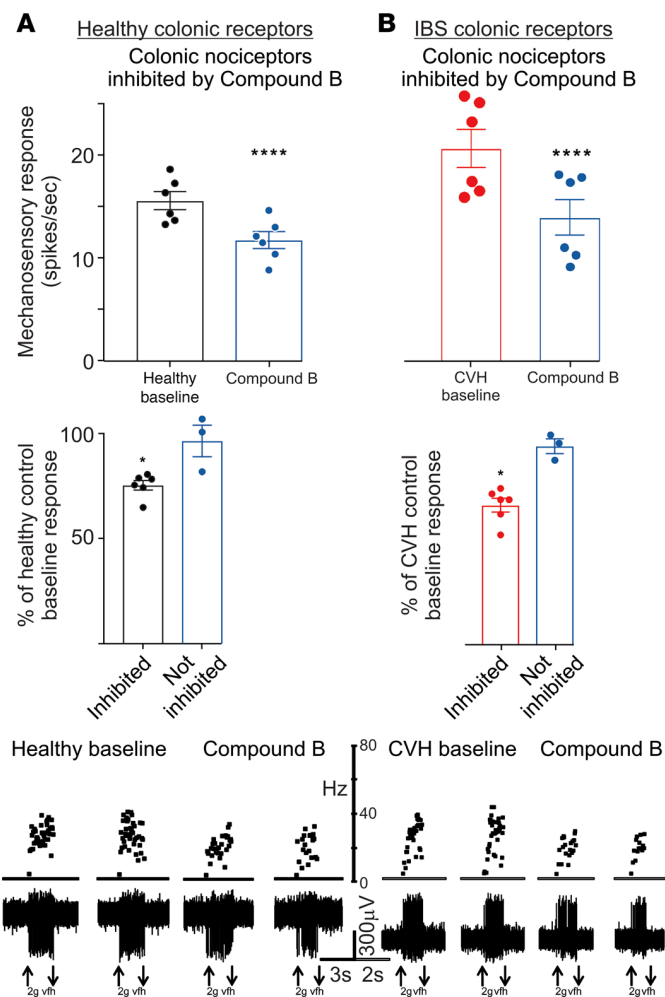
Figure 10.3: Effect of Compound B on colonic nociceptive afferents. (A) Top panel: Application of 100 μM Compound B inhibited a large subpopulation of colonic nociceptors from healthy control mice (n = 6, ****$P < 0.0001$, paired t test). Middle panel: In inhibited afferents, Compound B reduced responses to ~75% of healthy control baseline levels. *$P < 0.05$, unpaired t test. Lower panel: Representative examples of *ex vivo* healthy control colonic nociceptor recordings showing nociceptors in the absence and presence of Compound B. *$P < 0.05$, paired t test. (B) Top panel: In an IBS mouse

103

model of TNBS-induced chronic visceral hypersensitivity (CVH), Compound B (100 µM) inhibited a large subpopulation of CVH colonic nociceptors (n = 6, ****P < 0.0001, paired t test). Middle panel: In inhibited afferents, Compound B reduced responses to ~67% of CVH baseline levels. Lower panel: Representative examples of *ex vivo* CVH colonic nociceptor recordings showing nociceptors in the absence and presence of Compound B. vfh, von Frey hair. The vfh with upward arrow indicates start of the application, and a downward arrow signifies removal.

10.3.7 Visceral motor reflex (VMR) in response to colorectal distension (CRD)

In these studies, we monitored the VMR to CRD in 2 commonly used mouse models of IBS representing FBDs. The VMR technique involves placement of a flexible inflatable balloon wrapped around a pliable catheter into the descending colon (33). To quantify the effect of balloon pressures (in mmHg), we measured abdominal electromyogram (EMG) activity of the abdominal musculature via surgically implanted electrodes. As expected, IBS mice with TNBS-evoked CVH displayed significantly enhanced VMRs compared with healthy control animals. I.c. administration of Compound B (100µM) (i.e., directly applied to the peripheral endings of the colonic nociceptors) to IBS mice reduced VMRs to CRD to healthy control levels (**Figure 10.4**). Compared with healthy control mice, colonic compliance was unaltered in CVH mice or in CVH mice that were administered 100 µM Compound B (**Figure 10.14**), suggesting that changes in the VMR to CRD are not due to variations in smooth muscle function. These findings indicate that pharmacologically inhibiting $Na_v1.1$ could be a viable approach to reverse visceral hypersensitivity *in vivo*.
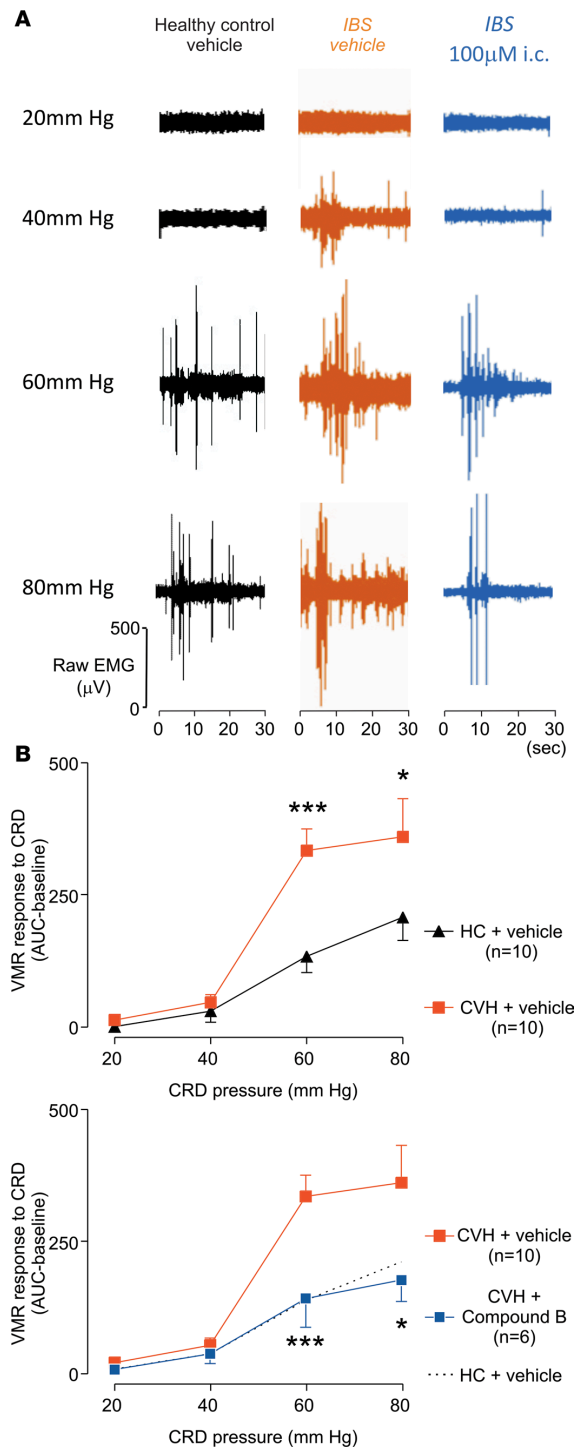
Figure 10.4 Effect of intracolonic administration of Compound B on VMR in an IBS mouse model of TNBS-induced CVH. (A) Representative EMG recordings at increasing colorectal distension pressures (mmHg) in healthy control mice with intracolonically (i.c.) administered vehicle (black), or IBS mice i.c. administered with vehicle (orange) or Compound B 100 μM (blue), 30 minutes before recordings. (B) Upper panel: Group data showing that IBS mice with CVH display increased VMRs (visceromotor reflexes) to CRD (colorectal distension) compared with healthy control mice, particularly at a distension pressure of 60 mmHg (***$P < 0.001$) and 80 mmHg (*$P < 0.05$). Lower panel: I.c. Compound B administration significantly reduced the VMR to CRD in IBS mice, normalizing responses to healthy control levels; 60 mmHg (***$P < 0.001$) and 80 mmHg (*$P < 0.05$). Significance of differences were analyzed by the Generalized Estimating Equation (GEE), followed by the Least Significant Difference (LSD) post hoc test. HC, healthy control; CVH, chronic visceral hypersensitivity.

In a second experiment, we systemically applied Compound B at 2 doses (i.p.) in control and acetic acid–evoked IBS mice and then measured the VMR to CRD. At 20 mg/kg, acute treatment with Compound B in IBS mice returned pain thresholds to those of the saline-injected healthy controls (**Figure 10.5**). At a higher dose (75 mg/kg), Compound B reduced mechanical pain thresholds in IBS mice to below the level of control mice. Based on the PK experiments, Compound B absorption via s.c. injection leads to a lower

105

peak concentration in plasma with a longer T_{max} of 1 hour. Therefore, higher concentrations may be needed to normalize mechanical pain thresholds in CVH mice. Indeed, acute treatment with Compound B at a dose of 75 mg/kg (s.c.) significantly reduced the increased pain thresholds in CVH mice to a level noted in saline-injected controls (**Figure 10.6**). Together, these *in vivo* experiments suggest that Na$_V$1.1 inhibition can be an effective approach to reduce mechanical hypersensitivity associated with CVH states.
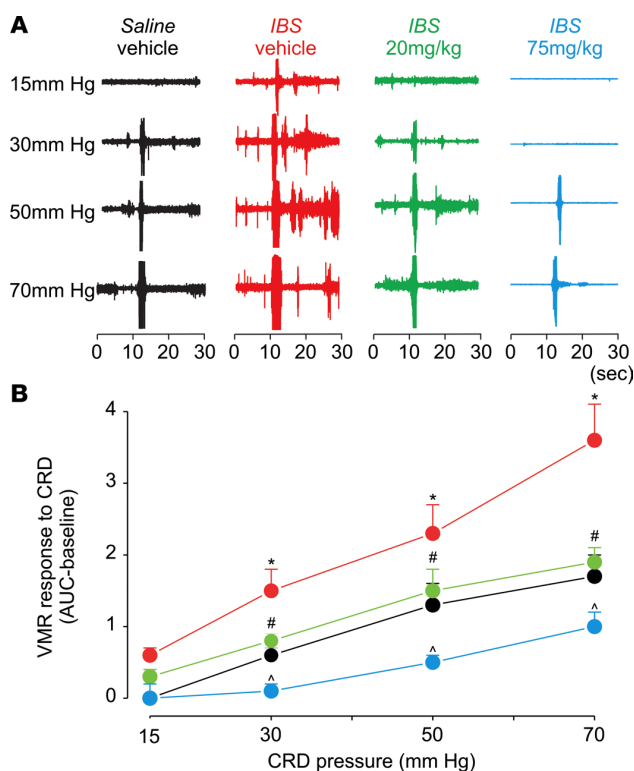
Figure 10.5: Effect (i.p.) of Compound B in an IBS mouse model of acetic acid–induced CVH. (A) Shown is the effect of Compound B (i.p. injection) at 20 and 75 mg/kg as measured by VMR response to CRD. Acute treatment at a dose of 20 mg/kg normalized the increased pain sensitivity in IBS mice, whereas 75 mg/kg compound reduced pain sensitivity in IBS mice to a level that is lower than control mice. (B) Two-way ANOVA showed main effect of treatment $F_{(3,76)} = 31.93$, $P < 0.001$; main effect of pressure $F_{(3,76)} = 44.09$, $P < 0.001$; interaction of treatment × pressure $F_{(9,76)} = 2.4$, $P = 0.017$. Data (n = 7) are presented as mean ± SEM. *$P < 0.05$, significantly different from saline-vehicle at the same pressure; #$P < 0.05$, significantly different at the same pressure from IBS vehicle; and ^$P < 0.05$, significantly different from saline-vehicle and IBS-vehicle at the same pressure (Student Newman-Keuls post hoc test). F represents F statistic obtained after 2-way ANOVA to test whether the means between 2 populations are significantly different.
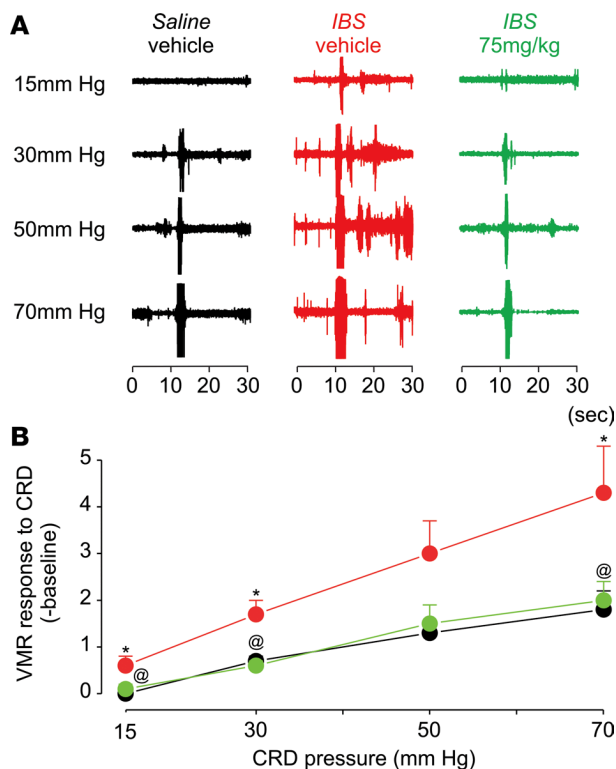
Figure 10.6: Effect (s.c.) of Compound B in an acetic acid–induced IBS mouse model. (A and **B)** Effect on hyperalgesia of s.c. Compound B treatment in an IBS mouse model measured by VMR response to CRD. Data are presented as mean ± SEM. *$P < 0.05$, significantly different from saline-vehicle at same pressure; @$P < 0.05$, significantly different from IBS-vehicle (Student Newman-Keuls post hoc test). Two-way ANOVA analysis showed the main effect of treatment $F_{(2,56)} = 14.02$, $P < 0.001$; main effect of pressure $F_{(3,56)} = 17.61$, $P < 0.001$; interaction of treatment x pressure $F_{(6,56)} = 1.13$, $P = 0.35$ (n = 7); these P values were obtained from the 2-way ANOVA test for the data shown in the figure.

10.4 Discussion

FBDs represent a major clinical problem in gastroenterology, with a large population of patients experiencing chronic abdominal pain secondary to visceral hypersensitivity to mechanical stimuli (1). Unfortunately, the mechanisms underlying CVH are unclear, and pharmacological management of chronic abdominal pain is therefore challenging (34–37). Accumulating evidence implicates a subset of Na$_v$ channel subtypes in normal gut sensory function and in the development of mechanical hypersensitivity and pain associated with injury (10, 23, 25, 29).

Together with previously reported observations (29), the results presented here suggest that Na$_v$1.1 is functionally upregulated under CVH conditions (**Figure 10.4**) and that pharmacologically inhibiting this channel subtype can reduce CVH in 2 mechanically distinct mouse IBS models (**Figure 10.4** - **Figure 10.6**) without altering colonic compliance (**Figure 10.14**). We show that Compound B, a Na$_v$1.1-targeting inhibitor of channel gating (30), reduces colonic nociceptor mechanical responses and can reduce the significantly enhanced VMRs in 2 mouse models of IBS to levels that are observed in healthy control animals. Importantly, as Compound B has ~79% oral bioavailability, without noticeable signs of toxicity upon acute or chronic dosing, our findings suggest a possible pathway toward the design of novel Na$_v$1.1-inhibiting therapeutics for FBD-related visceral pain (**Figure 10.9** and **Table 10.2**). Although extrapolating preclinical findings in rodents to human chronic conditions such as IBS is challenging, the ability to target the etiology at the level of the peripheral afferent may have many advantages. Therefore, it is worth exploring whether synthesis of compound derivatives that do not penetrate the blood-brain barrier could avoid potential adverse side effects that might occur when even higher but even more effective doses are introduced.

It is also of interest that mutations in Na$_v$1.1 have been linked to an array of epilepsy phenotypes (38). Via a subtle action on Na$_v$1.1 function, Compound B increases the threshold to action potential initiation

in hippocampal neurons, thereby reducing the frequency of seizures in various animal models (30). Given the role of $Na_v1.1$ in both epilepsy and CVH, it is therefore reasonable to assume that a subset of epilepsy patients may be prone to FBDs. Indeed, an observational study on 65 people with epilepsy showed a significantly increased prevalence of IBS compared with controls (39). Conversely, a large-scale study found that IBS patients had greater cumulative incidence of epilepsy compared with the control cohort (40). As people with epilepsy are not routinely screened for FBDs, appropriate treatment may be delayed; it is also conceivable that gastrointestinal complaints may be erroneously attributed to administration of antiepileptic drugs. Alternatively, the central contribution of $Na_v1.1$ in both disorders may provide a rationale to administer clinically used anticonvulsants in FBD patients to treat CVH.

10.5 Methods

10.5.1 Two-electrode voltage-clamp recording from Xenopus oocytes

Human $Na_v1.5$ (h$Na_v1.5$), h$Na_v1.7$, and h$Na_v1.8$ (*SCN5a*, *SCN9a*, and *SCN10a*, respectively) and hβ1 (*SCN1b*) clones were obtained from OriGene Technologies Inc. and expressed in *Xenopus laevis* oocytes (Xenopus 1). The DNA sequence of all constructs was confirmed by automated DNA sequencing. RNA was synthesized using T7 polymerase (Invitrogen). Channels were expressed with hβ1 in a 1:5 molar ratio, and currents were studied following incubation for 1–4 days after cRNA injection (incubated at 17°C in [mM] 96 NaCl, 2 KCl, 5 HEPES, 1 $MgCl_2$, 1.8 $CaCl_2$, and 50 µg/ml gentamycin [pH 7.6 with NaOH]) using 2-electrode voltage-clamp recording techniques (OC-725C, Warner Instruments). Data were filtered at 4 kHz and digitized at 20 kHz using pClamp10 (Molecular Devices). Microelectrode resistances were 0.5–1 MΩ when filled with 3M KCl. The external recording solution (ND100) contained (mM) 100 NaCl, 5 HEPES, 1 $MgCl_2$, and 1.8 $CaCl_2$ (pH 7.6 with NaOH). All experiments were performed at ~22°C. Leak and background conductances were subtracted by blocking Na_v channels with 10 µM tetrodotoxin. Chemicals were obtained from MilliporeSigma, unless otherwise stated. Voltage-activation relationships were obtained by measuring peak currents and calculating conductance (G). Compound B was dissolved in DMSO (~5 mg/ml stock) and diluted to 100 µM with ND100. Oocytes were incubated in solutions containing 100 µM drug (final DMSO concentration of ≤1%) for 1 hour. Data analysis was performed using Microsoft Excel and Origin 8 (OriginLab).

10.5.2 Compound safety screen on 44 targets

A saturating Compound B concentration (100 µM, LifeTein) was tested on 44 targets using a binding/competition assay with scintillation counting. Method and target are shown in **Table 10.1**. The study was carried out by Eurofins Pharma Discovery Services.

10.5.3 Metabolic stability of Compound B in plasma and liver microsomes

Plasma stability was evaluated using plasma from mice and humans as described previously (41, 42). Briefly, Compound B (10 µM) was spiked in plasma and incubated in an orbital shaker at 37°C. At predetermined times, aliquots of the mixture, in triplicate, were removed and the reaction quenched by the addition of 3× the volume of ice-cold acetonitrile spiked with the internal standard losartan (500 nM). The samples were vortexed for 30 seconds and centrifuged at 12,000 g for 10 minutes. Compound disappearance was monitored over time using a Liquid chromatography–tandem mass spectrometry (LC/MS/MS) method. Phase I metabolic stability assay was conducted in mouse and human liver microsomes as described previously (43). The reaction was carried out with 100 mM potassium phosphate buffer, pH 7.4, in the presence of a NADPH regenerating system (1.3 mM NADPH, 3.3 mM glucose 6-phosphate, 3.3 mM MgCl2, 0.4 U/ml glucose-6-phosphate dehydrogenase, 50 µM sodium citrate). Reactions in triplicate were initiated by the addition of liver microsomes to the incubation mixture (compound final concentration was 10 µM; 0.5 mg/ml microsomes). Negative controls in the absence of NADPH were performed to determine the specific cofactor–free degradation. Testosterone was used as a positive control. Chromatographic analysis was performed using an Accela ultra high–performance system consisting of an analytical pump and an autosampler coupled with a TSQ Vantage mass spectrometer (Thermo Fisher Scientific). Separation of analyte was achieved at ambient temperature using an Agilent Eclipse Plus column (100 × 2.1 mm i.d.) packed with a 1.8 µm C18 stationary phase.

`

The mobile phase used was composed of 0.1% formic acid in acetonitrile and 0.1% formic acid in H2O with gradient elution.

10.5.4 PK profiling of Compound B

Healthy male C57BL/6J mice (8–12 weeks old) weighing between 20–35 g were obtained from In Vivo Biosciences. Temperature and humidity were maintained at 22°C ± 3°C and 40%–70%, respectively, and illumination was controlled to give a sequence of 12-hour light and 12-hour dark cycle. Animals were administered with compound solution formulation (10 mg/kg) prepared in 40% w/v hydroxypropyl-β-cyclodextrin in normal saline through p.o., i.p., i.v., and s.c. route. A group of 12 mice was used in each study. Blood samples were collected under light isoflurane anesthesia at 0.1, 0.5, 1, 2, 4, and 8 hours in labeled micro centrifuge tube containing K2EDTA as anticoagulant. Immediately after blood collection, plasma was harvested by centrifugation and stored at –70°C until bioanalysis. Following blood collection, animals were euthanized by CO_2 asphyxiation, and brain and CSF were collected at each time point. Collected brain was dipped in 20 ml fresh phosphate buffer saline (pH 7.4) 3 times and dried on blotted paper. Brain was weighed and homogenized using ice-cold phosphate buffer saline (pH 7.4), and homogenates were stored below –70°C until bioanalysis. Total homogenate volume was 3× the brain weight. All samples were processed for analysis by protein precipitation using acetonitrile and analyzed with a fit-for-purpose LC/MS/MS method (lower limit of quantification [LLOQ] = 5 ng/ml in plasma, brain, and CSF).

10.5.5 Compound toxicity study in rats

This study consisted of 2 phases: A and B. In Phase A, the maximum tolerable dose (MTD) of the $Na_v1.1$ compound was determined. In Phase B, the dose range of the compound was investigated together with the toxicokinetic (TK) profile. Phase A consisted of 4 treatment groups of 3 male/female Sprague Dawley rats (Envigo) dosed with the compound orally, once daily for 5 days at 10 ml/kg. Phase A rats were treated with 10 mg/kg, 25 mg/kg, 50 mg/kg, and 100 mg/kg compound. Phase B consisted of 3 compound treatment groups of 5 male and 5 female — and 1 vehicle control group of 3 male and 3 female — Sprague Dawley rats dosed orally once daily for 7 days at 10 ml/kg. Phase B rats were treated with 25 mg/kg, 50mg/kg, and 100 mg/kg compound, and the group of 3 males/females received the vehicle, 15% DMSO, 35% PEG 400, and 50% sterile water and served as the vehicle control. Phase B included a TK cohort with 6 males/females in each treatment group and 3 males/females in the vehicle control group that were bled at 6 time points following dosing on study day 1 and day 7. Body and organ weights were collected, as well as urine for urinalysis. Food consumption was also monitored. Necropsies allowed 43 tissue types to be collected for clinical pathology examination. Tissues examined include adrenal mammary gland with skin, aorta ovaries with oviduct, brain, pancreas, cecum Peyer's patches, colon, pituitary gland, duodenum, prostate, epididymis, rectum, esophagus, salivary gland (mandibular), eyes with optic nerve, skeletal muscle (thigh) with sciatic nerve, femur with BM (articular surface of the distal end to include femorotibial joint), seminal vesicles with coagulating glands, heart, spinal cord (cervical, thoracic, and lumbar), ileum, spleen, sternum, jejunum, stomach, kidney, testes, lacrimal gland, thymus, larynx, thyroid with parathyroids, tongue, liver (sections from 2 lobes), trachea, lung with bronchi, urinary bladder, lymph node (mandibular), uterus with cervix, lymph node (mesenteric), and vagina. Animals were obtained from Envigo and were housed in an environmentally controlled room that maintained temperatures of 20°C–24°C and a relative humidity of 30%–70% with a 12-hour light/12-hour dark cycle. Animals were group housed based on group/sex designation, except for overnight urine collection, when animals were individually housed in metabolic caging for no more than 18 hours. The animals had ad libitum access to drinking water and to Rodent Diet 2916 (Harlan TEKLAD). The animals were acclimated for 48 or 25 days (Phase A and Phase B, respectively) prior to dosing.

10.5.6 Behavioral analysis in the SNI model of neuropathic pain

For these experiments, we used adult, male C57BL/6J mice from The Jackson Laboratory. Mice were anesthetized with isoflurane (2.0%). After skin and muscle incision at the level of the popliteal fossa, we tightly ligated the sural and superficial peroneal branches of the sciatic nerve with 8-0 silk sutures (Ethicon), leaving the tibial nerve intact. Next, the ligated branches were transected distal to the ligature,

and ~2.0 mm of each distal nerve stump was removed. Particular care was taken not to stretch or contact the intact spared branch. The overlying muscle and skin were sutured, and the animals were allowed to recover and then returned to their cages. We assessed mechanical sensitivity in this mouse model of neuropathic pain (44) by placing animals on an elevated wire mesh grid and stimulating the hind paw with vfh. We used an up-down paradigm (45) to define threshold. Animals were tested 3 times, once every other day before surgery to determine baseline threshold and once 3 days after surgery to assess the magnitude of the mechanical hypersensitivity. On day 7, mice received an i.p. injection of Compound B (60 mg/kg), and behavioral testing was performed 15, 30, and 60 minutes after the injection. On day 28 after SNI, mice received a single dose (60 mg/kg) of Compound B, and mechanical thresholds were measured 1 hour after. For behavioral tests, the investigator was blind to treatment. Motor performance of the mice injected with Compound B (60 mg/kg) was evaluated with the rotarod test.

10.5.7 Retrograde labeling to identify colonic neurons in DRG and dissociated DRG cell culture

Healthy, male C57BL/6J mice (The Jackson Laboratory) of 16 weeks were anesthetized with isoflurane, and — following midline laparotomy — five 2-µl injections of a fluorescent retrograde neuronal tracer (cholera toxin subunit B conjugated to AlexaFluor-488, Thermo Fisher Scientific) were made subserosally within the wall of the descending colon. Mice were administered analgesic (buprenorphine; 0.4 mg/10 kg s.c.) following completion of the surgery. Four days after tracer injection, mice were culled by CO_2 inhalation, and DRG from thoracolumbar (T10-L1) and lumbosacral spinal levels (L5-S1) were surgically removed. DRGs were digested with 4 mg/ml collagenase II (GIBCO, Invitrogen) and 4 mg/ml dispase (GIBCO) for 30 minutes at 37˚C, followed by 4 mg/ml collagenase II for 10 minutes at 37˚C. Neurons were mechanically dissociated into a single-cell suspension via trituration through fire-polished Pasteur pipettes. Neurons were resuspended in DMEM (GIBCO) containing 10% FCS (Invitrogen), 2 mM L-glutamine (GIBCO), 100 µM MEM nonessential amino acids (GIBCO), and 100 mg/ml penicillin/streptomycin (Invitrogen). Neurons were spot-plated on 15-mm coverslips coated with poly-D-lysine (800 µg/ml) and laminin (20 µg/ml) and maintained in an incubator at 37˚C in 5% CO_2.

10.5.8 Neuronal whole-cell electrophysiological recordings

Male C57BL/6J mice (The Jackson Laboratory) were used in all experiments. Twenty to 48 hours after plating, whole-cell recordings were made from fluorescent colon-innervating DRG neurons using fire-polished glass electrodes with a resistance of 0.7–2 MΩ (≥75% of series resistance was compensated). All recordings were performed at room temperature (20°C–22°C). Signals were amplified with an Axopatch 200A amplifier, digitized with a Digidata 1322A, recorded using pCLAMP 9 software (Molecular Devices), sampled at 20kHz, filtered at 5kHz, and analyzed in Clampfit 10.7 (Molecular Devices) and GraphPad Prism 7. Voltage-clamp intracellular solution contained (in mM) 60 CsF; 45 CsCl; 2 $MgCl_2$; 5 EGTA-Na; 10 HEPES-Cs; 30 TEA-Cl; and 2 MgATP adjusted to pH 7.2 with CsOH, 280 mOsm. Extracellular solution contained (in mM) 70 NaCl; 50 NMDG; 40 TEA-Cl; 4 CsCl; 2 $MgCl_2$; 2 $CaCl_2$; 10 HEPES; and 5 Glucose adjusted to pH 7.4, approximately 300 mOsm. Current-voltage (I_{Na}-V) relationships were determined by application of a prepulse to –100 mV (100 ms), followed by a series of step pulses from –65 mV to +60 mV (5 mV increments [100 ms]), before returning to hold at –70 mV (repetition interval of 3 sec, P/8 leak subtraction). Neurons inhibited by Compound B (LifeTein) were determined as a >15% reduction from baseline response. Extracellular (bath) solution containing Compound B at 100 µM (2-minute incubation) was applied with a gravity-driven multibarrel perfusion system positioned within ~1 mm of the neuron.

10.5.9 Colonic nociceptor afferent recordings

Male C57BL/6J mice (The Jackson Laboratory) were used in all experiments. *In vitro* single-unit extracellular recordings of action potential discharge were made of splanchnic colonic afferents from healthy control or IBS mice using standard protocols (12, 29, 46, 47). Baseline mechanosensitivity was determined in response to a 3-second application of a 2 g vfh probe to the afferent receptive field. This process was repeated 3–4 times, separated each time by 10 seconds. Mechanosensitivity was then retested after application of Compound B (100 µM). Afferents were considered inhibited by Compound B if we recorded a >10% reduction from baseline response. In some instances, data are presented as

`

percentage change from baseline. This value was calculated as the percentage change in mechanosensitivity of individual afferents between the baseline responses compared with the respective mechanical responses following compound addition. This difference is then averaged across all afferents to obtain a final mean ± SEM of percentage change in response from baseline. The spider toxin Hm1a was purified as previously described (29).

10.5.10 Animal models of FBDs

Male C57BL/6J mice (The Jackson Laboratory) were used in all experiments. In a first assay, colitis was induced by administration of TNBS as described previously (46, 47). Briefly, 13-week-old anesthetized mice were administered an i.c. enema of 0.1 ml TNBS (3.8 mg per mouse in 30% EtOH) via a polyethylene catheter. Histological examination of mucosal architecture, cellular infiltrate, crypt abscesses, and goblet cell depletion confirmed that TNBS induced significant damage by day 3 after treatment, largely recovered by day 7, and fully recovered at 28 days. High-threshold nociceptor recordings at the 28-day time point revealed significant mechanical hypersensitivity and lower mechanical activation thresholds. Based on these properties, we consider these mice an IBS model of TNBS-induced CVH.

An abdominal EMG allows assessment of visceral sensitivity *in vivo* in fully awake animals. Under isoflurane anesthesia, the bare endings of 2 Teflon-coated stainless-steel wires (Advent Research Materials Ltd.) were sutured into the right abdominal muscle, tunnelled s.c., and then exteriorized at the base of the neck for future access. At the end of the surgery, mice received prophylactic antibiotic (Baytril; 5 mg/kg s.c.) and analgesic (buprenorphine; 0.09 mg/kg s.c.), were housed individually, and were allowed to recover for at least 3 days before assessment of the VMR. On the day of VMR assessment, mice were briefly anesthetized using isoflurane and received a 100 µl enema of vehicle (sterile saline) or Compound B (100 µM). A lubricated balloon (2.5 cm length) was gently introduced through the anus and inserted into the colorectum, up to 0.25 cm past the anal verge. The balloon catheter was secured to the base of the tail and connected to a barostat (Isobar 3, G&J Electronics) for graded and pressure-controlled balloon distension. Mice were allowed to recover from anesthesia in a restrainer for 15 minutes prior to initiation of the distension sequence. Distensions were applied at 20, 40, 60, and 80 mmHg (20-second duration) at a 4-minute interval. The last distension was performed 30 minutes after i.c. treatment. The EMG electrodes were relayed to a data acquisition system, and the signal was recorded (NL100AK headstage), amplified (NL104), filtered (NL 125/126, Neurolog, Digitimer Ltd., bandpass 50–5000 Hz), and digitized (CED 1401, Cambridge Electronic Design) to a PC for off-line analysis using Spike2 (Cambridge Electronic Design). The analogue EMG signal was rectified and integrated. To quantify the magnitude of the VMR at each distension pressure, the AUC during the distension (20 seconds) was corrected for the baseline activity (AUC predistension, 20 seconds). After the final distension, the mice were killed by cervical dislocation. Colonic compliance was assessed by applying graded volumes (40–200 µl, 20-second duration) to the balloon in the colorectum of fully awake mice, while recording the corresponding colorectal pressure as described previously.

In a second assay, pain sensitivity was measured by VMR in response to CRD. As opposed to TNBS in the first assay, acetic acid was used to evoke mechanical hypersensitivity (48). A sterilized multistranded, Teflon-insulated, 40-gauge stainless steel wire (Cooner Wire) was implanted in the external oblique muscle and then s.c. tunneled through the back and fixed on the neck skin. One week after surgery, a balloon (made from 3 cm2 polyethylene membrane and attached to soft Tygon [PE60] tubing) was implanted into the colorectum. To test the VMR, the mouse was placed in a restrainer and allowed to adapt for 30–45 minutes. CRD was induced by applying pressure of 15, 30, 45, and 70 mmHg for 10 seconds each. There were at least 4-minute intervals between stimulations. The EMG was recorded from 2 externalized electrodes implanted in the external oblique muscle 20 seconds before, 10 seconds during, and 20 seconds after CRD. The EMG in the 10 seconds before (baseline) and during CRD were analyzed using CED 1401 plus and Spike 2 software. The AUC of the EMG 10 seconds before and during the CRD was measured. CRD response data were normalized to baseline. We used VMR response to CRD to determine the effect of Compound B on visceral hypersensitivity in this mouse model of IBS. This model was generated by colorectal infusion of 20 µl 0.5% acetic acid or saline (control) on postnatal days 9–12. The mice were weaned at 3 weeks. At 8 weeks of age, we conducted 2 studies. First, IBS mice (n = 6)

111

were treated with Compound B (75 mg/kg, 10 ml/kg) or vehicle (20% m/V 2-hydroxypropyl-β-cyclodextrin in saline) s.c. A group of mice (neonatal saline treated) was used together with the vehicle as control. In the second study, IBS mice were treated with vehicle, 20 or 75 mg/kg of Compound B i.p. alongside a control group that was saline treated. Thirty minutes after Compound B treatment, EMG responses to CRD were recorded. Analysis methods are specified in the appropriate sections. For these behavioral tests, the investigator was blind to treatment.

10.5.11 Statistics

PK parameters were calculated using the noncompartmental analysis tool of Phoenix WinNonlin (Version 6.3). For rat toxicity tests, animals were randomized but assigned a unique identification number. For Phase A, data were analyzed by parametric 1-way ANOVA if normally distributed and variances were homogeneous. Post hoc analysis was conducted by making all possible comparisons among the treatment groups with the Holm-Sidak test. If the assumptions of parametric analysis were not met, data were analyzed by Kruskal-Wallis 1-way ANOVA on ranks. Dunn's test was used to assess any post hoc differences by comparisons among all groups if the Kruskal-Wallis 1-way ANOVA was significant. For Phase B, data were analyzed by 1-way ANOVA followed by Dunnett's test if data were normally distributed and variances were homogeneous. Post hoc comparisons with Dunnett's test were only employed if treatment effect in the 1-way ANOVA was significant. If the assumptions of parametric analysis were not met, data were analyzed by Kruskal-Wallis 1-way ANOVA on ranks. Dunn's test was used to assess any post hoc differences among groups if the Kruskal-Wallis 1-way ANOVA was significant. For all statistical procedures, differences were considered significant if $P < 0.05$. All statistical analyses were performed with SigmaPlot 13.0 (Build 13.0.0.83), Systat Software Inc. For electrophysiological recordings, data are presented as mean ± SEM and analyzed using GraphPad Prism 7. More details about statistical methods used can be found in the text. If used, Student's t test was 2-tailed. For IBS mouse model experiments, data were statistically analyzed by generalized estimating equations followed by LSD post hoc tests when appropriate using SPSS 23.0. Analysis was typically carried out in GraphPad Prism 7 Software.

10.5.12 Study approval

PK profiling of Compound B was conducted at Sai Life Sciences Limited in accordance with Study Plan SAIDMPK/PK-16-05-213 and the guidelines of the Institutional Animal Ethics Committee (IAEC). Rat toxicity study was carried out by Sobran Inc. with an approved IACUC protocol, number SOB-051-2017. Behavioral analysis in the SNI model of neuropathic pain were approved by the UCSF IACUC. The Animal Ethics Committees of The Flinders University, The University of Adelaide, and the South Australian Health and Medical Research Institute (SAHMRI) approved experiments involving animals in FBD studies. The Animal Care and Use Committee of Johns Hopkins University approved the relevant IBS experiments.

10.6 Author contributions

JS, JC, AE, QL, JB, JG, AD, GYR, RR, BSS, AB, PJP, SMB, and FB designed the study. GFK provided Hm1a. JS, JC, AE, QL, JB, JG, AD, GYR, RR, BSS, AB, PJP, SMB, and FB generated or analyzed the data. JC, AE, LG, GYR, AD, and SMB designed, performed, and analyzed studies relating to colonic afferent, colon-innervating DRG neuron patch clamp and VMR to CRD studies from healthy control mice and the IBS mouse model of TNBS-induced CVH. BSS, AB, PJP, SMB, and FB wrote the manuscript.
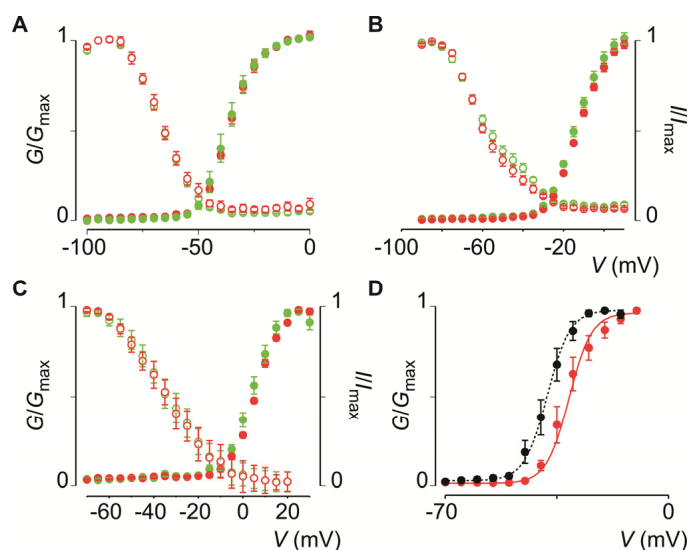
Figure 10.7: Effect of 100 μM Compound B on Na$_v$1.5, Na$_v$1.7, and Na$_v$1.8. A-C) Figure shows G/G$_{max}$ (G: conductance) and I/I$_{max}$ (I: current) relationships before (green, DMSO control) and after (red) addition of 100 μM Compound B to Na$_v$1.5 (A), Na$_v$1.7 (B), and Na$_v$1.8 (C). n = 5–8, and error bars represent SEM. No effects were observed. **D)** Effect of 1 μM Compound B (red) on Na$_v$1.1 (black; control) activation voltage.

	Mouse	Mouse Microsomes		Human	Human Microsomes		Testo* (Mouse)	Testo* (Human)
Time	*Plasma*	*Phase I*	*Negative Control*	*Plasma*	*Phase I*	*Negative Control*	*Phase I*	*Phase I*
0	100%	100%	100%	100%	100%	100%	100%	100%
30	93%	97%	96%	103%	111%	107%	4%	21%
60	*93%*	*98%*	*96%*	*85%*	*110%*	*108%*	*0%*	*8%*
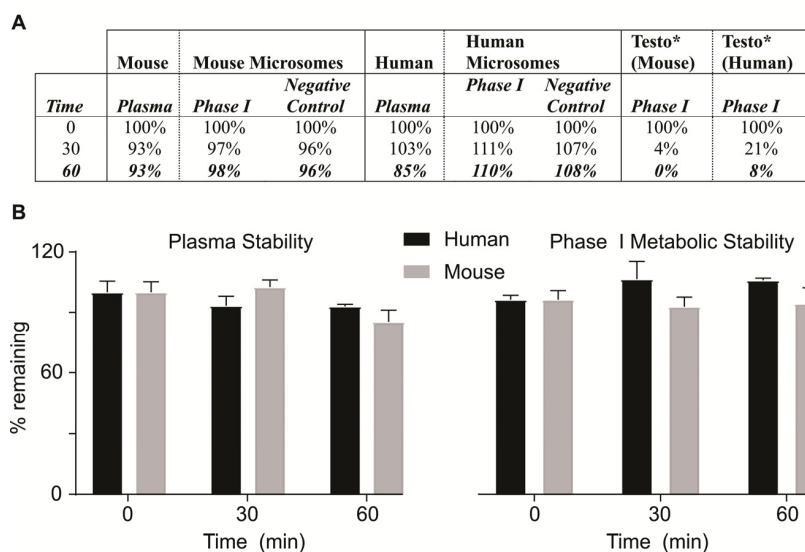
Figure 10.8: Metabolic stability of Compound B in plasma and liver microsomes. Compound B was completely stable in both plasma as well as microsomes from mouse and human fortified with NADPH suggesting that the compound is not susceptible to hydrolysis or CYP-450 dependent metabolism. * Testosterone (Testo) was used as a positive control.
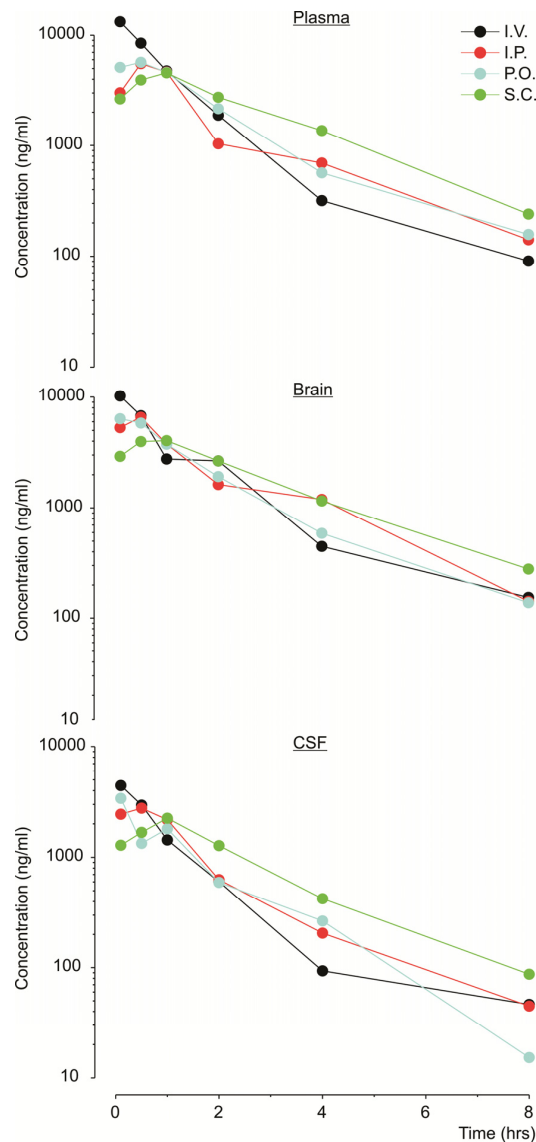
Figure 10.9: Pharmacokinetic (PK) profile of Compound B. Figure shows mean concentration (ng/ml) – time (hrs) profiles of plasma, brain, and CSF (cerebrospinal fluid) pharmacokinetics of Compound B in male C57BL/6 mice following a single intravenous (I.V.), intraperitoneal (I.P.), subcutaneous (S.C.), and oral (P.O.) dose administration at 10 mg/kg with 6 time points over 8 hrs. Deduced values are shown in **Table 10.2**.
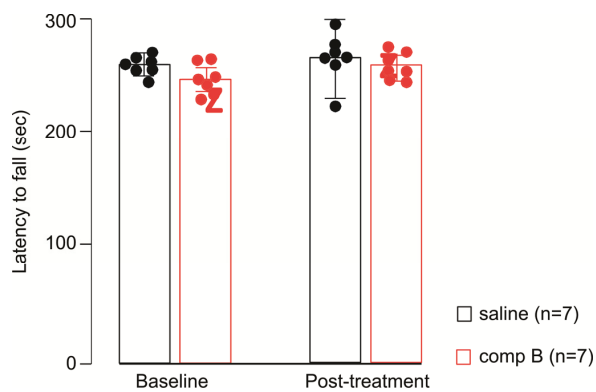
Figure 10.10: Compound B assessment in the rotarod test. Systemic administration of Compound B (I.P., 60 mg/kg) has no effect on motor performance on the rotarod test (baseline: 256 sec ± 5 vs Compound B: 261 sec ± 4, two-way ANOVA, p = 0.990, n = 7).
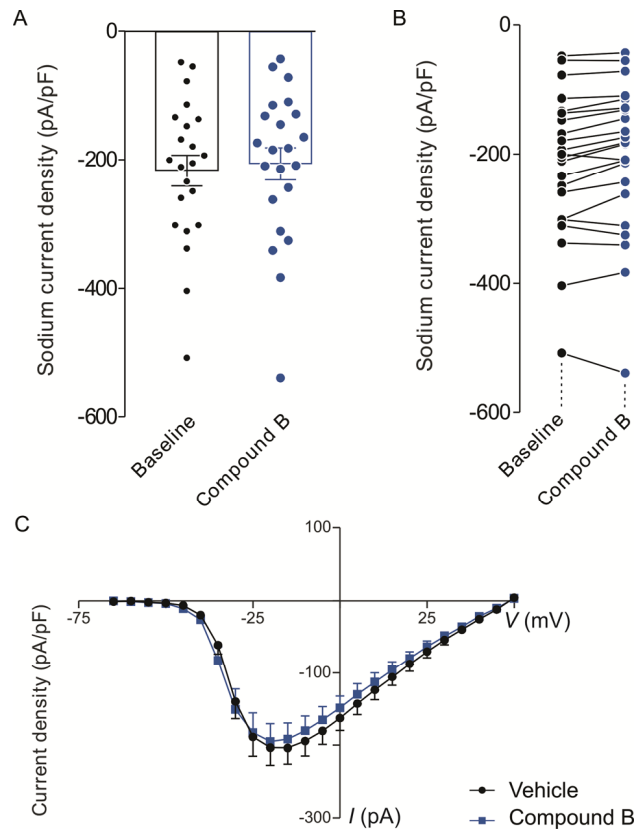
Figure 10.11: Compound B does not affect sodium currents in a subpopulation of colon-innervating DRG neurons. **A)** Group data showing that sodium current density (pA/pF) in a population of colon-innervating DRG neurons was not inhibited (defined as a ≥ 15% reduction from baseline responses) by Compound B ($p > 0.05$, n = 22 neurons, paired t-test). **B)** Individual data from the group data presented in **A)**. **C)** I-V (current-voltage) plots of sodium current density before (vehicle; black) and after (blue) Compound B application (100 μM) in uninhibited colon-innervating DRG neurons.
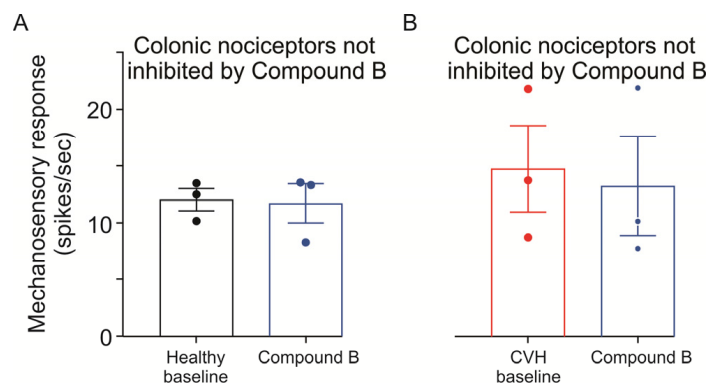
Figure 10.12: Compound B does not affect a subpopulation of colonic nociceptive afferents from healthy control and CVH mice. **A)** Healthy control mice: application of Compound B (100 μM) did not inhibit a population of nociceptors (n = 3, $p > 0.05$, paired t-test). **B)** TNBS colitis-induced CVH mouse model of IBS: application of Compound B (100 μM) did not inhibit a population of CVH nociceptors (n = 3, $p > 0.05$, paired t-test).

115

Figure 10.13: Effect of Compound B and Hm1a on colonic nociceptive afferents. Left: Healthy control mice with application of 100 μM Compound B inhibiting colonic nociceptors from control mice (n = 9 afferents). Addition of 100 nM Hm1a does not overcome Compound B inhibition. Right: In a TNBS colitis-induced CVH mouse model of IBS, application of Compound B inhibited colonic nociceptors from CVH mice (n = 9 afferents). Co-application of 100 nM Hm1a does not overcome Compound B inhibition. * $p < 0.05$; ** $p < 0.01$, repeated measures one-way ANOVA.
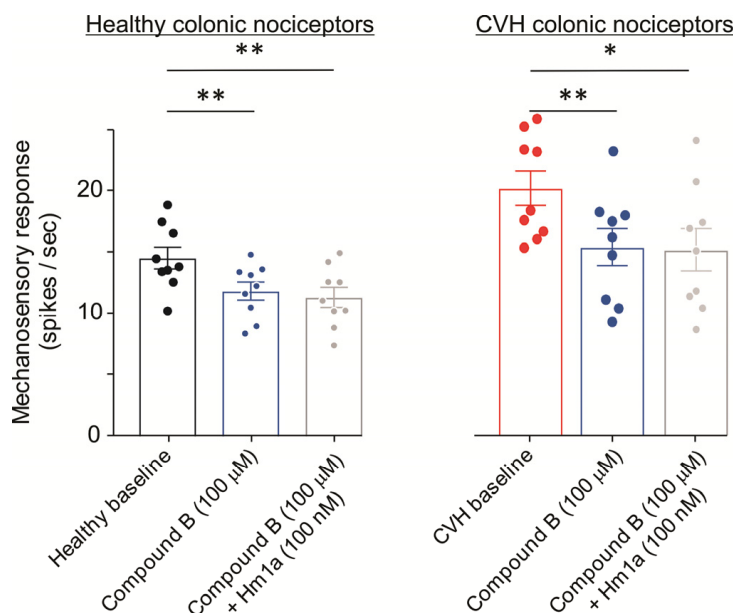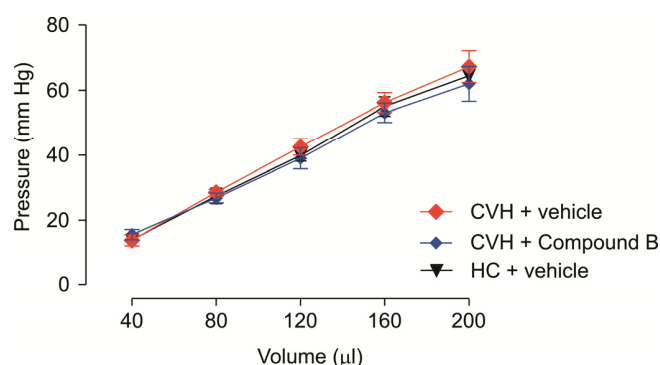

Figure 10.14: Colonic compliance. Compared with healthy control mice, colonic compliance is unaltered in a TNBS colitis-induced CVH mouse model of IBS or IBS mice dosed with 100 μM Compound B, suggesting that changes in the VMR to CRD are not due to changes in smooth muscle function. HC = Healthy Control.

Table 10.1.

Assay	Source	Ligand	Conc.	Kd	Non-specific	Incubation	Detection method	Result
Receptors								
A_{2A} (h) (agonist radioligand)	human recombinant (HEK-293)	[^{3}H]CGS 21680	6nM	27nM	NECA (10 μM)	120min RT	Scintillation counting	Negative
α1A (h) (antagonist radioligand)	human recombinant (CHO)	[^{3}H]prazosin	0.1nM	0.1nM	epinephrine (0.1mM)	60min RT	Scintillation counting	Negative
$α_{2A}$ (h) (antagonist radioligand)	human recombinant (CHO)	[^{3}H]RX 821002	1nM	0.8nM	epinephrine (100μM)	60min RT	Scintillation counting	Negative
$β_1$ (h) (agonist radioligand)	human recombinant (HEK-293)	[^{3}H](-)CGP 12177	0.3nM	0.39nM	alprenolol (50μM)	60min RT	Scintillation counting	Negative
$β_2$ (h) (antagonist radioligand)	human recombinant (CHO)	[^{3}H](-)CGP 12177	0.3nM	0.15nM	alprenolol (50μM)	120min RT	Scintillation counting	Negative
CB_1 (h)	human recombinant	[^{3}H]CP 55940	0.5nM	3.5nM	WIN 55212-2 (10μM)	120min 37°C	Scintillation counting	Negative

(agonist radioligand)	(CHO)							
CB$_2$ (h) (agonist radioligand)	human recombinant (CHO)	[^{3}H]WIN 55212-2	0.8nM	1.5nM	WIN 55212-2 (5 µM)	120min 37°C	Scintillation counting	Negative
CCK$_1$ (CCK$_A$) (h) (agonist radioligand)	human recombinant (CHO)	[^{125}I]CCK-8s	0.08nM	0.24nM	CCK-8s (1µM)	60min RT	Scintillation counting	Negative
D$_1$ (h) (antagonist radioligand)	human recombinant (CHO)	[^{3}H]SCH 23390	0.3nM	0.2nM	SCH 23390 (1µM)	60min RT	Scintillation counting	Negative
D$_{2S}$ (h) (agonist radioligand)	human recombinant (HEK-293)	[^{3}H]7-OH-DPAT	1nM	0.68nM	butaclamol (10µM)	60min RT	Scintillation counting	Negative
ET$_A$ (h) (agonist radioligand)	human recombinant (CHO)	[^{125}I]endothe lin-1	0.03nM	0.03nM	endothelin-1 (100nM)	120min 37°C	Scintillation counting	Negative
H$_1$ (h) (antagonist radioligand)	human recombinant (HEK-293)	[^{3}H]pyrilami ne	1nM	1.7nM	pyrilamine (1µM)	60min RT	Scintillation counting	Negative
H$_2$ (h) (antagonist radioligand)	human recombinant (CHO)	[^{125}I]APT	0.075nM	2.9nM	tiotidine (100µM)	120min RT	Scintillation counting	Negative
M$_1$ (h) (antagonist radioligand)	human recombinant (CHO)	[^{3}H]pirenze p ine	2nM	13nM	atropine (1µM)	60min RT	Scintillation counting	Negative
M$_2$ (h) (antagonist radioligand)	human recombinant (CHO)	[^{3}H]AF-DX 384	2nM	4.6nM	atropine (1µM)	60min RT	Scintillation counting	Negative
M$_3$ (h) (antagonist radioligand)	human recombinant (CHO)	[^{3}H]4-DAMP	0.2nM	0.5nM	atropine (1µM)	60min RT	Scintillation counting	Negative
N neuronal α4β2 (h) (agonist radioligand)	SH-SY5Y cells (human recombinant)	[^{3}H]cytisine	0.6nM	0.3nM	nicotine (10µM)	120min 4°C	Scintillation counting	Negative
δ (DOP) (h) (agonist radioligand)	human recombinant (CHO)	[^{3}H]DADLE	0.5nM	0.73nM	naltrexone (10µM)	120min RT	Scintillation counting	Negative
κ (KOP) (agonist radioligand)	rat recombinant (CHO)	[^{3}H]U 69593	1nM	2nM	naloxone (10µM)	60min RT	Scintillation counting	Negative
µ (MOP) (h) (agonist radioligand)	human recombinant (HEK-293 cells)	[^{3}H]DAMGO	0.5nM	0.35nM	naloxone (10µM)	120min RT	Scintillation counting	Negative
5-HT$_{1A}$ (h) (agonist radioligand)	human recombinant (HEK-293)	[^{3}H]8-OH-DPAT	0.5nM	0.5nM	8-OH-DPAT (10µM)	60min RT	Scintillation counting	Negative
5-HT$_{1B}$ (antagonist radioligand)	rat cerebral cortex	[^{125}I]CYP (+ 30µM isoproteren ol)	0.1nM	0.16nM	serotonin (10µM)	120min 37°C	Scintillation counting	Negative
5-HT$_{2A}$ (h) (agonist radioligand)	human recombinant (HEK-293)	[^{125}I](±)DOI	0.1nM	0.3nM	(±)DOI (1µM)	60min RT	Scintillation counting	Negative
5-HT$_{2B}$ (h) (agonist radioligand)	human recombinant (CHO)	[^{125}I](±)DOI	0.2nM	0.2nM	(±)DOI (1µM)	60min RT	Scintillation counting	Negative
GR (h) (agonist radioligand)	IM-9 cells (cytosol)	[^{3}H]dexame t hasone	1.5nM	1.5nM	Triamcino-lone (10µM)	6hr 4°C	Scintillation counting	Negative
AR (h) (agonist radioligand)	LNCaP cells (cytosol)	[^{3}H]methyltri enolone	1nM	0.8nM	testosterone (1µM)	24hr 4°C	Scintillation counting	Negative
V$_{1a}$(h) (agonist radioligand)	human recombinant (CHO)	[^{3}H]AVP	0.3nM	0.5nM	AVP (1µM)	60min RT	Scintillation counting	Negative
Ion channels								

117
`

BZD (central) (agonist radioligand)	rat cerebral cortex	[3H]flunitrazepam	0.4nM	2.1nM	diazepam (3µM)	60min 4°C	Scintillation counting	Negative
NMDA (antagonist radioligand)	rat cerebral cortex	[3H]CGP 39653	5nM	23nM	L-glutamate (100µM)	60min 4°C	Scintillation counting	Negative
5-HT$_3$ (h) (antagonist radioligand)	human recombinant (CHO)	[3H]BRL 43694	0.5nM	1.15nM	MDL 72222 (10µM)	120min RT	Scintillation counting	Negative
Ca^{2+} channel (L, dihydro-pyridine) (antagonist radioligand)	rat cerebral cortex	[3H]nitrendipine	0.1nM	0.18nM	nitrendipine (1µM)	90min RT	Scintillation counting	Negative
Potassium channel hERG (human)- [3H] Dofetilide	human recombinant (HEK-293)	[3H] Dofetilide	3nM	6.6nM	Terfenadine (25µM)	60min RT	Scintillation counting	Negative
K$_V$ channel (antagonist radioligand)	rat cerebral cortex	[125I]α-dendrotoxin	0.01nM	0.04nM	α-dendrotoxin (50nM)	60min RT	Scintillation counting	Negative
Transporters								
Nor epinephrine transporter (h) (antagonist radioligand)	human recombinant (CHO)	[3H]nisoxetine	1nM	2.9nM	desipramine (1µM)	120min 4°C	Scintillation counting	Negative
dopamine transporter (h) (antagonist radioligand)	human recombinant (CHO)	[3H]BTCP	4nM	4.5nM	BTCP (10µM)	120min 4°C	Scintillation counting	Negative
5-HT transporter (h) (antagonist radioligand)	human recombinant (CHO)	[3H]imipramine	2nM	1.7nM	imipramine (10µM)	60min RT	Scintillation counting	Negative
Enzymes								
MAO-A (antagonist radioligand)	rat cerebral cortex	[3H]Ro 41-1049	10nM	14nM	clorgyline (1µM)	60 min 37°C	Scintillation counting	Negative
Kinases and other enzymes								
Assay	Source	Substrate/stimulus/ tracer		Incu- bation		Measured component	Detection method	Result
Lck kinase (h)	human recombinant (Sf9 cells)	ATP + Ulight-Poly GAT[EAY(1:1:1)]n (25nM)		10 min RT		phospho-Ulight-Poly GAT[EAY(1:1:1)]n	LANCE	Negative
COX1 (h)	human recombinant	Arachidonic acid (3µM) + ADHP (25µM)		3min RT		Resorufin (oxydized ADHP)	Fluorimetry	Negative
COX2 (h)	human recombinant (Sf9 cells)	Arachidonic acid (2µM) + ADHP (25µM)		5min RT		Resorufin (oxydized ADHP)	Fluorimetry	Negative
PDE3A (h)	human recombinant (Sf9 cells)	[3H]cAMP + cAMP (0.5µM)		20min RT		[3H]5'AMP	Scintillation counting	Negative
PDE4D2 (h)	human recombinant (Sf9 cells)	[3H]cAMP + cAMP (0.5µM)		20min RT		[3H]5'AMP	Scintillation counting	Positive
acetylcholin esterase (h)	human recombinant (HEK-293)	Acetylthiocholine (400µM)		30min RT		5 thio 2 nitrobenzoic acid	Photometry	Negative

118
`

Table 10.2.

Route	Matrix	T_{max} (hrs)	C_0/C_{max} (ng/ml)	AUC_{last} (ng*hr/ml)	AUC_{inf} (ng*hr/ml)	$T_{1/2}$ (hrs)	CL (ml/min/kg)	Vss (l/kg)	% F^a
I.V.	Plasma	-	14442	15319	15479	1.4	10.8	0.8	-
	Brain[b]	-	11116	13861	14151	1.6	11.8	1.1	-
	CSF	-	4795	5016	5111	1.8	32.1	2.5	-
I.P.	Plasma	0.5	5523	10694	11134	-	-	-	-
	Brain[b]	0.5	6579	13505	13878	-	-	-	-
	CSF	0.5	2776	5179	5277	-	-	-	-
P.O.	Plasma	0.5	5681	12097	12437	-	-	-	79
	Brain[b]	0.25	6371	11525	11828	-	-	-	-
	CSF	0.25	3397	4426	4453	-	-	-	-
S.C.	Plasma	1.00	4570	14237	14839	-	-	-	-
	Brain[b]	1.00	4041	14010	14010	-	-	-	-
	CSF	1.00	2248	6190	6190	-	-	-	-

PK data (**Figure 10.9**): [a]AUClast was used for bioavailability calculation. [b]Brain concentration and exposure expressed as ng/g and ng/g*hr, density of brain tissue was considered to be 1 which is equivalent to plasma density.

10.8 Acknowledgments

Address correspondence to: Frank Bosmans, Johns Hopkins University School of Medicine 725 N Wolfe Street, 206 Biophysics, Baltimore, Maryland 21205, USA. Phone: 14109551609; Email: frankbosmans@jhmi.edu. Or to: Stuart Brierley, College of Medicine and Public Health, Flinders University, Level 7, South Australian Health and Medical Research Institute, North Terrace, Adelaide, South Australia 5000, Australia. Phone: 61881284848; Email: stuart.brierley@flinders.edu.au. Or to: Pankaj J Pasricha, Johns Hopkins University School of Medicine, 720 Rutland Street, Ross 958, Baltimore, Maryland 21205, USA. Phone: 14105501793; Email: ppasric1@jhmi.edu.

10.9 Conflict of interest

FB is an inventor on a patent for Compound B (US Patent and Trademark Office, 9505727).

10.10 References

1. Chey WD, Kurlander J, Eswaran S. Irritable bowel syndrome: a clinical review. *JAMA*. 2015;313(9):949–958.
2. Maxion-Bergemann S, Thielecke F, Abel F, Bergemann R. Costs of irritable bowel syndrome in the UK and US. *Pharmacoeconomics*. 2006;24(1):21–37.
3. Mayer EA. Clinical practice. Irritable bowel syndrome. N Engl J Med. 2008;358(16):1692–1699.
4. Farmer AD, Aziz Q. Gut pain & visceral hypersensitivity. *Br J Pain*. 2013;7(1):39–47.
5. Farzaei MH, Bahramsoltani R, Abdollahi M, Rahimi R. The Role of Visceral Hypersensitivity in Irritable Bowel Syndrome: Pharmacological Targets and Novel Treatments. *J Neurogastroenterol Motil*. 2016;22(4):558–574.
6. Akbar A, Walters JR, Ghosh S. Review article: visceral hypersensitivity in irritable bowel syndrome: molecular mechanisms and therapeutic agents. *Aliment Pharmacol Ther*. 2009;30(5):423–435.
7. Azpiroz F, et al. Mechanisms of hypersensitivity in IBS and functional disorders. *Neurogastroenterol Motil*. 2007;19(1 Suppl):62–88.
8. Brierley SM, Linden DR. Neuroplasticity and dysfunction after gastrointestinal inflammation. *Nat Rev Gastroenterol Hepatol*. 2014;11(10):611–627.

9. Akbar A, Yiangou Y, Facer P, Walters JR, Anand P, Ghosh S. Increased capsaicin receptor TRPV1-expressing sensory fibres in irritable bowel syndrome and their correlation with abdominal pain. *Gut.* 2008;57(7):923–929.

10. Beyder A, et al. Loss-of-function of the voltage-gated sodium channel $Na_v1.5$ (channelopathies) in patients with irritable bowel syndrome. *Gastroenterology.* 2014;146(7):1659–1668.

11. Brierley SM, et al. The ion channel TRPA1 is required for normal mechanosensation and is modulated by algesic stimuli. *Gastroenterology.* 2009;137(6):2084–2095.e3.

12. Castro J, et al. α-Conotoxin Vc1.1 inhibits human dorsal root ganglion neuroexcitability and mouse colonic nociception via $GABA_B$ receptors. *Gut.* 2017;66(6):1083–1094.

13. Cenac N, Altier C, Chapman K, Liedtke W, Zamponi G, Vergnolle N. Transient receptor potential vanilloid-4 has a major role in visceral hypersensitivity symptoms. *Gastroenterology.* 2008;135(3):937–946.

14. Cenac N, et al. Role for protease activity in visceral pain in irritable bowel syndrome. *J Clin Invest.* 2007;117(3):636–647.

15. Henström M, D'Amato M. Genetics of irritable bowel syndrome. *Mol Cell Pediatr.* 2016;3(1):7.

16. Hockley JR, Winchester WJ, Bulmer DC. The voltage-gated sodium channel $Na_v1.9$ in visceral pain. *Neurogastroenterol Motil.* 2016;28(3):316–326.

17. Hughes PA, et al. Increased κ-opioid receptor expression and function during chronic visceral hypersensitivity. *Gut.* 2014;63(7):1199–1200.

18. Laird JM, Souslova V, Wood JN, Cervero F. Deficits in visceral pain and referred hyperalgesia in $Na_v1.8$ (SNS/PN3)-null mice. *J Neurosci.* 2002;22(19):8352–8356.

19. Marger F, et al. T-type calcium channels contribute to colonic hypersensitivity in a rat model of irritable bowel syndrome. *Proc Natl Acad Sci* USA. 2011;108(27):11268–11273.

20. Page AJ, et al. Different contributions of ASIC channels 1a, 2, and 3 in gastrointestinal mechanosensory function. *Gut.* 2005;54(10):1408–1415.

21. Defrees DN, Bailey J. Irritable Bowel Syndrome: Epidemiology, Pathophysiology, Diagnosis, and Treatment. *Prim Care.* 2017;44(4):655–671.

22. Lacy BE, Weiser K, De Lee R. The treatment of irritable bowel syndrome. *Therap Adv Gastroenterol.* 2009;2(4):221–238.

23. Ahern CA, Payandeh J, Bosmans F, Chanda B. The hitchhiker's guide to the voltage-gated sodium channel galaxy. *J Gen Physiol.* 2016;147(1):1–24.

24. Mao Y, Wang B, Kunze W. Characterization of myenteric sensory neurons in the mouse small intestine. *J Neurophysiol.* 2006;96(3):998–1010.

25. Osorio N, Korogod S, Delmas P. Specialized functions of $Na_v1.5$ and $Na_v1.9$ channels in electrogenesis of myenteric neurons in intact mouse ganglia. *J Neurosci.* 2014;34(15):5233–5244.

26. Copel C, Clerc N, Osorio N, Delmas P, Mazet B. The $Na_v1.9$ channel regulates colonic motility in mice. *Front Neurosci.* 2013;7:58.

27. Erickson A, et al. Voltage-gated sodium channels: (Na_v)igating the field to determine their contribution to visceral nociception. *J Physiol* (Lond). 2018;596(5):785–807.

28. Woods CG, Babiker MO, Horrocks I, Tolmie J, Kurth I. The phenotype of congenital insensitivity to pain due to the $Na_v1.9$ variant p.L811P. *Eur J Hum Genet.* 2015;23(10):1434.

29. Osteen JD, et al. Selective spider toxins reveal a role for the $Na_v1.1$ channel in mechanical pain. *Nature.* 2016;534(7608):494–499.

30. Gilchrist J, et al. $Na_v1.1$ modulation by a novel triazole compound attenuates epileptic seizures in rodents. *ACS Chem Biol.* 2014;9(5):1204–1212.

31. Wheeler DW, Lee MC, Harrison EK, Menon DK, Woods CG. Case Report: Neuropathic pain in a patient with congenital insensitivity to pain. *F1000Res.* 2014;3:135.

32. Zhang HT. Cyclic AMP-specific phosphodiesterase-4 as a target for the development of antidepressant drugs. *Curr Pharm Des.* 2009;15(14):1688–1698.

33. Whitehead WE, et al. Tolerance for rectosigmoid distention in irritable bowel syndrome. *Gastroenterology.* 1990;98(5 Pt 1):1187–1192.

34. Bradesi S, Herman J, Mayer EA. Visceral analgesics: drugs with a great potential in functional disorders? *Curr Opin Pharmacol.* 2008;8(6):697–703.

35. Drossman DA. Beyond tricyclics: new ideas for treating patients with painful and refractory functional gastrointestinal symptoms. *Am J Gastroenterol.* 2009;104(12):2897–2902.

36. Ford AC, Talley NJ, Schoenfeld PS, Quigley EM, Moayyedi P. Efficacy of antidepressants and psychological therapies in irritable bowel syndrome: systematic review and meta-analysis. *Gut.* 2009;58(3):367–378.

37. Houghton LA, Fell C, Whorwell PJ, Jones I, Sudworth DP, Gale JD. Effect of a second-generation alpha2delta ligand (pregabalin) on visceral sensation in hypersensitive patients with irritable bowel syndrome. *Gut.* 2007;56(9):1218–1225.

38. Catterall WA, Kalume F, Oakley JC. $Na_v1.1$ channels and epilepsy. *J Physiol* (Lond). 2010;588(Pt 11):1849–1859.

39. Camara-Lemarroy CR, Escobedo-Zúñiga N, Ortiz-Zacarias D, Peña-Avendaño J, Villarreal-Garza E, Díaz-Torres MA. Prevalence and impact of irritable bowel syndrome in people with epilepsy. *Epilepsy Behav.* 2016;63:29–33.

40. Chen CH, Lin CL, Kao CH. Irritable Bowel Syndrome Increases the Risk of Epilepsy: A Population-Based Study. *Medicine* (Baltimore). 2015;94(36):e1497.

41. Nedelcovych MT, et al. N-(Pivaloyloxy)alkoxy-carbonyl Prodrugs of the Glutamine Antagonist 6-Diazo-5-oxo-l-norleucine (DON) as a Potential Treatment for HIV Associated Neurocognitive Disorders. *J Med Chem.* 2017;60(16):7186–7198.

42. Rais R, et al. Discovery of 6-Diazo-5-oxo-l-norleucine (DON) Prodrugs with Enhanced CSF Delivery in Monkeys: A Potential Treatment for Glioblastoma. *J Med Chem.* 2016;59(18):8621–8633.

43. Zou MF, et al. Structure-Activity Relationship Studies on a Series of 3α-[Bis(4-fluorophenyl)methoxy]tropanes and 3α-[Bis(4-fluorophenyl)methylamino]tropanes As Novel Atypical Dopamine Transporter (DAT) Inhibitors for the Treatment of Cocaine Use Disorders. *J Med Chem.* 2017;60(24):10172–10187.

44. Shields SD, Eckert WA, Basbaum AI. Spared nerve injury model of neuropathic pain in the mouse: a behavioral and anatomic analysis. *J Pain.* 2003;4(8):465–470.

45. Chaplan SR, Bach FW, Pogrel JW, Chung JM, Yaksh TL. Quantitative assessment of tactile allodynia in the rat paw. *J Neurosci Methods.* 1994;53(1):55–63.

46. Castro J, et al. Linaclotide inhibits colonic nociceptors and relieves abdominal pain via guanylate cyclase-C and extracellular cyclic guanosine 3',5'-monophosphate. *Gastroenterology.* 2013;145(6):1334–46.e1.

47. de Araujo AD, et al. Selenoether oxytocin analogues have analgesic properties in a mouse model of chronic abdominal pain. *Nat Commun.* 2014;5:3165.

48. Winston J, Shenoy M, Medley D, Naniwadekar A, Pasricha PJ. The vanilloid receptor initiates and maintains colonic hypersensitivity induced by neonatal colon irritation in rats. *Gastroenterology.* 2007;132(2):615–627.

Statement of Authorship

Title of Paper	Tetrodotoxin-sensitive voltage-gated sodium channels regulate bladder afferent responses to distension
Publication Status	☑ Published ☐ Accepted for Publication ☐ Submitted for Publication ☐ Unpublished and Unsubmitted work written in manuscript style
Publication Details	Grundy, L., Erickson, A., Caldwell, A., Garcia-Caraballo, S., Rychkov, G., Harrington, A., & Brierley, S. M. (2018). Tetrodotoxin-sensitive voltage-gated sodium channels regulate bladder afferent responses to distension. Pain, 159(12), 2573-2584. doi:10.1097/ j.pain.0000000000001368

Principal Author

Name of Principal Author (Candidate)	Andelain Erickson (co-author)
Contribution to the Paper	Retrograde labeling, DRG culture, whole-cell patch clamp electrophysiology and analysis, single-cell isolation, single-cell PCR and analysis, editing of manuscript.
Overall percentage (%)	20
Certification:	This paper reports on original research I conducted during the period of my Higher Degree by Research candidature and is not subject to any obligations or contractual agreements with a third party that would constrain its inclusion in this thesis. I am the primary author of this paper.
Signature	Date 15/1/2019

Co-Author Contributions

By signing the Statement of Authorship, each author certifies that:

i. the candidate's stated contribution to the publication is accurate (as detailed above);

ii. permission is granted for the candidate in include the publication in the thesis; and

iii. the sum of all co-author contributions is equal to 100% less the candidate's stated contribution.

Name of Co-Author	Luke Grundy (first author, corresponding author)
Contribution to the Paper	Project conception, experimental design, experiments, analysis, composition + editing of manuscript
Signature	Date 19.3.19

Name of Co-Author	Ashlee Caldwell
Contribution to the Paper	bladder distension, & pERK labelling, imaging, cording for spinal cord experiments, editing of manuscript
Signature	Date 25.3.19

Name of Co-Author	Sonia Garcia-Caraballo		
Contribution to the Paper	single cell experiments.		
Signature		Date	25/3/19

Name of Co-Author	Grigori Rychkov		
Contribution to the Paper	Supervision of patch clamping and data analysis, editing of manuscript		
Signature		Date	14.03.2015

Name of Co-Author	Andrea M. Harrington		
Contribution to the Paper	Bladder distension for pERK labelling in the spinal cord experiments, editing of manuscript		
Signature		Date	14/3/2019

Name of Co-Author	Stuart M. Brierley		
Contribution to the Paper	SUPERVISION, PROJECT LEAD, DRAFTING/WRITING MANUSCRIPT		
Signature		Date	14/3/2019

123

Chapter 11 Tetrodotoxin-sensitive voltage-gated sodium channels regulate bladder afferent responses to distension

Grundy, Luke[a,b,*]; Erickson, Andelain[a,b]; Caldwell, Ashlee[a,b]; Garcia-Caraballo, Sonia[a,b]; Rychkov, Grigori[b]; Harrington, Andrea[a,b]; Brierley, Stuart M.[a,b]

[a]Visceral Pain Research Group, Centre for Neuroscience, College of Medicine and Public Health, Flinders University, Bedford Park, South Australia, Australia. [b]Centre for Nutrition and Gastrointestinal Diseases, Discipline of Medicine, University of Adelaide, South Australian Health and Medical Research Institute (SAHMRI), Adelaide, South Australia, Australia. Corresponding author. Address: Visceral Pain Research Group, Flinders University, Level 7, South Australian Health and Medical Research Institute (SAHMRI), North Terrace, Adelaide, South Australia 5000, Australia. Tel.: +61 8 8128 4858. E-mail address: luke.grundy@flinders.edu.au (L. Grundy).

11.1 Abstract

Interstitial cystitis/bladder pain syndrome (IC/BPS) is a prevalent, chronic bladder disorder that negatively impacts the quality of life for ~5% of the western population. Hypersensitivity of mechanosensory afferents embedded within the bladder wall is considered a key component in mediating IC/BPS symptoms. Bladder infusion of voltage-gated sodium (Na_v) channel blockers show clinical efficacy in treating IC/BPS symptoms; however, the current repertoire of Na_v channels expressed by and contributing to bladder afferent function is unknown. We used single-cell reverse-transcription polymerase chain reaction of retrogradely traced bladder-innervating dorsal root ganglia (DRG) neurons to determine the expression profile of Na_v channels, and patch-clamp recordings to characterise the contribution of tetrodotoxin-sensitive (TTX-S) and tetrodotoxin-resistant (TTX-R) Na_v channels to total sodium current and neuronal excitability. We determined the TTX-S and TTX-R contribution to mechanosensitive bladder afferent responses *ex vivo* and spinal dorsal horn activation *in vivo*. Single-cell reverse-transcription polymerase chain reaction of bladder-innervating DRG neurons revealed significant heterogeneity in Na_v channel coexpression patterns. However, TTX-S Na_v channels contribute the vast majority of the total sodium current density and regulate the neuronal excitability of bladder DRG neurons. Furthermore, TTX-S Na_v channels mediate almost all bladder afferent responses to distension. *In vivo* intrabladder infusion of TTX significantly reduces activation of dorsal horn neurons within the spinal cord to bladder distension. These data provide the first comprehensive analysis of Na_v channel expression within sensory afferents innervating the bladder. They also demonstrate an essential role for TTX-S Na_v channel regulation of bladder-innervating DRG neuroexcitability, bladder afferent responses to distension, and nociceptive signalling to the spinal cord.

Keywords: Bladder, Afferent, Spinal cord, Nociception, DRG, Na_v, TTX

11.2 Introduction

Interstitial cystitis/bladder pain syndrome (IC/BPS) is a prevalent, chronic bladder disorder that negatively impacts the quality of life for ~5% of the western population.[2,38] Patients with IC/BPS exhibit hyperalgesia and allodynia to cystometric bladder filling compared with healthy controls, reporting sensations of urgency and pain at lower bladder distension volumes.[27] Although the pathophysiology of bladder disorders is not completely understood, changes in peripheral afferent responsiveness likely play a key role in their associated urgency, frequency, and pain.[10]

The bladder wall contains a dense spinal afferent nerve innervation that responds to a range of stimuli,[10,17] including the direct transduction of mechanical distortion. Activation of these afferents supplies input to

124

autonomic spinal/brainstem reflex pathways and is essential for efferent modulation of normal bladder filling and the conscious perception of bladder fullness.[15] Secondary to these primary transducers, but also essential in neuronal response to nonnoxious and noxious stimuli, are the voltage-gated sodium (Na$_v$) channels, which have been shown to regulate neuronal excitability by amplifying cation influx to generate and propagate action potentials.[5,6,11,12,28]

The Na$_v$ channel family consists of 9 isoforms (Na$_v$1.1-Na$_v$1.9) that are historically characterised by their relative sensitivity to the neurotoxin tetrodotoxin (TTX) as either TTX-sensitive (Na$_v$1.1-Na$_v$1.4, Na$_v$1.6, and Na$_v$1.7) or TTX-resistant (Na$_v$1.5, Na$_v$1.8, and Na$_v$1.9).[5,6] Na$_v$ channels also display localised tissue distribution, with Na$_v$1.1, Na$_v$1.7, Na$_v$1.8, and Na$_v$1.9 most commonly expressed in the peripheral nervous system.[6,35,37] Na$_v$ isoform channelopathies in *SCN9A* (Na$_v$1.7), *SCN10A* (Na$_v$1.8), and *SCN11A* (Na$_v$1.9) are primarily responsible for enhanced or diminished pain sensitivity phenotypes in humans.[11,42] These studies have since generated widespread interest into the therapeutic potential of Na$_v$ channels for the treatment of acute and chronic visceral pain,[12,25] a defining symptom of IC/BPS. More recently, neosaxitoxin, a pan-Na$_v$ inhibitor, showed outstanding efficacy in relieving the symptoms of IC/BPS in a small clinical trial,[30] and another pan-Na$_v$ channel inhibitor, lidocaine, also shows efficacy in the treatment of IC/BPS symptoms.[9] These findings directly implicate Na$_v$ channels and bladder afferent signalling in the symptomology of IC/BPS. However, the full complement of Na$_v$ channels expressed by bladder afferents and their contribution to bladder afferent function remains unresolved.

In this study, we addressed this issue using single-cell reverse-transcription polymerase chain reaction (RT-PCR) to determine the distribution of Na$_v$ channels in retrogradely traced bladder-innervating dorsal root ganglia (DRG) neurons. We also characterised the contribution of TTX-S and TTX-R Na$_v$ channels to the total sodium current and neuronal excitability of retrogradely traced bladder-innervating DRG neurons and to bladder afferent responses to distension in *ex vivo* recordings. Finally, we determined the capacity of TTX to modulate neuronal activation within the dorsal horn of the spinal cord in response to noxious bladder distension *in vivo*. These data provide the first comprehensive analysis of Na$_v$ channels in the sensory afferents innervating the bladder and provide a platform for the pharmacological characterisation of the Na$_v$ channel isoforms contributing to bladder afferent mechanosensation.

11.3 Methods

In this study, 12- to 16-week-old male and female C57BL/6 mice were used. They were obtained from an in-house breeding facility within the South Australian Health and Medical Research Institute (SAHMRI). Mice were group-housed (5 mice per cage) in specific housing rooms within a temperature-controlled environment of 22°C and a 12-hour light/12-hour dark cycle. Mice had free access to food and water at all times. Mice were randomly assigned to experimental procedures and individual mice were used for a single experiment only. All experiments were performed in accordance with SAHMRI Animal Ethics Committee (application # SAM195, SAM190, and SAM281).

11.3.1 Bladder retrograde tracing

A small aseptic abdominal incision was made in anesthetised (isoflurane 2%-4% in oxygen) mice. Cholera toxin subunit B conjugated to Alexa Fluor 488 (CTB-488; 0.5% diluted in 0.1M phosphate buffered saline [PBS]; Thermo Fisher Scientific, Victoria, Australia) was injected at 4 sites into the bladder wall (2 μL/injection) using a 5-μL Hamilton syringe attached to a 33-gauge needle. The abdominal incision was sutured closed and analgesic (buprenorphine; 2.7 μg/30 **G)** and antibiotic (ampicillin; 50 mg/kg) were given subcutaneously as mice regained consciousness. Mice were then allowed to recover, housed individually, and monitored for 4 days, to visualise CTB-labelled afferent neurons in the DRG.

11.3.2 Real-time quantitative reverse-transcription polymerase chain reaction

11.3.2.1 Tissue collection

Dorsal root ganglia (L5-S1) and bladder tissues were collected immediately after euthanasia by CO$_2$ inhalation. For DRG, whole lumbosacral (LS) (L5-S1) DRG pairs were surgically removed, frozen in dry

ice, and stored at -80°C before RNA extraction. For bladder mucosa and detrusor tissue layers, bladders were removed, cut open, stretched out, and rinsed with 1x PBS before gently peeling the mucosal layer from the underlying muscle. Each layer of tissue was frozen in dry ice and stored at -80°C before RNA extraction.

11.3.2.2 RNA extraction

RNA was extracted using the PureLink RNA Micro kit (Invitrogen, Victoria, Australia, cat #12183-016; DRG pairs) or the PureLink RNA Mini kit (Invitrogen, 12183018A; bladder mucosa or detrusor) followed by a DNAse treatment (Life Technologies, cat #12185-010) according to the manufacturer's instructions. RNA was transcribed to cDNA using SuperScript VILO Master Mix (Invitrogen, cat # 11755250) as per the manufacturer's instructions. cDNA was stored at -20°C.

11.3.2.3 Quantitative reverse-transcription polymerase chain reactions

Quantitative reverse-transcription polymerase chain reaction (qRT-PCR) was performed using Taqman Gene Expression Master Mix (Applied Biosystems, Victoria, Australia, Cat #4369016) with commercially available hydrolysis probes (TaqMan; Life Technologies, see **Table 11.1** for details) and RNAse-free water (AMBION, Victoria, Australia, cat #AM9916). For each reaction, 10 µL of qPCR SuperMix, 1 µL of TaqMan primer assay, 4 µL of water, and 5 µL of cDNA (1:10 dilution in RNA free H_2O) from each sample was tested in duplicate for each Na_v channel subtype. β-Actin was used as an endogenous control for all tissues. Assays were run for 45 cycles on a 7500 Fast Real-Time PCR System (Applied Biosystems) machine, using 7500 Fast software, v2.0.6. mRNA quantities are expressed as ΔCt relative to reference gene β-actin. Using Prism 7 software (San Diego, CA), data were analysed by 1-way analysis of variance (ANOVA) with Bonferroni post hoc analysis. Statistical significance is reported when $*P < 0.05$, $**P < 0.01$, and $***P < 0.001$.

Table 11.1: Taqman primers used for qRT-PCR and single-cell PCR, obtained from Life Technologies.

Gene name	Gene target	Assay ID
β-Actin (reference gene)	*Actb*	Mm00607939_s1
Na_v1.1	*Scn1a*	Mm00450580_m1
Na_v1.2	*Scn2a1*	Mm01270359_m1
Na_v1.3	*Scn3a*	Mm00658167_m1
Na_v1.4	*Scn4a*	Mm00500103_m1
Na_v1.5	*Scn5a*	Mm01342518_m1
Na_v1.6	*Scn8a*	Mm00488110_m1
Na_v1.7	*Scn9a*	Mm00450762_s1
Na_v1.8	*Scn10a*	Mm00501467_m1
Na_v1.9	*Scn11a*	Mm00449367_m1
Tubulin, β 3 class III	*Tubb3*	Mm00727586_s1

qRT-PCR, quantitative reverse-transcription polymerase chain reaction.

11.3.3 Isolation of dorsal root ganglia neurons for single-cell reverse-transcription polymerase chain reaction, calcium imaging, and patch-clamp recordings

Dorsal root ganglia from lumbosacral (L5-S1) spinal levels of the mouse spinal cord, which correspond to the pelvic innervation of the bladder, were isolated and incubated in Hanks balanced salt solution (pH 7.4) containing collagenase (4 mg/mL) and dispase (4.5 mg/mL), at 37°C for 30 minutes. The collagenase/dispase solution was aspirated and replaced with Hanks balanced salt solution containing collagenase (4 mg/mL) for 10 minutes at 37°C. The collagenase solution was aspirated and replaced with 600 µL of DMEM (GIBCO) containing 10% FCS (Invitrogen), 2 mM of L-glutamine (GIBCO), 100 µM of MEM nonessential amino acids (GIBCO), and 100 mg/mL of penicillin/streptomycin (Invitrogen). Neurons were dissociated via trituration with a Pasteur pipette and spot-plated onto 15-mm coverslips coated with laminin (20 µg/mL) and poly-D-lysine (800 µg/mL) and maintained in an incubator at 37°C in 5% CO_2. Calcium imaging and patch-clamp recordings were performed on DRG neurons 18 to 30 hours after isolation.

11.3.4 Single-cell reverse-transcription polymerase chain reaction of bladder dorsal root ganglia neurons

Under continuous perfusion of sterile and RNA-/DNase-free PBS, retrogradely traced single DRG neurons were identified using a fluorescent microscope and picked using a micromanipulator into the end of a fine glass capillary. The glass capillary containing the cell was then broken into a sterile Eppendorf tube containing 10 µL of lysis buffer with DNAse (TaqMan Gene Expression Cells-to-CT Kit; Life Technologies). For each coverslip of cells, a bath control was also taken and analysed together with cells. After lysis and termination of DNAse treatment, samples were immediately frozen on dry ice and stored at -80°C until cDNA synthesis was performed. Tubulin-3 expression served as a neuronal marker and positive control. PCR products were stored at -20°C and resolved on a 3% to 4% TBE agarose gel (UltraPure Agarose 1000; cat#16550-100, Invitrogen). All samples were visualized by adding 1 µL of Midori Green Direct to 20 µL of post-PCR sample and 5 µL of samples was loaded into each well for gel electrophoresis. A 20-bp marker (Bio-Rad, New South Wales, Australia) was used to check for correct size.

11.3.5 Calcium imaging

Cultured DRG neurons (18-30 hours) were loaded with 2 µM of fura-2-acetoxymethyl ester (fura-2) for 15 minutes at 37°C and washed with HEPES buffer (10 mM, NaCl 142 mM, KCl 2 mM, glucose 10 mM, CaCl2 2 mM, MgCl2 1 mM, HEPES 10 mM; pH 7.4) for 30 minutes before imaging at room temperature (23°C). Fura-2 was excited at 340 and 380 nm (emissions 510 nM) using a Nikon TE300 Eclipse microscope equipped with a Sutter DG-4/OF wavelength switcher, Omega XF04 filter set for Fura-2, Photonic Science ISIS-3 intensified CCD camera, and Universal Interface Card MetaFluor software. Retrogradely traced bladder DRG were identified by the presence of the CTB-488 tracer. Fluorescence images were obtained every 5 seconds using a 20x objective. Data were recorded and further analysed using MetaFluor software. After an initial baseline reading to ensure cell fluorescence was stable (an indication of healthy cells), DRG were stimulated with veratridine (50 µM), with or without TTX (300 nM), and changes in intracellular calcium $[Ca^{2+}]i$, were monitored in real time. KCl (40 mM) was applied as a positive control for neuronal phenotype and cell viability.

11.3.6 Patch-clamp electrophysiology of bladder-innervating dorsal root ganglia neurons

11.3.6.1 Compound application

Cells were continually perfused with bath solution by a gravity-driven multibarrel perfusion system positioned within 1 mm of the neuron under investigation. After baseline recordings in voltage or current-clamp mode, TTX (100 nM; 1-minute incubation) was applied and a second recording was made.

11.3.6.2 Current-clamp recordings

Rheobase (amount of current required to fire an action potential) was determined by application of a series of depolarising pulses from a holding potential of −70 mV (10 or 25 pA increments [480 ms]) followed by hold at −70 mV (100 ms) (supplemental Fig 1A, available at http://links.lww.com/PAIN/A655). Borosilicate glass pipettes were fire-polished to 4 to 8 MΩ (Ra = 66 ± 17 MΩ). Bladder-innervating DRG neuron resting membrane potential was −49 ± 5 mV (cutoff ≤ -40 mV). Current-clamp intracellular solution contained (in mM): 135 KCl; 2 MgCl₂; 2 MgATP; 5 EGTA-Na; 10 HEPES-Na; adjusted to pH 7.3, 275 mOsm. Extracellular solution contained (in mM): 140 NaCl; 4 KCl; 2 MgCl₂; 2 CaCl₂; 10 HEPES; 5 glucose, adjusted to pH 7.4, 285 mOsm.

11.3.6.3 Voltage-clamp recordings

The current–voltage (I_{Na}-V) relationship was determined by application of a prepulse to −100 mV (100 ms), followed by a series of step pulses from −70 mV to +60 mV (5-mV increments of 100-ms duration), before returning to hold at −70 mV (repetition interval of 3 seconds, P/8 leak subtraction, supplemental Fig 1A, available at http://links.lww.com/PAIN/A655). Voltage dependence of the steady-state fast inactivation was determined by application of a series of prepulses from −110 to +2.5 mV (7.5-mV increments [100 ms]), then a pulse at −30 mV, followed by hold at −70 mV (50 ms; 3-second repetition interval) (supplemental Fig 1B, available at http://links.lww.com/PAIN/A655). Peak inward currents (I)

were normalised to the maximal inward current (I_{max}) and fitted using a Boltzmann equation: $I/I_{max} = 1/(1 + \exp[(V_m - V_{1/2})/k])$, where $V_{1/2}$ is the half-maximal sodium current, V_m is the preconditioning potential, and k is the slope factor. Pipettes were fire-polished to 0.7 to 2 MΩ and ≥75% of series resistance was compensated. Neuron membrane capacitance ranged from 20 to 65 pF, with a median of 36 pF. Voltage-clamp intracellular solution contained (in mM): 60 CsF; 45 CsCl; 2 $MgCl_2$; 5 EGTA-Na; 10 HEPES-Cs; 30 TEA-Cl; 2 MgATP; adjusted to pH 7.2 with CsOH, 280 mOsm. Extracellular solution contained (in mM): 70 NaCl; 50 NMDG; 40 TEA-Cl; 4 CsCl; 2 $MgCl_2$; 2 $CaCl_2$; 10 HEPES; 5 glucose; adjusted to pH 7.4, 300 mOsm.

11.3.6.4 Data acquisition and analysis
Recordings were amplified with Axopatch 200A, digitised with Digidata 1322A, sampled at 20 kHz, filtered at 5 kHz, recorded with pCLAMP 9 software (Molecular Devices), and analysed in Clampfit and GraphPad Prism 7 (San Diego, CA). Groups were compared using paired Student t test and statistical significance is reported as ***$P < 0.001$.

11.3.7 *Ex vivo* bladder afferent nerve recordings
Afferent nerve recordings were conducted using an *ex vivo* model previously described.[18] Mice were humanely killed by CO_2 asphyxiation using a Quietek induction system (Next Advance), and the entire lower abdomen was removed and immediately placed in ice-cold Krebs-bicarbonate solution (composition in mmol/L: NaCl 118.4, $NaHCO_3$ 24.9, $CaCl_2$ 1.9, $MgSO_4$ 1.2, KCl 4.7, KH_2PO_4 1.2, glucose 11.7). Submerged in a modified organ bath under continual perfusion with gassed (95% O_2, 5% CO_2) Krebs-bicarbonate solution at 35°C, excess tissue was removed to expose the bladder, urethra, and ureters. Ureters were tied with perma-hand silk (ETHICON). The bladder was catheterised through the urethra (PE 50) that was connected to a syringe pump (NE-1000) to allow for a controlled fill rate. A second catheter was inserted through the dome of the bladder, secured with silk, and connected to a pressure transducer (NL108T2; Digitimer Ltd, Hertfordshire, United Kingdom) to enable recording of intravesical pressure during graded distension. Pelvic nerves were dissected into fine multiunit branches and placed within a sealed glass pipette containing a microelectrode (WPI) attached to a neurolog headstage (NL100AK; Digitimer Ltd), amplified (NL104), filtered (NL 125/126, Neurolog; Digitimer Ltd, bandpass 50-5000 Hz), and digitized (CED 1401; Cambridge Electronic Design, Cambridge, United Kingdom) to a PC for offline analysis using Spike2 (Cambridge Electronic Design). To quantify the magnitude of the afferent response, the number of action potentials crossing a preset threshold was determined per second. Using Prism 7 software (San Diego, CA), data were analysed by repeated-measures 2-way ANOVA with Bonferroni post hoc analysis. Statistical significance is reported as *$P < 0.05$, **$P < 0.01$, and ***$P < 0.001$.

11.3.7.1 Experimental protocols
At the start of all afferent recording experiments, control bladder distensions were performed with intravesical infusion of isotonic saline (NaCl, 0.9%) at a rate of 100 µL/minute to a maximum pressure of 50 mm Hg until afferent nerve output was stable. The volume in the bladder was extrapolated from the known fill rate (100 µL/minute) and the time taken (seconds) to reach the maximum pressure of 30 mm Hg. After a stable baseline was maintained, the saline in the infusion pump was replaced by either TTX (1 µM), the pan-Na_v activator veratridine (50 µM), or both in combination.

11.3.8 *In vivo* bladder distension
Female mice were anesthetised (isoflurane 2%-4% in oxygen) and a catheter (PE 50 tubing) was inserted into the bladder through the urethra. Urine was removed using a suction syringe and a new catheter (PE 50 tubing) was inserted primed with either vehicle (saline; N = 4) or TTX (1 µM, N = 4), and 100 µL of solution was then infused into the bladder and allowed to incubate for 10 minutes before being removed with a suction syringe. A new catheter was inserted and a fine silk suture was used to tie around the catheter and the urethral opening to secure the tube and to limit loss of pressure through the urethra during distension. Mice remained under anaesthesia for 5 minutes before the first distension administered using a syringe attached to a sphygmomanometer pressure gauge. Distension was performed at 60 mm Hg pressure for 20 seconds and then deflated for 10 seconds. This process was repeated 5 times. Thirty

seconds after the final deflation, mice were administered an anaesthetic overdose (0.125 mL/250 g lethabarb) and by 4 minutes, had undergone transcardial perfuse fixation.

11.3.9 Transcardial perfuse fixation and tissue dissection

After anaesthetic overdose, the chest cavity was opened and 0.5 mL of heparin saline was injected into the left ventricle followed by insertion of a 22-gauge needle, attached to tubing and a peristaltic perfusion pump. The right atrium was snipped, allowing for perfusate drainage. Warm saline (0.85% physiological sterile saline) was perfused before ice-cold 4% paraformaldehyde in 0.1 M phosphate buffer (Sigma-Aldrich, St. Louis, MO). After complete perfusion, L5-S1 spinal cord segments (determined by level of DRG root insertion points) were removed and postfixed in 4% paraformaldehyde in 0.1 M phosphate buffer at 4°C for 18 to 20 hours. The lowest rib was used as an anatomical marker of T13. After postfixation, spinal cords were cryoprotected in 30% sucrose/phosphate buffer (Sigma-Aldrich) overnight at 4°C and then an additional 24-hour incubation at 4°C in 50% OCT/30% sucrose/phosphate buffer solution before freezing in 100% OCT. Spinal cord were cryosectioned (12-µm thick) and placed onto gelatin-coated slides for immunofluorescence labelling. Lumbosacral spinal cord sections used for dorsal horn neuron quantification were serially sectioned and distributed over 7 slides, which were used for immunofluorescence of neuronal activation marker phosphorylated MAP kinase ERK 1/2 (pERK).

11.3.10 Spinal cord–phosphorylated MAP kinase ERK 1/2 and neurochemical marker immunofluorescence

The spinal cord dorsal horn neurons activated by bladder distension were identified by labelling for neuronal activation marker pERK using a similar immunofluorescent labelling method as previously described.[19,20] Antibody details are provided in **Table 11.2**. Negative controls were prepared as above with the primary antibody omitted. After air drying for 1 hour, sections were washed with 0.2% Triton-TX 100 (Sigma-Aldrich, MO) in 0.1 M PBS (T-PBS) to remove excess OCT. Nonspecific binding of secondary antibodies was blocked with 5% normal chicken serum diluted in 0.2% Triton-TX 100/(Sigma-Aldrich, MO) in 0.1 M PBS. Tissue sections were incubated with primary antisera and diluted in T-PBS overnight (greater than 16 hours but less than 24 hours) at room temperature. Sections were then washed in T-PBS and incubated for 1 hour at room temperature with a secondary antibody conjugated to Alexa Fluor (**Table 11.2**). Sections were then washed in T-PBS before mounting in ProLong Gold Antifade and cover-slipped. Slides were allowed to dry for 24 hours before visualisation.

Table 11.2: Primary and secondary antisera details.

Antigen		Species raised in	Manufacturer code	Manufacturer	Dilution	RIID
Primary Phospho-p44/42 MAPK (Erk1/2) (Thr202/ Tyr204) (D13.14.4E) XP(tm) mAb (pERK)		Rabbit	4370	Cell Signalling	1:100	AB_2315112
Antigen	Species raised in	AF conjugate	Manufacturer code	Manufacturer	Dilution	RIID
Secondary Rabbit IgG H + L	Chicken	594	A21442	Thermo Fisher	1:200	AB_141840

11.3.11 Microscopy

Fluorescence was visualised with an epifluorescence microscope (Olympus, Tokyo, Japan) using 10x objective and 3-second exposure. Visualization of Alexa Fluor was achieved using a 590 nm excitation and 610/630 nm emission settings. Images were analysed using ImageJ software (NIH). Other than making moderate adjustments for contrast and brightness, the images were not manipulated in any way.

11.3.12 Spinal cord pERK neuronal counts and analysis

Neuronal counts were analysed from previously saved digital photomicrographs, with only neurons with intact nuclei counted. The number of pERK-immunoreactive (IR) dorsal horn neurons/animal was obtained from 10 sections. The total number of pERK-IR neurons from 10 sections/spinal regions was then averaged across mice following noxious pressures of bladder distension after vehicle or TTX bladder infusion (N = 4), and the mean number of neurons (+/-SEM) localised within the dorsal horn, only within

129

the superficial dorsal horn (laminae I-II), or only within dorsal gray commissure (DGC) indicative of spinal dorsal column nuclei was compared between experimental groups. Using Prism 7 software (San Diego, CA), data were analysed by 1-way ANOVA with Bonferroni post hoc analysis. Statistical significance is reported as $*P < 0.05$, $**P < 0.01$, and $***P < 0.001$.

11.4 Results

11.4.1 Voltage-gated sodium (Na_v) channels regulate bladder afferent responses to distension

It has previously been shown that a single intrabladder instillation of the pan-Na_v blocker neosaxitoxin is able to relieve symptoms in patients with IC/BPS for at least 3 months.[30] Given that Na_v channels are historically localised on sensory neurons and have been shown to mediate a number of pain phenotypes,[42] we hypothesised the reduction in painful sensation that occurs after neosaxitoxin treatment is through a modulation of bladder afferent excitability. To test this hypothesis, we performed *ex vivo* recordings of bladder afferents (**Figure 11.1**). We evaluated bladder afferent mechanosensitivity before and during instillation with the neurotoxin TTX (1 µM) and observed an almost complete abolishment of bladder afferent firing to distension during TTX instillation (**Figure 11.1** Ai, **iii)**. Notably, these effects were observed throughout the duration of bladder distension, indicating that there was no differential effect of TTX on high- or low-threshold mechanosensitive afferents. Furthermore, the reduction in bladder mechanosensitivity occurred in the absence of changes in muscle compliance (pressure/volume relationship; **Figure 11.1** Aii), indicating that the effects of TTX on afferent firing when instilled into the bladder are at the level of the primary afferent, not secondary to changes in muscle function. In separate experiments, bladder mechanosensitivity was evaluated before and during instillation with the pan-Na_v channel activator, veratridine (50 µM) (**Figure 11.1 B)**. Veratridine induced significant, immediate mechanical hypersensitivity to distension, prompting greater afferent firing compared with saline at the same intravesical pressures (**Figure 11.1** Bi, **iii)**. As with the effects of TTX, veratridine had no effect on bladder compliance (**Figure 11.1** Bii). Furthermore, veratridine failed to induce mechanical hypersensitivity to distension when applied in the presence of TTX (**Figure 11.1 C)**. Overall, these data show that Na_v channels mediate bladder afferent responses to distension and that TTX-S Na_v isoforms may have a predominant role in this process.
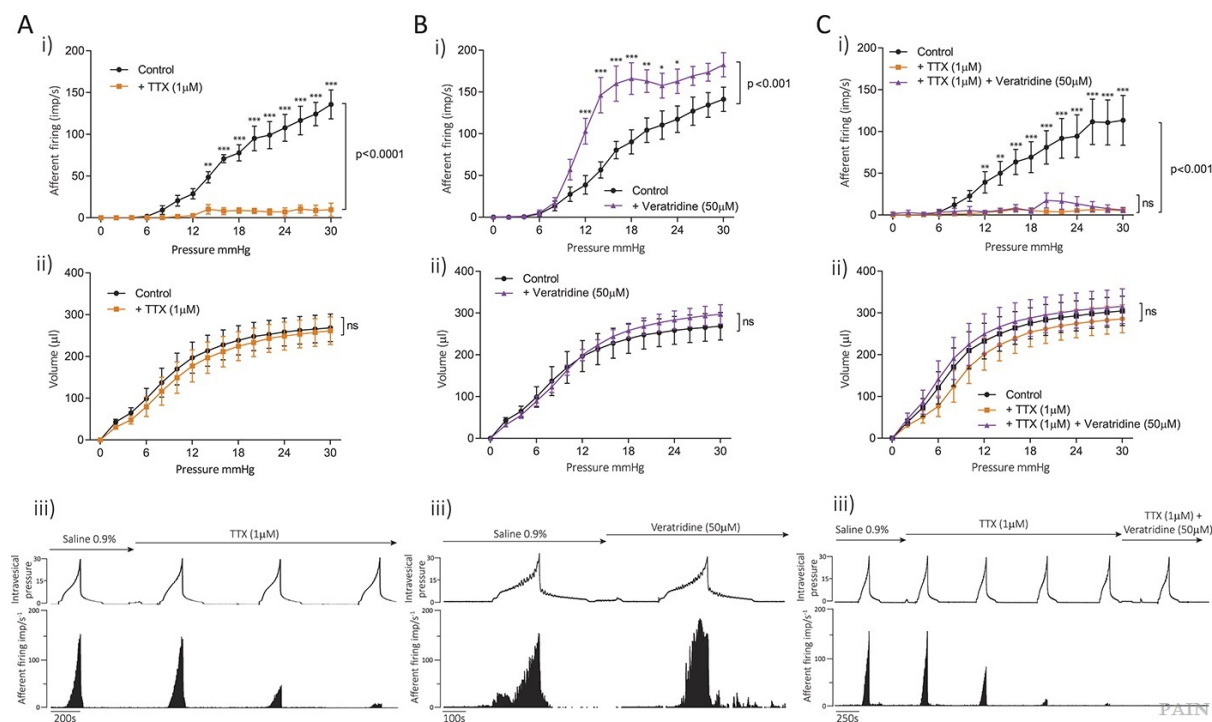

Figure 11.1: Voltage-gated sodium (Na_v) channels underlie bladder afferent responses to mechanical stimuli. (A) (i) Bladder afferent sensitivity to graded distension is significantly attenuated by intravesical infusion of TTX (1 µM; $P < 0.0001$, repeated-measures 2-way ANOVA), particularly at distension pressures of 16 to 30 mm Hg ($***P < 0.001$ Bonferroni post hoc tests, N = 5 mice). (ii) The

130

pressure/volume relationship during graded bladder distension is not changed with intravesical instillation of TTX (1 μM, P > 0.05, repeated-measures 2-way ANOVA). (iii) Original recordings of bladder afferent firing and intravesical pressure show a progressively reduced afferent response to intravesical infusion with TTX (1 μM). (B) (i) Bladder afferent sensitivity to graded distension is significantly enhanced by intravesical instillation of the pan-Na_v activator veratridine (50 μM; P < 0.001, repeated-measures 2-way ANOVA), particularly at distension pressures of 12 to 20 mm Hg (*P < 0.05, **P < 0.01, **P < 0.001, Bonferroni post hoc tests, N = 5 mice). (ii) The pressure/volume relationship during graded bladder distension is not changed with intravesical instillation of veratridine (50 μM, P > 0.05, repeated-measures 2-way ANOVA). (iii) Original recordings of bladder afferent firing and intravesical pressure show an enhanced afferent response during intravesical infusion with veratridine (50 μM). (C) (i) Bladder afferent sensitivity to graded distension is significantly inhibited by intravesical infusion of TTX (1 μM, repeated-measures 2-way ANOVA, P < 0.001, *P < 0.05, **P < 0.01, ***P < 0.001, Bonferroni post hoc test, N = 5 mice), which also prevents veratridine-induced enhancements in bladder mechanosensitivity (ns, P ≥ 0.05 repeated-measures 2-way ANOVA, N = 5 mice). (ii) Neither TTX (1 μM) nor TTX (1 μM) and veratridine (50 μM) have any effect on muscle compliance during graded bladder distension. (iii) Original recordings of bladder afferent firing and intravesical pressure show a reduced afferent response during intravesical infusion with TTX (1 μM), which is unchanged in the presence of veratridine (50 μM). ANOVA, analysis of variance.

11.4.2 Na_v channels are expressed in retrogradely traced bladder-innervating dorsal root ganglia neurons

As we observed a significant effect of Na_v channel modulation on bladder afferent response to distension, we next sought to elucidate the relative expression of the genes encoding Na_v channels within the different tissue structures of the bladder. To do this, we performed qRT-PCR on bladder mucosa, detrusor smooth muscle, as well as whole LS DRG and single-cell RT-PCR of retrogradely traced LS bladder-innervating DRG neurons (**Figure 11.2**). In whole LS DRG (**Figure 11.2 A**), we see abundant expression of genes encoding the TTX-S Na_v channel isoforms $Na_v1.1$, $Na_v1.7$, and TTX-R isoforms $Na_v1.8$ and $Na_v1.9$. Quantitative reverse-transcription polymerase chain reaction of bladder muscle (supplemental Figure 2A, available at http://links.lww.com/PAIN/A655) and mucosa (supplemental Figure 2B, available at http://links.lww.com/PAIN/A655) reveal only minor expression of Na_v channels compared with DRG, with Na_v expression ~1000-fold greater in LS DRG compared with bladder mucosa or muscle. When present in the bladder mucosa, $Na_v1.1$, $Na_v1.2$, and $Na_v1.4$ display the most abundant expression, whereas $Na_v1.2$ and $Na_v1.5$ were most abundant in the bladder muscle. These expression data support our afferent recording data, which indicates that TTX and veratridine are acting through a neuronal mechanism.

As our qRT-PCR data indicated that Na_v channels are expressed in greater amounts in the LS DRG than in the bladder wall, we endeavoured to provide further detail on the specific and individual expression profiles of Na_v channels in bladder-innervating DRG neurons. This is important because whole DRG contain both somatic and visceral innervating cell bodies as well as nonneuronal cells. Using retrograde tracer injected into the bladder allowed us to isolate individual bladder-innervating neurons and investigate the expression and coexpression of Na_v channels in these neurons using single-cell RT-PCR. 98% of bladder-innervating DRG neurons coexpress $Na_v1.7$, $Na_v1.8$, and $Na_v1.9$ (**Figure 11.2** B-D). A significant proportion of these neurons also express $Na_v1.1$ (78%), $Na_v1.2$ (92%), $Na_v1.3$ (86%), and $Na_v1.6$ (82%) (**Figure 11.2** B-D). We observed marked heterogeneity between individual neurons (**Figure 11.2** C and **D**), with only a small proportion of cells expressing the same patterns of Na_v channel-mRNA, and only 4/50 (8%) of cells expressing the full repertoire of Na_v channel genes.
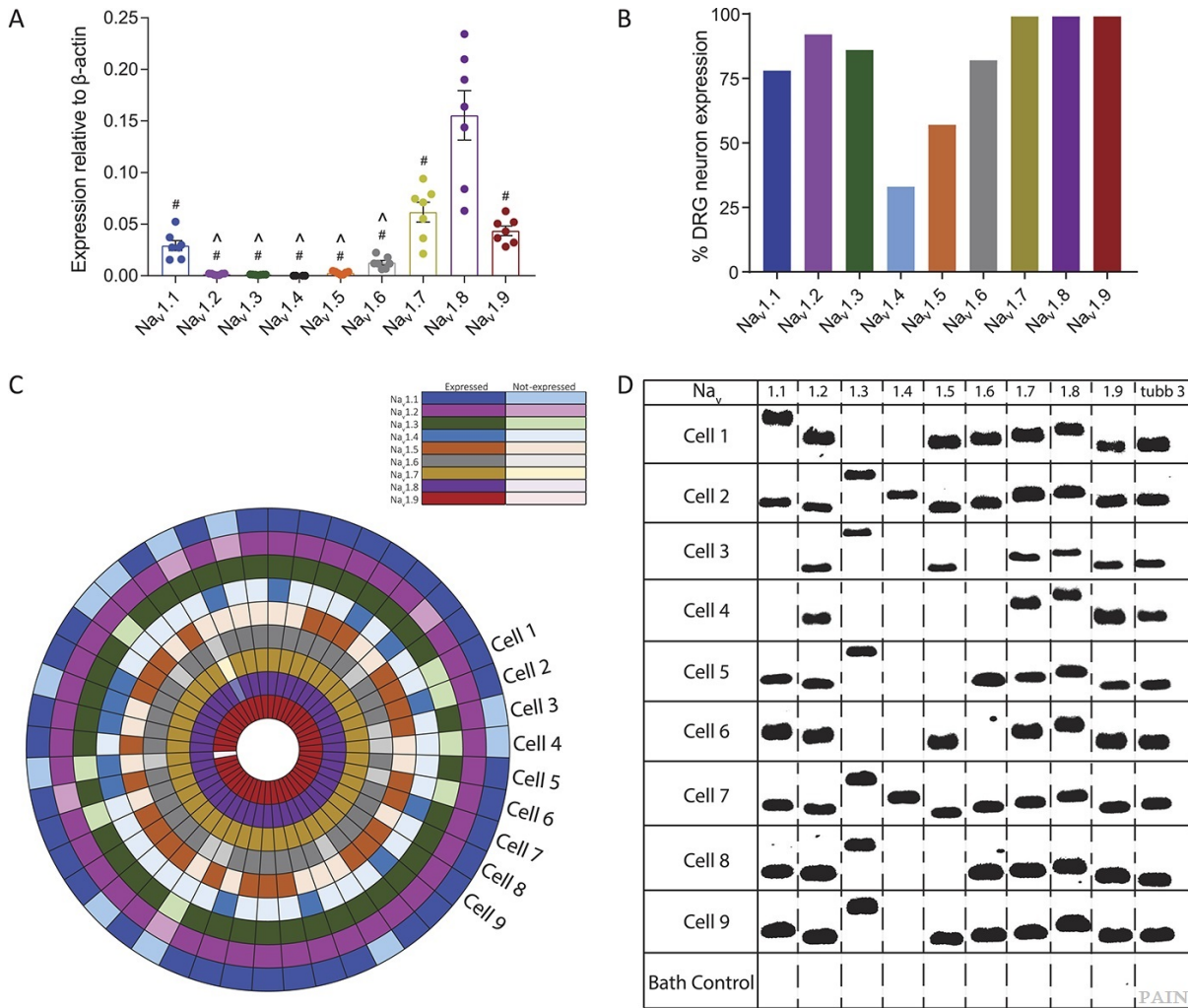
Figure 11.2: Na_v channels are expressed in whole LS DRG and retrogradely labelled bladder-innervating DRG neurons. (A) mRNA expression of genes (*Scn1a-Scn11a*) encoding Na_v channels (Na_v1.1-1.9) in whole LS (L5-S1) DRG relative to the housekeeper gene β-actin. Expression of genes encoding TTX-S Na_v isoforms Na_v1.1 (*Scn1a*), Na_v1.6 (*Scn8a*), Na_v1.7 (*Scn9a*), and TTX-R Na_v isoforms Na_v1.8 (*Scn10a*) and Na_v1.9 (*Scn11a*) is abundant in LS DRG, with Na_v1.8 (*Scn10a*) having the overall highest expression. Considerably lower expression of Na_v1.2 (*Scn2a*), Na_v1.3 (*Scn3a*), Na_v1.4 (*Scn4a*), and Na_v1.5 (*Scn5a*) are found in LS DRG (#$P < 0.05$ vs Na_v1.8, ^$P < 0.05$ vs Na_v1.7, 1-way ANOVA, Tukey post hoc test, N = 7 mice). (B) Single-cell RT-PCR of retrogradely traced bladder-innervating DRG neurons reveals the percentage of neurons expressing genes encoding Na_v channels (*Scn1a-Scn11a*) (n = 50 single cells from N = 6 mice). 98% of bladder DRG neurons express transcripts for Na_v1.7 (*Scn9a*), Na_v1.8 (*Scn10a*), and Na_v1.9 (*Scn11a*). Na_v1.1 (*Scn1a*, 78%), Na_v1.2 (*Scn2a*, 92%), Na_v1.3 (Scn3a, 86%), and Na_v1.6 (Scn8a, 82%) are expressed in 75% to 90% of all bladder-traced neurons. Na_v1.4 (*Scn4a*) and Na_v1.5 (*Scn5a*) are expressed by considerably fewer bladder-innervating DRG neurons. (C) Donut plot showing expression and coexpression of genes encoding Na_v channels (Na_v1.1-1.9) in 50 individual retrogradely traced bladder-innervating DRG neurons. Each colour represents an individual gene with expression marked by bold (see legend). (Na_v1.1) *Scn1a* is represented in the outer ring, and (Na_v1.9) *Scn11a* in the inner ring. Individual neurons are arranged radially, such that coexpression of genes in a single neuron can be easily identified running from outside to inside. Cell numbers correspond to gel electrophoresis numbers in (D). Four of 50 cells expressed the full repertoire of all Na_v channel genes. All cells represented expressed the neuronal marker tubulin-3. (D) Collated and colour-inverted images of single-cell RT-PCR products after gel electrophoresis showing Na_v expression in 9 individual retrogradely traced bladder-innervating DRG neurons and a bath control (no cell). Individual neurons show significant heterogeneity of expression and substantial coexpression of Na_v channels in individual retrogradely traced DRG. Na_v1.7, Na_v1.8, and Na_v1.9 are coexpressed in 99% of all bladder-innervating neurons. ANOVA, analysis of variance; DRG, dorsal root ganglia; LS, lumbosacral; RT-PCR, reverse-transcription polymerase chain reaction.

11.4.3 Na$_v$ channels are functionally expressed by bladder-innervating dorsal root ganglia neurons

Given the Na$_v$ channel expression profile in lumbosacral DRG and within retrogradely traced bladder-innervating DRG neurons, we sought to confirm the functional role of Na$_v$ channels in bladder afferent excitability. Using calcium imaging as a proxy for neuronal activation revealed that 90% of bladder neurons are responsive to the pan-Na$_v$ activator veratridine (**Figure 11.3** A and **B)**. Furthermore, responses to veratridine in both retrogradely bladder-traced and the general population of LS DRG neurons were abolished by prior and concurrent incubation with TTX (**Figure 11.3** C-E). Overall, these findings are consistent with our *ex vivo* afferent studies, which demonstrate that TTX prevents veratridine-induced mechanical hypersensitivity of bladder afferents.
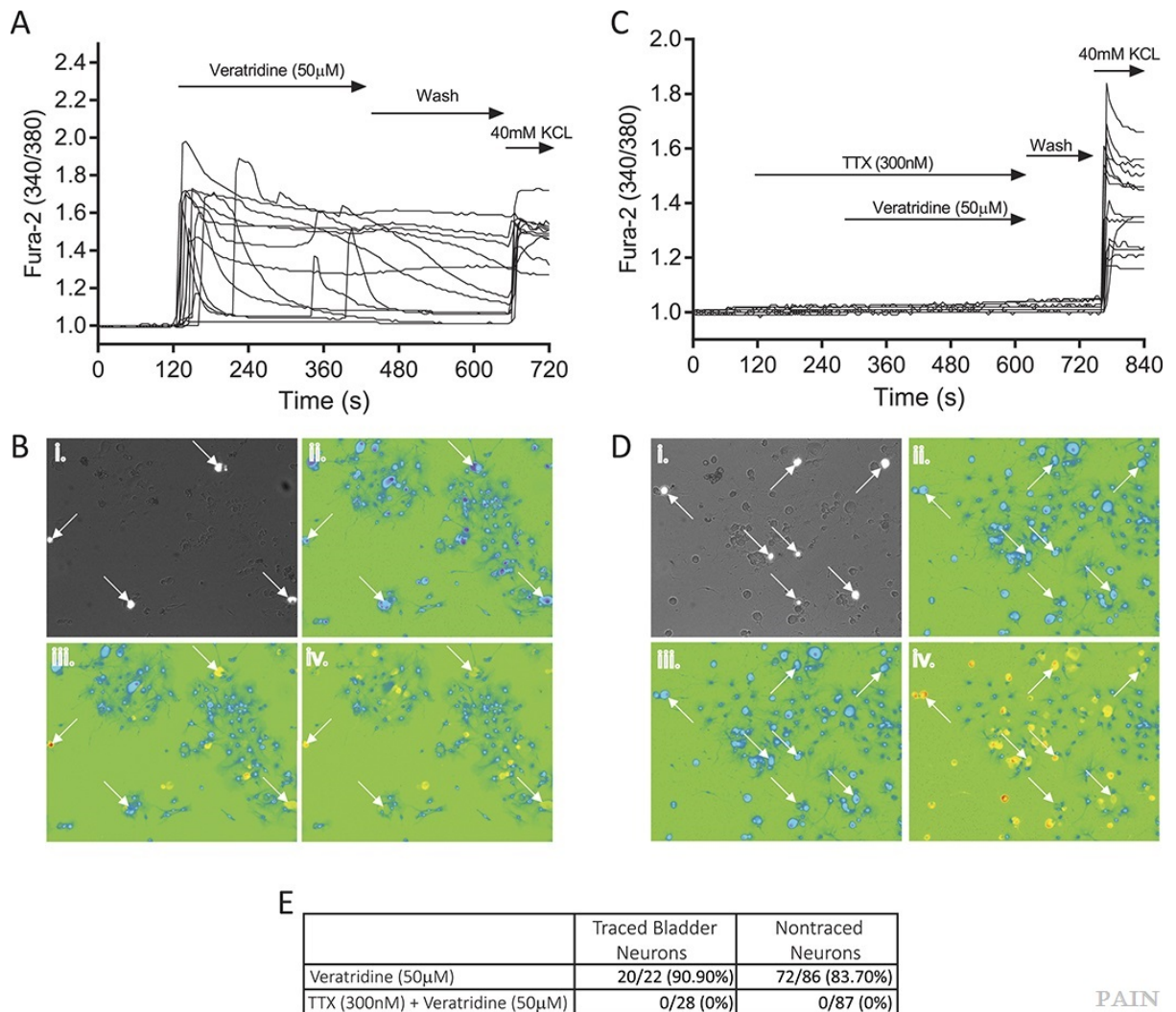

	Traced Bladder Neurons	Nontraced Neurons
Veratridine (50μM)	20/22 (90.90%)	72/86 (83.70%)
TTX (300nM) + Veratridine (50μM)	0/28 (0%)	0/87 (0%)

PAIN

Figure 11.3: Veratridine induces calcium transients in TTX-sensitive bladder-innervating DRG neurons. (A) Calcium responses elicited by veratridine (50 μM) in isolated bladder-innervating LS DRG neurons loaded with Fura-2. An increase in fluorescent ratio (340/380) indicates calcium influx after channel opening. KCl (40 mM) was added at the end of each experiment to confirm cell viability and neuronal phenotype. Each line represents an individual neuron. (B) (i) Retrogradely traced bladder-innervating LS DRG neurons are identified under a fluorescent microscope (with 488 nm excitation and 503-538 nm emission detection). White arrows indicate traced neurons. (ii) Low fluorescent ratio (F340/380) during continuous perfusion with control external solution indicates neurons are healthy before the start of experiment. (iii) The addition of veratridine (50 μM) opens Na$_v$ channels and allows calcium to enter neurons through voltage-gated calcium channels. Excited neurons are indicated by an increase in fluorescent ratio (yellow colour and red colour). (iv) Neurons responding to KCl (40 mM). (C) Veratridine (50 μM)-elicited Ca^{2+} responses in isolated bladder-innervating LS DRG neurons are inhibited by TTX (300 nM). TTX has no effect on baseline fluorescence, but neurons respond to KCl (40 mM) indicating neurons are healthy and voltage-gated calcium channels are functional. Each line represents an individual neuron. (D) (i) Retrogradely traced bladder-innervating LS DRG neurons are identified under a fluorescent microscope (488 nm excitation and 503-538 nm emission detection). White arrows indicate traced cells. (ii) Low fluorescent ratio (F340/380) during continuous perfusion with

control external solution indicates cells are healthy before the start of experiment. (iii) The addition of veratridine (50 µM) in the presence of TTX has no effect on Ca^{2+} responses. Excited cells indicated by an increase in fluorescent ratio (yellow colour and red colour). (iv) Cells responding to KCl (40 mM). (E) Table showing number of bladder-innervating LS DRG neurons investigated and % responding to veratridine (50 µM) in the presence (n = 87 individual neurons from N = 5 mice) and absence (n = 86 individual neurons from N = 5 mice) of TTX (300 nM). All veratridine responses are abolished in the presence of TTX. Cells failing to respond to KCl were omitted from analysis. DRG, dorsal root ganglia; LS, lumbosacral.

Using whole-cell patch-clamp electrophysiology of retrogradely traced bladder DRG neurons allowed us to further investigate the contribution of TTX-S and TTX-R sodium currents to neuronal excitability of bladder-innervating DRG neurons. In the presence of TTX, the robust sodium current density observed in control bath solution was significantly reduced by 71.1 ± 4.4% (**Figure 11.4 A)**, showing that the majority of the sodium current entering bladder-innervating DRG neurons during steady-state voltage activation is through TTX-S Na_v channels. Furthermore, the fast inactivation current is almost completely abolished in the presence of TTX (supplemental Figure 3, available at http://links.lww.com/PAIN/A655). Importantly, in support of our afferent data, the decrease in sodium current density we observed in the presence of TTX translated to a significant decrease in neuronal excitability, as indicated by an increase in the current required to elicit action potential firing (rheobase), in the presence of TTX (**Figure 11.4 B)**. TTX-induced increases in rheobase were observed for all but one neuron (23/24 cells) supporting the importance of TTX-S currents in modulating bladder-innervating DRG neuroexcitability. Overall, these findings indicate that sodium currents in bladder DRG neurons are largely mediated by TTX-S Na_v channels, and these isoforms are essential in mediating neuronal excitability.
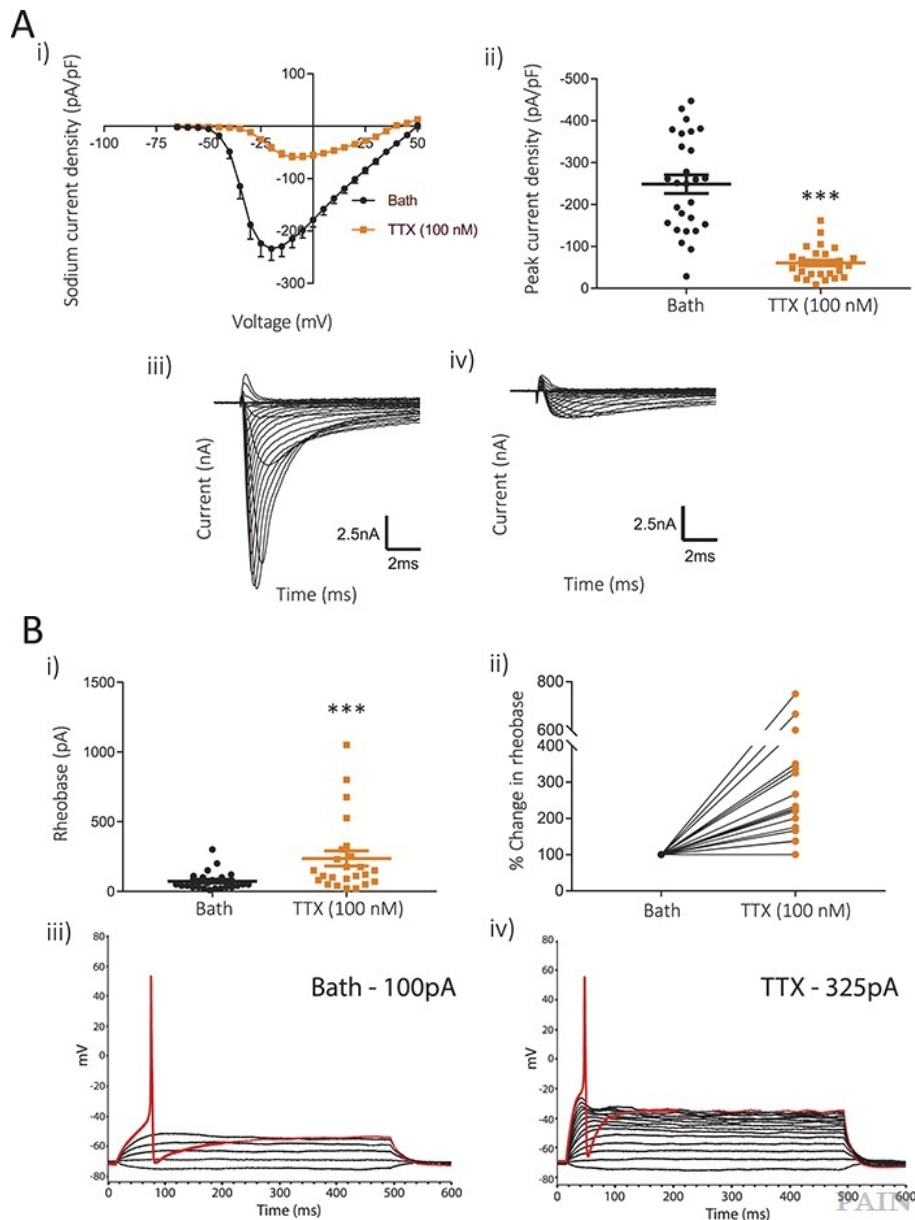
Figure 11.4: TTX attenuates bladder-innervating DRG neuron excitability through a significant reduction in sodium current density. (A) Whole-cell voltage-clamp recordings of retrogradely traced bladder-innervating LS DRG neurons reveal that the activated sodium current is predominantly TTX-S. (i) Activated sodium current density and (ii) peak sodium current density are significantly attenuated in the presence of TTX (***$P < 0.001$, paired Student t test, n = 26 neurons from N = 9 mice). (iii) Original recording of sodium currents in response to a series of voltage step pulses from −70 mV to +60 mV (5 mV increments of 100 ms duration) before and (iv) after incubation with TTX. The sodium current is almost completely abolished in the presence of TTX, suggesting a small contribution of TTX-R channels to the voltage-gated sodium current in bladder-innervating LS DRG. (B) Whole-cell current-clamp recordings of retrogradely traced bladder-innervating LS DRG neurons. (i) TTX significantly increases the amount of current required to elicit an action potential (rheobase; ***$P < 0.001$, paired Student t test, n = 24 neurons from N = 9 mice). (ii) Percent change in rheobase from baseline highlights the individual changes to rheobase observed in the presence of TTX. 23/24 cells exhibited sensitivity to TTX with an increase in rheobase. (iii) Original recording of membrane voltage from a single bladder-innervating DRG neuron during current ramp protocols. Each line represents a 25-pA increase in current. In this example, a 100-pA current was required to elicit an action potential under control conditions. (iv) Perfusion with TTX for 1 minute onto the same DRG neuron increases the amount of current required to elicit an action potential to 325 pA, indicating decreased neuronal excitability. DRG, dorsal root ganglia; LS, lumbosacral.

11.4.4 Mechanosensitive bladder afferents are predominantly TTX-S

Post hoc analysis of multiunit bladder afferent recordings allows for the examination of distinct spike waveforms and a more precise understanding of the contribution of individual afferent units to the entire

mechanosensitive response. On grouping single afferent units together, we found the same pattern of response as seen in **Figure 11.1**, with a dramatic reduction in mechanosensitivity during the course of graded bladder distension (**Figure 11.5 A**). When we dissect apart these single units, however, it becomes clear that not all units are equally sensitive to TTX (**Figure 11.5** Aii, **iii**). Out of a total of 53 single units, we identified 49 (92%) as TTX-S (**Figure 11.5** Aii), exhibiting a significant reduction in action potential firing rate to distension compared with control, whereas 4 single units (8%) showed a remarkable resistance to TTX during mechanical distension (**Figure 11.5** Aiii, C; see unit 1). These data support those from our patch-clamp studies of retrogradely traced bladder DRG neurons, showing that the vast majority, but not all, bladder-innervating DRG exhibit reduced excitability in the presence of TTX.
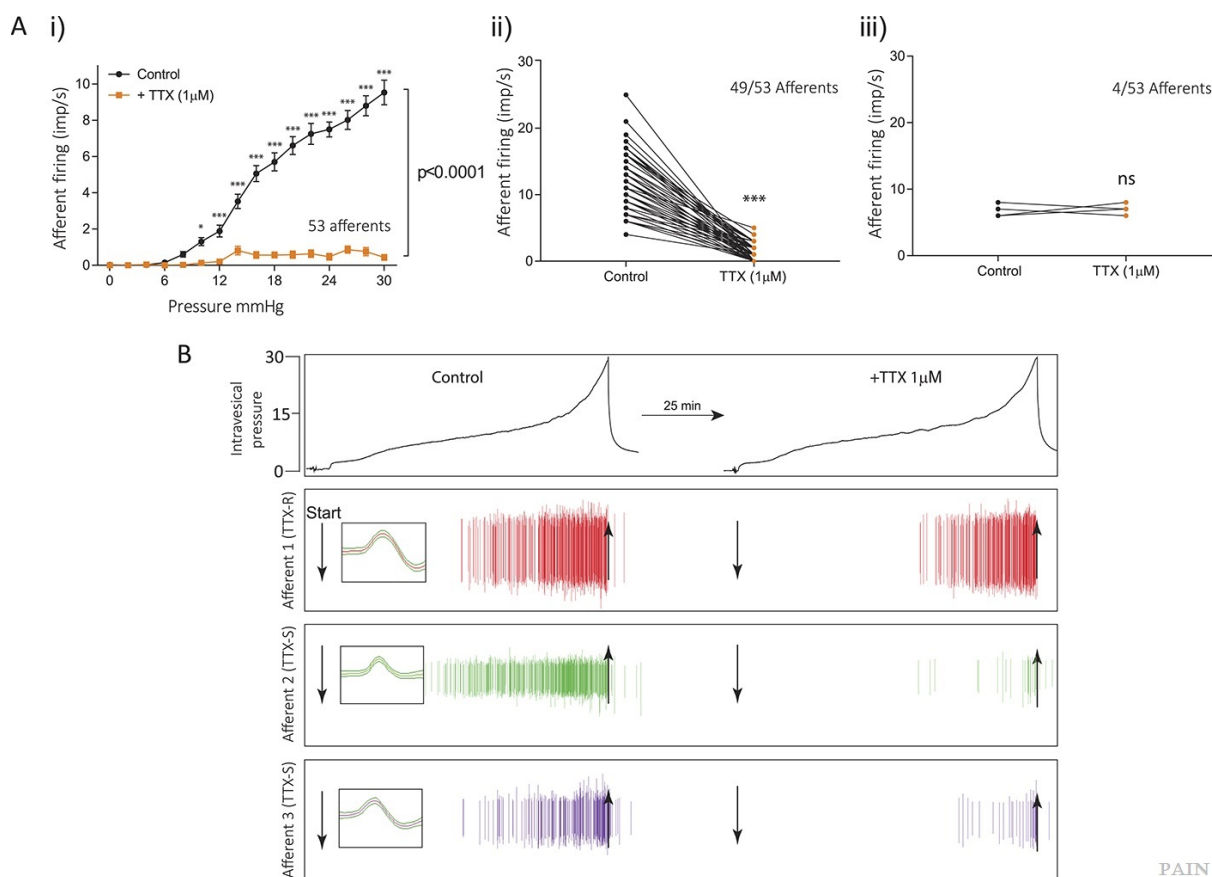

Figure 11.5. Single-unit analysis reveals a predominant TTX-S and minor TTX-R component of bladder afferent responses to distension. (A) Post hoc analysis of multiunit bladder afferent recordings reveals single-unit sensitivity to graded distension before and after intravesical infusion of TTX (1 μM; n = 53 individual bladder afferents from N = 5 mice). (i) When all single units are grouped together, TTX (1 μM) significantly attenuates afferent firing compared with control saline solution (1 μM; ***P < 0.001, repeated-measures 2-way ANOVA, Bonferroni post hoc test). (ii) Individual afferents can be characterised by their responsiveness to TTX. Of 53 single afferents, 49 units showed greater than 50% reductions in mechanosensory responses in the presence of TTX (1 μM) (88.6% mean reduction). (iii) Only 4 afferents maintained sensitivity to distension in the presence of TTX (5.8% mean increase). (B) Original traces of single-unit afferent firing in response to an increase in intravesical pressure. Individual units are determined by spike profile (inserts) and colour coded for ease of discrimination. Each coloured line represents the spike of that individual waveform. Individual units show marked differences in waveform, amplitude, frequency, and mechanosensitivity under control distensions. In these examples, units 2 and 3 show significant sensitivity to TTX, with an almost complete abolishment of action potential firing. Unit 1 shows little sensitivity to TTX and is a rare example of a TTX-R bladder afferent. ANOVA, analysis of variance.

11.4.5 *In vivo* intravesical administration of TTX reduces neuronal activation within the lumbosacral spinal cord in response to noxious bladder distension

Based on our findings that TTX inhibits bladder afferent responses to mechanical distension *ex vivo* and reduces neuronal excitability of bladder DRG neurons *in vitro*, we hypothesised that intrabladder (intravesical) infusion of TTX should correspondingly reduce signalling of noxious bladder distension within the spinal cord *in vivo* (**Figure 11.6**). We identified activated neurons within the dorsal horn of the

lumbosacral spinal cord in response to noxious bladder distension with saline by pERK immunoreactivity. These pERK-activated neurons were located within the superficial dorsal horn and the DGC (**Figure 11.6** A and **B)**. In mice undergoing noxious bladder distension after TTX instillation, significantly fewer dorsal horn neurons were activated within the lumbosacral spinal cord (**Figure 11.6** A and **B)**. The overall reduction in pERK immunoreactivity within the dorsal horn was a result of decreased activation within the DGC (**Figure 11.6** A and **B)**.
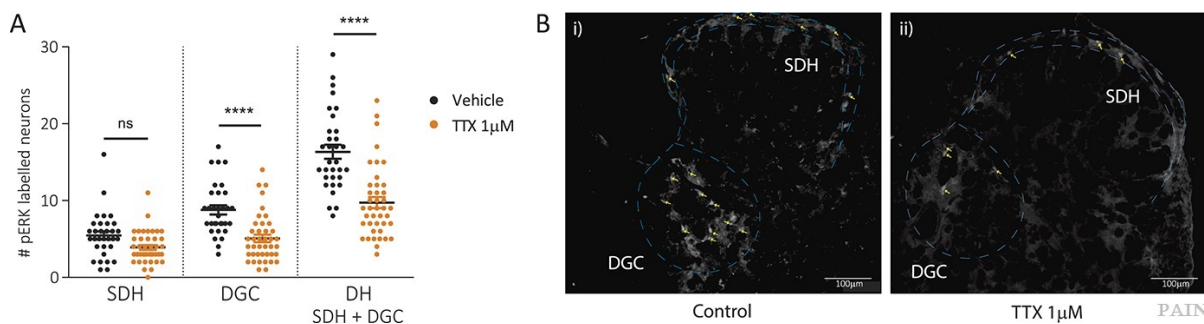

Figure 11.6: Intrabladder TTX reduces nociceptive signalling in the dorsal horn of the spinal cord in response to noxious bladder distension. (A) Noxious bladder distension (60 mm Hg) with saline (black dots) in healthy mice results in activation of dorsal horn (DH) neurons in the lumbosacral (LS) spinal cord, as indicated by pERK immunoreactivity (pERK-IR). In mice undergoing noxious bladder distension (60 mm Hg) with TTX (1 µM, orange dots), significantly fewer DH (SDH + DGC) neurons are activated (**** $P \leq 0.001$, N = 4 mice). There is a significant reduction in the number of pERK-IR neurons in the dorsal gray commissure (DGC) of mice receiving intrabladder TTX compared with saline (*** $P < 0.001$, N = 4 mice). By contrast, there is no significant change in the number of pERK-IR neurons within the superficial dorsal horn (SDH). (B) Example images from the LS spinal cord showing pERK-IR in the absence and presence of TTX. (i) In healthy mice, neurons activated by noxious bladder distension are predominantly located in the SDH and DGC of the dorsal horn. (ii) In the presence of intrabladder TTX (1 µM), the number of pERK-IR dorsal horn neurons is reduced. Blue dashed lines distinguish the boundaries between the DGC and SDH. Yellow arrows indicate activated neurons.

11.5 Discussion

Bladder afferent input into the central nervous system is required for normal bladder function, triggering the autonomic circuits that regulate detrusor relaxation during storage, and at greater intrabladder pressures, to initiate urge sensations necessary for conscious control of micturition.[15] Accordingly, aberrant bladder afferent signalling in preclinical models of bladder inflammation, bladder infection, or pharmacological/genetic modulation correlates with bladder dysfunction.[45-47]

Recently, Na$_v$ channels have been implicated in mediating bladder pain signalling after the successful trial of intravesical neosaxitoxin or lidocaine instillation in patients with IC/BPS.[9,30] However, the precise role of Na$_v$ channels in bladder mechanosensation and nociception has remained unknown. In this study, we show that TTX significantly attenuates *ex vivo* bladder afferent mechanosensitivity to graded distension and nociceptive signalling within the LS dorsal horn *in vivo*, providing the first direct demonstration for a role of Na$_v$ channels in regulating bladder sensation. We also identify, for the first time, the complete profile of Na$_v$ channel coexpression within individual retrogradely traced bladder-innervating DRG neurons. Finally, we confirm the relative proportions of TTX-S and TTX-R Na$_v$ current in bladder-innervating DRG neurons and the significance of TTX-S Na$_v$ channel activation on bladder DRG neuroexcitability. These data highlight the importance of TTX-S Na$_v$ channels in bladder afferent signalling and support a peripheral sensory-mediated mechanism by which neosaxitoxin and lidocaine exert their antinociceptive effect in patients with IC/BPS.

Due to their documented role in action potential activation and propagation, Na$_v$ channels are consistently implicated in mediating nociceptive neurotransmission from the periphery,[11,44] and pharmacological modulation of Na$_v$ channels in both visceral and somatic paradigms supports these findings.[12,24,28] Consumption of the pan-Na$_v$ activators pacific ciguatoxin-1 or veratridine induces severe gastrointestinal dysfunction and abdominal pain in humans and mice.[12] Similarly, the Na$_v$ channel blocker lidocaine can reduce abdominal pain in humans and rodents.[12]

For the first time, we demonstrate a direct role for Na$_v$ channels in mediating bladder afferent signalling, observing enhanced afferent firing to bladder distension after pan-Na$_v$ activation with veratridine and almost ubiquitous sensitivity of mechanosensitive bladder afferents to TTX. The initial effects of both TTX and veratridine occur at similar distension pressures, suggesting that these effects are mediated by the same TTX-S Na$_v$ channels. We found that *in vivo* noxious distension of the bladder predominantly activated neurons in the DGC that were significantly attenuated after TTX instillation. As we observe a significant decrease in bladder afferent firing to graded distension in the presence of TTX *ex vivo*, this observation is likely due to reduced peripheral drive from the bladder to the spinal cord. Peripheral afferents synapse within the spinal dorsal horn and modulate autonomic spinal/brainstem reflex pathways that determine bladder sensation.[15] Postsynaptic DGC neurons project to the nucleus gracilis before continuing on to activate thalamic regions, forming an important pelvic pain pathway.[1,21,43] The DGC is also innervated by projections from preganglionic neurons located within the sacral parasympathetic nucleus of the lumbosacral spinal cord, allowing for coordination of afferent signals with sympathetic and parasympathetic efferent neurons that control bladder detrusor contractions.[15,33,34,39] Likewise, interneurons involved in autonomic bladder function are also located in the lumbosacral DGC and regulate inputs onto preganglionic dendrites.[3,4,15,31,34,41] Thus, we provide evidence that the symptom relief experienced by patients with IC/BPS after lidocaine or neosaxitoxin bladder infusion is due to reduced bladder afferent firing in response to distension and a consequential reduction in spinal cord activation.

Our qRT-PCR data identified abundant Na$_v$ channel expression within lumbosacral DRG but limited expression of Na$_v$ channel subtypes within the bladder mucosa and detrusor. Furthermore, neither TTX nor veratridine effected bladder muscle compliance *ex vivo*, indicating that the changes in mechanosensation we observed with either TTX or veratridine were mediated directly by the primary afferent. Na$_v$ channel expression has not previously been reported in bladder tissue, but we report similar relative Na$_v$ expression to that previously observed for whole-mouse DRG, with Na$_v$1.8 the most ubiquitously expressed subtype.[7] Conversely, our functional data with TTX in afferent studies demonstrate only a small TTX-resistant component. Furthermore, we show that the majority of the sodium current found in bladder-innervating LS DRG neurons is carried by TTX-S Na$_v$ channels. In addition, TTX significantly decreased neuronal excitability of bladder DRG as indicated by an increase in rheobase. Previous studies have shown that the majority of Na$^+$ current in bladder DRG neurons from rats is also TTX-S;[29,48] however, in contrast to the data presented here, the majority of small-diameter bladder-innervating DRG neurons exhibited TTX-R action potentials.[45,46] A recent study reporting Na$_v$ expression in human DRG showed striking species differences in the relative proportion of Na$_v$1.7 and Na$_v$1.8 expression, with Na$_v$1.7 contributing almost 50% of the total percentage expression in humans, compared with 18% in mouse.[7] By contrast, Na$_v$ channel expression in rats seems distinct, with greater expression of TTX-R Na$_v$1.8 and Na$_v$1.9 [22] than both mice and humans, and it may be this differential expression that mediates the dichotomy of TTX sensitivity.

In this study, we identified significant variability in the effect of TTX on rheobase (from 0% to 750% increase) that likely reflects the heterogeneity of Na$_v$ channel coexpression in individual bladder-innervating neurons. These data demonstrate the importance of using single-cell PCR to highlight intricacies that are overlooked by traditional qPCR of whole DRG. The single-cell RT-PCR data revealed coexpression of Na$_v$1.7, Na$_v$1.8, and Na$_v$1.9 in virtually all bladder-innervating DRG neurons, suggesting that the balance of effect may be mediated by the coexpression of the other TTX-S Na$_v$ subtypes. This variable expression also likely mediates the heterogeneity of the calcium responses we and others observed in response to veratridine.[32] Veratridine induced calcium transients in approximately 90% of bladder-innervating DRG, which were abolished by prior incubation with TTX. Veratridine differentially activates TTX-R and TTX-S sodium channel currents when examined under clamped conditions at lower concentrations (25 μM).[13] However, at the concentration used in the current experiments, veratridine has been demonstrated to induce TTX-R calcium transients in DRG neurons, showing that it can open TTX-R channels and induce voltage-gated calcium channel opening in the presence of TTX.[32] However, no TTX-R calcium transients were observed in this study, in contrast to a general population of DRG neurons.[32] These differences may relate to the subpopulation of DRG studied, lumbosacral in the current

study vs all spinal levels in the study by Mohammed et al.[32] that may reflect a greater heterogeneity of neurons, Na_v channel expression, or coexpression, and therefore responses to veratridine.

The ability of TTX to modify bladder afferent responses to distension in this study is likely attributable to a combination of TTX-S Na_v channels, including $Na_v1.1$, $Na_v1.2$, $Na_v1.3$, $Na_v1.4$, $Na_v1.6$, and $Na_v1.7$, which we found to be expressed in a high proportion of bladder-innervating DRG neurons. A polymorphism in the gene *SCN9A*, encoding $Na_v1.7$, correlates with pain perception in a subset of patients with IC/BPS;[36] however, previous characterisation of individuals with *SCN9A* channelopathy-associated insensitivity to pain revealed normal bladder control.[8] Moreover, recent studies using an indirect measure of visceral pain and a conditional nociceptor-specific $Na_v1.7$ knockout mouse ($Na_v1.7^{Nav1.8}$) revealed comparable levels of referred hyperalgesia before and during acute cyclophosphamide-induced cystitis, suggesting $Na_v1.7$ is neither essential in mediating bladder afferent responses to distension nor bladder nociception.[16,23] In this study, we identified 98% of bladder DRG neurons as expressing $Na_v1.7$; however, the current data are inconclusive for a specific role of $Na_v1.7$ in normal or nociceptive bladder signalling.

We see low expression of $Na_v1.2$ in lumbosacral DRG, consistent with its known restricted expression in the central nervous system, and there are currently no functional data to indicate a role for $Na_v1.2$ in peripheral sensory signalling or pain.[11] Similarly, $Na_v1.4$ expression is low within lumbosacral DRG and is expressed in relatively few individual bladder DRG neurons. Consistent with this, $Na_v1.4$ is the predominant isoform in skeletal muscle,[40] and channelopathies of this receptor seem to exclusively involve deficits in skeletal muscle function.[26]

Although no studies have directly investigated a role for $Na_v1.1$ or $Na_v1.6$ in the bladder, experimental evidence in other hollow organs, namely the colon, which shares similarities in afferent function with the bladder, suggests that these isoforms could contribute to the observed effects of TTX.[12,17] Colonic nociception is enhanced in the presence of the selective $Na_v1.1$ agonist δ-theraphotoxin-Hm1a (Hm1a)[35] and reduced by selective inhibition of $Na_v1.1$ by Compound B.[37] In similar experiments, antagonism of $Na_v1.6$ reduced the excitability of stretch-sensitive colorectal afferents *in vitro*.[14] Of the TTX-S Na_v channels we identified in LS DRG, $Na_v1.1$ and $Na_v1.6$ combined contribute ~40% of the total mRNA expression of TTX-S Na_v subunits, whereas ~80% of bladder-innervating DRG neurons express transcripts for $Na_v1.1$ or $Na_v1.6$ and these channels are coexpressed in 86% of bladder DRG neurons.

In conclusion, our findings demonstrate an essential role for Na_v channels in bladder afferent responses to distension and nociceptive signalling into the spinal cord. TTX-S Na_v channels mediate these effects by regulating sodium current and neuronal excitability of bladder sensory afferents. These data represent a novel insight and enhanced understanding of the channels responsible for mediating bladder sensation. Because altered bladder sensory signalling is a trademark of IC/BPS, these data also provide a mechanistic basis for the development of novel therapeutics targeting Na_v channels for the treatment of this disorder.

11.6 Conflict of interest statement

11.7 Acknowledgements

11.8 Supplemental digital content

Supplemental digital content associated with this article can be found online at http://links.lww.com/PAIN/A655.

11.9 References

[1] Al-Chaer ED, Lawand NB, Westlund KN, Willis WD. Pelvic visceral input into the nucleus gracilis is largely mediated by the postsynaptic dorsal column pathway. *J Neurophysiol* 1996;76:2675–90.

[2] Berry SH, Elliott MN, Suttorp M, Bogart LM, Stoto MA, Eggers P, Nyberg L, Clemens JQ. Prevalence of symptoms of bladder pain syndrome/interstitial cystitis among adult females in the United States. *J Urol* 2011; 186:540–4.

[3] Birder LA, de Groat WC. Induction of c-fos expression in spinal neurons by nociceptive and nonnociceptive stimulation of LUT. *Am J Physiol* 1993; 265:R326–33.

[4] Birder LA, Roppolo JR, Erickson VL, de Groat WC. Increased c-fos expression in spinal lumbosacral projection neurons and preganglionic neurons after irritation of the lower urinary tract in the rat. *Brain Res* 1999; 834:55–65.

[5] Catterall WA. Voltage-gated sodium channels at 60: structure, function and pathophysiology. *J Physiol* 2012;590:2577–89.

[6] Catterall WA, Goldin AL, Waxman SG. International Union of Pharmacology. XLVII. Nomenclature and structure-function relationships of voltage-gated sodium channels. *Pharmacol Rev* 2005;57:397–409.

[7] Chang W, Berta T, Kim YH, Lee S, Lee SY, Ji RR. Expression and role of voltage-gated sodium channels in human dorsal root ganglion neurons with special focus on $Na_v1.7$, species differences, and regulation by paclitaxel. *Neurosci Bull* 2018;34:4–12.

[8] Cox JJ, Reimann F, Nicholas AK, Thornton G, Roberts E, Springell K, Karbani G, Jafri H, Mannan J, Raashid Y, Al-Gazali L, Hamamy H, Valente EM, Gorman S, Williams R, McHale DP, Wood JN, Gribble FM, Woods CG. An *SCN9A* channelopathy causes congenital inability to experience pain. *Nature* 2006;444:894.

[9] Cvach K, Rosamilia A. Review of intravesical therapies for bladder pain syndrome/interstitial cystitis. *Transl Androl Urol* 2015;4:629–37.

[10] de Groat WC, Yoshimura N. Afferent nerve regulation of bladder function in health and disease. *Handb Exp Pharmacol* 2009;194:91–138.

[11] Dib-Hajj SD, Cummins TR, Black JA, Waxman SG. Sodium channels in normal and pathological pain. Annu Rev Neurosci 2010;33:325–47.

[12] Erickson A, Deiteren A, Harrington AM, Garcia-Caraballo S, Castro J, Caldwell A, Grundy L, Brierley SM. Voltage-gated sodium channels: (Na_v)igating the field to determine their contribution to visceral nociception. *J Physiol* 2018;596:785–807.

[13] Farrag KJ, Bhattacharjee A, Docherty RJ. A comparison of the effects of veratridine on tetrodotoxin-sensitive and tetrodotoxin-resistant sodium channels in isolated rat dorsal root ganglion neurons. *Pflugers Arch* 2008; 455:929–38.

[14] Feng B, Zhu Y, La JH, Wills ZP, Gebhart GF. Experimental and computational evidence for an essential role of $Na_v1.6$ in spike initiation at stretch-sensitive colorectal afferent endings. *J Neurophysiol* 2015;113: 2618–34.

[15] Fowler CJ, Griffiths D, de Groat WC. The neural control of micturition. *Nat Rev Neurosci* 2008;9:453–66.

[16] Gonzalez-Cano R, Tejada MA , Artacho-Cordon A, Nieto FR, Entrena JM, Wood JN, Cendan CM. Effects of tetrodotoxin in mouse models of visceral pain. *Mar Drugs* 2017;15:188.

[17] Grundy L, Brierley SM. Cross-organ sensitization between the colon and bladder: to pee or not to pee? *Am J Physiol Gastrointest Liver Physiol* 2018;314:G301–8.

[18] Grundy L, Daly DM, Chapple C, Grundy D, Chess-Williams R. TRPV1 enhances the afferent response to P2X receptor activation in the mouse urinary bladder. *Sci Rep* 2018;8:197.

[19] Harrington AM, Brierley SM, Isaacs N, Hughes PA, Castro J, Blackshaw LA. Sprouting of colonic afferent central terminals and increased spinal MAP kinase expression in a mouse model of chronic visceral hypersensitivity. *J Comp Neurol* 2012;520:2241–55.

[20] Harrington AM, Brierley SM, Isaacs NJ, Young RL, Blackshaw LA. Identifying spinal sensory pathways activated by noxious esophageal acid. *Neurogastroenterol Motil* 2013;25:e660–668.

[21] Hirshberg RM, Al-Chaer ED, Lawand NB, Westlund KN, Willis WD. Is there a pathway in the posterior funiculus that signals visceral pain? *PAIN* 1996;67:291–305.

[22] Ho C, O'Leary ME. Single-cell analysis of sodium channel expression in dorsal root ganglion neurons. *Mol Cell Neurosc*i 2011;46:159–66.

[23] Hockley JRF, Gonzalez-Cano R, McMurray S, Tejada-Giraldez MA, McGuire C, Torres A, Wilbrey AL, Cibert-Goton V, Nieto FR, Pitcher T, Knowles CH, Baeyens JM, Wood JN, Winchester WJ, Bulmer DC, Cendan CM, McMurray G. Visceral and somatic pain modalities reveal Na$_v$1.7-independent visceral nociceptive pathways. *J Physiol* 2017;595: 2661–79.

[24] Inserra MC, Israel MR, Caldwell A, Castro J, Deuis JR, Harrington AM, Keramidas A, Garcia-Caraballo S, Maddern J, Erickson A, Grundy L, Rychkov GY, Zimmermann K, Lewis RJ, Brierley SM, Vetter I. Multiple sodium channel isoforms mediate the pathological effects of Pacific ciguatoxin-1. *Sci Rep* 2017;7:42810.

[25] Jami S, Erickson A, Brierley S, Vetter I. Pain-causing venom peptides: insights into sensory neuron pharmacology. *Toxins* (Basel) 2018;10:15.

[26] Jurkat-Rott K, Holzherr B, Fauler M, Lehmann-Horn F. Sodium channelopathies of skeletal muscle result from gain or loss of function. *Pflugers Archiv* 2010;460:239–48.

[27] Kim SH, Kim TB, Kim SW, Oh SJ. Urodynamic findings of the painful bladder syndrome/interstitial cystitis: a comparison with idiopathic overactive bladder. *J Urol* 2009;181:2550–4.

[28] King GF, Vetter I. No gain, no pain: Na$_v$1.7 as an analgesic target. *ACS Chem Neurosci* 2014;5:749–51.

[29] Lei Q, Malykhina AP. Colonic inflammation up-regulates voltage-gated sodium channels in bladder sensory neurons via activation of peripheral transient potential vanilloid 1 receptors. *Neurogastroenterol Motil* 2012; 24:575–e257.

[30] Manriquez V, Castro Caperan D, Guzman R, Naser M, Iglesia V, Lagos N. First evidence of neosaxitoxin as a long-acting pain blocker in bladder pain syndrome. *Int Urogynecol J* 2015;26:853–8.

[31] Marson L. Identification of central nervous system neurons that innervate the bladder body, bladder base, or external urethral sphincter of female rats: a transneuronal tracing study using pseudorabies virus. *J Comp Neurol* 1997;389:584–602.

[32] Mohammed ZA, Doran C, Grundy D, Nassar MA. Veratridine produces distinct calcium response profiles in mouse Dorsal Root Ganglia neurons. *Sci Rep* 2017;7:45221.

[33] Morgan CW, De Groat WC, Felkins LA, Zhang SJ. Intracellular injection of neurobiotin or horseradish peroxidase reveals separate types of preganglionic neurons in the sacral parasympathetic nucleus of the cat. *J Comp Neurol* 1993;331:161–82.

[34] Nadelhaft I, Vera PL, Card JP, Miselis RR. Central nervous system neurons labelled following the injection of pseudorabies virus into the rat urinary bladder. *Neurosci Lett* 1992;143:271–4.

[35] Osteen JD, Herzig V, Gilchrist J, Emrick JJ, Zhang C, Wang X, Castro J, Garcia-Caraballo S, Grundy L, Rychkov GY, Weyer AD, Dekan Z, Undheim EAB, Alewood P, Stucky CL, Brierley SM, Basbaum AI, Bosmans F, King GF, Julius D. Selective spider toxins reveal a role for Na$_v$1.1 channel in mechanical pain. *Nature* 2016;534:494–9.

[36] Reeder JE, Byler TK, Foster DC, Landas SK, Okafor H, Stearns G, Wood RW, Zhang Y, Mayer RD. Polymorphism in the SCN9A voltage-gated sodium channel gene associated with interstitial cystitis/bladder pain syndrome. *Urology* 2013;81:210.e211–214.

[37] Salvatierra J, Castro J, Erickson A, Li Q, Braz J, Gilchrist J, Grundy L, Rychkov GY, Deiteren A, Rais R, King GF, Slusher BS, Basbaum A, Pasricha PJ, Brierley SM, Bosmans F. Na$_v$1.1 inhibition can reduce visceral hypersensitivity. *JCI Insight* 2018;3:121000.

[38] Suskind AM, Berry SH, Ewing BA, Elliott MN, Suttorp MJ, Clemens JQ. The prevalence and overlap of interstitial cystitis/bladder pain syndrome and chronic prostatitis/chronic pelvic pain syndrome in men; results of the RAND Interstitial Cystitis Epidemiology (RICE) male study. *J Urol* 2013;189:141–5.

[39] Thor KB, de Groat WC. Neural control of the female urethral and anal rhabdosphincters and pelvic floor muscles. *Am J Physiol Regul Integr Comp Physiol* 2010;299:R416–38.

[40] Trimmer JS, Cooperman SS, Agnew WS, Mandel G. Regulation of muscle sodium channel transcripts during development and in response to denervation. *Dev Biol* 1990;142:360–7.

[41] Vizzard MA, Erickson VL, Card JP, Roppolo JR, Groat WCd. Transneuronal labeling of neurons in the adult rat brainstem and spinal cord after injection of pseudorabies virus into the urethra. *J Comp Neurol* 1995;355:629–40.

[42] Waxman SG, Merkies IS, Gerrits MM, Dib-Hajj SD, Lauria G, Cox JJ, Wood JN, Woods CG, Drenth JP, Faber CG. Sodium channel genes in pain-related disorders: phenotype-genotype associations and recommendations for clinical use. *Lancet Neurol* 2014;13:1152–60.

[43] Willis WD Jr. A novel visceral pain pathway in the posterior funiculus of the spinal cord. *J Med Sci* 2009;1:33–37.

[44] Wood JN, Boorman JP, Okuse K, Baker MD. Voltage-gated sodium channels and pain pathways. *J Neurobiol* 2004;61:55–71.

[45] Yoshimura N, Bennett NE, Hayashi Y, Ogawa T, Nishizawa O, Chancellor MB, de Groat WC, Seki S. Bladder overactivity and hyperexcitability of bladder afferent neurons after intrathecal delivery of nerve growth factor in rats. *J Neurosci* 2006;26:10847–55.

`

[46] Yoshimura N, de Groat WC. Increased excitability of afferent neurons innervating rat urinary bladder after chronic bladder inflammation. *J Neurosci* 1999;19:4644–53.

[47] Yoshimura N, Oguchi T, Yokoyama H, Funahashi Y, Yoshikawa S, Sugino Y, Kawamorita N, Kashyap MP, Chancellor MB, Tyagi P, Ogawa T. Bladder afferent hyperexcitability in bladder pain syndrome/interstitial cystitis. *Int J Urol* 2014;21(suppl 1):18–25.

[48] Yoshimura N, Seki S, Novakovic SD, Tzoumaka E, Erickson VL, Erickson KA, Chancellor MB, de Groat WC. The involvement of the tetrodotoxin-resistant sodium channel $Na_v1.8$ (PN3/SNS) in a rat model of visceral pain. J Neurosci 2001;21:8690–6.

Chapter 12 Discussion

Visceral pain is a symptom of gastrointestinal disorders such as irritable bowel syndrome (IBS) and inflammatory bowel disease. Investigation of mechanisms of visceral pain and evaluation of analgesics specific for visceral pain has been challenging due to the internal site(s) of origin, diffuse sensory output from visceral organs, and the complexity in causes of gastrointestinal disorders and visceral pain. Research has identified several contributing factors to chronic pain experienced in the colon and bladder, including infection, inflammation, long-term plasticity of sensory afferents, neuro-immune interactions, neuro-epithelial interactions, stress, microbiome-related changes, and cancer (**Chapter 1**). In the search for better suited analgesics for visceral pain, a range of rodent models of visceral pain conditions have been developed. For colon-specific pain, models include chemically-induced colitis, pathogen-induced colitis, maternal separation, stress, diabetes, and colonic obstruction (Brierley & Linden 2014; Jiminez et al. 2015; Moloney, Rachel D. et al. 2015). For bladder-specific pain, models include chemically-induced cystitis, colitis-induced comorbidity, and stress (Birder & Andersson 2018). A range of cell membrane receptors has been investigated for the contribution to visceral pain and potential as suitable visceral pain targets (Sadeghi et al. 2018). Members of the voltage-gated sodium (Na_v) channel family ($Na_v1.1$-$Na_v1.9$) enable signal generation in all excitable cells, and have been researched extensively for their contribution to somatic pain disorders, and increasingly also in visceral pain disorders (**Chapter 2**). The work presented in this thesis was designed to investigate electrophysiological characteristics of colon-innervating neurons from mice with chronic visceral hypersensitivity (CVH) following chemically-induced colitis (section 12.1), and evaluate the effects of selective Na_v channel modulation on electrophysiological properties in colon-innervating and bladder-innervating neurons (section 12.2).

12.1 Electrophysiological properties in thoracolumbar and lumbosacral colon-innervating dorsal root ganglia neurons from healthy and chronic visceral hypersensitivity mice

In vivo measures of hypersensitivity in animal models, such as abdominal muscle contraction in response to colorectal distension, or the number of nocifensive behaviors in response to intracolonic instillation of a compound, have enabled *in vivo* screening of novel analgesics (Grundy et al. 2018). However, to be able to draw conclusions about the molecular mechanism of hypersensitivity and drug responses, the study of hypersensitivity on the order of a tissue, system, or single-cell level is necessary. In this thesis, long-term plasticity of visceral sensory neurons *in vitro* in a chemically induced colitis mouse model of *in vivo* hypersensitivity was evaluated. Four measures of neuronal hypersensitivity in colon-innervating dorsal root ganglia (DRG) neurons were selected and evaluated based on previously published findings using similar visceral hypersensitivity models: 1) the minimum current required to elicit an action potential (rheobase); 2) the number of neurons eliciting multiple action potentials at 2-times rheobase; 3) the peak sodium current density; and 4) the effect of a Na_v channel blocker, tetrodotoxin (TTX), on rheobase and the peak sodium current density. Expression levels of genes encoding Na_v channels in thoracolumbar (TL) and lumbosacral (LS) DRG, and in colon-innervating TL DRG between healthy and CVH mice were also evaluated.

12.1.1 TNBS treatment induced post-colitis visceral hypersensitivity *in vivo*

A trinitrobenzenesulfonic acid (TNBS)-induced colitis model was used to study the effect of CVH on colon-innervating sensory neurons in mice. In this model, TNBS suspended in ethanol is administered intracolonically, which is known to cause inflammation of the colonic epithelium and mucosa (Antoniou et al. 2016). In most cases, the local inflammation resolves without intervention by 28 days post TNBS, a timepoint where visceral hypersensitivity is present and histological signs of inflammation are absent (Castro et al. 2017; Hughes et al. 2009). All TNBS-treated mice included in this thesis exhibited weight loss following treatment, which was -8.3 ± -3.0% on average and lasted for 4 ± 3 days (**Table 4.2**). Mice also exhibited clinical signs of colitis, including diarrhea and constipation. Mice from a subset of TNBS treatment cohorts used in electrophysiology experiments exhibited enhanced visceromotor responses to colorectal distension compared to healthy mice 28 days post TNBS treatment (**Figure 10.4**) (Grundy et al. 2018), a common measure of *in vivo* hypersensitivity in chronic visceral pain models. Taken together,

143

these measurements support the use of this model to study the effect of post-colitis visceral hypersensitivity on colon-innervating sensory neurons in mice.

12.1.2 TNBS treatment was not associated with Na$_v$ channel mRNA abundance in thoracolumbar or lumbosacral dorsal root ganglia or with colon-innervating dorsal root ganglia single-cell expression percentages

Several studies have found changes in Na$_v$ channel gene expression in visceral pain models (**Table 2.2**), although this does not necessarily appear to be correlated with an electrophysiological response. The expression of Na$_v$ channel isoforms and the four auxiliary β-subunits (β1-β4) in TL and LS DRG from healthy and CVH mice was measured to gain an overview of Na$_v$ channel abundance in the experimental line. Individual TL colon-innervating DRG neurons from healthy and CVH mice were also collected and gene expression of Na$_v$ isoforms and β-subunits was measured to compare with the electrophysiological and pharmacological data. Na$_v$1.8 was the most abundant isoform in TL and LS DRG from healthy and CVH mice, followed by Na$_v$1.7, Na$_v$1.9, and Na$_v$1.1 (**Figure 5.1**). These findings correspond well with gene expression data obtained by others (Chang et al. 2018; Inserra et al. 2017). At the single-cell level, the majority of neurons expressed Na$_v$1.7, Na$_v$1.8, and Na$_v$1.9, and approximately one third expressed Na$_v$1.1 (**Figure 5.2**), which is in agreement with previously published results (Hockley, James R. F. et al. 2017). It was also discovered that the majority (> 70%) of colon-innervating TL and LS neurons from healthy mice expressed β1, β2, and β3 transcripts, whereas approximately one third expressed the β4 transcript. There was insufficient evidence to support any differences in abundance of Na$_v$ channel isoforms between DRG from healthy and CVH mice from the TL (**Table 5.1**) and LS (**Table 5.2**) regions. Similarly, there were no indications of a change in the percentage of neurons that expressed each Na$_v$ channel between colon-innervating TL DRG neurons from healthy and CVH mice (**Table 5.3**). Taken together, the majority of Na$_v$ channels and the four main β-subunits were identified in whole TL and LS DRG, and in DRG neurons specifically innervating the colon, however, a TNBS-related difference in Na$_v$ channel expression was not evident in the dataset.

12.1.3 Duration in culture and soma diameter can affect electrophysiological properties of colon-innervating dorsal root ganglia neurons.

Multivariable regression analyses showed that several variables are associated with rheobase levels and peak sodium current density in colon-innervating DRG neurons. The number of days (1 vs 2) following dissociation of DRG neurons was significantly associated with rheobase levels and peak sodium current density; neurons recorded on day 2 post culture (38 – 48 hrs) were more likely to exhibit a higher rheobase and a greater peak sodium current density compared to neurons recorded on day 1 (16 – 28 hrs). This pattern has previously been reported for DRG neurons between acute dissociation and day 1 following dissociation (Song et al. 2018). The difference in active electrophysiological properties as a function of time in culture may be related to changes in ion channel expression due to growth factors in culturing media. Furthermore, primary neuron cultures develop neuronal processes over time (see **Figure 4.1** for an example image of immediately dissociated neurons compared 2 days following dissociation), which reflects changes in cellular processes that can affect ion channel expression. A significant association of rheobase levels with soma diameter and resting membrane potential was obtained, where smaller diameter neurons and neurons with a more depolarized resting membrane potential were more likely to have a low rheobase (**Table 5.7**). Similar findings of diameter and neuronal excitability in DRG neurons have been reported (Gong et al. 2014; Song et al. 2018). Taken together, these findings demonstrate that several variables can influence electrophysiological responses obtained in patch-clamp recordings of primary neurons, which may be considered when comparing neuronal populations to strengthen conclusions of results.

12.1.4 TNBS treatment was not associated with rheobase levels in colon-innervating dorsal root ganglia neurons

Allodynia, the experience of pain sensation in response to stimuli that under normal circumstances would not be perceived as painful, has been described for IBS patients in response to colorectal distension (Mayer et al. 2008). In electrophysiology terms, allodynia can be explained as a lowering of the threshold

`

for action potential generation in neurons that generate, relay, or receive pain signals. Generation of action potentials follows an all-or-none principle, and two measures of the threshold for action potential generation are often used to reflect neuronal excitability: the threshold value (in volts) or the minimum amount of current required to elicit an action potential (in amperes), also known as the rheobase. Several studies on acute and post-inflammatory visceral pain models in rodents have reported a reduction in rheobase in colon-innervating DRG neurons during the acute phase of TNBS-induced colitis (Beyak et al. 2004) and dextran sodium sulfate-induced colitis in mice (R Abdrakhmanova et al. 2010), and during experimentally induced diabetes in rats (Hu, J et al. 2016; Meerupally, Singh & Sharma 2014). Rheobase levels in colon-innervating DRG neurons from the TL and LS spinal levels from healthy and CVH mice were investigated (**Table 5.5**). Multivariable regression analysis was applied to correct for variables that could confound the effect of health status on rheobase (analyzed as the natural log value), which included spinal level (TL vs LS), soma diameter, resting membrane potential, and number of days in culture. In this analysis, there was insufficient evidence to support an effect of the TNBS treatment on rheobase levels (**Table 5.7**). In summary, a TNBS-related reduction in rheobase levels in colon-innervating DRG neurons from mice was not observed.

12.1.5 TNBS treatment was not associated with a higher number of action potentials at 2-times rheobase in colon-innervating dorsal root ganglia neurons

Hyperalgesia refers to an elevated perception of painful stimuli. This phenomenon is often observed in patients with chronic pain, particularly following treatment with opioids (Ji et al. 2018; Stoicea et al. 2015), and has been reported for patients with IBS (Mohammad et al. 2016). The firing rate (action potentials per unit time) in nociceptive neurons is believed to be related to the intensity of pain (Dubin & Patapoutian 2010; Momin & McNaughton 2009). Studies that demonstrated a reduction in rheobase in visceral hypersensitivity models also found an increase in the percentage of neurons that elicited multiple action potentials at 2-times rheobase (Beyak et al. 2004; R Abdrakhmanova et al. 2010). To evaluate enhanced firing in colon-innervating DRG neurons from CVH mice, the number of action potentials elicited at 2-times rheobase was measured. There was no statistically significant increase in the percentage of neurons that elicited multiple action potentials compared to a single action potential at 2-times rheobase in neurons from CVH mice compared to healthy mice in this data (**Table 5.9**). In summary, a TNBS-related increase in the proportion of neurons eliciting multiple action potentials at 2-times rheobase in colon-innervating TL and LS DRG neurons from mice was not evident.

12.1.6 TNBS treatment was not associated with peak sodium current density in colon-innervating dorsal root ganglia neurons

Na_v channels are highly sensitive to small depolarizations and facilitate the rising phase of action potential generation in mammalian neurons (Bean 2007). Human genetic studies have shown that gain-of-function mutations in Na_v channel isoforms underlie enhanced pain disorders such as erythromelalgia, paroxysmal extreme pain disorder, and painful neuropathy (Emery, Luiz & Wood 2016; Faber et al. 2012; Huang et al. 2014), whereas loss-of-function mutations in the $Na_v1.7$ isoform is related to congenital insensitivity to pain (Cox et al. 2006; Goldberg et al. 2007). Collectively, these findings indicate that there is a direct link between Na_v channel activity and nociceptive signaling. Increased peak sodium current density in colon-innervating DRG neurons from rodents with visceral hypersensitivity has been reported and may be related to the neuronal excitability in these studies (Beyak et al. 2004; Qu et al. 2013). To investigate the role of Na_v channels in neurons from TNBS-treated mice, peak sodium currents in colon-innervating TL and LS DRG neurons from healthy and CVH mice were measured (**Table 5.10**). Multivariable regression analysis with the dependent variable peak sodium current density was run with health status, spinal level, and number of days in culture as the independent variables. In this analysis, no evidence to support an effect of the TNBS treatment on peak sodium current density was obtained (**Table 5.12**). In summary, although Na_v channel isoforms and Na^+ currents are involved in pain signaling, a TNBS-related change in peak sodium current in colon-innervating DRG neurons from mice was not supported.

12.1.7 TNBS treatment was not associated with a change in the tetrodotoxin-resistant component of peak sodium current density

Several studies on inflammatory and non-inflammatory pain models in rodents have found differences in voltage-gated Na^+ channel components that are sensitive and resistant to the Na_v inhibitor tetrodotoxin (TTX) in pathological states (**Table 2.2**). TTX is a potent inhibitor of $Na_v1.1$, $Na_v1.2$, $Na_v1.3$, $Na_v1.4$, $Na_v1.6$ and $Na_v1.7$, and has very low affinity for $Na_v1.5$, $Na_v1.8$, and $Na_v1.9$ (Goldin 2001). Increases in the TTX-resistant (TTX-R) fraction of total sodium current has been reported in studies on colon-innervating DRG neurons from mice with acute TNBS-induced colitis (Beyak et al. 2004), and in colon-innervating DRG neurons from rats following maternal separation-induced visceral hypersensitivity (Hu, S et al. 2013), streptozotocin-induced diabetes (Hu, J et al. 2016), and partial colonic obstruction (Lin et al. 2017). In these studies, the enhanced TTX-R component of total current was postulated to be associated with enhanced neuronal activity and visceral hyperalgesia. In contrast to these studies, no association between the magnitude of the TTX-R component of total current and TNBS treatment (section 7.5), nor in the fold-change in rheobase in the presence of TTX (**Table 7.5**) was obtained in the work presented in this thesis. Furthermore, there was no association between TNBS treatment and the fold-change in rheobase and reduction in peak sodium current density in the presence of a more selective Na_v-modulator, Hs1a (section 8.5). Taken together, while TTX-sensitive or TTX-resistant channels may contribute to pathological pain conditions, there was insufficient evidence to support a TNBS-related change in the sensitivity to TTX in colon-innervating DRG neurons from mice.

12.1.8 Colon-innervating lumbosacral and thoracolumbar dorsal root ganglia neurons exhibit differences in electrophysiological properties and tetrodotoxin-sensitivity

Based on multivariable regression analyses, the variable that had the highest impact on rheobase levels in colon-innervating dorsal root ganglia neurons was whether neurons had a TL or LS origin. LS neurons had, on average, a significantly lower rheobase compared to TL neurons when all other variables were held constant (**Table 5.7**). This result corresponds well with the theory that pelvic nerves (terminating in the LS region) predominantly relay physiological stimuli, whereas splanchnic nerves (terminating in the TL region) also relay noxious stimuli. This theory is further supported by the finding that pelvic nerves predominantly contain low-threshold afferents, whereas splanchnic nerves also contain a population of high-threshold afferents (Brierley et al. 2004). It was also discovered that incubation with TTX had a greater effect on rheobase (section 7.6) and peak sodium current (section 7.5) in LS neurons compared to TL neurons. Although Na_v channel expression, specifically, has not been compared between colon-innervating TL and LS neurons, clustering analyses have identified several non-overlapping neuronal subtypes in terms of gene expression between these two populations (Hockley, J. R. F. et al. 2018). Taken together, these findings support a functional distinction between TL and LS DRG neurons that is evident *in vitro*.

12.1.9 Potentially confounding variables of *in vitro* hyperexcitability that were not considered in regression analyses include strain variation, dietary changes and stress

Four measures of neuronal hypersensitivity in colon-innervating DRG neurons were evaluated; rheobase, action potential firing rate at 2-times rheobase, peak sodium current density, and TTX-sensitivity. In these analyses, insufficient evidence to support an effect of TNBS treatment on the response variables was obtained. Collectively, these findings contrast to previously published results that demonstrate a change in at least one of the aforementioned variables in colon-innervating neurons in experimentally induced CVH. While it is possible that *in vitro* hypersensitivity is not a stable measurement in post-colitis visceral hypersensitivity models, the influence of other factors that may have affected the disease model cannot be excluded. Other factors may include strain variation and the degree of outbreeding, which can significantly influence the response to experimental colitis (Moloney, R. D., Dinan & Cryan 2015; te Velde, Verstege & Hommes 2006). A change in the standardized diet of the animal facility was also in process, which can alter the gut mucus layer and microbiome composition (Desai et al. 2016) and introduce changes in visceral sensitivity. Stress is also a factor that can have unforeseen effects on experimentally induced visceral hypersensitivity in mice under certain circumstances (Larauche et al. 2010; Larsson, Miketa & Martinez 2009), and may have incurred during an extended facility restructuring process.

12.2 Pharmacological modulation of Na$_v$ isoforms in colon-innervating thoracolumbar and lumbosacral dorsal root ganglia neurons from mice

The search for a compound that is selective for a single pain target such as Na$_v$1.7 without affecting other Na$_v$ isoforms that could have deleterious effects, such as disruption of cardiac activity via Na$_v$1.5, skeletal muscle activity via Na$_v$1.4, or central processes via Na$_v$1.1 and Na$_v$1.6, has been the focus of research in the past two decades. In this search, there have been extensive investigations into naturally occurring neurotoxins, modifications to and repurposing of existing compounds. Despite the discovery of predominantly Na$_v$1.7-selective compounds, such as a monoclonal antibody (Lee et al. 2014), the aryl sulfonamide PF-05089771 (Alexandrou et al. 2016), and the spider venom peptide Pn3a (Deuis et al. 2017), administration of these and other Na$_v$1.7-selective compounds has not been able to demonstrate adequate analgesia in preclinical studies or in clinical trials (McDonnell et al. 2018). Furthermore, peripherally restricted Na$_v$1.7 knock-out models do not reflect the human loss-of-function phenotype (Minett et al. 2012). For these reasons, the focus of Na$_v$ modulation as a therapeutic strategy may benefit from moving away from the single-isoform approach to one that focuses more on optimizing and localizing target site delivery.

In conditions where pain originates in a low permeability organ, such as the colon or bladder, the issue of selectivity of a compound across Na$_v$ isoforms is potentially a less critical condition compared to systemic delivery. This is exemplified by the finding that bladder infiltration with neosaxitoxin, a Na$_v$ pore blocker, produced analgesia in patients with interstitial cystitis/bladder pain syndrome (Manriquez et al. 2015), and that subcutaneous injections of TTX reduced chemically-induced acute visceral pain in mice (González-Cano et al. 2017) and cancer-related pain in patients (Hagen, Neil A. et al. 2017; Hagen, N. A. et al. 2011). Another strategy in providing pain relief in gastrointestinal illness is by localized delivery of compounds with limited absorption, such as peptides. This study evaluated the effect of seven Na$_v$-modulating compounds on active electrophysiological properties in colon-innervating DRG neurons, and the effect of one Na$_v$-modulating compound on active electrophysiological properties in bladder-innervating DRG neurons.

12.2.1 Veratridine induces membrane depolarization and decreases action potential overshoot in colon-innervating dorsal root ganglia neurons

Veratridine is a non-selective Na$_v$ channel agonist that has been used in high-throughput screening of novel Na$_v$ modulators for pain therapeutics (Deuis et al. 2017; Klint et al. 2015). Veratridine is a lipid-soluble alkaloid neurotoxin found in the seeds of lilaceous plants and is believed to interact with Na$_v$ channels through neurotoxin site 2, which is accessible from the cell membrane and comprises the S6 segments of domains I and IV, and possibly also II and III (Stevens, Peigneur & Tytgat 2011; Ulbricht, W. 1998; Wang & Wang 2003). Veratridine is only able to bind Na$_v$ channels in the open conformation, likely due to steric hindrances of the S6 segment during closed and inactivated conformations. Furthermore, the re-entrant loop of S5-S6 comprises the ion selectivity filter, which may explain why veratridine also impairs ion permeation, leading to a reduction in peak sodium current density (Ulbricht, Werner 2005).

Veratridine at 50 µM significantly reduced action potential overshoot and depolarized the membrane potential following generation of the first action potential in colon-innervating TL and LS DRG neurons (**Figure 6.1**). The estimated reduction in action potential overshoot in the presence of veratridine was 18% on average, and the change in membrane potential was 0.63-fold on average, in colon-innervating DRG neurons. The reduction in overshoot is likely due to the impairment of sodium permeation by veratridine, and the depolarization following the first action potential reflects the open-state preference. The membrane potential repolarized in subsequent current applications (**Figure 6.1 Eii**) and approached baseline levels during washout. Veratridine also increased action potential half-width in the lumbosacral subset, which likely reflects the impairment of steady-state fast inactivation by veratridine. Finally, only modest effects of veratridine on rheobase were observed, which is consistent with the state-dependent mechanism for this modulator. In summary, veratridine induces membrane depolarization and decreases action potential overshoot in colon-innervating DRG neurons from mice.

12.2.2 OD1 reduces rheobase and increases action potential half-width in colon-innervating dorsal root ganglia neurons

To build on the finding that veratridine exerted substantial effects on action potential generation in colon-innervating neurons, action potential generation in the presence of a more selective Na_v agonist was investigated. OD1 is a scorpion venom peptide isolated from *Odonthobuthus doriae* and exhibits characteristics of both α-scorpion and β-scorpion toxins. The α-scorpion toxins interact with neurotoxin site 3, which is comprised of the S5-S6 pore loops of domain I and IV and the voltage sensor S3-S4 linker region in domain IV (Cestele & Catterall 2000; Durek et al. 2013; Stevens, Peigneur & Tytgat 2011), and β-scorpion toxins interact with neurotoxin site 4, which comprises S1-S2 and S3-S4 of domain II (Stevens, Peigneur & Tytgat 2011). In line with α- and β-scorpion toxin mechanisms, OD1 impairs steady-state fast inactivation and hyperpolarizes steady-state activation of targeted Na_v channels (Durek et al. 2013). Patch-clamp studies using heterologous expression systems have found that OD1 has nanomolar potentiating effects on $Na_v1.4$ (EC_{50} = 9.6 ± 0.1 nM), $Na_v1.6$ (EC_{50} = 30 ± 1 nM) and $Na_v1.7$ (EC_{50} = 8 ± 1 nM) (Durek et al. 2013). The compound is much less sensitive to $Na_v1.3$ and $Na_v1.5$ (EC_{50} > 1 μM), and inactive on $Na_v1.2$ and $Na_v1.8$ (Jalali et al. 2005; Maertens et al. 2006).

In the presence of 30 nM OD1, colon-innervating DRG neurons exhibited a significantly lower rheobase and an increase in the action potential half-width in the form of a prolonged repolarization phase, without changes in action potential overshoot (**Figure 6.2**). The estimated fold change in rheobase in the presence of OD1 was 0.76 and the action potential half-width was increased by on average 1.9-fold in colon-innervating DRG neurons. The extension of the repolarization phase is likely via impairment of Na_v channel inactivation, as observed with other neurotoxin site 3 peptide toxins such as the spider venom peptide Hm1a and the sea anemone peptide ATX-II on primary neurons (Browne, L, Smith & Jagger 2017; Osteen et al. 2016). These findings confirm that one or more of $Na_v1.4$, $Na_v1.6$, and $Na_v1.7$ contribute to action potential generation in dissociated colon-innervating DRG neurons from mice.

12.2.3 Tetrodotoxin increases rheobase and reduces peak sodium current density in colon-innervating and bladder-innervating dorsal root ganglia neurons

TTX is a neurotoxin produced by symbiotic bacteria carried by marine species, such as pufferfish, blue ringed octopus, and starfish, where it is believed to confer defense against predation (Soong & Venkatesh 2006). TTX acts as a pore blocker by binding re-entrant loop regions between S5-S6 from the four Na_v domains, which confer ion selectivity and conductance (Klint et al. 2012). Interaction in this site impairs sodium conductance, leading to a reduction in peak sodium current. TTX is a potent inhibitor of $Na_v1.1$, $Na_v1.2$, $Na_v1.3$, $Na_v1.4$, $Na_v1.6$, and $Na_v1.7$, with an IC_{50} of 1-10 nM, and is much less active on $Na_v1.5$, $Na_v1.8$, and $Na_v1.9$, with an IC_{50} of > 1 μM (Goldin 2001). The low nanomolar efficacy, fast binding kinetics, and clear separation of two target groups has made TTX useful in classifying voltage-gated Na^+ currents.

TTX effectively increased the rheobase and reduced peak sodium current in DRG neurons retrogradely labeled from the bladder (**Figure 11.4**) and colon (**Figure 7.1** and **Figure 7.2**). The estimated TTX-sensitive component of total sodium current was 71% in bladder-innervating LS neurons, 60% in colon-innervating LS neurons, and 47% in colon-innervating TL neurons, and rheobase was increased by on average 2.4-fold in LS neurons and 2.0-fold in TL neurons. In the presence of TTX, the half-maximal voltage (V_{50}) of steady-state activation was depolarized by 5.3 mV and the V_{50} of steady-state fast inactivation was depolarized by 28.8 mV. The shift in steady-state fast inactivation is consistent with kinetics of TTX-R channels (Catterall, Goldin & Waxman 2005; Inserra et al. 2017), and similar studies using primary neurons (Beyak et al. 2004; Cummins & Waxman 1997). These findings demonstrate that action potential generation and voltage-dependent sodium influx in colon- and bladder-innervating DRG neurons are effectively impaired by TTX.

12.2.4 Hs1a increases rheobase and reduces peak sodium current density in colon-innervating dorsal root ganglia neurons

Hs1a is a tarantula venom peptide with a putative inhibitor cysteine knot motif and structural similarity to Family 1 of spider peptide toxins that target Na_v channels (NaSpTx1), which is comprised of peptides isolated from tarantula species (Klint et al. 2012). Peptides in this family commonly interact with neurotoxin site 4, which consists of the extracellular linker regions in S1-S2 and S2-S4 of domain II of Na_v channels (Klint et al. 2012). Interaction of the peptide in this site reduces mobility of the voltage sensor in domain II and reduces sodium conductance through the pore, and may also induce a hyperpolarizing shift in steady-state activation (Stevens, Peigneur & Tytgat 2011). Whole-cell patch-clamp electrophysiology using recombinantly produced Hs1a found that this compound is an equipotent inhibitor of human $Na_v1.1$ ($hNa_v1.1$) (IC_{50} = 19 nM) and $hNa_v1.7$ (IC_{50} = 27 nM), a potent inhibitor of $hNa_v1.2$ (IC_{50} = 82 nM), $hNa_v1.3$ (IC_{50} = 107 nM), and $hNa_v1.6$ (IC_{50} 168 nM). Hs1a did not show a preference for $hNa_v1.4$ (IC_{50} > 10 µM) or $hNa_v1.5$ (IC_{50} > 10 µM), however, was found to potentiate $hNa_v1.8$ (EC_{50} = 146 nM).

Hs1a at 100 nM was not effective in increasing the average rheobase (**Figure 8.1**) or decreasing peak sodium current density (**Figure 8.2**) in colon-innervating TL DRG neurons. However, a significant increase in the average rheobase (**Figure 8.1**) and a decrease in peak sodium current density (**Figure 8.2**) was observed in the presence of 500 nM of Hs1a, which was not accompanied by changes in steady-state activation (**Figure 8.3**) or fast inactivation (**Figure 8.4**). The estimated component of total sodium current that was sensitive to 500 nM of Hs1a was 24%, and rheobase was increased by on average 1.2-fold. At this concentration, Hs1a is most likely modulating several Na_v isoforms, predominantly $Na_v1.1$, $Na_v1.7$, $Na_v1.2$, $Na_v1.3$, and $Na_v1.6$. The reduction in peak current without accompanying changes in steady-state activation or fast inactivation is similar to that of Huwentoxin-IV, an inhibitor cysteine knot peptide isolated from the *Ornithoctonus huwena* tarantula, which targets neurotoxin site 4 in rat $Na_v1.2$, $Na_v1.3$, and $Na_v1.4$, and human $Na_v1.7$ as shown by patch-clamp electrophysiology in heterologous expression systems (Xiao et al. 2008). In summary, Hs1a is an inhibitor of action potential generation and voltage-dependent sodium influx in colon-innervating DRG neurons at a concentration where a subset of TTX-S isoforms are targeted.

12.2.5 Compound B increases rheobase and reduces peak sodium current density in colon-innervating dorsal root ganglia neurons

$Na_v1.1$ has recently gained attention as a potential therapeutic target for visceral pain from a preclinical study using a mouse model of CVH (Osteen et al. 2016). In this study, action potential firing in colon-innervating DRG neurons and mechanosensitive responses in colonic splanchnic afferents from mice were elevated by a novel spider venom peptide δ-theraphotoxin-Hm1a. The mechanism behind this enhanced neuronal activity is thought to include inhibition of fast inactivation of $Na_v1.1$ via interaction of the peptide with S1-S2 and S3-S4 of domain IV, and possibly also by inhibition of $Na_v1.2$ (Osteen et al. 2016). To advance the understanding of the role of $Na_v1.1$ in colonic nociception, electrophysiological properties of colon-innervating DRG neurons was investigated in the presence of a selective $Na_v1.1$ modulator.

Compound B is a structural derivative of rufinamide, an anticonvulsant that exerts inhibitory effects on $hNa_v1.1$ and $hNa_v1.6$ in heterologous expression systems (Atkin et al. 2018; Gilchrist et al. 2014). Anticonvulsants commonly bind to a local anesthetic binding site on Na_v channels, where the compound-channel association reduces ion permeation and blocks sodium conductance (Lipkind & Fozzard 2005). Two-electrode voltage-clamp studies using oocytes have shown that incubation with compound B or rufinamide at 100 µM creates a depolarizing shift in the steady-state activation of $hNa_v1.1$ without affecting steady-state fast inactivation, thereby reducing the window current. In the presence of compound B, there were no changes in recovery from inactivation or persistent current, suggesting that compound B may be stabilizing a closed conformation of $hNa_v1.1$ (Gilchrist et al. 2014). Compound B was not found to be active on $hNa_v1.2$, $hNa_v1.3$, $hNa_v1.6$ (Gilchrist et al. 2014), $hNa_v1.5$, $hNa_v1.7$, or $hNa_v1.8$ (Salvatierra et al. 2018) With the exception of $Na_v1.4$ and $Na_v1.9$, for which activity information is not available, compound B is believed to selectively inhibit $Na_v1.1$ within the Na_v channel family.

In the current studies on colon-innervating DRG neurons from mice, compound B effectively reduced peak sodium current density (**Figure 10.2**) and increased rheobase (**Figure 9.1**) at 100 µM. The estimated component of total sodium current that was sensitive to 100 µM Compound B was 0.20, and rheobase was increased by on average 1.1-fold. These results support the hypothesis that $Na_v1.1$ contributes to action potential generation and sodium current properties in colon-innervating DRG neurons from mice.

12.2.6 ICA-121341 increases rheobase in colon-innervating dorsal root ganglia neurons

Following the finding that rheobase can be modulated using a $Na_v1.1$-selective compound, a less selective $Na_v1.1$ inhibitor was investigated for comparison. ICA-121341 belongs to the chemical class of aryl sulfonamides, which appear to target Na_v channels by interacting with the S1-S4 of domain IV (McCormack et al. 2013). This interaction may stabilize the inactivated conformation of Na_v channels (Ahuja et al. 2015), and is observed as a reduction in peak sodium current and a hyperpolarizing shift in steady-state fast inactivation (McCormack et al. 2013). This mechanism of inhibition is state-dependent and the inhibition is generally more effective in depolarized and rapidly firing neurons (Focken et al. 2016; Theile, Fuller & Chapman 2016). Patch-clamp electrophysiology using heterologous systems have shown that ICA-121341 has low nanomolar potency for $hNa_v1.1$ (IC_{50} = 23 ± 6 nM), $hNa_v1.3$ (IC_{50} = 13 ± 9 nM) and $hNa_v1.2$ (IC_{50} = 240 ± 80 nM), with low sensitivity for $Na_v1.4$-$Na_v1.8$ (IC_{50} > 10 µM) (McCormack et al. 2013).

Rheobase levels in colon-innervating DRG neurons were unaffected in the presence of 50 and 200 nM ICA-121341, but significantly increased in the presence of 500 nM of ICA-121341 (**Figure 9.2**), by on average 1.2-fold. The differences between results obtained using Compound B and ICA-121341 may be due to the mechanism of inhibition, whereby inhibition of rheobase is more effective using Compound B which may interact more with the channel pore, compared to ICA-121341, which is believed to be interacting more with one of the four voltage sensing domains. In summary, ICA-121341 effectively reduces rheobase in colon-innervating DRG neurons from mice at a concentration where the compound is likely to be targeting $Na_v1.1$, $Na_v1.2$, and $Na_v1.3$.

12.2.7 A-803467 increases rheobase and reduces action potential overshoot in colon-innervating dorsal root ganglia neurons

$Na_v1.8$ has been researched extensively for its contribution to visceral pain signaling (**Table 2.2**), and is the only isoform that is predominantly confined to the peripheral nervous system over other nervous systems (**Table 2.1**), making it an attractive therapeutic target for pain originating in the periphery. Mutagenesis studies have shown that A-803467, a synthetic furyl carboxamide, interacts with S6 segments, particularly in domain IV, and exhibited sensitivity to residues in the local anesthetic neurotoxin binding site of $Na_v1.8$ (Browne, LE et al. 2009). Like other compounds acting on S6 segments, such as local anesthetics and veratridine, the potency of A-803467 as a modulator is state- or voltage-dependent. A-803467 has an IC_{50} of 8 ± 2 nM for $hNa_v1.8$ when the prepulse in the voltage protocol is -40 mV, and an IC_{50} of 80 ± 10 nM when the prepulse is -100 mV (Jarvis et al. 2007). Similarly, A-803467 inhibited the TTX-R component of sodium current in rat LS DRG neurons with an IC_{50} of 140 nM when the prepulse potential was -40 mV, and an IC_{50} of 1 µM when the prepulse potential was -100 mV, and inhibited action potential generation at a concentration of 300 nM only when the neuron was held at -40 mV (Jarvis et al. 2007). A-803467 exhibited low nanomolar affinity for $Na_v1.8$, low micromolar affinity for $hNa_v1.2$, $hNa_v1.3$, $hNa_v1.5$, and $hNa_v1.7$ as determined by patch-clamp electrophysiology in heterologous expression systems (Jarvis et al. 2007; Kort et al. 2008), and unknown activity on $Na_v1.1$, $Na_v1.4$, $Na_v1.6$ and $Na_v1.9$. On the basis of the structure-activity information available, A-803467 is believed to selectively inhibit $Na_v1.8$ within the Na_v channel family.

In the current study, A-803467 at 500 nM was effective in increasing the rheobase in colon-innervating LS DRG neurons (**Figure 9.3**), by on average 1.4-fold. Furthermore, the action potential overshoot was significantly reduced in the presence of A-803467 (**Figure 9.3**), by on average 15%, which is similar to results obtained with knock-down of $Na_v1.8$ in LS DRG from mice (Renganathan, Cummins & Waxman 2001). A lower concentration of 250 nM was also investigated, however, no changes in action potential generation was observed with this concentration (**Figure 9.3**), likely due to the lower affinity of A-803467

150

at holding potential -70 mV. In summary, selective modulation of $Na_v1.8$ using A-803467 was effective in increasing rheobase in colon-innervating DRG neurons from mice.

12.3 Conclusion

This thesis investigated expression of Na_v channels in DRG neurons retrogradely labeled from the colon and bladder in mice, and demonstrated that pharmacological manipulation of subsets, as well as individual Na_v isoforms, is effective in altering active electrophysiological properties in these neurons. $Na_v1.8$ was the most abundant isoform detected in TL and LS DRG, followed by $Na_v1.7$, $Na_v1.9$, and $Na_v1.1$. In colon-innervating and bladder-innervating DRG neurons, transcripts for all nine Na_v channel isoforms were detected, with $Na_v1.7$-$Na_v1.9$ expressed by the majority of neurons. In the pharmacological section of this study, it was shown that inhibition of $Na_v1.1$-$Na_v1.4$, $Na_v1.6$, and $Na_v1.7$ using TTX was effective in inhibiting action potential generation and voltage-gated sodium influx in colon-innervating and bladder-innervating DRG neurons, and furthermore that this set of ion channels is required to mediate bladder afferent responses to distension and nociceptive signaling to the spinal cord in mice. Electrophysiological properties of colon-innervating DRG neurons were also effectively modulated by veratridine, which targets $Na_v1.1$-$Na_v1.9$; Hs1a, which targets $Na_v1.1$, $Na_v1.2$, $Na_v1.3$, $Na_v1.6$, and $Na_v1.7$; OD1, which targets $Na_v1.4$, $Na_v1.6$ and $Na_v1.7$; ICA-121341, which targets $Na_v1.1$-$Na_v1.3$; A-803467, which targets $Na_v1.8$; and Compound B, which targets $Na_v1.1$. Administration of Compound B was also shown to reduce pain responses to colorectal distension in CVH mice. The use of colon-innervating DRG neurons from CVH mice as an *in vitro* model for hypersensitivity was also evaluated. In this evaluation, there was no evidence to support a disease-related phenotype *in vitro*, however, further studies are encouraged to fully elucidate the relationship between external factors and electrophysiological parameters in this disease model. Collectively, the findings presented in this thesis support further preclinical investigation of Na_v modulation as a treatment for pain originating in the viscera.

12.4 Literature cited

Ahuja, S, Mukund, S, Deng, L, Khakh, K, Chang, E, Ho, H, Shriver, S, Young, C, Lin, S, Johnson, JP, Wu, P, Li, J, Coons, M, Tam, C, Brillantes, B, Sampang, H, Mortara, K, Bowman, KK, Clark, KR, Estevez, A, Xie, Z, Verschoof, H, Grimwood, M, Dehnhardt, C, Andrez, J-C, Focken, T, Sutherlin, DP, Safina, BS, Starovasnik, MA, Ortwine, DF, Franke, Y, Cohen, CJ, Hackos, DH, Koth, CM & Payandeh, J 2015, 'Structural basis of Na$_v$1.7 inhibition by an isoform-selective small-molecule antagonist', *Science*, vol. 350, no. 6267, p. aac5464.

Alexandrou, AJ, Brown, AR, Chapman, ML, Estacion, M, Turner, J, Mis, MA, Wilbrey, A, Payne, EC, Gutteridge, A, Cox, PJ, Doyle, R, Printzenhoff, D, Lin, Z, Marron, BE, West, C, Swain, NA, Storer, RI, Stupple, PA, Castle, NA, Hounshell, JA, Rivara, M, Randall, A, Dib-Hajj, SD, Krafte, D, Waxman, SG, Patel, MK, Butt, RP & Stevens, EB 2016, 'Subtype-Selective Small Molecule Inhibitors Reveal a Fundamental Role for Na$_v$1.7 in Nociceptor Electrogenesis, Axonal Conduction and Presynaptic Release', *PLoS One*, vol. 11, no. 4, p. e0152405.

Antoniou, E, Margonis, GA, Angelou, A, Pikouli, A, Argiri, P, Karavokyros, I, Papalois, A & Pikoulis, E 2016, 'The TNBS-induced colitis animal model: An overview', *Annals of medicine and surgery (2012)*, vol. 11, pp. 9-15.

Atkin, TA, Maher, CM, Gerlach, AC, Gay, BC, Antonio, BM, Santos, SC, Padilla, KM, Rader, J, Krafte, DS, Fox, MA, Stewart, GR, Petrovski, S, Devinsky, O, Might, M, Petrou, S & Goldstein, DB 2018, 'A comprehensive approach to identifying repurposed drugs to treat *SCN8A* epilepsy', *Epilepsia*, vol. 59, no. 4, 2018/04/01, pp. 802-813.

Bean, BP 2007, 'The action potential in mammalian central neurons', *Nature Reviews Neuroscience*, vol. 8, 06/01/online, p. 451.

Beyak, MJ, Ramji, N, Krol, KM, Kawaja, MD & Vanner, SJ 2004, 'Two TTX-resistant Na$^+$ currents in mouse colonic dorsal root ganglia neurons and their role in colitis-induced hyperexcitability', *Am. J. Physiol. GI. Liver Physiol.*, vol. 287, no. 4, Oct, pp. G845-855.

Birder, L & Andersson, K-E 2018, 'Animal Modelling of Interstitial Cystitis/Bladder Pain Syndrome', *International neurourology journal*, vol. 22, no. Suppl 1, pp. S3-S9.

Brierley, SM, Jones, RCW, Gebhart, GF & Blackshaw, LA 2004, 'Splanchnic and pelvic mechanosensory afferents signal different qualities of colonic stimuli in mice', *Gastroenterology*, vol. 127, no. 1, Jul, pp. 166-178.

Brierley, SM & Linden, DR 2014, 'Neuroplasticity and dysfunction after gastrointestinal inflammation', *Nat Rev Gastroenterol Hepatol*, vol. 11, no. 10, Oct, pp. 611-627.

Browne, L, Smith, KE & Jagger, DJ 2017, 'Identification of Persistent and Resurgent Sodium Currents in Spiral Ganglion Neurons Cultured from the Mouse Cochlea', *eneuro*, vol. 4, no. 6, pp. ENEURO.0303-0317.2017.

Browne, LE, Blaney, FE, Yusaf, SP, Clare, JJ & Wray, D 2009, 'Structural Determinants of Drugs Acting on the Na$_v$1.8 Channel', *Journal of Biological Chemistry*, vol. 284, no. 16, pp. 10523-10536.

Castro, J, Harrington, AM, Garcia-Caraballo, S, Maddern, J, Grundy, L, Zhang, J, Page, G, Miller, PE, Craik, DJ, Adams, DJ & Brierley, SM 2017, 'alpha-Conotoxin Vc1.1 inhibits human dorsal root ganglion neuroexcitability and mouse colonic nociception via GABA$_B$ receptors', *Gut*, vol. 66, no. 6, Jun, pp. 1083-1094.

Catterall, WA, Goldin, AL & Waxman, SG 2005, 'International Union of Pharmacology. XLVII. Nomenclature and Structure-Function Relationships of Voltage-Gated Sodium Channels', *Pharmacological Reviews*, vol. 57, no. 4, pp. 397-409.

Cestele, S & Catterall, WA 2000, 'Molecular mechanisms of neurotoxin action on voltage-gated sodium channels', *Biochimie*, vol. 82, no. 9-10, Sep-Oct, pp. 883-892.

Chang, W, Berta, T, Kim, YH, Lee, S, Lee, SY & Ji, RR 2018, 'Expression and Role of Voltage-Gated Sodium Channels in Human Dorsal Root Ganglion Neurons with Special Focus on Na$_v$1.7, Species Differences, and Regulation by Paclitaxel', *Neurosci Bull*, vol. 34, no. 1, Feb, pp. 4-12.

Cox, JJ, Reimann, F, Nicholas, AK, Thornton, G, Roberts, E, Springell, K, Karbani, G, Jafri, H, Mannan, J, Raashid, Y, Al-Gazali, L, Hamamy, H, Valente, EM, Gorman, S, Williams, R, McHale, DP, Wood, JN, Gribble, FM & Woods, CG 2006, 'An *SCN9A* channelopathy causes congenital inability to experience pain', *Nature*, vol. 444, 12/14/online, p. 894.

Cummins, TR & Waxman, SG 1997, 'Downregulation of Tetrodotoxin-Resistant Sodium Currents and Upregulation of a Rapidly Repriming Tetrodotoxin-Sensitive Sodium Current in Small Spinal Sensory Neurons after Nerve Injury', *The Journal of Neuroscience*, vol. 17, no. 10, p. 3503.

Desai, MS, Seekatz, AM, Koropatkin, NM, Kamada, N, Hickey, CA, Wolter, M, Pudlo, NA, Kitamoto, S, Terrapon, N, Muller, A, Young, VB, Henrissat, B, Wilmes, P, Stappenbeck, TS, Núñez, G & Martens, EC 2016, 'A Dietary Fiber-Deprived Gut Microbiota Degrades the Colonic Mucus Barrier and Enhances Pathogen Susceptibility', *Cell*, vol. 167, no. 5, pp. 1339-1353.e1321.

Deuis, JR, Dekan, Z, Wingerd, JS, Smith, JJ, Munasinghe, NR, Bhola, RF, Imlach, WL, Herzig, V, Armstrong, DA, Rosengren, KJ, Bosmans, F, Waxman, SG, Dib-Hajj, SD, Escoubas, P, Minett,

MS, Christie, MJ, King, GF, Alewood, PF, Lewis, RJ, Wood, JN & Vetter, I 2017, 'Pharmacological characterisation of the highly Na$_v$1.7 selective spider venom peptide Pn3a', *Sci Rep*, vol. 7, 01/20/online, p. 40883.

Dubin, AE & Patapoutian, A 2010, 'Nociceptors: the sensors of the pain pathway', *The Journal of clinical investigation*, vol. 120, no. 11, pp. 3760-3772.

Durek, T, Vetter, I, Wang, C-IA, Motin, L, Knapp, O, Adams, DJ, Lewis, RJ & Alewood, PF 2013, 'Chemical Engineering and Structural and Pharmacological Characterization of the α-Scorpion Toxin OD1', *ACS Chemical Biology*, vol. 8, no. 6, 2013/06/21, pp. 1215-1222.

Emery, EC, Luiz, AP & Wood, JN 2016, 'Na$_v$1.7 and other voltage-gated sodium channels as drug targets for pain relief', *Expert opinion on therapeutic targets*, vol. 20, no. 8, pp. 975-983.

Faber, CG, Lauria, G, Merkies, ISJ, Cheng, X, Han, C, Ahn, H-S, Persson, A-K, Hoeijmakers, JGJ, Gerrits, MM, Pierro, T, Lombardi, R, Kapetis, D, Dib-Hajj, SD & Waxman, SG 2012, 'Gain-of-function Na$_v$1.8 mutations in painful neuropathy', *Proceedings of the National Academy of Sciences of the United States of America*, vol. 109, no. 47, pp. 19444-19449.

Focken, T, Liu, S, Chahal, N, Dauphinais, M, Grimwood, ME, Chowdhury, S, Hemeon, I, Bichler, P, Bogucki, D, Waldbrook, M, Bankar, G, Sojo, LE, Young, C, Lin, S, Shuart, N, Kwan, R, Pang, J, Chang, JH, Safina, BS, Sutherlin, DP, Johnson, JP, Jr., Dehnhardt, CM, Mansour, TS, Oballa, RM, Cohen, CJ & Robinette, CL 2016, 'Discovery of Aryl Sulfonamides as Isoform-Selective Inhibitors of Na$_v$1.7 with Efficacy in Rodent Pain Models', *ACS medicinal chemistry letters*, vol. 7, no. 3, pp. 277-282.

Gilchrist, J, Dutton, S, Diaz-Bustamante, M, McPherson, A, Olivares, N, Kalia, J, Escayg, A & Bosmans, F 2014, 'Na$_v$1.1 Modulation by a Novel Triazole Compound Attenuates Epileptic Seizures in Rodents', *ACS Chemical Biology*, vol. 9, no. 5, 2014/05/16, pp. 1204-1212.

Goldberg, YP, MacFarlane, J, MacDonald, ML, Thompson, J, Dube, MP, Mattice, M, Fraser, R, Young, C, Hossain, S, Pape, T, Payne, B, Radomski, C, Donaldson, G, Ives, E, Cox, J, Younghusband, HB, Green, R, Duff, A, Boltshauser, E, Grinspan, GA, Dimon, JH, Sibley, BG, Andria, G, Toscano, E, Kerdraon, J, Bowsher, D, Pimstone, SN, Samuels, ME, Sherrington, R & Hayden, MR 2007, 'Loss-of-function mutations in the Na$_v$1.7 gene underlie congenital indifference to pain in multiple human populations', *Clinical Genetics*, vol. 71, no. 4, pp. 311-319.

Goldin, AL 2001, 'Resurgence of Sodium Channel Research', *Annu Rev Physiol*, vol. 63, no. 1, 2001/03/01, pp. 871-894.

Gong, K, Kung, L-H, Magni, G, Bhargava, A & Jasmin, L 2014, 'Increased Response to Glutamate in Small Diameter Dorsal Root Ganglion Neurons after Sciatic Nerve Injury', *PLoS One*, vol. 9, no. 4, p. e95491.

González-Cano, R, Tejada, MÁ, Artacho-Cordón, A, Nieto, FR, Entrena, JM, Wood, JN & Cendán, CM 2017, 'Effects of Tetrodotoxin in Mouse Models of Visceral Pain', *Marine Drugs*, vol. 15, no. 6, p. 188.

Grundy, L, Harrington, AM, Castro, J, Garcia-Caraballo, S, Deiteren, A, Maddern, J, Rychkov, GY, Ge, P, Peters, S, Feil, R, Miller, P, Ghetti, A, Hannig, G, Kurtz, CB, Silos-Santiago, I & Brierley, SM 2018, 'Chronic linaclotide treatment reduces colitis-induced neuroplasticity and reverses persistent bladder dysfunction', *JCI Insight*, vol. 3, no. 19, p. e121841.

Hagen, NA, Cantin, L, Constant, J, Haller, T, Blaise, G, Ong-Lam, M, du Souich, P, Korz, W & Lapointe, B 2017, 'Tetrodotoxin for Moderate to Severe Cancer-Related Pain: A Multicentre, Randomized, Double-Blind, Placebo-Controlled, Parallel-Design Trial', *Pain Research & Management*, vol. 2017, pp. 7212713-7212713.

Hagen, NA, Lapointe, B, Ong–Lam, M, Dubuc, B, Walde, D, Gagnon, B, Love, R, Goel, R, Hawley, P, Ngoc, AH & du Souich, P 2011, 'A multicentre open-label safety and efficacy study of tetrodotoxin for cancer pain', *Current Oncology*, vol. 18, no. 3, pp. e109-e116.

Hockley, JRF, González-Cano, R, McMurray, S, Tejada-Giraldez, MA, McGuire, C, Torres, A, Wilbrey, AL, Cibert-Goton, V, Nieto, FR, Pitcher, T, Knowles, CH, Baeyens, JM, Wood, JN, Winchester, WJ, Bulmer, DC, Cendán, CM & McMurray, G 2017, 'Visceral and somatic pain modalities reveal Na$_v$1.7-independent visceral nociceptive pathways', *J Physiol*, vol. 595, no. 8, pp. 2661-2679.

Hockley, JRF, Taylor, TS, Callejo, G, Wilbrey, AL, Gutteridge, A, Bach, K, Winchester, WJ, Bulmer, DC, McMurray, G & Smith, ESJ 2018, 'Single-cell RNAseq reveals seven classes of colonic sensory neuron', *Gut*, Feb 26.

Hu, J, Song, Z-Y, Zhang, H-H, Qin, X, Hu, S, Jiang, X & Xu, G-Y 2016, 'Colonic Hypersensitivity and Sensitization of Voltage-gated Sodium Channels in Primary Sensory Neurons in Rats with Diabetes', *Journal of Neurogastroenterology and Motility*, vol. 22, no. 1, pp. 129-140.

Hu, S, Xiao, Y, Zhu, L, Li, L, Hu, CY, Jiang, X & Xu, GY 2013, 'Neonatal maternal deprivation sensitizes voltage-gated sodium channel currents in colon-specific dorsal root ganglion neurons in rats', *American Journal of Physiology - Gastrointestinal and Liver Physiology*, vol. 304, no. 4, Feb 15, pp. G311-321.

Huang, J, Han, C, Estacion, M, Vasylyev, D, Hoeijmakers, JG, Gerrits, MM, Tyrrell, L, Lauria, G, Faber, CG, Dib-Hajj, SD, Merkies, IS, Waxman, SG & Group, PS 2014, 'Gain-of-function mutations in sodium channel Na$_v$1.9 in painful neuropathy', *Brain*, vol. 137, no. Pt 6, Jun, pp. 1627-1642.

Hughes, PA, Brierley, SM, Martin, CM, Brookes, SJ, Linden, DR & Blackshaw, LA 2009, 'Post-inflammatory colonic afferent sensitisation: different subtypes, different pathways and different time courses', *Gut*, vol. 58, no. 10, Oct, pp. 1333-1341.

Inserra, MC, Israel, MR, Caldwell, A, Castro, J, Deuis, JR, Harrington, AM, Keramidas, A, Garcia-Caraballo, S, Maddern, J, Erickson, A, Grundy, L, Rychkov, GY, Zimmermann, K, Lewis, RJ, Brierley, SM & Vetter, I 2017, 'Multiple sodium channel isoforms mediate the pathological effects of Pacific ciguatoxin-1', *Sci Rep*, vol. 7, Feb 22, p. 42810.

Jalali, A, Bosmans, F, Amininasab, M, Clynen, E, Cuypers, E, Zaremirakabadi, A, Sarbolouki, M-N, Schoofs, L, Vatanpour, H & Tytgat, J 2005, 'OD1, the first toxin isolated from the venom of the scorpion Odonthobuthus doriae active on voltage-gated Na$^+$ channels', *FEBS Letters*, vol. 579, no. 19, 2005/08/01, pp. 4181-4186.

Jarvis, MF, Honore, P, Shieh, CC, Chapman, M, Joshi, S, Zhang, XF, Kort, M, Carroll, W, Marron, B, Atkinson, R, Thomas, J, Liu, D, Krambis, M, Liu, Y, McGaraughty, S, Chu, K, Roeloffs, R, Zhong, C, Mikusa, JP, Hernandez, G, Gauvin, D, Wade, C, Zhu, C, Pai, M, Scanio, M, Shi, L, Drizin, I, Gregg, R, Matulenko, M, Hakeem, A, Gross, M, Johnson, M, Marsh, K, Wagoner, PK, Sullivan, JP, Faltynek, CR & Krafte, DS 2007, 'A-803467, a potent and selective Na$_v$1.8 sodium channel blocker, attenuates neuropathic and inflammatory pain in the rat', *Proceedings of the National Academy of Sciences of the United States of America*, vol. 104.

Ji, R-R, Nackley, A, Huh, Y, Terrando, N & Maixner, W 2018, 'Neuroinflammation and Central Sensitization in Chronic and Widespread Pain', *Anesthesiology: The Journal of the American Society of Anesthesiologists*, vol. 129, no. 2, pp. 343-366.

Jiminez, JA, Uwiera, TC, Douglas Inglis, G & Uwiera, RRE 2015, 'Animal models to study acute and chronic intestinal inflammation in mammals', *Gut Pathogens*, vol. 7, no. 1, 2015/11/10, p. 29.

Klint, JK, Senff, S, Rupasinghe, DB, Er, SY, Herzig, V, Nicholson, GM & King, GF 2012, 'Spider-venom peptides that target voltage-gated sodium channels: Pharmacological tools and potential therapeutic leads', *Toxicon*, vol. 60, no. 4, 2012/09/15/, pp. 478-491.

Klint, JK, Smith, JJ, Vetter, I, Rupasinghe, DB, Er, SY, Senff, S, Herzig, V, Mobli, M, Lewis, RJ, Bosmans, F & King, GF 2015, 'Seven novel modulators of the analgesic target Na$_v$1.7 uncovered using a high-throughput venom-based discovery approach', *British Journal of Pharmacology*, vol. 172, no. 10, pp. 2445-2458.

Kort, ME, Drizin, I, Gregg, RJ, Scanio, MJC, Shi, L, Gross, MF, Atkinson, RN, Johnson, MS, Pacofsky, GJ, Thomas, JB, Carroll, WA, Krambis, MJ, Liu, D, Shieh, C-C, Zhang, X, Hernandez, G, Mikusa, JP, Zhong, C, Joshi, S, Honore, P, Roeloffs, R, Marsh, KC, Murray, BP, Liu, J, Werness, S, Faltynek, CR, Krafte, DS, Jarvis, MF, Chapman, ML & Marron, BE 2008, 'Discovery and Biological Evaluation of 5-Aryl-2-furfuramides, Potent and Selective Blockers of the Nav1.8 Sodium Channel with Efficacy in Models of Neuropathic and Inflammatory Pain', *Journal of Medicinal Chemistry*, vol. 51, no. 3, 2008/02/01, pp. 407-416.

Larauche, M, Gourcerol, G, Million, M, Adelson, DW & Taché, Y 2010, 'Repeated psychological stress-induced alterations of visceral sensitivity and colonic motor functions in mice: influence of surgery and postoperative single housing on visceromotor responses', *Stress (Amsterdam, Netherlands)*, vol. 13, no. 4, pp. 343-354.

Larsson, MH, Miketa, A & Martinez, V 2009, 'Lack of interaction between psychological stress and DSS-induced colitis affecting colonic sensitivity during colorectal distension in mice', *Stress*, vol. 12, no. 5, 2009/01/01, pp. 434-444.

Lee, J-H, Park, C-K, Chen, G, Han, Q, Xie, R-G, Liu, T, Ji, R-R & Lee, S-Y 2014, 'A monoclonal antibody that targets a Na$_v$1.7 channel voltage sensor for pain and itch relief', *Cell*, vol. 157, no. 6, pp. 1393-1404.

Lin, YM, Fu, Y, Winston, J, Radhakrishnan, R, Sarna, SK, Huang, LM & Shi, XZ 2017, 'Pathogenesis of abdominal pain in bowel obstruction: Role of mechanical stress-induced upregulation of nerve growth factor in gut smooth muscle cells', *Pain*, Jan 06.

Lipkind, GM & Fozzard, HA 2005, 'Molecular Modeling of Local Anesthetic Drug Binding by Voltage-Gated Sodium Channels', *Molecular Pharmacology*, vol. 68, no. 6, p. 1611.

Maertens, C, Cuypers, E, Amininasab, M, Jalali, A, Vatanpour, H & Tytgat, J 2006, 'Potent Modulation of the Voltage-Gated Sodium Channel Na$_v$1.7 by OD1, a Toxin from the Scorpion *Odonthobuthus doriae*', *Molecular Pharmacology*, vol. 70, no. 1, p. 405.

Manriquez, V, Castro Caperan, D, Guzman, R, Naser, M, Iglesia, V & Lagos, N 2015, 'First evidence of neosaxitoxin as a long-acting pain blocker in bladder pain syndrome', *Int Urogynecol J*, vol. 26, no. 6, Jun, pp. 853-858.

Mayer, EA, Bradesi, S, Chang, L, Spiegel, BMR, Bueller, JA & Naliboff, BD 2008, 'Functional GI disorders: from animal models to drug development', *Gut*, vol. 57, no. 3, pp. 384-404.

McCormack, K, Santos, S, Chapman, ML, Krafte, DS, Marron, BE, West, CW, Krambis, MJ, Antonio, BM, Zellmer, SG, Printzenhoff, D, Padilla, KM, Lin, Z, Wagoner, PK, Swain, NA, Stupple, PA,

de Groot, M, Butt, RP & Castle, NA 2013, 'Voltage sensor interaction site for selective small molecule inhibitors of voltage-gated sodium channels', *Proceedings of the National Academy of Sciences of the United States of America*, vol. 110, no. 29, 07/01, pp. E2724-E2732.

McDonnell, A, Collins, S, Ali, Z, Iavarone, L, Surujbally, R, Kirby, S & Butt, RP 2018, 'Efficacy of the Na$_v$1.7 blocker PF-05089771 in a randomised, placebo-controlled, double-blind clinical study in subjects with painful diabetic peripheral neuropathy', *Pain*, vol. 159, no. 8.

Meerupally, R, Singh, JN & Sharma, SS 2014, 'Diabetic-induced increased sodium channel activity attenuated by tetracaine in sensory neurons *in vitro*', *Biochemical and Biophysical Research Communications*, vol. 453, no. 3, 2014/10/24/, pp. 296-301.

Minett, MS, Nassar, MA, Clark, AK, Passmore, G, Dickenson, AH, Wang, F, Malcangio, M & Wood, JN 2012, 'Distinct Na$_v$1.7-dependent pain sensations require different sets of sensory and sympathetic neurons', *Nature Communications*, vol. 3, p. 791.

Mohammad, HF, Roodabeh, B, Mohammad, A & Roja, R 2016, 'The Role of Visceral Hypersensitivity in Irritable Bowel Syndrome: Pharmacological Targets and Novel Treatments', *Journal of Neurogastroenterology and Motility*, vol. 22, no. 4, 10, pp. 558-574.

Moloney, RD, Dinan, TG & Cryan, JF 2015, 'Strain-dependent variations in visceral sensitivity: relationship to stress, anxiety and spinal glutamate transporter expression', *Genes, Brain and Behavior*, vol. 14, no. 4, 2015/04/01, pp. 319-329.

Moloney, RD, O'Mahony, SM, Dinan, TG & Cryan, JF 2015, 'Stress-Induced Visceral Pain: Toward Animal Models of Irritable-Bowel Syndrome and Associated Comorbidities', *Frontiers in Psychiatry*, vol. 6, p. 15.

Momin, A & McNaughton, PA 2009, 'Regulation of firing frequency in nociceptive neurons by pro-inflammatory mediators', *Experimental Brain Research*, vol. 196, no. 1, 2009/06/01, pp. 45-52.

Osteen, JD, Herzig, V, Gilchrist, J, Emrick, JJ, Zhang, C, Wang, X, Castro, J, Garcia-Caraballo, S, Grundy, L, Rychkov, GY, Weyer, AD, Dekan, Z, Undheim, EAB, Alewood, P, Stucky, CL, Brierley, SM, Basbaum, AI, Bosmans, F, King, GF & Julius, D 2016, 'Selective spider toxins reveal a role for the Na$_v$1.1 channel in mechanical pain', *Nature*, vol. 534, no. 7608, 06/23/print, pp. 494-499.

Qu, R, Tao, J, Wang, Y, Zhou, Y, Wu, G, Xiao, Y, Hu, C-Y, Jiang, X & Xu, G-Y 2013, 'Neonatal colonic inflammation sensitizes voltage-gated Na$^+$ channels via upregulation of cystathionine beta-synthetase expression in rat primary sensory neurons', *American Journal of Physiology-Gastrointestinal and Liver Physiology*, vol. 304, no. 9, May, pp. G763-G772.

R Abdrakhmanova, G, Alsharari, S, Kang, M, Imad Damaj, M & Akbarali, H 2010, *7-nAChR-mediated suppression of hyperexcitability of colonic dorsal root ganglia neurons in experimental colitis*, vol. 299.

Renganathan, M, Cummins, TR & Waxman, SG 2001, 'Contribution of Na$_v$1.8 sodium channels to action potential electrogenesis in DRG neurons', *Journal of Neurophysiology*, vol. 86, no. 2, Aug, pp. 629-640.

Sadeghi, M, Erickson, A, Castro, J, Deiteren, A, Harrington, AM, Grundy, L, Adams, DJ & Brierley, SM 2018, 'Contribution of membrane receptor signalling to chronic visceral pain', *Int J Biochem Cell Biol*, vol. 98, May, pp. 10-23.

Salvatierra, J, Castro, J, Erickson, A, Li, Q, Braz, J, Gilchrist, J, Grundy, L, Rychkov, GY, Deiteren, A, Rais, R, King, GF, Slusher, BS, Basbaum, A, Pasricha, PJ, Brierley, SM & Bosmans, F 2018, 'Na$_v$1.1 inhibition can reduce visceral hypersensitivity', *JCI Insight*, vol. 3, no. 11, Jun 7.

Song, Y, Zhang, M, Tao, X, Xu, Z, Zheng, Y, Zhu, M, Zhang, L, Qiao, J & Gao, L 2018, 'Difference of acute dissociation and 1-day culture on the electrophysiological properties of rat dorsal root ganglion neurons', *Journal of Physiology and Biochemistry*, vol. 74, no. 2, 2018/05/01, pp. 207-221.

Soong, TW & Venkatesh, B 2006, 'Adaptive evolution of tetrodotoxin resistance in animals', *Trends in Genetics*, vol. 22, no. 11, 2006/11/01/, pp. 621-626.

Stevens, M, Peigneur, S & Tytgat, J 2011, 'Neurotoxins and their binding areas on voltage-gated sodium channels', *Frontiers in Pharmacology*, vol. 2, pp. 71-71.

Stoicea, N, Russell, D, Weidner, G, Durda, M, Joseph, NC, Yu, J & Bergese, SD 2015, 'Opioid-induced hyperalgesia in chronic pain patients and the mitigating effects of gabapentin', *Frontiers in Pharmacology*, vol. 6, pp. 104-104.

te Velde, AA, Verstege, MI & Hommes, DW 2006, 'Critical appraisal of the current practice in murine TNBS-induced colitis', *Inflammatory Bowel Diseases*, vol. 12, no. 10, 2006/10/01, pp. 995-999.

Theile, JW, Fuller, MD & Chapman, ML 2016, 'The Selective Na$_v$1.7 Inhibitor, PF-05089771, Interacts Equivalently with Fast and Slow Inactivated Na$_v$1.7 Channels', *Molecular Pharmacology*, vol. 90, no. 5, p. 540.

Ulbricht, W 1998, 'Effects of veratridine on sodium currents and fluxes', in *Reviews of Physiology Biochemistry and Pharmacology, Volume 133*, Springer Berlin Heidelberg, Berlin, Heidelberg, pp. 1-54.

Ulbricht, W 2005, 'Sodium Channel Inactivation: Molecular Determinants and Modulation', *Physiological Reviews*, vol. 85, no. 4, 2005/10/01, pp. 1271-1301.

`

Wang, S-Y & Wang, GK 2003, 'Voltage-gated sodium channels as primary targets of diverse lipid-soluble neurotoxins', *Cellular Signalling*, vol. 15, no. 2, 2003/02/01/, pp. 151-159.

Xiao, Y, Bingham, J-P, Zhu, W, Moczydlowski, E, Liang, S & Cummins, TR 2008, 'Tarantula huwentoxin-IV inhibits neuronal sodium channels by binding to receptor site 4 and trapping the domain ii voltage sensor in the closed configuration', *The Journal of biological chemistry*, vol. 283, no. 40, pp. 27300-27313.

`